High-throughput Screening and Chemical Synthesis for the Discovery of
APOBEC3 DNA Cytosine Deaminase Inhibitors

A THESIS
SUBMITTED TO THE FACULTY OF
UNIVERSITY OF MINNESOTA
BY

MARGARET EMILY OLSON

IN PARTIAL FULFILLMENT OF THE REQUIREMENTS
FOR THE DEGREE OF
DOCTOR OF PHILOSOPHY

Adviser: Daniel A. Harki

September 2015

Acknowledgements

First and foremost, I want to sincerely thank my advisor, Professor Daniel Harki, for his unwavering support over the course of my graduate career. My successes as a graduate student are a direct result of his mentorship style, including his encouragement to apply for fellowships, present and publish often, and explore original research ideas. I would also like to acknowledge Professor Reuben Harris, my co-mentor and research collaborator, who envisioned the project of APOBEC3 inhibitor discovery, which ultimately became the focus of my thesis. I am truly grateful to have had such a close collaboration with Harris laboratory and for the opportunities Reuben provided me to train at the interface of medicinal chemistry and molecular biology. Finally, I would like to recognize Professor Courtney Aldrich, Professor Elizabeth Amin, and Professor Gunda Georg for serving on my dissertation committee, and for invaluable critiques and advice throughput my graduate career.

The research accomplished in this thesis would not be possible without the collaboration and camaraderie of many gifted scientists at the University of Minnesota. Foremost, I would like to thank Dr. Ming Li (Harris Lab), who not only performed many of the biochemical experiments presented in this thesis, but was responsible for my training in the Harris laboratory. Additionally, I would like to recognize my colleagues in the Harki Lab, especially the fellow doctoral students Kellan Passow, Nick Struntz, and John Widen, who created an intellectual, productive and fun work environment. I would also like to acknowledge members of the Harki and Harris laboratories who have specifically contributed to the APOBEC3 project including: Daniel Abate-Pella, Stephanie Breunig, Tenley

didn't have the four of you. To all of my family and friends, thank you for all of your encouragement and interest in my developing career.

Finally, I'd like to acknowledge my fiancé Dr. Elbek Kurbanov. I couldn't imagine going through graduate school without you. Thank you for everything you've done for me, your patience for all the late nights and last minute deadlines, and your undying support. I can't wait to see what the next chapter of life has in store for us.

Dedication

This thesis is lovingly dedicated to my parents, Leonard and Judith Olson, who instilled in me the hard work and passion for learning that made this thesis a success.

Abstract

APOBEC3 (APOBEC3A-APOBEC3H) enzymes catalyze single-stranded (ss)DNA cytosine-to-uracil (C-to-U) deamination as a function of innate immune defense against foreign DNA. Host cellular protection results from APOBEC3-catalyzed lethal mutagenesis of the offending genome. When misregulated, however, APOBEC3 enzymes have been demonstrated to drive the genetic evolution of numerous cancers and HIV-1. Specifically, sub-lethal levels of APOBEC3D/F/G/H-catalyzed mutation can enable HIV-1 escape from immune defense and antiretroviral therapies. Moreover, APOBEC3B over-expression in breast, bladder, cervical, lung, and head/neck cancers generates high levels of C-to-U mutation, which drives tumor formation, metastasis, and chemotherapeutic resistance. Thus, small molecule inhibition of APOBEC3-catalyzed deamination may provide a novel strategy for HIV-1 and cancer drug development.

This thesis highlights efforts to discover small molecule inhibitors of the APOBEC3s through high-throughput screening (HTS) and chemical synthesis. Chapter 2 discusses an HTS of 168,192 compounds against APOBEC3B and APOBEC3G. In this effort, MN23 was discovered as a potent inhibitor of APOBEC3B (IC_{50} = 150 nM) and APOBEC3G (IC_{50} = 5.5 μM). Chapter 2 also reports a novel synthesis of MN23, and preliminary efforts to elucidate its mechanism of inhibition. Chapter 3 presents a class of covalent APOBEC3G-specific inhibitors based on a 1,2,4-triazole-3-thiol substructure. This compound class is predicted to inhibit APOBEC3G by covalently binding C321, forcing an inhibitory conformational change within the enzyme active site. Chapter 4 reports

the discovery of a novel APOBEC3G inhibitory chemotype, which was discovered from the deconvolution of an impure HTS hit. In this effort, we also identified a previously unreported Pan Assay Interference Scaffold (PAINS), and characterized the mechanism by which compounds of this class undergo oxidative decomposition. Finally, Chapter 5 describes how benzthiazolinone-based APOBEC3 inhibitors are being developed into probes of APOBEC3 structure and function. Brief descriptions of two unrelated projects performed concurrent with these studies are also detailed in the Appendices.

TABLE OF CONTENTS

List of Tables

List of Figures

List of Schemes

Chapter 1

INTRODUCTION

1.1 Overview of the APOBEC Enzyme Family

The APOBEC3 family of single-stranded DNA (ssDNA) cytosine-to-uracil deaminases belongs to the larger human apolipoprotein B mRNA-editing enzyme catalytic polypeptide-like (APOBEC) gene family. In total, the APOBEC family consists of 11 polynucleotide cytosine-to-uracil (C-to-U) editing enzymes including activation induced deaminase (AID), APOBEC1 (A1), APOBEC2 (A2), seven APOBEC3s (APOBEC3A/B/C/D/F/G/H), and APOBEC4 (A4). AID functions as an essential element of the adaptive immune system, catalyzing antibody gene diversification through somatic hypermutation and class switch recombination.[2-8] APOBEC1, the sole RNA-editing enzyme of the family, functions in lipid metabolism[9], while the activities of APOBEC2 and APOBEC4 are currently unknown.

The seven APOBEC3s constitute a vital defense network of the innate immune system. Specifically, APOBEC3-catalyzed DNA cytosine deamination of exogenous viruses and endogenous retroelements restricts their replication and protects immune cells from infection. The 7 APOBEC3s are encoded in tandem on chromosome 22 of the human genome.[10] A possible explanation for the repetitive function of these polynucleotide deaminases is to provide overlapping protection against a broad spectrum of DNA-based pathogens.

The APOBEC3 sub-family is further divided into the Z1, Z2, and Z3 phylogenetic sub-groups, which are defined by structural features of the zinc(Zn)-coordinating motif.[8,11] Z1 APOBEC3s contain a $Hx_1Ex_5\underline{XV/I}$; $\underline{S}WS/TPCx_{2-4}C$ Zn-coordinating motif, and a unique isoleucine in a RIY sequence C-terminal to the

Zn-coordinating residues.[11-13] Z2 APOBEC3s are characterized by a $Hx_1Ex_5\underline{WF}$; $\underline{S}WS/TPCx_{2-4}C$ Zn-coordinating motif – differing from Z1 APOBEC3s by a conserved tryptophan-phenylalanine (WF) sequence five amino acids after the catalytic Glu.[11,12] Finally, Z3 APOBEC3s have a distinct $\underline{T}WSCx_2C$ Zn-coordinating motif. APOBEC3s may be expressed as either single domain or double domain enzymes (Figure 1.1).[11] APOBEC3A, APOBEC3C, and APOBEC3H are characterized as single domain APOBEC3s, though APOBEC3A exhibits a Z1 domain, APOBEC3C exhibits a Z2 domain, and APOBEC3H uniquely exhibits a Z3 domain (Figure 1.1). APOBEC3B, APOBEC3D, APOBEC3F, and APOBEC3G contain two structural domains, where APOBEC3B and APOBEC3G are structurally defined as having Z2-Z1 domains and APOBEC3D and APOBEC3F have Z2-Z2 domains (Figure 1.1).[11]

Figure 1.1. Schematic Representation of the Human APOBEC3 Loci. The APOBEC3s are encoded in tandem on chromosome 22 of the human genome. The seven family members can be individually distinguished by the number of structural domains (represented as one or two ellipses) and the phylogenetic characterization of those domains. Three phylogenetic sub-groups exist (Z1, Z2, Z3), which are assigned based on the structural homology of the zinc-coordinating motif.[11] The Z1 sub-group is represented in green, the Z2 sub-group in orange, and the Z3 sub-group in blue as implemented by LaRue et al.[11] Graphic inspired by Hultquist et al. *J. Virol.* **2011**, *85*, 11220.[14]

Human APOBEC3s are expressed in most tissues in the human body.[15-17] In freshly isolated peripheral blood mononuclear cells (PBMCs), APOBEC3C/D/F/G and H are more highly expressed in B cells and T cells than

in monocytes as determined by quantitative PCR (qPCR).[15] Accordingly, expression levels of APOBEC3C/D/F/G and H are high in lymphoid organs, such as the thymus and spleen, which are abundant in T lymphocytes (thymus) and B lymphocytes (thymus/spleen).[16] Like PMBCs, the thymus shows virtually no expression of APOBEC3A or APOBEC3B. The spleen, however, is also rich in undifferentiated monocytes.[18] As APOBEC3A is predominantly expressed in monocytes (CD14$^+$ cells)[15,19,20] and APOBEC3B is predominately expressed in B cells, the spleen exhibits relatively high expression levels of all seven APOBEC3s.[15,16] Interesting, the APOBEC3s are also expressed to a wide degree outside of immune tissues. Harris and coworkers have observed that five APOBEC3s (A,B,C,D,H) are expressed at appreciable levels in lung tissue, with APOBEC3A being over-expressed almost 70-fold.[16] APOBEC3A is also over-expressed 5-fold in adipose tissue.[16] Expression levels likely reflect the large quantity of CD14$^+$ macrophages in these tissues types.[21,22] Other notable observations included that APOBEC3C/F and G are over-expressed between 3-to-5-fold in ovarian tissues, and that APOBEC3B can be over-expressed up to 10-fold in breast cancer tissues.[16,17] The over-expression of various APOBEC3s in many of these tissues types has pathological consequences for overall health. An in-depth discussion of these situations can be found in Section 1.5. Also of note, at least two of the studied tissue types exhibit virtually no APOBEC3 expression.[16] Specifically, brain and testicular tissues may not require protection by the APOBEC3s because of their innate immune physical barriers from general circulation, namely the blood-brain-barrier and blood-tubular barrier.[16]

Within cells, differences in sub-cellular localization among the APOBEC3s can also be noted. Using fluorescence microscopy, GFP-tagged APOBEC3s

transfected into HeLa cells demonstrated that APOBEC3D, APOBEC3F, APOBEC3G, and APOBEC3H localize to the cytoplasm; APOBEC3B localizes to the nucleus, and APOBEC3A and APOBEC3C are distributed cell wide.[14] The fact that multiple APOBEC3s can access the host genome and that many cancers show evidence of APOBEC3-mediated mutation patterns prompted Harris and co-workers to investigate the role of the APOBEC3s in cancer mutagenesis. This work will be discussed in Section 1.5.

1.2 Mechanism of APOBEC3-Catalyzed DNA Cytosine-to-Uracil Deamination

To elicit their immunoprotective effect, the APOBEC3 family catalyzes DNA C-to-U deamination on ssDNA substrates.[5,7,23-30] Catalytic activity is dependent on zinc-mediated hydrolysis at the 4-position of the DNA cytosine nucleobase. Characteristic of this enzyme family, the APOBEC3s contain a consensus zinc-binding motif of Histidine(His)-X-Glutamic Acid(Glu)-X_{23-28}-Proline(Pro)-Cysteine(Cys)-X_{2-4}-Cysteine(Cys), where X represents any amino acid and the His and Cys residues coordinate the zinc metal (Figure 1.2).[10,11,31-33] The active site of the APOBEC3s also contains a water molecule, giving the zinc metal a tetrahedral coordination environment (Figure 1.2).
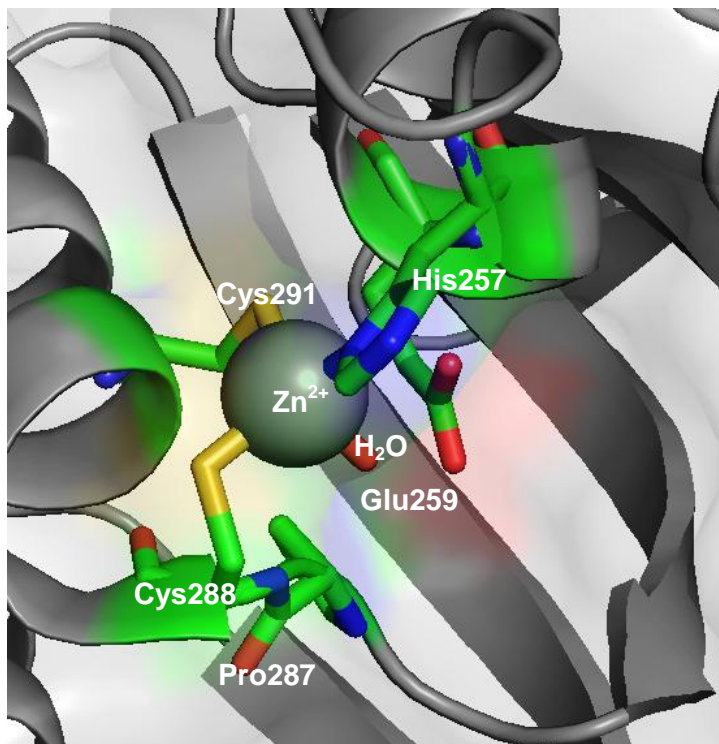
Figure 1.2. The APOBEC3G Active Site (PDB: 3V4K; Rendered in PyMOL 1.3).[1]
Key residues of the zinc-coordinating motif (His257, Pro287, Cys288, Cys291),
the catalytic Glu (Glu259), and the active site water are shown as sticks. The His
and Cys residues coordinate the zinc metal. Analogous active sites characterize
the other APOBEC3s.

The proposed mechanism of deamination is based on previous structural
studies of bacterial[34,35] and yeast[36-38] cytidine deaminases, and relies on the
activation of the active site water molecule through deprotonation by a
conserved, catalytic Glu (Figure 1.3). The resulting zinc-stabilized hydroxide ion
($^-$OH) attacks the 4-position of the DNA cytosine nucleobase yielding an unstable
tetrahedral intermediate. A DNA uracil nucleobase is achieved through formation
of the C4-O double bond and the release of ammonia.
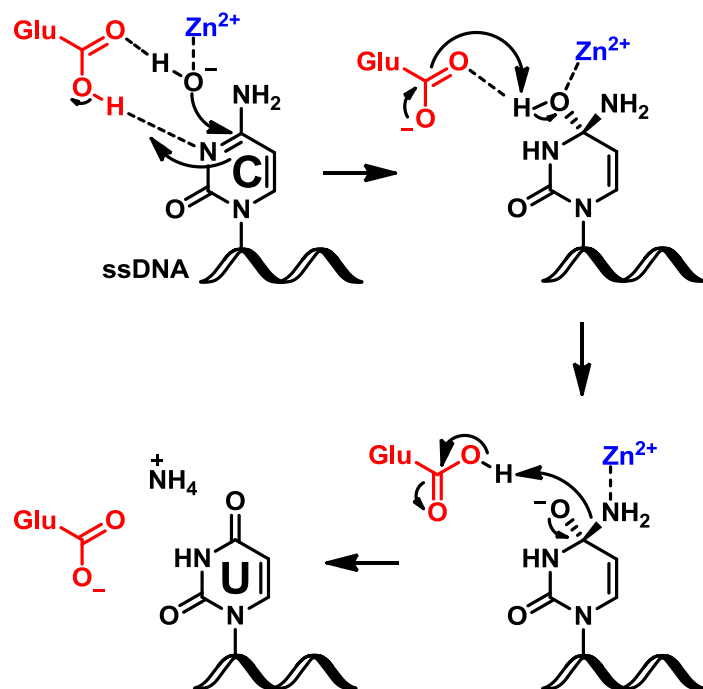
Figure 1.3. Proposed Mechanism of APOBEC3-Catalyzed DNA Cytosine-to-Uracil Deamination.

Unlike the bacterial and yeast cytidine deaminases on which this mechanism is based, the APOBEC3 family cannot turnover single cytidine nucleosides/nucleotides. For deamination, the APOBEC3 enzymes require a minimum of a 5-mer DNA oligomer, where the targeted DNA cytosine is preceded by three nucleotides on its 5′ end and one nucleotide on its 3′ end.[39,40] Importantly, because the APOBEC3s require substrate oligomers, previously designed transition state analogues zebularine (**1.1**) and tetrahydrouridine (**1.2**), which are known inhibitors of cytidine deaminase,[41,42] fail to inhibit the APOBEC3 enzymes (Figure 1.4; unpublished results from the Harki and Harris labs). To date, there is no crystal structure of an APOBEC3 bound to DNA, and thus the mechanism of deamination remains hypothetical. The currently accepted model

predicts that positively charged residues around the active site position the DNA substrate so that the target DNA cytosine flips about the phosphodiester backbone. This conformational change in the DNA substrate would be required for the target DNA cytosine to contact the catalytic Glu residue.[13]

1.1 (Zebularine)   **1.2 (Tetrahydrouridine)**
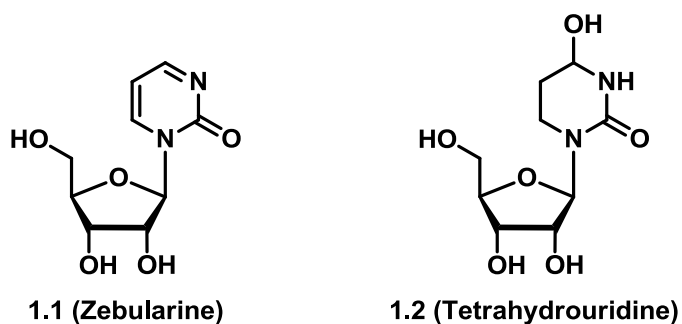
Figure 1.4. Chemical Structures of Zebularine and Tetrahydrouridine.

The APOBEC3s can also be differentiated by individual preferences for targeted dinucleotide deamination sequences. Specifically, APOBEC3G is unique in targeting DNA cytosines that are immediately preceded (5′) by another DNA cytosine. The other APOBEC3s (APOBEC3A/B/C/D/F/H) prefer to deaminate DNA cytosines with a 5′-DNA thymine.[43-46] Structurally, current models predict that a loop positioned adjacent to the enzyme active site, loop 7, garners the APOBEC3's substrate sequence preferences.[13,44,46-49] In addition to a strong preference for the preceding nucleobase, the minus-two and plus-one bases additionally affect APOBEC3 deamination efficiency, though specific trends are less concrete.[40,50-52]

1.3 Structural Characteristics of the APOBEC3s

Acquiring detailed structural information about the APOBEC3 enzymes has been an arduous process, and to date, no X-ray or NMR structure exists that depicts the details of APOBEC3-nucleic acid binding. The APOBEC3 enzymes have been particularly difficult to study because of poor solubility associated with the Z2 N-terminal domain (NTD) of double domain APOBEC3s.[53] Significant efforts have accomplished *apo* X-ray and NMR structures of APOBEC3A, APOBEC3C, APOBEC3F CTD, APOBEC3G CTD, and APOBEC3G NTD.[1,13,26,30,48,54-61] Consistent with over-lapping function, many structural characteristics of the APOBEC3 family are conserved. Each domain can be characterized as having an overall globular structure with a hydrophobic core consisting of five beta strands, three of which are arranged in parallel ($\beta3$, $\beta4$, $\beta5$) (Figure 1.5).[30,62] The hydrophobic core is surrounded by six peripheral alpha helices (Figure 1.5).[30,62] Importantly, the parallel organization of $\beta3$-$\beta4$-$\beta5$ contrasts the antiparallel construction of bacterial and yeast cytidine deaminases, on which the proposed deamination mechanism is based. (For a detailed description of the mechanism of APOBEC3-catalyzed deamination, see Section 1.2). It has been suggested that this parallel $\beta3$-$\beta4$-$\beta5$ arrangement may be the key structural feature that distinguishes polynucleotide deaminases from mono-nucleotide deaminases.[30] The loops that link the secondary structures exhibit a high degree of variability (length/composition) among the APOBEC3s, and are predicted to play an important role in enzyme function, substrate specificity, and substrate binding.[62] Representative of the larger family of cytosine deaminases,

9

the APOBEC3s contain the conserved zinc-binding motif in α2-β3-α3, with the

conserved zinc-binding sequence motif described above.
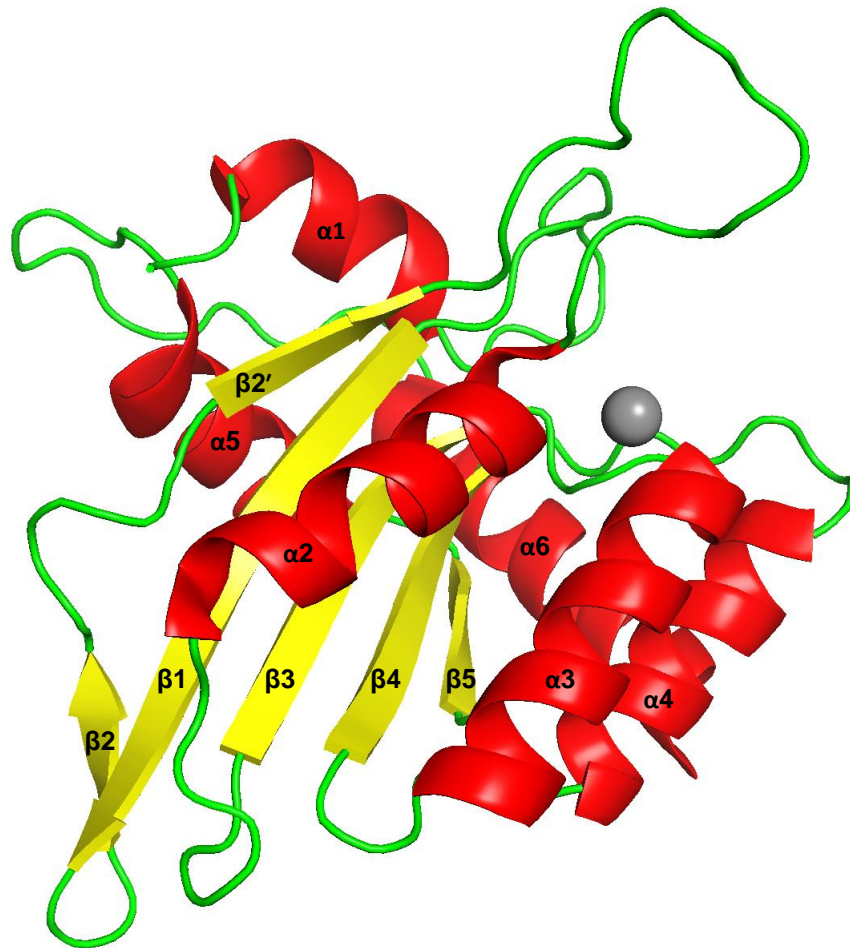
Figure 1.5. Structure of APOBEC3G CTD (PDB: 3V4K; Rendered in PyMOL 1.3). Each APOBEC3 domain has six alpha helices (red) and five beta strands (yellow). The flexible and variable loops are depicted in green. The active site contains a zinc metal, which is depicted in grey as a sphere.

1.4 The Role of APOBEC3D/F/G/H in Human Immunodeficiency Virus-1 (HIV-1) Restriction

Members of the APOBEC3 family, particularly APOBEC3D, APOBEC3F,

APOBEC3G, and APOBEC3H, potently inhibit HIV-1 replication in the absence of

viral counter mechanisms.[25,30,63] This biological activity characterizes the

APOBEC3s as viral restriction factors. By definition, restriction factors (1) have the ability to directly inhibit viral replication, (2) undergo positive selection as a result of competition with the virus, (3) are responsive to interferon, and (4) are neutralized by a counter strategy encoded by the virus.[28,64,65] Although APOBEC3G offers the prototypical example in the field of HIV-1, additional restriction factors, including TRIM5α[66], Tetherin/BST-2[67], and SAMHD1[68], also play important roles in immune defense against viral restriction. To achieve a productive infection, HIV-1 must overcome the network of restriction factors furnished by the host. In the case of APOBEC3D/F/G/H, HIV-1 encodes virion infectivity factor (Vif), a 23 kDa and positively charged accessory protein that enables degradation of the APOBEC3s.

1.4.1 APOBEC3s Potently Inhibit HIV-1 in the Absence of VIF

In the absence of Vif, the APOBEC3s can potently protect host cells from HIV-1 infection. The accepted model of APOBEC3 viral restriction is primarily based on experiments with APOBEC3G, and posits that APOBEC3G, which is expressed in the cytoplasm of an HIV-1 infected cell, incorporates into budding viral particles through an RNA-Gag-mediated mechanism, hijacking transport with the viral particle in a Trojan horse-like fashion until the particle fuses with the target cell (Figure 1.6).[30,69-75] To access the viral genome, the APOBEC3s must breach the viral nucleocapsid; however, the mechanism by which this occurs is not known.[76-78] APOBEC3 inhibition of viral replication occurs through both deamination-independent[79-81] and deamination-dependent mechanisms.[65,82-85] Once the viral particle has fused with an uninfected target cell, the viral RNA undergoes reverse transcription (Figure 1.6). Independent of deamination, the

APOBEC3s have been shown to directly bind viral genomic RNA, sterically blocking the progression of reverse transcriptase (RT).[53,80,81,86-89] Deamination dependant restriction, however, is likely the dominant mechanism, where APOBEC3G-catalyzes extensive C-to-U deamination events on the minus-strand viral cDNA.[50,90-93] The resulting uracilated positive-stand cDNA is either degraded or immortalized as G-to-A hypermutations once complemented and integrated into the target cell genome (Figure 1.6).[88,90-95] Studies which expressed APOBEC3G catalytic mutants at physiological levels demonstrated the ability of Vif-deficient virus to replicate, implicating deamination-dependent restriction as the principle protective mechanism.[83,84,96,97]

Though APOBEC3G has been characterized as the archetypal deaminator, strong evidence implicates APOBEC3D/F and H as playing complementary roles in restricting HIV-1.[14] The mutation patterns of proviral sequences from HIV-1+ patients reflect both 5′-GG-to-AG and 5′-GA-to-AA hypermutation.[98-104] As APOBEC3G preferentially deaminates the second DNA cytosine of a 5′-CC dinucleotide yielding GG-to-AA hypermutation, one or more of the other APOBEC3s must account for the observed 5′-GA-to-AA mutation.[32,50,90,92,93,97,105] In 2011, the Harris laboratory identified that four of the seven APOBEC3 family members play an integral role in HIV-1 restriction.[14] Although the literature reports that all seven APOBEC3s can inhibit HIV-1 replication, APOBEC3D/F/G and H are the only APOBEC3s to package into viral particles and restrict HIV-1 replication in human T cell lines.[14] It is likely, then, that APOBEC3D, APOBEC3F, and APOBEC3H combine to elicit the 5′-GA-to-AA hypermutation observed in HIV-1.

Impressively, if left uncontested by Vif, the APOBEC3s can mutate up to 10% of the HIV-1 cDNA cytosines in a single round of viral replication.[50,90] Such a substantial accumulation of deamination forces the mutation rate of HIV-1 across the error catastrophe threshold, effectively lethally mutagenizing the virus.[106,107] Thus, the APOBEC3 enzymes have the ability to wholly combat infection by HIV-1.
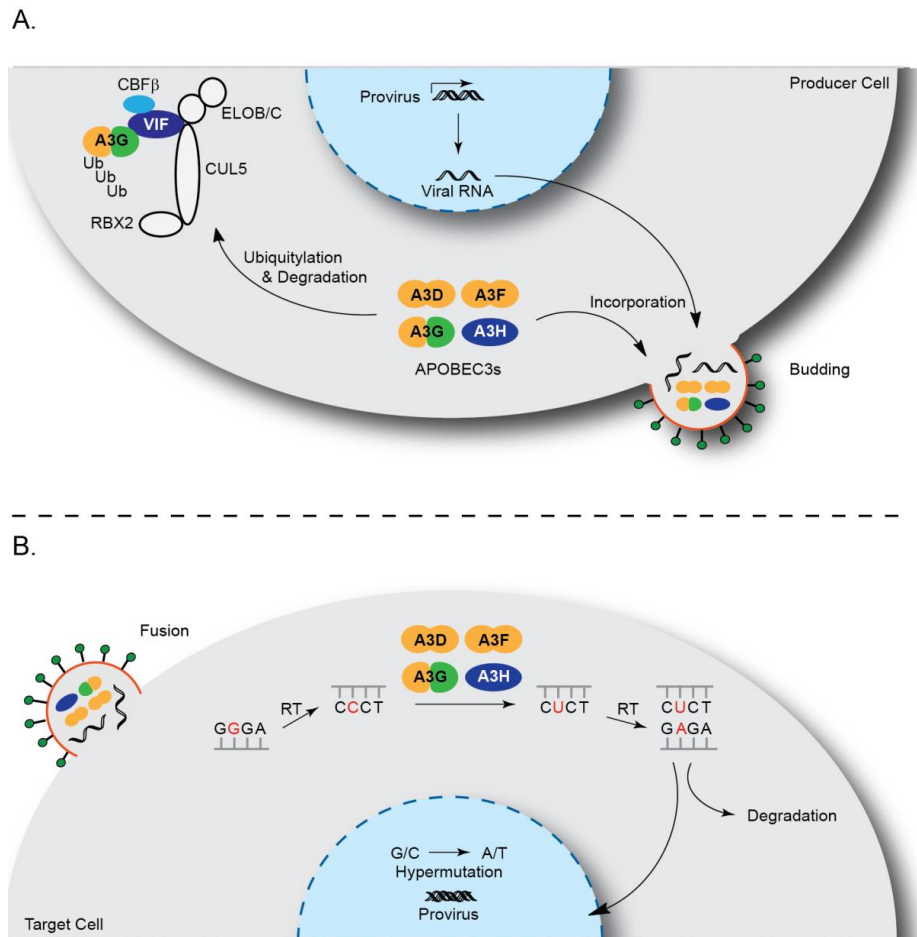
Figure 1.6. Model for APOBEC3-Mediated HIV-1 Restriction. (A) In an infected cell, sublethal amounts of the APOBEC3s incorporate into budding viral particles and hijack transport to virus naïve cells. HIV-1 modulates APOBEC3 expression through Vif. Vif targets the APOBEC3s for degradation at the 26S proteasome through ubiquitylation. (B) The APOBEC3s restrict viral replication through both deamination-dependant lethal mutagenesis and deamination-independent inhibition of RT. Graphic inspired by Hultquist et al. *J. Virol.* **2011**, *85*, 11220.[14]

1.4.2 Vif Modulates APOBEC3 Activity

Following the observation that Vif was required by HIV-1 to infect some T-cell lines (CEM, H9; non-permissive cell lines), but not others (CEM-SS, SupT1; permissive cell lines), multiple laboratories elucidated the fundamental interplay between the APOPEC3 restriction factors and the counteracting protein Vif.[10,23,90-93,108-111] Vif is required by the virus to evade the APOBEC3 immune defense network *in vivo* and *ex vivo* in monocytes, macrophages, primary T CD4+ lymphocytes, and non-permissive T cell lines.[108-110,112-115] Wild-type HIV-1 employs Vif to nucleate the formation of an E3 ubiquitin ligase complex consisting of CUL5/NEDD8, ELOB, ELOC, RBX2, and CBFβ, which flags the APOBEC3s for degradation at the 26S proteasome and enables viral replication in APOBEC3-expressing cells (Figure 1.6A).[116-122] Moreover, secondary mechanisms of APOBEC3 neutralization by Vif may exist including: direct inhibition of APOBEC3 deaminase activity, physical blockage of APOBEC3 packaging in budding viral particles, sequestration of APOBEC3 in the cytoplasm, and/or inhibition of APOBEC3 translation.[123-129] The APOBEC3-Vif interaction is therefore essential for HIV-1 infection and provides a novel, and minimally explored, target in HIV-1 drug discovery (See Chapter 1.4.3).

1.4.3 Therapy by Hypermutation

The ability of the APOBEC3s to lethally mutagenize HIV-1 in the absence of Vif insinuates that this natural defense network can be reinstated if the APOBEC3s are protected from degradation (Figure 1.6A).[130,131] The most obvious approach is the direct inhibition of HIV-1 Vif. Vif is an attractive

therapeutic target because it possesses sole responsibility for APOBEC3

degradation and it has no known mammalian homologues.[132]
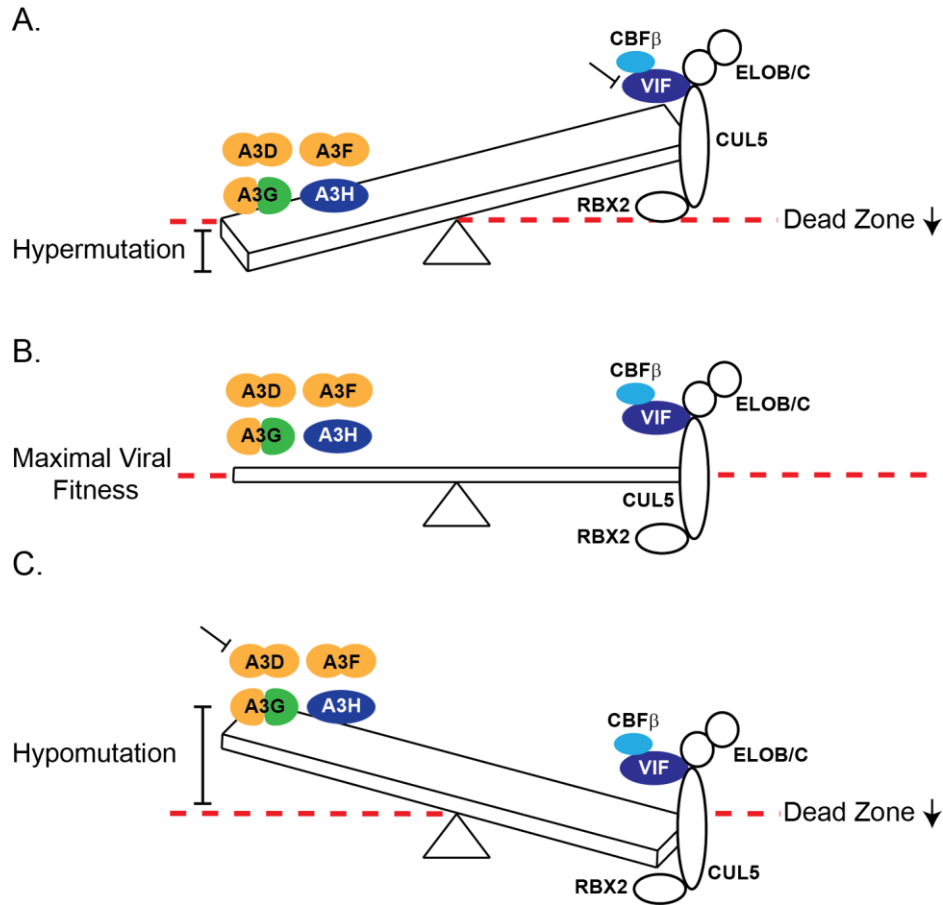
Figure 1.7. Therapeutic strategies to Target the APOBEC3-Vif Interface. (A) Therapy by hypermutation. This therapeutic strategy seeks to inhibit Vif and/or block the Vif-APOBEC3 interface thereby reinstating the restrictive capabilities of the APOBEC3s. Upon Vif inhibition, the relevant APOBEC3s can lethally mutate the viral genome. (B) In a clinical infection, APOBEC3-catalyzed restriction is inhibited by Vif-mediated ubiquitylation and degradation of the APOBEC3s. Despite this inhibition, a sub-lethal level of APOBEC3 deamination is observed. Thus, the activities of Vif and the APOBEC3s are balanced to achieve optimum viral fitness. (C) Therapy by hypomutation. Inhibition of the APOBEC3s may deprive the virus of a needed mutation source. Inhibiting viral fitness may enable immunological or antiretroviral HIV-1 clearance. Graphic inspired by Refsland, E. W. et al. *Curr. Top. Microbiol. Immunol.* **2013**, *371*, 1-27.[30] Concept originally proposed by Harris, R. S. in *Nat. Biotech.* **2008**, *26*, 1089.[130]

The earliest efforts to inhibit Vif employed lentiviral delivery of HIV-1 Vif siRNA to silence Vif gene expression.[134,135] When used synergistically with another anti-HIV-1 siRNA, the Vif siRNA exhibited >80% inhibition of HIV-1 replication in Jurkat cells. These initial studies offered proof-of-concept that Vif siRNA could be used to target HIV-1 mRNA through gene therapy; however, after these initial reports in the mid-2000s, there have been no further studies.[133,134] Multiple laboratories have undertaken programs in recent years to discover small molecule Vif inhibitors, with the first-in-class Vif inhibitor being discovered in 2008. This small molecule, entitled RN-18 (**1.3**), was identified through cell-based high through screening (HTS) of 30,000 small molecules.[132] Specifically, the HTS assay probed for molecules that maintained APOBEC3-GFP fluorescence in the presence of Vif.[132] Of the 25 identified hits, two benzamides, RN-18 (**1.3**, Figure 1.8) and RN-19, exhibited Vif antagonism and anti-HIV-1 activity in non-permissive cell lines.[132] It was also demonstrated that RN-18 (**1.3**) and RN-19 increase cellular levels of APOBEC3G and APOBEC3G encapsidation into budding viral particles.[132] Ultimately, RN-18 was prioritized for further optimization because of its better potency (IC_{50} = 4.5 μM (CEM cells) and 10 μM (H9 cells)) as compared to RN-19.[132] Follow-up work by the Rana Lab explored the structure activity relationship studies of RN18 (**1.3**), identifying a number of tolerated isosteric and water-solubilizing modifications to the parent molecule.[135,136] However, these analogues only offered modest potency improvements (from 10 μM to 1.0 μM in H9 cells) on RN-18 (**1.3**).[135,136]

1.3 (RN-18)

1.4 (IMB-26); X =NH
1.5 (IMB-35); X = O

1.6 (MM-2)

1.7

1.8 (VEC-5)

1.9 (SN-2)
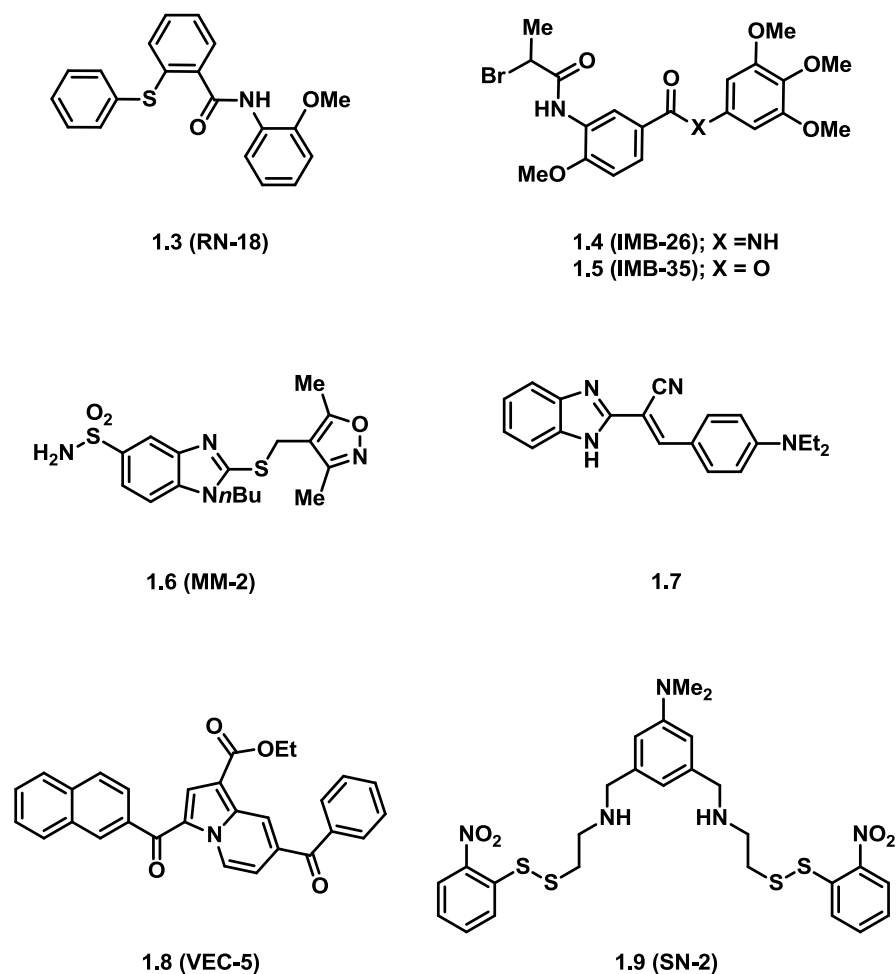
Figure 1.8. Chemical Structures of Small Molecule Leads that Function through "Therapy by Hypermutation."[133,138-140,142,143,147,148]

Work by Cen and colleagues may shed light on the mechanism of RN-18 (**1.3**) inhibition and its structurally related analogues. Using the HTS assay reported by the Rana laboratory, a HTS of 8634 small molecules and natural products identified two compounds, IMB-26 (**1.4**) and IMB-35 (**1.5**), as inhibitors of Vif-mediated APOBEC3G degradation (1.8).[137] Specifically, at 2 µM, IMB-26/35 (**1.4**, **1.5**) reduced HIV-1 infectivity by 97% in H9 cells.[137] Interestingly, IMB-26/35 (**1.4**, **1.5**) are structurally analogous to RN-18 (**1.3**) and like RN-18,

17

IMB-26 (**1.4**) and IMB-35 (**1.4**) stabilize APOBEC3G expression and packaging in the presence of Vif.[137] Surface plasmon resonance experiments with IMB-26/35 (**1.4**, **1.5**) determined that molecules of this class directly interact with APOBEC3G, but have no binding affinity to Vif.[137] The authors propose a possible inhibitory mechanism where IMB-26/35 (**1.4**, **1.5**) bind APOBEC3G and prevent the enzyme from interfacing with Vif.[137] However, additional data are needed to further test this model. Due to the structural similarity between these inhibitors and RN-18 (**1.3**), similar mechanisms of Vif inhibition / APOBEC3G protection are possible. However, it is important to note that despite their structural similarity, treatment with RN-18 (**1.3**) leads to a reduction of Vif expression in the cell, while treatment with IMB-25/35 has no effect on cellular levels of Vif.[137] This observation could imply that RN-18 (**1.3**) is a direct Vif binder.

The above-mentioned successes of using this fluorescence-based HTS assay in identifying inhibitors of Vif-mediated APOBEC3G degradation have prompted its use by additional labs. An HTS of 20000 compounds (Enamine) performed by Matsui and colleagues identified a unique class of Vif-inhibitors.[138] In this effort, secondary screening with an analogous luciferase-based assay was also employed. In brief, expression vectors for Luc-APOBEC3G and Vif were transfected into 293T cells and challenged with small molecules.[138] Compounds that also recovered chemiluminescence intensity validated the findings from the primary fluorescence-based screen. Ultimately, two small molecules, MM-1 and MM-2 (**1.6**), were discovered to inhibit HIV-1 replication in non-permissive cells, increase APOBEC3G expression in a dose dependant manner, and increase APOBEC3G packaging into Vif-proficient viral particles (Figure 1.8).[138] To

elucidate the mechanism of inhibition, immunoprecipitation studies were performed to determine if the small molecules inhibited APOBEC3G-Vif binding. Co-precipitation was unaffected in the presence of inhibitor suggesting that the APOBEC3G-Vif binding interface was untouched. Moreover, immunoblotting experiments with an anti-ubiquitin antibody demonstrated that MM-1 and MM-2 (**1.6**) did not inhibit ubiquitylation of APOBEC3G. In the last set of experiments, the authors also noted that MM-1 and MM-2 (**1.6**) do not inhibit the 26S proteasome.[138] As a result, the target of the MM series remains elusive and additional studies are required to improve upon these early leads.

Most recently, the APOBEC3G-GFP reporter assay was used to screen >20000 small molecules from Enamine.[139] Of the 372 initial hits that restored A3G-GFP fluorescence, 133 were found to additionally inhibit HIV-1 replication in non-permissive H9 cells.[139] With potent activity (50% inhibition at 5 μM), a drug-like scaffold, and ease of SAR investigation, Pan and co-workers prioritized a benzimidazole hit for further investigation.[139] Extensive SAR studies identified compound **1.7** as the most potent Vif inhibitor discovered to date, with an IC_{50} value of 3.5 nM (Figure 1.8).[139] Like the Vif inhibitors described above, **1.7** protects cellular levels of APOBEC3G, and dampens Vif-regulated ubiquitylation and degradation of APOBEC3G, and overall HIV-1 infectivity.[139] There is noteworthy structural similarity between the discovered Vif inhibitors **1.6** and **1.7**. Accordingly, one could envision similar mechanisms of inhibition for these two scaffolds. As described above, **1.6** did not inhibit the co-precipitation of Vif and APOBEC3G.[138] In surface plasmon resonance experiments with **1.7**, however, a modest reduction (17% of max resonance) in Vif-APOBEC3G binding was

19

observed.[139] Although this observation is conservative, the results suggest that **1.7** and its analogues, and potentially **1.6**, could inhibit at the Vif-APOBEC3G interface.[139] Moreover, co-immunoprecipitation experiments demonstrated that **1.7** and its analogues have no effect on Vif binding to ELOB, ELOC and CUL5.

Improving upon these initial inhibitory scaffolds has been limited by the lack of a full-length crystal structure of Vif and thus, the opportunity for structure-based drug design. In 2013, Zhou and co-workers explored the binding modes of the RN-18 (**1.3**) series by computer modelling using a previously reported Vif-homology model.[140,141] Through blind and focused docking, binding free energy calculations, and molecular dynamics simulations, a common binding conformation at the C-terminal interface of Vif-ELOC-CUL5 was purported to be the binding site of RN-18 (**1.3**) and analogues.[140] These computational studies additionally support the hypothesis that RN-18 (**1.3**) and IMB-26/35 (**1.4**, **1.5**) have unique mechanisms of action despite their structural similarities. The authors subsequently offered a number of suggested structural modifications to RN-18 (**1.3**) to improve upon compound binding affinity for Vif.[140] Taken with this study and the recent achievement of the first Vif crystal structure, structure-based rational design and/or structure-guided optimization of existing Vif inhibitors can finally be pursued.

Although a feasible strategy for achieving APOBEC3-catalyzed lethal mutagenesis has been demonstrated, concerns about the rapid development of drug resistance must be taken into consideration. As HIV-1 Vif undergoes rapid evolution as a result of positive selection by the APOBEC3s and other sources of HIV-1 genetic variation, the attainment of mutations that confer small molecule resistance is a likely probability.

A secondary strategy to enable APOBEC3 mutagenesis focuses on interrupting essential Vif interaction surfaces. To achieve APOBEC3 degradation, Vif requires the recruitment of numerous cellular proteins including CUL5/NEDD8, ELOB, ELOC, RBX2, and CBFβ to the E3 ubiquitin ligase complex. Being host proteins, these targets are inherently more stable – undergoing a drastically reduced rate of evolution. There are four protein-protein interactions (PPI) that are required to inhibit the APOBEC3s: the APOBEC3-Vif interaction, the CBFβ-Vif interaction,[121] the ELOC-Vif interaction,[117,119] and the CUL5-Vif interaction.[117,119] Interruption of any of these interfaces would prevent complex assembly and thus, APOBEC3 degradation. As proof of concept, genetic knockdown of CBFβ diminishes Vif expression and function.[121]

The recently achieved Vif-E3 ligase complex x-ray structure has offered an enormous amount of structural information on the interfaces in this complex.[122] As such, drug discovery efforts targeting these interfaces should benefit immensely. Structural information on the APOBEC3-Vif interface remains a considerable gap in the field, and inhibition of this interface may be difficult due to the high degree of Vif disorganization and the discontinuous surface by which it engages the APOBEC3s. While previous work has identified potently conserved structural motifs, an NMR or X-ray structure has not been achieved.[56,105] Moreover, recent evidence suggests that APOBEC3G may engage Vif through an interface unique to that of APOBEC3F, and potentially the other APOBEC3s. As a result, a protein-protein interface (PPI) inhibitor that disrupts one APOBEC3-Vif interface may not necessary inhibit the others.

21

Using a previously reported Vif-ELOB/ELOC homology model, Zuo and co-workers virtually screened 1.2 million small molecules from the Available Chemicals Directory (ACD) to identify a benzoylindolizine (**1.8**), designated VEC-5, as a first-in-class Vif-ELOC protein-protein interface (PPI) inhibitor with micromolar potency (Figure 1.8).[141,142] Similar to the previous studies, VEC-5 (**1.8**) inhibits HIV-1 replication only in non-permissive (A3G-positive) cell lines, stabilizes cellular levels of APOBEC3G in the presence of Vif, augments A3G packaging in budding viral particles, and reduces HIV-1 infectivity with an IC_{50} value of 24 μM.[142] Coimmunoprecipitation assays and label-free biolayer interferometry (BLI) technology demonstrated that VEC-5 (**1.8**) treatment abolished the binding interaction of Vif to ELOC/CUL5, while having no affect on the Vif-APOBEC3G interface[142] As seen with the follow-up studies on RN-18 (**1.3**), however, subsequent efforts to improve upon the potency of VEC-5 (**1.8**) yielded only modest improvements (from $IC_{50} = 24$ μM to 19 μM).[143]

While the development of drug resistance by host enzymes is less likely, the approach of targeting host enzymes also has liabilities. Small molecules that bind and inhibit ELOC, CUL5, and/or CBFβ may interfere with essential cellular processes, yielding off-target effects or toxicities. Inhibitory molecules that function via these mechanisms must be thoroughly vetted to characterize inhibitor safety.

A final drug design strategy in this arm seeks to identify compounds that agonize APOBEC3 activity or increase APOBEC3 expression to overcome Vif-mediated degradation.[137,144,145] Fujita and co-workers reported the first small molecule to agonize APOBEC3G. Inspired by the discovery that N,N,N′,N′-

22

tetrakis(2-pyridylmethyl)ethane-1,2-diamine (TPEN) leaches zinc from the zinc-coordinating motif of Vif, which in turn prevents APOBEC3G-Vif binding, Ejima and co-workers examined the effect of a previously reported zinc chelator named SN-1 on the Vif-APOBEC3 interface.[145] SN-1 and related analogue SN-2 (**1.9**, 4-(dimethylamine)-2,6-bis[(N-(2-[(2-nitrophenyl)dithio]ethyl)amino)methyl]pyridine) had been previously investigated as inhibitors of the HIV-EP1 zinc finger (Figure 1.8).[146,147] Unexpected to the authors, SN-2 (**1.9**) was found to increase A3G expression and inhibit HIV-1 replication at a concentration of 5 μM.[145] Unique to SN-2 (**1.9**), as compared to the previously discussed small molecules, was that while SN-2 (**1.9**) promoted the stabilization of APOBEC3G expression and packaging, it had no affect on Vif expression or function.[145] Conversely, MG-132, a proteasome inhibitor, stabilizes both APOBEC3G and Vif, as both proteins are ubiquitylated and degraded through the E3 ligase complex and the 26S proteasome.[145] This finding suggests multiple possibilities: (1) there is an additional cellular protein that can mediate APOBEC3G degradation and that SN-2 inhibits this process or (2) that SN-2 can protect APOBEC3G from ubiquitylation and thus, degradation at the proteasome.[145] With the wealth of genetic and biochemical literature on the Vif-APOBEC3G interaction, it would seem that the second hypothesis is more probable. If SN-2 can bind APOBEC3G and block its ubiquitylation, APOBEC3G would be saved from proteasomal degradation while the ubiquitylation and degradation of Vif would remain unscathed.

Although growing excitement in the field exists for this novel strategy in HIV-1 therapeutic design and the number of publications increases every year,

small molecules that restore the pro-mutagenic capacity of the APOBEC3s remain in their infancy. Most notably, there is an absence of data regarding the biological targets and mechanisms of action of these lead Vif inhibitors. Moreover, none of the above mentioned studies discussed the selection of Vif resistance mutants by the small molecule inhibitors. Resistance remains the gold standard for validating that a small molecule specifically targets a viral protein. Failure to identify resistance mutants implies that the small molecule functions via a non-specific mechanism of action in these cellular studies. Significant work is required in the future to elucidate the specific protein-ligand interactions so that improvements upon the current leads can be achieved.

1.4.4 Therapy by Hypomutation

Despite the ability of Vif to counteract APOBEC3-catalyzed mutation through proteasomal degradation, strong evidence exists to support the hypothesis that APOBEC3G is being exploited by HIV-1 through Vif modulation.[14,116-118,124,125] Namely, isolated proviral sequences from HIV-1+ individuals demonstrate the two characteristic patterns of APOBEC3-catalyzed deamination: 5′-GG-AG and 5′-GA-to-AA.[98-104] Moreover, deep sequencing has shown that antiretroviral resistance mutations occur more frequently in the presence of APOBEC3G.[148,149] This suggests that the APOBEC3s remain functional to a sub-lethal level in a clinical infection. Thus, a paradigm exists where HIV-1, by taking advantage of the pro-mutagenic capabilities of the APOBEC3s, may regulate APOBEC3 activity to accomplish an advantageous level of mutation enabling optimal viral fitness.[106,150-152] As a result, genetic variation attributable to the APOBEC3s likely

24

contributes to the characteristically high mutation rate of HIV-1, its ability to evade immune clearance mechanisms, and its rapid evolution of antiretroviral resistance.[106,130] In fact, a number of common resistance mutations to antiretroviral therapies may result from APOBEC3-catalyzed deamination.[106,148,149,151,153-155] The reality that APOBEC3-catalyzed mutation occurs frequently in clinical infection begs the question of whether the APOBEC3s function as an *essential* source of mutation for HIV-1.

One hypothesis is that APOBEC3-catalyzed deamination is an indispensable source of mutation for HIV-1, and is required by the virus to achieve its unprecedented level of fitness (Figure 1.7C). Therefore, current therapies and vaccination strategies may benefit from removing the APOBEC3s as enablers of HIV-1 evolution. Our strategy to reduce HIV-1 mutation by inhibiting the APOBEC3s can be classified as *"therapy by hypomutation"*.[150] Therapy by hypomutation may be the key to offsetting the unprecedented balance between HIV-1 mutagenesis and pathogenesis. For example, a small molecule APOBEC3 inhibitor that limits viral evolution, in combination with host immune clearance mechanisms and/or the effective toolbox of antiretroviral drugs, may offer the final piece to obtaining a curative HIV-1 strategy.
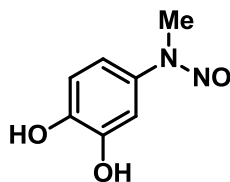
1.10 (MN30)

Figure 1.9. Chemical Structure of APOBEC3G Inhibitor MN30 (**1.10**).

25

A high-throughput screen of 1280 pharmacologically active compounds (LOPAC, Sigma) completed by the Harris lab against recombinant APOBEC3A and APOBEC3G accomplished the first-in-class small molecule inhibitors of APOBEC3G.[1] Of the 34 initial HTS hits, the majority encompassed a catechol-based core. Representative of this inhibitor class, MN30 (**1.10**) was prioritized for further investigation (Figure 1.9).[1] Through systematic site directed mutagenesis, x-ray crystallography, and mass spectrometry experiments, MN30 (**1.10**) was determined to covalently engage Cys321 upon auto-oxidation from the catechol to the ortho-quinone.[1] Interestingly, electrophoretic mobility shift assays (EMSAs) demonstrated that although MN30 (**1.10**) binds near the APOBEC3G active site; enzyme - substrate binding was not inhibited.[1] This observation is likely explained by the ability of APOBEC3G NTD to bind substrate, while the CTD is covalently bound to and inhibited by MN30 (**1.10**). As a result, MN30 (**1.10**)-mediated inhibition of APOBEC3G is proposed to be competitive with substrate binding within the active site, as an energy-minimized model of MN30 bound to C321 suggested that the added steric bulk of MN30 forces the adjacent Y315 to flip and negatively contact W285, an active site residue.[13,1] Both Y315 and W285 are conserved and essential for enzyme function.[13] Thus, despite the ability of APOBEC3G to bind its DNA substrate while inhibited by MN30 (**1.10**), the resulting conformational change may prevent the targeted DNA cytosine from entering the APOBEC3G active site or positioning appropriately for catalytic turnover.[1]
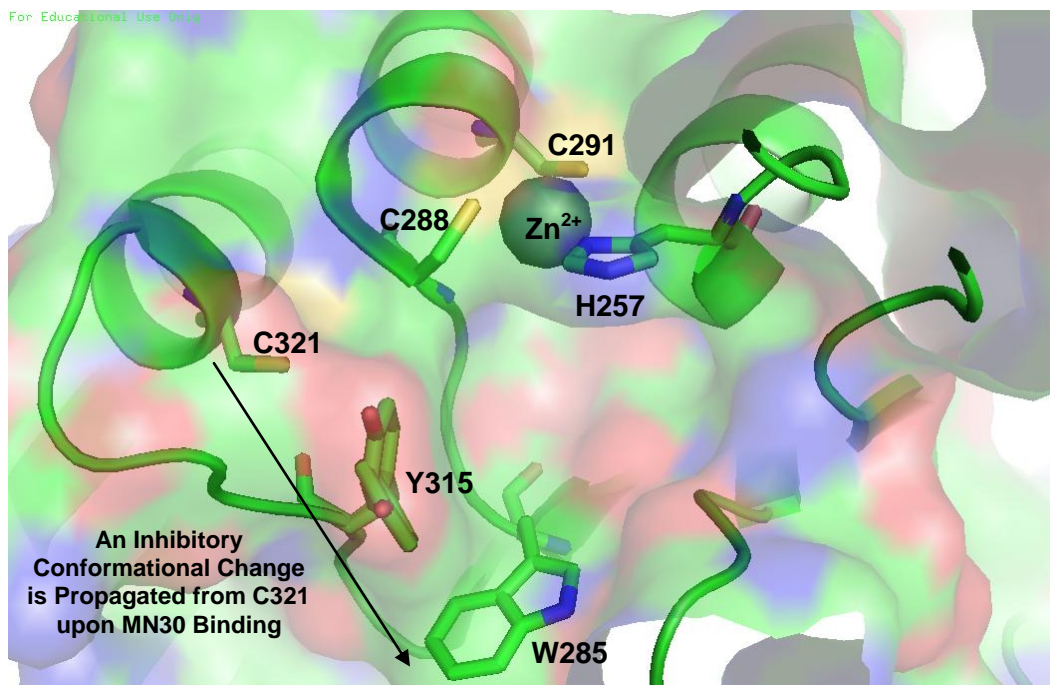
Figure 1.10. Crystal Structure of APOBEC3G CTD Emphasizing the Proximity of C321 to the Active Site (PDB: 3V4K; Rendered in PyMOL 1.3).[1] Additional residues that are key to MN30's mechanism of inhibition, such as Y315 and W285, are represented as sticks. Molecular modelling suggests that MN30 binding to C321 causes Y315 to flip, forcing negative interactions with W285.[1]

Importantly, this work identified that a cysteine residue located within 8 Å of the zinc-containing active site is a unique structural feature of APOBEC3G.[1] As a result, electrophilic small molecules specifically inhibit APOBEC3G versus other APOBEC3 family members, with IC_{50}'s ~ 1-20 μM for APOBEC3G versus >200 μM for other APOBEC3s.[1,156] Sensitivity to MN30 (**1.10**) could be engineered into APOBEC3A by grafting the entire C321-containing loop (loop 7) from APOBEC3G into APOBEC3A.[1] Following this seminal work to deliver the first APOBEC3G inhibitors, multiple follow-up studies were pursued collaboratively by the Harki and Harris laboratories. The details of those studies will be presented in the course of this thesis.

27

1.5 The Role of APOBEC3B in Cancer

As described in the preceding sections, targeted mutagenesis, as catalyzed by the APOBEC3s, represents a powerful defense mechanism of the human innate immune system. However, the existence of a pro-mutagenic host enzyme raises concerns about what pathological consequences exist when the APOBEC3s are misregulated. As cancer progression requires the continued acquisition of somatic mutations, APOBEC3s that have access to host genetic material could rapidly mutate the human genome. A number of observations suggested that one of more of the APOBEC3s could contribute to mutagenesis in cancer. First, multiple reports over the last decade demonstrated that the mutation patterns in various cancers are dominated by cytosine-to-thymine (C-to-T) transition mutations.[157-165] DNA cytosine deamination, as catalyzed by the APOBEC3s, destroys Watson-Crick base pairing by producing uracils that template the insertion of adenines, which subsequently template thymines during DNA replication. Additionally, related members of the APOBEC gene family, APOBEC1 and AID, offer examples of enzyme dependant mutator states that catalyze endogenous genomic mutation. AID evolved to diversify antibody gene variable regions to promote antibody isotype switching (class switch recombination) for greater recognition of pathogens.[7] However, erroneous processing of AID-dependant lesions can cause chromosomal translocations, such as the Ig-Myc translocation that initiates B cell lymphomas.[166-168] APOBEC1 is specifically located in hepatocytes and is implicated in cancers of the liver.[169] Finally, APOBEC3B is nuclear localized, having the opportunity to access and mutate the human genome.[14,170]

28

Employing breast cancer as a model, Burns et al. demonstrated that *APOBEC3B* messenger RNA (mRNA) is up-regulated in 65% of patient-derived primary breast cancer specimens and 90% of breast cancer cell lines.[17] In 12 of the 38 lines tested, APOBEC3B was over-expressed 10-fold compared to healthy mammary epithelial lines.[17] Tumors that over-express APOBEC3B also have twice as many overall mutations compared to low APOBEC3B expressing breast tumors and are more likely to have mutations in *TP53*, the well-known tumor suppressor gene.[17] Knockdown experiments performed by the Harris laboratory have directly correlated APOBEC3B activity with increased genomic uracil content, overall mutation load, frequency of C-to-T transitions, cell cycle deviations, cell death, and DNA fragmentation, each individual event contributing to breast cancer development, propagation and relapse.[17] The mutagenic capacity of APOBEC3B suggests a chronic source of DNA damage is innate, and further, offers a mechanism by which *TP53* is endogenously inactivated.

A model of chronic endogenous mutation may explain the heterogeneity, rapid evolution and therapeutic resistance characteristic of many tumors. In that vein, APOBEC3B expression was found to be similarly up-regulated in ovarian,[158] lung, bladder, head/neck,[163] and cervical cancers.[157,171] It is now widely accepted that APOBEC3B over-expression prompts a 'hypermutable cancer state', similar to misregulated AID and APOBEC1, allowing for rapid tumor growth, aggressive metastasis, and therapeutic and/or immunological resistance (Figure 1.10).

29
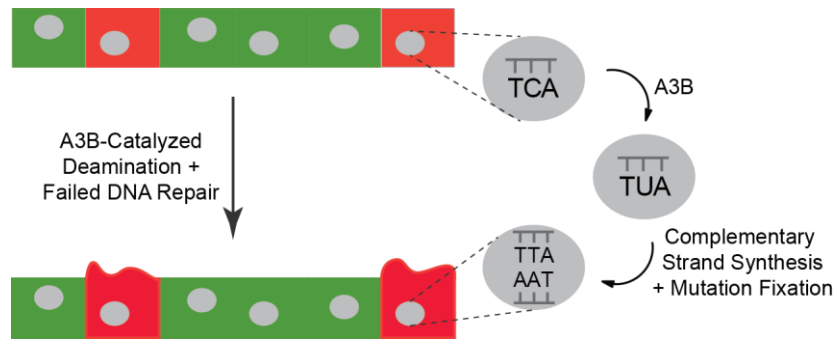
Figure 1.11. Model for APOBEC3B-Catalyzed Transition Mutations in Cancer. Acquired somatic mutation over the course of an individual's lifetime can transform a healthy cell into a tumor cell. In the figure, darker shades of blue represent a higher mutational load. APOBEC3B represents one source of endogenous somatic mutation. Mutation catalyzed by APOBEC3B can give rise to tumor cell growth, metastasis, and the development of therapeutic resistance. APOBEC3B preferentially deaminates DNA cytosines in 5′-TCA contexts. The resulting uracil templates the insertion of adenine during complementary strand synthesis and uracil base excision repair will convert the U-A base pair to T-A (a C-to-T transition mutation).

A clear relationship between APOBEC3B over-expression and clinical breast cancer progression has recently been elucidated through survival studies of a cohort of estrogen receptor-positive breast cancer patients (ER+).[172,173] In this study, APOBEC3B mRNA levels in previously cryopreserved breast cancer samples were determined by qPCR. The large cohort was divided into two groups, APOBEC3B-high and APOBEC3B-low expressers, and overall and disease-free survival was correlated for each of the patients.[81] Ultimately, patients in the high APOBEC3B-expressing cohort were found to have shorter durations of both disease-free and overall survival.[172] For example, of 633 lymph-node-negative, ER+ breast cancer patients, 201/317 APOBEC3B-low expressing patients were alive after six years, compared to 171/316 APOBEC3B-high expressing patients.[172] As a result, the level of APOBEC3B expression may serve as a prognostic marker for ER+ breast cancers in the future.

As a result of these paradigm shifting observations, APOBEC3B serves as a candidate drug target to control pro-cancerous mutations that likely result in cancer recurrence, metastasis, and the development of chemotherapeutic resistance. Moreover, APOBEC3B is a non-essential enzyme in humans, confirmed by the existence of a prevalent polymorphic deletion allele in the general population.[102] Efforts to discover the first APOBEC3B small molecule inhibitor for further development into a useful cellular probe of APOBEC3B-catalyzed mutation will be discussed in the course of this thesis.

1.6 Preface to this Thesis

The following chapters disclose my efforts to discover novel APOBEC3 inhibitors for development as HIV-1 and cancer therapeutic leads. Chapter 2 discusses optimization and implementation of the first APOBEC3B-focused HTS of approximately 168,000 small molecules. This screen identified inhibitory lead MN23 (**2.16**), which is currently under investigation for APOBEC3B and APOBEC3G inhibition. Chapter 3 builds on the work described in Section 1.4.4. Specifically, a novel APOBEC3G inhibitor, based on a 1,2,4-triazole-3-thiol substructure, was discovered to inhibit APOBEC3G through a mechanism similar to MN30 (**1.10**). The synthesis, SAR, and mechanism of action studies regarding this scaffold are reported therein. Chapter 4 communicates the discovery of an APOBEC3B/G inhibitor from a decomposed HTS hit. An extensive study on the mechanism and scope of this decomposition was investigated to properly annotate HTS libraries in the future. Chapter 5 continues the work reported in Chapter 3 by designing and synthesizing small molecule covalent probes of APOBEC3G to investigate protein – ligand structure and possible mechanisms of

inhibition. Appendix A highlights work conducted on the characterization of guanosine monophosphate synthetase (GMPS) enantioselectivity, an essential enzyme in nucleotide biosynthesis. Finally, Appendix B discusses the *in vitro* thiol reactivity of EPI-001, a small molecule of interest for future development into a next-generation prostate cancer therapy.

Chapter 2

HIGH-THROUGHPUT SCREENING FOR APOBEC3B INHIBITOR DISCOVERY

2.1 Introduction

APOBEC3B (apolipoprotein B mRNA editing enzyme, catalytic polypeptide-like 3B) is a single stranded (ss)DNA cytosine-to-uracil (C-to-U) deaminase that functions in innate immunity to protect host cells from viral infection.[5,7,23-30] APOBEC3B belongs to a larger family of polynucleotide DNA cytosine deaminases, which includes AID, APOBEC1, APOBEC2, APOBEC3A/B/C/D/F/G/H, and APOBEC4.[30] The protective mechanism catalyzed by this enzyme family is C-to-U deamination of DNA parasites, such as retroviruses and retrotransposons, which translates to an elevated level of DNA uracil content in the foreign genome. Importantly, DNA uracils (U) are pre-mutagenic lesions because DNA polymerases incorrectly read these nucleobases as thymines (T), templating the insertion of adenines (A) during replication. As a result, APOBEC3B can initiate C-to-T transition mutations when the DNA uracils resulting from APOBEC3B-dependant deamination go unrepaired. Moreover, uracil DNA glycosylase (UDG), a DNA proofreading enzyme, can excise DNA uracils to generate abasic sites, which are often incorrectly repaired. For example, the REV1 polymerase inserts a C opposite an abasic site, which in the case of APOBEC3B-dependant deamination, results in a C-to-G transversion mutation.[174,175] Taken together, the biological function of APOBEC3B underlies a number of simple and complex mutagenic outcomes.[17,171,176,177]

The existence and widespread expression of the APOBEC3 family prompted the APOBEC mutator hypothesis, whereby one or more of the APOBEC3s was proposed to provide an endogenous source of somatic mutation

in cancer.[23,178,179] Accumulated somatic mutation not only transforms healthy cells into tumor cells, but continuously provides the evolutionary fuel to enable tumor cell growth, cancer metastasis, and chemotherapeutic resistance.[177] Following this hypothesis, array hybridization experiments suggested that at least one APOBEC3 was over-expressed in several cancers,[23] and genetic experiments in yeast indicated that the APOBEC3 enzymes could mutate eukaryotic genomic DNA.[180] Further, genome sequencing of many cancers displayed somatic mutation patterns dominated by C-to-T transitions, the characteristic pattern of APOBEC3-catalyzed mutation.[157-165,181]

Evidence for enzyme-dependent mutator states can be demonstrated by the APOBEC3-related proteins AID and APOBEC1. AID evolved to diversify antibody gene variable regions to promote antibody isotype switching (class switch recombination) for greater recognition of pathogens.[7] However, erroneous processing of AID-dependent lesions can cause chromosomal translocations, such as the Ig-Myc translocation that initiates B cell lymphomas.[2-8,166,167] Moreover, mis-regulation of APOBEC1-catalyzed deamination has recently been implicated in esophageal adenocarcinomas.[182] Recent evidence suggests that APOBEC3B similarly prompts a 'hypermutable' cancer state, which allows for rapid tumor growth, aggressive metastasis, and therapeutic and/or immunological resistance.[17]

Quantitative PCR (qPRC) experiments were employed by Harris and colleagues to determine which APOBEC3s were expressed at higher levels in breast cancer cells in comparison to normal breast tissues.[17] APOBEC3B was the sole APOBEC family member found to be up-regulated in cancerous tissues, and was virtually non-detectable in matched normal tissues.[17] The other

APOBEC3s (APOBEC3A/D/F/G and H) were expressed at similar levels in both cancerous and normal cells.[17] Specifically, APOBEC3B was over-expressed in 65% of primary breast cancers and 90% of breast cancer cell lines.[17] The distinct pattern of APOBEC3B up-regulation in breast tumors and cells lines suggested that this enzyme may have a role in breast cancer mutagenesis.[17]

To provide evidence for this hypothesis, the Harris laboratory demonstrated that over-expression of APOBEC3B in breast tumors correlates to an increase in C-to-T transition mutations as compared to low APOBEC3B-expressing tumors.[17] Moreover, genetic knockdown of APOBEC3B mRNA produces cells with lower levels of genomic uracil content and lower mutation frequencies in *TP53*, the well-known tumor suppressor gene.[17] Ultimately, tumors that over-express APOBEC3B have twice as many overall mutations when compared to their low APOBEC3B-expressing counterparts. As a result, APOBEC3B has become widely accepted as a cancer facilitator, driving the genetic diversity of tumors through deamination-mediated mutational events.[177,183] This foundational work, which implicated APOBECB as a source of genetic diversity in breast cancer, has since been extended to mutagenesis paradigms in head/neck, cervical, bladder, lung, and ovarian cancers.[171,176,184-188]

APOBEC3B over-expression also correlates to negative outcomes in a clinical setting. Survival in a large cohort of estrogen receptor-postive breast cancer patients was recently analyzed for a relationship to APOBEC3B expression levels.[172] Strikingly, the duration of survival in APOBEC3B-high expressing patients was significantly shorter than in APOBEC3B-low expressers.[172] Consequently, APOBEC3B may offer a prime therapeutic target for preventing the evolution of tumors, and thus, detrimental mutation-dependent

outcomes such as cancer recurrence, metastasis and drug resistance. Importantly, APOBEC3B is a non-essential enzyme, as a natural 29.5 kb deletion allele is prevalent in some populations.[189] Specifically, the frequency of the deletion allele is 93% in Oceanic populations, 37% in Asian populations, and 58% in North American Indian populations.[189] Moreover, APOBEC3B is rarely expressed in most normal tissues, highlighting its benefits as a novel therapeutic target for cancer.

2.2 Previous APOBEC3 Screening Efforts

The Harki and Harris Labs previously collaborated with the University of Minnesota Institute for Therapeutics Discovery & Development (ITDD) and the Sanford-Burnham Medical Research Institute to accomplish the HTS of ~350,000 small molecules for APOBEC3A (88% amino acid identity to APOBEC3B CTD) and APOBEC3G (65% amino acid identity to APOBEC3A CTD) inhibition.[1,156,190] A fluorescence-based DNA deamination assay was employed (Figure 2.1), and relied on the 2 h incubation of full-length human APOBEC3A or APOBEC3G with a ssDNA oligonucleotide substrate that contains the target DNA cytosine, a 5′-6-FAM fluorophore, and a 3′-TAMRA quenching molecule.[1] Subsequent addition of *E. coli* uracil DNA glycosylase (UDG) enabled excision of the deamination-dependant DNA uracil lesion, and treatment with NaOH promoted cleavage of the phosphodiester backbone at the abasic site.[1] Upon cleavage, the 6-FAM fluorophore was released from the quenching TAMRA, and deaminase activity was quantified directly with a fluorescence plate reader.[1] The average Z-score for these screens was ~0.85, highlighting the robust and reproducible nature of the

assay. Using this fluorescence-based assay, 32 APOBEC3A-specific, 154 APOBEC3G-specific, and 161 APOBEC3A/APOBEC3G-dual inhibitory compounds were identified through primary HTS and confirmatory biochemical evaluation with commercially purchased materials. On-going studies of small molecules leads identified through these screening efforts form the basis of Chapters 3-5 in this thesis.

2.3 Design of the APOBEC3B-Focused HTS Assay

With the characterization of APOBEC3B as an enabler of genetic evolution in multiple cancers, we sought to identify the first small molecule inhibitors of APOBEC3B. An APOBEC3B inhibitor would complement the current arsenal of chemotherapeutics by decreasing the overall DNA mutation rate in cancer cells, reducing the ability of tumors to adapt to chemotherapeutic and/or immunological pressures. We employed the previously reported fluorescence-based DNA deamination assay to discover APOBEC3B inhibitory leads.[1,156,191] In short, recombinant APOBEC3B CTD was incubated with a ssDNA oligomer containing a 5′-6-FAM fluorophore and a 3′-TAMRA quenching molecule (Figure 2.1).[1] In this absence of a small molecule inhibitor, APOBEC3B CTD deaminates the target DNA cytosine to a DNA uracil, which is excised by *E. coli* UDG.[1] Addition of NaOH prompts cleavage of the phosphodiester backbone at the abasic site, which releases the 6-FAM fluorophore from the TAMRA quench.[1] Deaminase activity is quantified by measuring fluorescence.[1] Small molecule inhibition of APOBEC3B CTD deamination preserves the DNA oligomer, maintaining the substrate with quenched fluorescence.[1] Based on the recommended guidelines for reporting HTS assays proposed by Inglese, Shamu

& Guy, a detailed description of this fluorescence-based DNA C-to-U HTS assay is described in Table 2.1.[192]
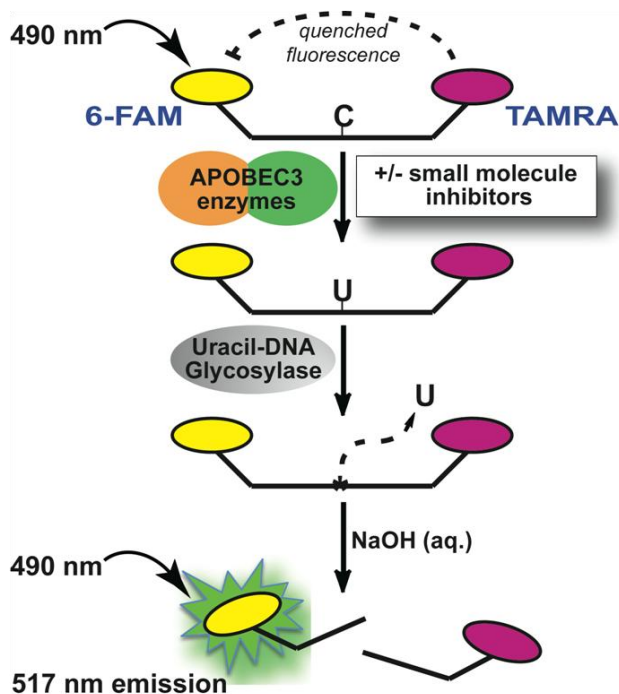
Figure 2.1. Fluorescence-Based C-to-U Deamination Assay for High-Throughput Screening. Uninhibited APOBEC3-catalyzed deamination results in a high fluorescence readout, while potent APOBEC3 inhibition reads as background fluorescence signal. This figure is inspired by an earlier version published in Li, M. et al. *ACS Chem. Biol.*, **2012**, *7*, 506.517.[1]

This assay was employed by Ms. Margaret Olson and Dr. Ming Li to screen 168,192 small molecules against APOBEC3B CTD at the ICCB-Longwood Screening Center at Harvard Medical School (Boston, MA). Specificity for APOBEC3B CTD inhibition was gauged by counter-screening against related APOBEC3 family member APOBEC3G. APOBEC3G has been previously shown to contain a reactive and readily modified cysteine residue nearby the active site

(for a detailed description, see Chapter 1.4.4).[1,156] As a result, counter-screening against APOBEC3G flagged many predicted electrophilic inhibitors present in the HTS libraries. The average Z-scores for the HTS were 0.8 for APOBEC3B CTD and 0.6 for APOBEC3G, indicating that the assay was robust and reproducible. Though this effort, a small molecule pan inhibitor of the APOBEC3 family was discovered, offering an exciting starting point for further development as a molecular probe of the APOBEC3B mutator hypothesis.

Table 2.1 Step-Wise HTS Protocol and Description

Assay Protocol (384 Well Plate Format)		
Parameter	**Value**	**Description**
Enzymes	40 ng	APOBEC3B CTD or APOBEC3G-mycHis in Protein Dilution Buffer[a]
Compounds	33 nL	Library Compounds as 10 mM DMSO Stock Solutions
Substrate	2 pmol	5′-6-FAM-AAA-TAT-CCC-AAA-GAG-AGA-TAMRA-3′
Reaction Volume	12 μL	Protein Dilution Buffer[a] and TE Buffer[b]
Reaction Time	30 min	RT Incubation
Detection Volume	17.2 μL	Protein Dilution Buffer[a], TE Buffer[b], 4 N NaOH, 2 M Tris-Cl[c]
Detection Time	60 min	RT
Readout	517 nm	Fluorescence

Assay Steps	
1	Add 10 μL enzyme in protein dilution buffer[a] to each well.
2	Compound transferred to each well via pin array.
3	Add substrate and UDG (0.01 unit) in 2 μL TE buffer[b].
4	Add 1.2 μL 4 N NaOH to quench reaction.
5	Add 4 μL 2 M Tris-Cl[c] to neutralize reaction.
6	Measure fluorescence with Perkin Elmer Envision® (Ex: 490 nm; Em: 517 nm)

[a]50 mM Tris-Cl, pH 7.4 150 mM NaCl, 10% glycerol, 0.5% Triton X-100
[b]1x TE Buffer: 10 mM Tris, 1 mM EDTA, pH = 8.0
[c]Tris-Cl: 2 M Tris, HCl to adjust pH to 7.4

2.3.1 Assay Optimization from Previous Screens

The assay described above was previously employed in a large scale HTS to discover the first inhibitors of APOBEC3G.[1,156] A total of 330,000 small molecules were interrogated, and ultimately, a disproportionately high number of covalent APOBEC3G modifiers were identified. We reasoned that the conditions of the previous assay enriched for inhibitors with covalent mechanisms of action because of an excessively long incubation time (2 h). When initiating this APOBEC3B-focused HTS, we sought to optimize the assay as to identify inhibitors that were more likely to exhibit non-covalent mechanisms of action. To

enrich for a desired mechanism of inhibition, such as allosteric, competitive, slow-binding, or uncompetitive, important considerations for optimizing an HTS assay include incubation time, substrate concentration, and order of reagent addition.[193,194] In optimizing this screen, we interrogated the assay incubation time as it related to the kinetics of APOBEC3B deamination. Previous screening efforts with this assay employed a 2 h incubation time; however, in studying the extent of APOBEC3B/G deamination over time, it was evident that the enzyme was well outside its initial rate period at 2 h. Thus, the previous screen effectively enriched for HTS 'hits' that were slow-binding and irreversible covalent inhibitors that saturated the enzyme. It was hypothesized that quenching the reaction at an earlier time point could eliminate the identification of irreversible inhibitors. As a result, this APOBEC3B-focused screen relied on an incubation time of 30 min, which would query the enzyme during initial velocity, yet logistically allow for the handling of large numbers of plates.
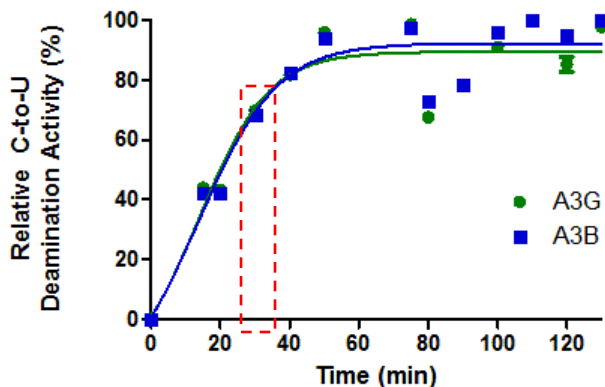
Figure 2.2. Activity vs. Time Plot of APOBEC3 Deamination Activity. The linear period lasts for 50 min. For HTS, a 30 min incubation was selected to enable screening during the initial velocity of APOBEC3B and APOBEC3G.

42

The HTS assay was also miniaturized for resource efficiency in comparison with previous screening efforts. Formerly, small molecules, as 10 mM DMSO stock solutions, were transferred to 15 μL of enzyme (APOBEC3A/G) in protein dilution buffer.[1] ssDNA substrate and UDG diluted in 15 μL of oligomer buffer were added, resulting in a 30 μL reaction volume.[1] In this screen, the final reaction volume was 12 μL, which was comprised of 10 μL of 150 nM APOBEC3B CTD and 67.5 nM APOBEC3G in protein dilution buffer, to which the small molecule stock solutions were transferred, and 2 μL ssDNA substrate and UDG in TE buffer. Though our strategy was to reduce the reaction volume further, the 12 μL reaction volume was selected for compatibility with ICCB-Longwood's compound transfer technology. Specifically, a robotic platform with a stainless steel pin array (V&P Scientific, Inc.) was employed to transfer nanoliter volumes of small molecule stock solutions. After being submerged in the source plate, small droplets of the small molecule DMSO stock form on the pin heads. Compound transfer is accomplished when the droplets, which are held to the pin head by surface tension, are immersed into the experimental wells. For accurate transfer, we needed 10 μL of pre-dispensed volume in the experimental plates.

For the APOBEC3B-focused screen, small molecule controls were also incorporated into each experimental plate. Specifically, aurintricarboxylic acid (ATA), a potent and non-specific inhibitor of the APOBEC3s, was used as a positive control for APOBEC3B inhibition. MN256.0102 (**3.8**), an APOBEC3G-specific inhibitor, was employed as a positive control for APOBEC3G-specific inhibition. These controls were used in addition to the high and low protein controls employed previously. The high protein control reports the fluorescent

reading when the APOBEC3s are unchallenged by small molecule inhibitor, and the low protein control contains all assay reagents except protein. The low control enables the measurement of background fluorescence.

The final modification to this APOBEC3B-focused screen was the strategy to test every compound in duplicate against both enzymes. In other words, each library member was screened four times, two times against APOBEC3B and two times against APOBEC3G. Our earlier screens were characterized by a significant number of false positive hits, slowing efforts in both the discovery and development of APOBEC3 inhibitors. In this screen, duplicate screening was employed to reduce the number of false positive hits. Duplicate screening enables the removal of experimental outliers during data analysis (Figure 2.3). While these outliers would have been characterized as hits in previous screening efforts, they were easily reclassified as false positives using this strategy. Compounds were only prioritized for further investigation after two confirmatory data points in the primary screen.
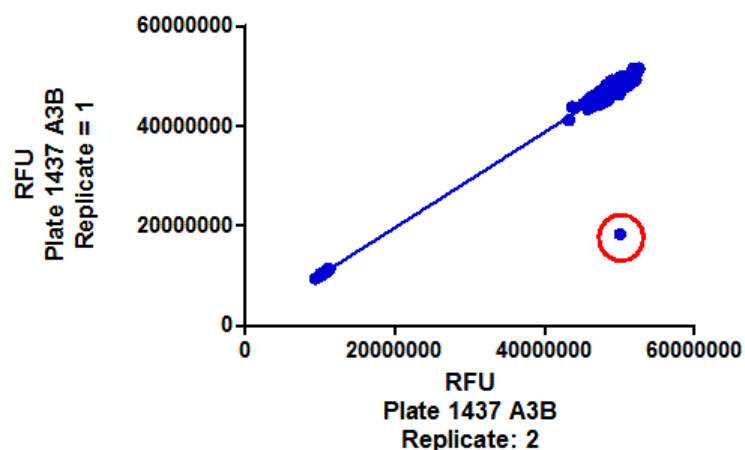
Figure 2.3. Reproducibility of the Screening Data. Duplicate data for plate 1436 are displayed to represent results of the primary screen. Data that are consistent between the two plates fall on the linear plot with good fit ($R^2 > 0.99$). Control data are observed on the far left of the plot with RFU readings ~1.0×10^7. Non-active compounds fall on the far right of the plot with RFU readings ~5.0×10^7. Confirmed hits would be observed in between. Outliers are observed askew from the linear fit as demonstrated by the data point circled in red. RFU = Relative Fluorescence Units.

2.4 Implementation of the Primary Screen and Identification of Hits

In this effort, 168,192 small molecules from 20 commercially-available libraries were screened at 27.5 µM. The screened libraries included: the Library of Pharmacologically Active Compounds (LOPAC, Sigma), the NIH Chemical Collection (NIHCC), Maybridge Libraries 3-5, Asinex1, Biomol4 (FDA Approved Library), the Prestwick 2 Collection, MicroSource Discovery 1, Tocrisscreen Mini-Library, ChemDiv 5-7, SYNthesis Med Chem Kinase Inhibitor 1, the ChemBridge Focused G-Protein Coupled Receptor Library, the ChemBridge Focused Ion Channel Core, the ChemBridge Focused Nuclear Hormone Receptor-Based Core, the ChemBridge Focused Kinase-Based Core, LINCS3 Chromatin

45

Targeting Library, Enamine 2, ChemBridge 3, and Life Chemicals 1. The primary screen resulted in 83 APOBEC3B-specific inhibitors (0.05% hit rate), 1099 APOBEC3G-specific inhibitors (0.7% hit rate), and 253 APOBEC3B/G dual inhibitors (0.2% hit rate), after filtering to remove pan assay inference scaffolds (PAINS).[195] Compounds that reduced APOBEC3B CTD deaminase activity by at least 20%, and inhibited APOBEC3G no more than 15% were defined as APOBEC3B-specific. Compounds that reduced APOBEC3G deaminase activity by at least 40% and inhibited APOBEC3B CTD no more than 15% were defined as APOEC3G-specific. Finally, compounds that inhibited APOBEC3B by at least 20% and APOBEC3G by at least 40% were identified as dual inhibitors. The number of identified hits in each library is displayed in Table 2.2. After visual inspection to ensure drug-likeness of the primary hits, 371 small molecules were selected for further dose response experiments. The 371 compounds included 69 A3B-specific inhibitors, 184 A3B/A3G dual inhibitors, and 119 APOBEC3G-specific inhibitors.

Table 2.2. Summary of Screened Libraries and Hit Rates

Primary Screening Report	A3B CTD	A3G	Dual	Total
LOPAC (1,280)	1	14	12	27
	0.1%	1.1%	0.9%	2.1%
NIHCC (727)	0	8	4	12
	0.0%	1.1%	0.6%	1.7%
Maybridge(15,427)	3	180	21	204
	0.0%	1.2%	0.1%	1.3%
Asinex 1 (12,378)	4	200	43	247
	0.0%	1.6%	0.3%	2.0%

Biomol 4 - FDA Approved Drug Library (640)	2	2	0	4
	0.3%	0.3%	0.0%	0.6%
Prestwick2 Collection (1,120)	0	2	1	3
	0.0%	0.2%	0.1%	0.3%
MicroSource Discovery 1 (270)	0	2	1	3
	0.0%	0.7%	0.4%	1.1%
Tocriscreen™ Mini Library-Makoto (1,120)	7	3	4	14
	0.6%	0.3%	0.4%	1.3%
ChemDiv7 (49,128)	1	476	63	540
	0.1%	1.0%	0.1%	1.1%
ChemDiv6 (44,000)	28	147	54	229
	0.1%	0.3%	0.1%	0.5%
ChemDiv5 (1,249)	0	1	0	1
	0.0%	0.1%	0.0%	0.1%
SYNthesis med chem Kinase Inhibitor 1 (288)	0	0	0	0
	0.0%	0.0%	0.0%	0.0%
ChemBridge Focused G-Protein Coupled Receptor Library (250)	0	0	0	0
	0.0%	0.0%	0.0%	0.0%
ChemBridge Focused Ion Channel Core (250)	0	0	0	0
	0.0%	0.0%	0.0%	0.0%
ChemBridge Focused Nuclear Hormone Receptor-Based Core (250)	0	1	0	1
	0.0%	0.4%	0.0%	0.4%
ChemBridge Focused Kinase-Based Core (250)	0	0	0	0
	0.0%	0.0%	0.0%	0.0%
LINCS3 Chromatin-Targeting Library (164)	0	3	2	5
	0.0%	1.8%	1.2%	3.0%
Enamine 2 (26,576)	37	806	193	1,036
	0.1%	3.0%	0.7%	3.9%

47

ChemBridge3 (9,504/10,560)	3	112	14	129
	0.0%	1.1%	0.1%	1.2%
Life Chemicals 1 (3,893)	0	96	24	120
	0.0%	2.5%	0.6%	3.1%
Total (168,192)	**83**	**1,099**	**253**	**1,645**
	0.05%	**0.7%**	**0.2%**	**1.0%**

2.5 Dose Response Assays

Twelve-point dose response curves (100 µM – 49 nM, 1:2 dilutions) were generated for the 371 primary hits to reconfirm the observed inhibitory activity and to determine IC_{50} values. Of the 69 APOBEC3B-specific primary hits, none of the compounds exhibited APOBEC3B inhibition in dose response assays. Forty-two dual APOBEC3B/G inhibitors of the 184 primary hits (~22%) maintained APOBEC3B inhibition in dose response experiments, displaying IC_{50} values from 2 µM – 500 µM. Similarly, 36 of the 119 primary APOBEC3G-specific hits (30%) maintained inhibition in dose response experiments, with IC_{50} values from 2 µM - 60 µM. All of the APOBEC3B/G dual inhibitory leads were purchased, if commercially available, for further interrogation in-house. Five of the 42 prioritized leads were not commercially available.

2.6 Quality Control and Dose Response on Commercial Material

The 37 purchased small molecules were analyzed for chemical integrity by two wavelength HPLC and LCMS (Table 2.3).

Table 2.3. Purities and Activities of Purchased APOBEC3B/G Dual Inhibitory Leads from Commercial Vendors.

MN Number[a]	Vendor	Purity[b]	IC$_{50}$ (A3B)	IC$_{50}$ (A3G)
MN23	Aldrich	>99%	0.15 μM	5.5 μM
MN59	Microsource	>99%	>100 μM	>100 μM
MN347	Life Chemicals	>99%	83 μM	>100 μM
MN348	TimTec	>99%	8 μM	3.5 μM
MN349	ChemBridge	N/A	3.9 μM	18 μM
MN350	ChemBridge	41%	>100 μM	7.0 μM
MN351	ChemBridge	>99%	>100 μM	>100 μM
MN352	Asinex	>99%	>100 μM	>100 μM
MN353	Asinex	>99%	4.8 μM	3.2 μM
MN354	Asinex	>99%	4.5 μM	4.2 μM
MN355	Asinex	N/A	<1 μM	2.7 μM
MN356	Asinex	<99%	4.8 μM	23 μM
MN357	Asinex	>99%	>100 μM	>100 μM
MN358	ChemDiv	>99%	3.6 μM	13 μM
MN359	ChemDiv	>99%	5.1 μM	16 μM
MN360	ChemDiv	>99%	0.2 μM	2.4 μM
MN361	ChemDiv	>99%	36 μM	70 μM

MN362	ChemDiv	>99%	2.3 μM	8.2 μM
MN363	ChemDIv	>99%	>100 μM	>100 μM
MN364	ChemDiv	77%	11 μM	14 μM
MN365	ChemDiv	>99%	8.4 μM	4.9 μM
MN366	Alfa Aesar	N/A	8.6 μM	0.3 μM
MN367	ChemDiv	>99%	17 μM	12 μM
MN368	ChemDiv	>99%	>100 μM	>100 μM
MN369	Ambinter	>99%	>100 μM	>100 μM
MN370	Enamine	N/A	>100 μM	>100 μM
MN371	Enamine	>99%	5.0 μM	5.1 μM
MN372	Enamine	83%	>100 μM	>100 μM
MN373	Enamine	N/A	>100 μM	>100 μM
MN374	Enamine	>99%	13 μM	16 μM
MN375	Enamine	>99%	>100 μM	94 μM
MN376	Enamine	89%	6.4 μM	6.7 μM
MN377	Enamine	90%	>100 μM	>100 μM
MN378	Enamine	60%	11 μM	15 μM
MN379	Enamine	>99%	96 μM	54 μM
MN380	Enamine	45%	15 μM	19 μM
MN381	Enamine	>99%	7.8 μM	12 μM

HPLC and LCMS analysis confirmed that 24 of the 37 purchased leads were >95% pure by two wavelengths (254/215 nm). Dose response assays were performed in-house to reconfirm the APOBEC3B inhibitory activity associated with the leads. Thirteen of the repurchased compounds evaluated at the University of Minnesota showed no APOBEC3B inhibition when tested up to 100 μM. To be prioritized for further investigation, the purchased compounds had to demonstrate >95% purity by two wavelengths and an IC_{50} value against APOBEC3B < 100 μM. After these quality control experiments, 16 potential APOBEC3B inhibitors were identified and are shown in Figure 2.4.

2.1 (MN347)   **2.2 (MN348)**   **2.3 (MN353)**

2.4 (MN354)   **2.5 (MN356)**   **2.6 (MN359)**

2.7 (MN360)   **2.8 (MN361)**   **2.9 (MN362)**

2.10 (MN365)   **2.11 (MN367)**   **2.12 (MN371)**

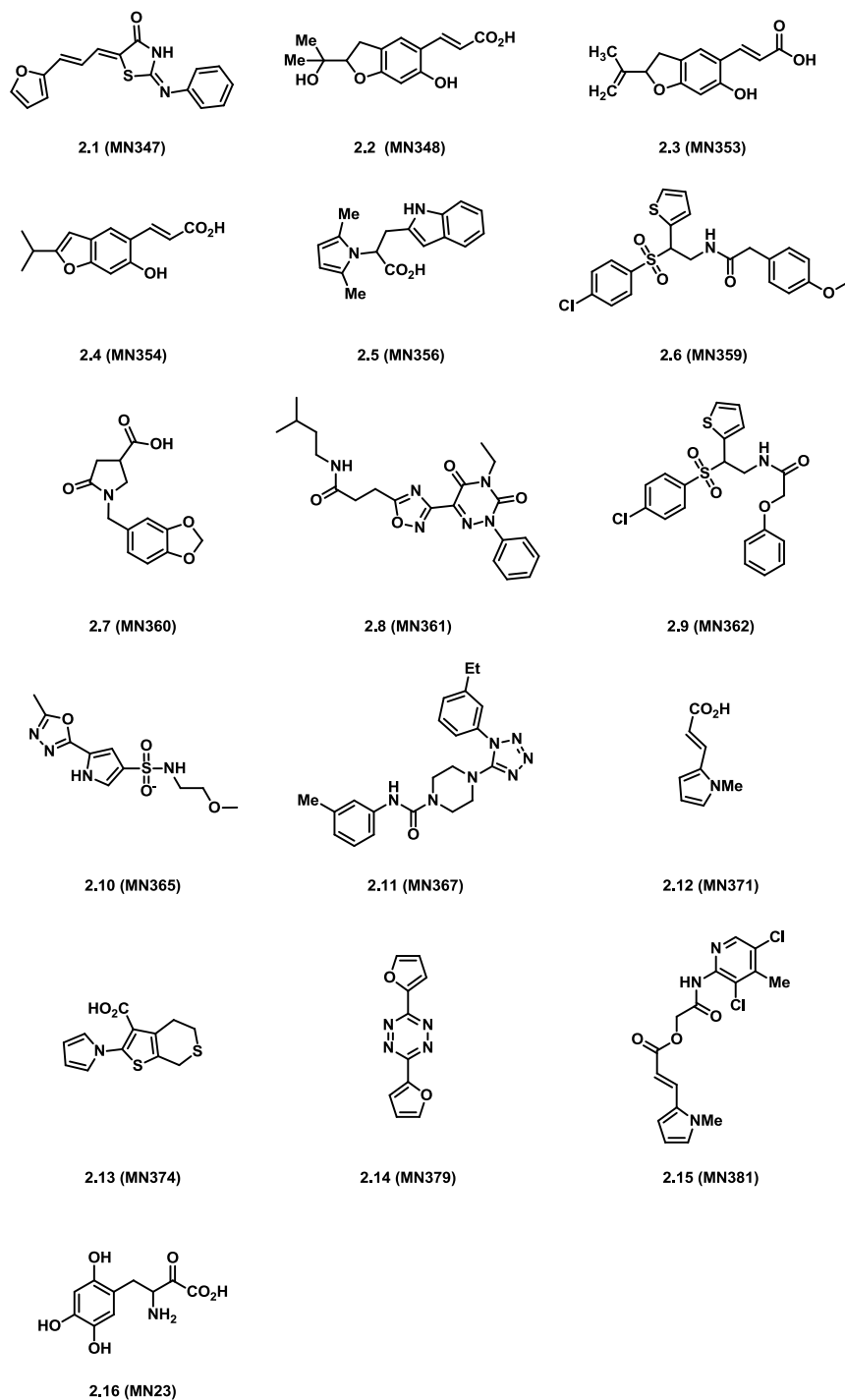**2.13 (MN374)**   **2.14 (MN379)**   **2.15 (MN381)**

2.16 (MN23)

Figure 2.4. Chemical Structures of APOBEC3B Inhibitory Leads Identified at ICCB-Longwood, Harvard Medical School. Compounds in this graphic were >95% pure by two-wavelengths (254/215 nm) and inhibited A3B with an $IC_{50} <$ 100 μM, when purchased commercially. The majority of these compounds were promoted for further interrogation.

52

2.7 Lead Triage of Active Commercial APOBEC3B Inhibitors

Despite passing the computational PAINS filter, MN347 (**2.1**) and MN356 (**2.5**) were disqualified from further analysis as a result of containing PAINS-like substructures, an α, β, λ, δ-unsaturated carbonyl and a tri-substituted pyrrole, respectively. Moreover, MN379 (**2.14**) was eliminated because of its unimpressive inhibitory activity. The remaining 13 compounds were further interrogated by Ms. Olson and members of the Harki laboratory through purification of commercially available samples, synthesis of compounds that could not be purchased in suitable quantities for purification, and then biochemical evaluation of the pure samples to reconfirm APOBEC3B inhibitory activity. Commercial materials were purified by SiO_2 flash column chromatography and/or reverse phase HPLC. Following purification of the commercially available compounds and synthesis of those that were not available, 12/13 compounds failed to demonstrate APOBEC3B inhibition when tested up to 200 µM (Table 2.4). The following compounds failed to be validated as 'real' APOBEC3B inhibitors through these studies: MN348 (**2.2**), MN353 (**2.3**), MN354 (**2.4**), MN359 (**2.6**), MN360 (**2.7**), MN362 (**2.9**), MN365 (**2.10**) MN367 (**2.11**), MN371 (**2.12**), and MN381 (**2.14**). Moreover, MN361 (**2.8**) and MN374 (**2.13**) were removed from further consideration due to significantly reduced APOBEC3B inhibitory activity after purification. MN23 (**2.16**) was the sole confirmed APOBEC3B inhibitor.

Table 2.4. Activities of Commercial APOBEC3B/G Dual Inhibitory Leads Post Purification.

MN Number	$IC_{50}s$ (A3B/A3G)
MN348	>200 µM
MN353	>200 µM
MN354	>200 µM
MN359	>200 µM
MN360	>200 µM
MN361	>200 µM
MN362	>200 µM
MN365	>200 µM
MN367	>200 µM
MN371	>200 µM
MN374	>200 µM
MN381	>200 µM

This disappointing result raises serious concerns regarding contamination of HTS libraries and commercial chemicals. Through quality control analysis, we ruled out any potential organic contaminants as no additional resonances or peaks were identified by ^{1}H NMR or HPLC, respectively. The lack of data to support the presence of organic contamination points towards an inorganic contaminant, such as a metal or salt. In an effort to prioritize the discovery of APOBEC3B inhibitors, further investigation into the origin of the false positive hits was not undertaken. Importantly, the employed fluorescence-based deamination assay has exhibited an exceedingly high rate of false positive identification. This observation has prompted the Harki-Harris collaboration to investigate alternative assays for future screening endeavors.

2.8 Re-Discovery of MN23 (2.16)

MN23 (2.16), a non-natural amino acid analogue of tyrosine commonly known as 6-hydroxy-DL-DOPA, was re-discovered as a small molecule inhibitor of APOBEC3A, APOBEC3B and APOBEC3G in this HTS (Figure 2.5, See Chapter 2.2 for a discussion of the previous screen).
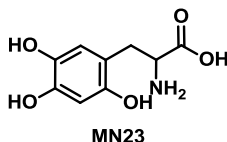

MN23

Figure 2.5. Chemical Structure of MN23 (2.16).

MN23 (2.16) was previously reported by the Harris and Harki groups to be a potent inhibitor of APOBEC3A and APOBEC3G with IC_{50} values of 0.3 μM and 4.0 μM, respectively.[1] Moreover, MN23 (2.16) maintained potent inhibitory activity against APOBEC3A and APOBEC3G in the context of cellular lysates, with IC_{50}s = 30 μM (A3A) and 15 μM (A3G). Importantly, purification of the commercial material by HPLC had no affect on the potency of the small molecule. Interestingly, MN23 (2.16) inhibits APOBEC3-catalyzed deamination through a novel and under-investigated mechanism of action.[1] Electrophoretic mobility shift assays (EMSAs) demonstrated that MN23 (2.16) inhibits APOBEC3G from binding its ssDNA substrate (Figure 2.6). Conversely, MN30 (1.8) is proposed to inhibit APOBEC3G by covalently engaging C321, a residue proximal to the active site (See Chapter 1.4.4 for an in-depth description).[1] Molecular modeling of this covalent binding event suggested that in order to accommodate the steric bulk of MN30 (1.8), APOBEC3G undergoes a conformational change in its active site, which inhibits enzymatic activity. This

55

conformational change, however, does not interfere with APOBEC3G - DNA binding.
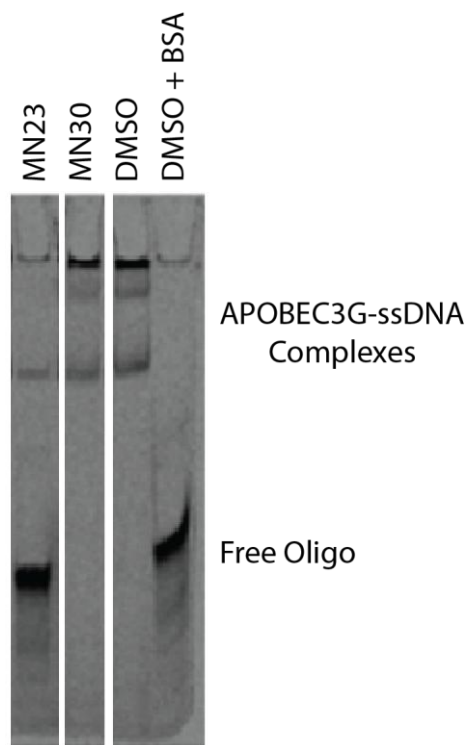
Figure 2.6. Electrophoretic Mobility Shift Assay of MN23 (**2.16**) and MN30 (**1.8**). The figure is modified from Li et al. *ACS Chem. Biol.*, **2012**, *7*, 506.[1] MN23 (**2.16**) inhibits APOBEC3G – DNA binding at 50 μM as evidenced by a distinct band, which correlates to free oligo. Conversely, in the presence of 50 μM MN30 (**1.8**), the DNA substrate was entirely enzyme bound. No band corresponding to free oligo was observed. Controls show that in the presence of DMSO, APOBEC3G-DNA binding occurs unhindered. However, in the presence of BSA, DNA-protein binding is inhibited.

Recent experiments demonstrate that in addition to APOBEC3A and APOBEC3G, MN23 (**2.16**) potently inhibits APOBEC3B, with an IC_{50} of 0.15 μM against recombinant APOBEC3B CTD and an IC_{50} of 11 μM in cellular lysates. The potent activity of MN23 (**2.16**) and its unique mechanism of inhibition have

prompted the Harki Lab to pursue this putative APOBEC3B inhibitor in more depth.

2.9 Synthesis of MN23

The synthesis of MN23 (**2.16**) was accomplished in 5 steps from commercially available 2,4,5-trimethoxybenzaldehyde (**2.17**) (Scheme 2.1). This synthesis was modified from a published synthesis of *o*-methoxytyrosine.[196] From **2.17**, the azlactone intermediate was synthesized through the Erlenmeyer azlactone procedure,[197,198] and was subsequently opened to the protected amino acid acrylate under basic conditions. Hydrogenation of acrylic acid **2.19** in the presence of Pd/C at 50 psi H_2 gave the protected amino acid (**2.20**) in 89% yield. Deprotection of the trimethoxy intermediate was accomplished in excess BBr_3 in 61% yield. A final deprotection under acidic conditions yielded the free amino acid (MN23, **2.16**). This synthesis can also be performed asymmetrically with a commercially available Rhodium Deguphos catalyst (3*R*,4*R*-(+)-bis(diphenylphosphino)-1-benzylpyrrolidine(1,5-cyclooctadiene)rhodium(I)) to afford the enantioselective hydrogenation of **2.19**.[196,199] The asymmetric syntheses of MN23 (**2.16**) will be pursued upon confirming the biochemical inhibitory activity of this compound against APOBEC3A/B and G.
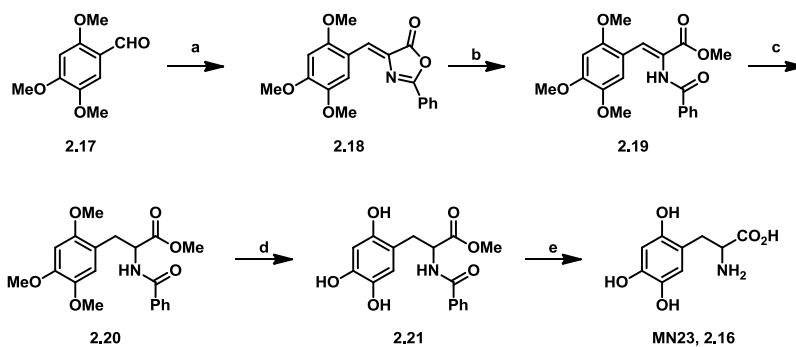
Scheme 2.1 Synthesis of MN23 (**2.16**). (a) hippuric acid, NaOAc, AcOH, 100 $^{\circ}$C, 84%; (b) Na_2CO_3, MeOH, 94%; (c) H_2, Pd/C, MeOH, 50 bar, 89%; (d) BBr$_3$, DCM, 61%; (e) HCl, H_2O, 110 $^{\circ}$C.

2.10 MN23 SAR by Commerce

A series of MN23 (**2.16**) analogues were purchased from commercial vendors and evaluated for inhibitory activity against APOBEC3A/B and G. The commercially available series included 3-hydroxy-DL-tyrosine (**2.22**), DL-*o*-tyrosine (**2.23**), DL-*m*-tyrosine (**2.24**), DL-tyrosine (**2.25**), tyramine (**2.26**), and phenylephrine (**2.27**). Ultimately, none of the investigated compounds showed APOBEC3B inhibition up to 200 µM, and only **2.22** showed weak inhibitory activity against APOBEC3G. These results show that at minimum trihydroxy substitution of the phenyl ring is required for APOBEC3B inhibition.
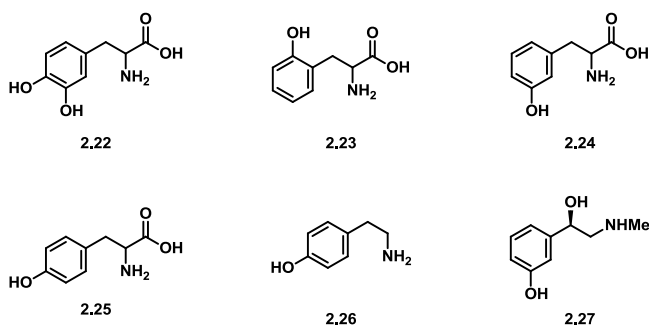

Figure 2.7 Chemical Structures of Purchased **MN23** analogues.

58

2.11 Conclusions

A HTS of 168,192 small molecules for APOBEC3B inhibition identified 40 dual APOBEC3B/G inhibitors upon reconfirmation in dose response assays. Disappointingly, none of the 40 small molecules passed stringent follow-up quality control interrogation, which included HPLC, LCMS, and biochemical evaluation both pre- and post- purification. The results of this screen mirror our previous efforts in screening against APOBEC3A and APOBEC3G, which also employed the fluorescence-based deamination assay described above. As a result, our future efforts will be focused on the design and implementation of a complementary assay, which could be employed as either the primary or secondary screening assay. HTS assays based on fluorescence polarization, Förster resonance energy transfer (FRET), and biophysical fragment screening will be individually investigated as alternative methodologies.

Our screening efforts also highlight the obstacle that false positives present to an inhibitor discovery campaign. Extensive efforts have been undertaken in recent years to annotate common chemical libraries to flag "frequent hitters".[200-203] Although a number of scaffolds and chemical substructures have been identified, these guidelines are incomplete, and active screeners must invest time and resources to validate hits. Recently, our laboratory discovered and characterized a novel pan assay inference class as a result of our own screening efforts, and this work is presented in Chapter 4. With the widespread popularity of HTS-driven in drug discovery campaigns, continued efforts towards the identification of factors that complicate successful HTS endeavors and strategies to overcome them will be invaluable to the field.

This APOBEC3B-focused screen did, however, re-discover **MN23** (**2.16**), a tyrosine analogue from the Sigma LOPAC library. **MN23** (**2.16**) exhibited potent inhibition of APOBEC3B with an IC_{50} = 0.15 μM against recombinant APOBEC3B CTD and an IC_{50} = 11 μM in cellular lysates. EMSA experiments with **MN23** (**2.16**) demonstrate that **MN23** (**2.16**) potently inhibits APOBEC3G-ssDNA binding, which is a unique mechanism of action compared to previously published APOBEC3 inhibitors. The synthesis of **MN23** (**2.16**) has recently been completed, and further work will focus on the rigorous validation of this small molecule inhibitor. If upheld, the asymmetric synthesis of **MN23** (**2.16**), comprehensive SAR investigation, and mechanism of action studies will be performed to develop **MN23** (**2.16**) into a probe of APOBEC3B-dependent cancer mutagenesis.

2.12 Experimental

Cell Culture and Protein Purification: A3B 193-382 mychis was purified from stably transfected T-REx-293 cells using a C-terminal hexahistidine tag.[1,19,204] Cells were maintained in DMEM (Invitrogen)/high glucose (Hyclone) supplemented with 10% FBS (Hyclone), 50 units/mL penicillin and 50 μg/mL streptomycin (Corning) at 5% CO_2 and 37°C. Cells were harvested 48 hours after induction with 5 ng/mL doxycycline and lysed in 25 mM HEPES, pH 7.4, 150 mM NaCl, 1 mM $MgCl_2$, 0.5% Triton X-100 and 10% glycerol. Insoluble materials were removed from crude cell lysates by centrifugation (12,000 rpm, 10 min), and A3B-mychis was captured by Ni-NTA agarose (Qiagen). The resins were intensively washed with 50 mM Tris, pH 8.0, 0.3 M NaCl, 10% glycerol, 0.5%

Triton X-100 and 50 mM imidazole. Then, the target protein was eluted with 50 mM Tris, pH 8.0, 0.3 M NaCl, 10% glycerol, 0.5% Triton X-100 and 250 mM imidazole. APOBEC3G-mycHis was expressed and purified as previously reported.[1]

DNA Deaminase Assay and HTS: The fluorescence-based DNA C-to-U deaminase assay was modified for this screen from previous reports.[1,19,191,204] Recombinant human proteins APOBEC3B- or APOBEC3G-mycHis were diluted with 15 mM Tris-Cl, pH 7.4, 50 mM NaCl, 10% glycerol, 0.5% triton X-100 to working concentrations, and 10 µL of 150 nM APOBEC3B CTD or 67.5 nM APOBEC3G were added to each well. Small molecules were transferred as 10 mM DMSO stock solutions using a pin array to achieve a final concentration of 27.5 µM. Finally, 2 pmol of ssDNA substrate (5′-6-FAM-AAA-CCC-AAA-GAG-AGA-ATG-TGA-TAMRA-3′, Biosearch Technologies, Inc.) and 0.01 units of UDG (New England Bioloabs) diluted in 2 µL TE buffer (10 mM Tris-HCl, 1 mM EDTA, pH = 7.4) were added to the experimental wells. The assay plates were incubated for 30 min at rt. To quench the reaction, 1.2 µL of 4 N NaOH was added, followed by another rt incubation for 30 min. Four microliters of 2 M Tris-Cl were then added for neutralization. All reagents transfers were performed using a Combi nL. Relative fluorescence intensity was quantified by reading fluorescence with excitation at 485 nm and emission at 520 nm on an Envision® plate reader (Perkin Elmer).

Dose Response Assay: DMSO (120 nL) was dispensed by HP D300 into each well of a Corning® black low volume 384 well plate (3820) to normalize DMSO
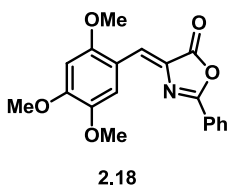
61

content to the highest concentration. Compounds as 10 mM DMSO stocks were diluted over 12-pts with the highest concentration at 100 µM and the lowest concentration at 49 nM. These concentrations represent a 1:2-fold dilution. Protein (40 ng in 10 µL) was added to each experimental well, followed by the immediate addition of substrate oligo (2 pmol in 2 µL). The assay plates were incubated for 30 min at rt, before 1.2 µL of 4 N NaOH was added into each experimental. The assay plates were incubated for 30 min at rt, followed by final neutralization with 4 µL of 2 M Tris·HCl. Fluorescence was quantified with excitation at 485 nm and emission at 520 nm.

EMSA. Previously reported in Li et al. *ACS Chem. Biol.* **2011**, *7*, 506.[1]

General Synthesis.

Chemical reagents were purchased from commercial sources and used without additional purification. Bulk solvents were from Fisher Scientific. Anhydrous solvents were obtained from an MBraun Solvent Purification system. Reactions were performed under an atmosphere of dry N_2 where noted. Silica gel chromatography was performed on a Teledyne-Isco Combiflash Rf-200 instrument using Redisep *R*f Gold High Performance silica gel columns (Teledyne-Isco) or self-packed columns with SiliaFlash 60Å silica gel (SiliCycle). HPLC analyses were performed on an Agilent 1200 series instrument equipped with a diode array detector and a Zorbax SB-C18 column (4.6 x 150 mm, 3.5 µm, Agilent Technologies). Compounds used in biological testing were no less than 95% pure as determined by two-wavelength HPLC analysis (254 and 215 nm). Nuclear magnetic resonance (NMR) spectroscopy was performed using a Bruker

Avance instrument operating at 400 MHz or 500 MHz (for ^{1}H) and 100 MHz or 125 MHz (for ^{13}C) at ambient temperature. Chemical shifts are reported in parts per million and normalized to internal solvent peaks or tetramethylsilane (0 ppm). LC-MS analyses were performed on an Agilent 1100 series instrument equipped with an Agilent MSD SL Ion Trap mass spectrometer (positive-ion mode) and a Zorbax SB-C18 column (0.5 x 150 mm, 5 μm, Agilent Technologies). The analysis method (15 μL/min flow rate) involved isocratic 10% MeCN (containing 0.1% TFA) in ddH$_2$O (containing 0.1% HCO$_2$H; 0 to 2 mins) followed by a linear gradient of 10% to 90% MeCN (containing 0.1% TFA) in ddH$_2$O (containing 0.1% HCO$_2$H; 2 to 24 mins), and isocratic 90% MeCN (containing 0.1% TFA) in ddH$_2$O (containing 0.1% HCO$_2$H; 24-26 mins). The column was heated to 40 ^{o}C. Wavelengths monitored = 214 nm and 254 nm.


2.18

(*Z*)-2-Phenyl-4-(2,4,5-trimethoxybenzylidene)oxazol-5(4*H*)-one (2.18). 2,4,5-Trimethoxybenzaldehyde (**2.17**, 2.5 g, 12.7 mmol), hippuric acid (2.3 g, 12.7 mmol), NaOAc (1.1 g, 13.1 mmol), and Ac$_2$O (2.9 mL, 30.6 mmol) were melted with a heat gun, then heated with an oil bath for 2 h at 100 ^{o}C. The resulting mixture was cooled to rt and dH$_2$O (100 mL) was added. The precipitate was collected via vacuum filtration, washed with NaHCO$_3$ (100 mL), and dried under vacuum. SiO$_2$ purification (20% MeOH in DCM) gave 3.2 g (73%) of **2.18** as an orange solid. ^{1}H NMR (CDCl$_3$) δ = 8.64 (s, 1H), 8.11 (d, 2H, *J* = 7.1 Hz), 7.82 (s, 1H), 7.58 (t, 1H, *J* = 7.3 Hz), 7.51 (t, 2H, *J* = 7.3), 6.49 (s, 1H), 4.02 (s, 3H), 3.98

(s, 3H), 3.92 (s, 3H); ^{13}C (CDCl$_3$): δ = 168.3, 161.7, 156.2, 153.9, 143.6, 132.9, 129.1, 128.0, 126.3, 126.2, 115.0, 114.5, 95.9, 56.6, 56.4, 56.2. HRMS-ESI$^+$ *m/z* [M+H]$^+$ calc'd for C$_{19}$H$_{17}$NO$_5$: 340.1179, found: 340.1165.


2.19
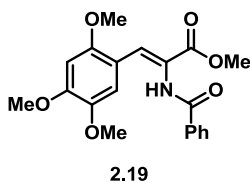
(*Z*)-Methyl-2-benzamido-3-(2,4,5-trimethoxyphenyl)acrylate (2.19). To a solution of **2.18** (3.2 g, 9.3 mmol) in MeOH/DCM (110 mL, 1:1, v/v) was added Na$_2$CO$_3$ (0.5 g, 4.7 mmol) and the reaction was stirred at rt. After 16 h, the reaction mixture was filtered over Celite, and the filtrate was concentrated *in vacuo*. SiO$_2$ purification (100% DCM) gave 3.4 g (97%) of **2.19** as an orange powder. ^{1}H NMR (CDCl$_3$) δ = 8.22 (bs, 1H, NH), 7.86 (d, 2H, *J* = 7.2 Hz), 7.54 (s, 1H), 7.54 (t, 1H, *J* = 7.5 Hz), 7.46 (t, 2H, *J* = 7.1 Hz), 7.00 (s, 1H), 6.53 (s, 1H), 3.90 (s, 3H), 3.90 (s, 3H), 3.88 (s, 3H), 3.63 (s, 3H); ^{13}C (CDCl$_3$) δ = 166.2, 165.5, 152.3, 151.2, 143.4, 134.0, 132.2, 128.9, 127.5, 126.0, 124.0, 114.8, 112.6, 97.8, 57.4, 56.2, 56.1, 52.8. HRMS-ESI$^+$ *m/z* [M+H]$^+$ calc'd for C$_{20}$H$_{21}$NO$_6$: 372.1442, found: 372.1447.


2.20
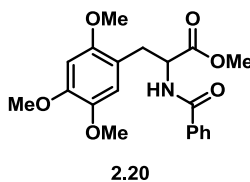
Methyl 2-benzamido-3-(2,4,5-trimethoxyphenyl)propanoate (2.20). To a suspension of **2.19** (1.0 g, 2.7 mmol) in MeOH (40 mL) was added Pd/C (0.3 g, 10% w/w) and the reaction hydrogenated in a Parr shaker under 50 bar H$_2$

atmosphere. After 24 h, the grey/brown mixture was concentrated onto SiO_2 and

purified using a gradient of EtOAc (0% to 100%) in hexanes to afford 0.9 g (89%)

of **2.20** as a white powder. ^1H NMR (CDCl$_3$) δ = 7.73 (d, 2H, J = 7.2 Hz), 7.49 (t,

1H, J = 7.4 Hz), 7.41 (t, 2H, J = 7.6 Hz), 7.11 (d, 1H, J = 6.9 Hz), 6.66 (s, 1H),

6.52 (s, 1H), 4.85 (q, 1H, J = 12.2 Hz, 7.1 Hz), 3.88 (s, 3H), 3.83 (s, 3H), 3.76 (s,

3H), 3.75 (s, 3H), 3.18 (ddd, 2H, J = 33.1 Hz, 13.9 Hz, 7.5 Hz); ^{13}C (CDCl$_3$) δ =

172.4, 167.1, 151.7, 149.0, 143.4, 134.1, 131.8, 128.6, 127.1, 116.0, 115.0, 97.7,

56.6, 56.6, 56.3, 54.4, 52.4, 31.9. HRMS-ESI$^+$ m/z [M+H]$^+$ calc'd for $C_{20}H_{23}NO_6$:

374.1598, found: 374.1578.

2.21
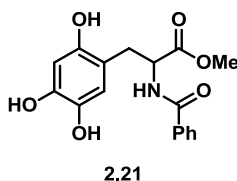
Methyl 2-benzamido-3-(2,4,5-trihydroxyphenyl)propanoate (2.21). To a

solution of **2.20** (400.0 mg, 1.1 mmol) in DCM (12 mL) was added BBr$_3$ (10.7 mL,

10.7 mmol, 1 M in heptanes) at -78 °C under N$_2$. The reaction was stirred at -78

°C for 10 min, before it was allowed to warm to rt. After 24 h, the reaction was

quenched with MeOH (15 mL), concentrated onto SiO_2 *in vacuo*, and purified

using a gradient of MeOH (0% to 15%) in DCM to yield 158.0 mg (45%) of **2.21**

as a brown crystalline solid. ^1H NMR (DMSO-d$_6$) δ = 8.63 (d, 1H, J = 7.2 Hz, NH),

7.80 (d, 2H, J = 7.6 Hz), 7.54 (t, 1H, J = 7.4 Hz), 7.46 (t, 2H, J = 7.6 Hz) 6.50 (s,

1H), 6.30 (s, 1H), 4.57 (m, 1H), 3.60 (s, 3H), 3.16 (s, 1H, OH), 2.99 (dd, 1H, J =

13.6 Hz, 5.2 Hz), 2.89 (s, 1H, OH), 2.79 (dd, 1H, J = 13.8 Hz; 9.4 Hz), 2.73 (s,

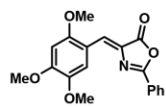1H, OH); ^{13}C (DMSO-d$_6$) δ = 172.4, 166.2, 147.6, 144.2, 137.2, 133.7, 131.4,

128.3, 127.2, 117.8, 113.1, 103.3, 53.5, 51.7, 31.0. HRMS-ESI$^+$ m/z [M+H]$^+$ calc'd for $C_{17}H_{17}NO_6$: 332.1129, found: 332.1111.
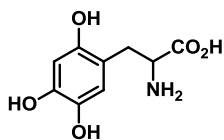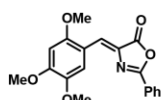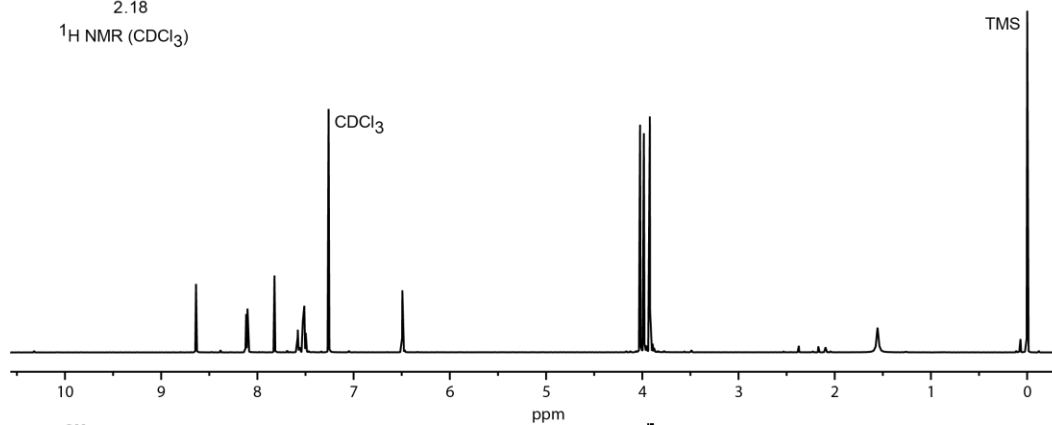

MN23, 2.16

2-Amino-3-(2,4,5-trihydroxyphenyl)propanoic acid (MN23, 2.16). A solution of **2.21** (177.0 mg, 0.5 mmol) in 5 M aq. HCl (5 mL) was stirred for 18 h at 110 ^{o}C. After the reaction cooled to rt, the solvent was removed *in vacuo*. The resulting residue was taken up in H_2O (10 mL), and the aq. mixture was extracted with DCM (3 x 10 mL). The aq. layer was concentrated *in vacuo* to yield the HCl salt of MN23 (**2.16**) as a brown powder. ^{1}H NMR (D$_2$O) δ = 6.71 (s, 1H), 6.50 (s, 1H), 4.13 (m, 1H), 3.24 (dd, 1H, J = 15.0 Hz, 5.4 Hz), 2.96 (dd, 1H, J = 14.6 Hz, 7.6 Hz); ^{13}C (D$_2$O) δ = 171.6, 148.1, 144.4, 137.0, 118.7, 112.1, 104.0, 53.4, 30.0. HRMS-ESI$^+$ m/z [M+Na]$^+$ calc'd for $C_9H_{11}NO_5$: 236.0529, found: 236.0544. Note: MN23 (**2.16**) is air and photosensitive. Exposure to air and light triggers MN23 (**2.16**) polymerization.

2.13 NMR Spectra of Synthesized Compounds

2.18
^{1}H NMR (CDCl$_3$)

TMS

CDCl$_3$

2.18
^{13}C NMR (CDCl$_3$)

CDCl$_3$

TMS

2.19
^{1}H NMR (CDCl$_3$)

2.19
^{13}C NMR (CDCl$_3$)

68

2.20
^{1}H NMR (CDCl$_3$)

2.20
^{13}C NMR (CDCl$_3$)

69

^{1}H NMR (DMSO-d$_6$)

^{13}C NMR (DMSO-d$_6$)

70

MN23 (2.16)
^{1}H NMR (D$_2$O)

D$_2$O

10.0 9.5 9.0 8.5 8.0 7.5 7.0 6.5 6.0 5.5 5.0 4.5 4.0 3.5 3.0 2.5 2.0 1.5 1.0 0.5 0.0

MN23 (2.16)
^{13}C NMR (D$_2$O)

200 190 180 170 160 150 140 130 120 110 100 90 80 70 60 50 40 30 20 10 0
ppm

71
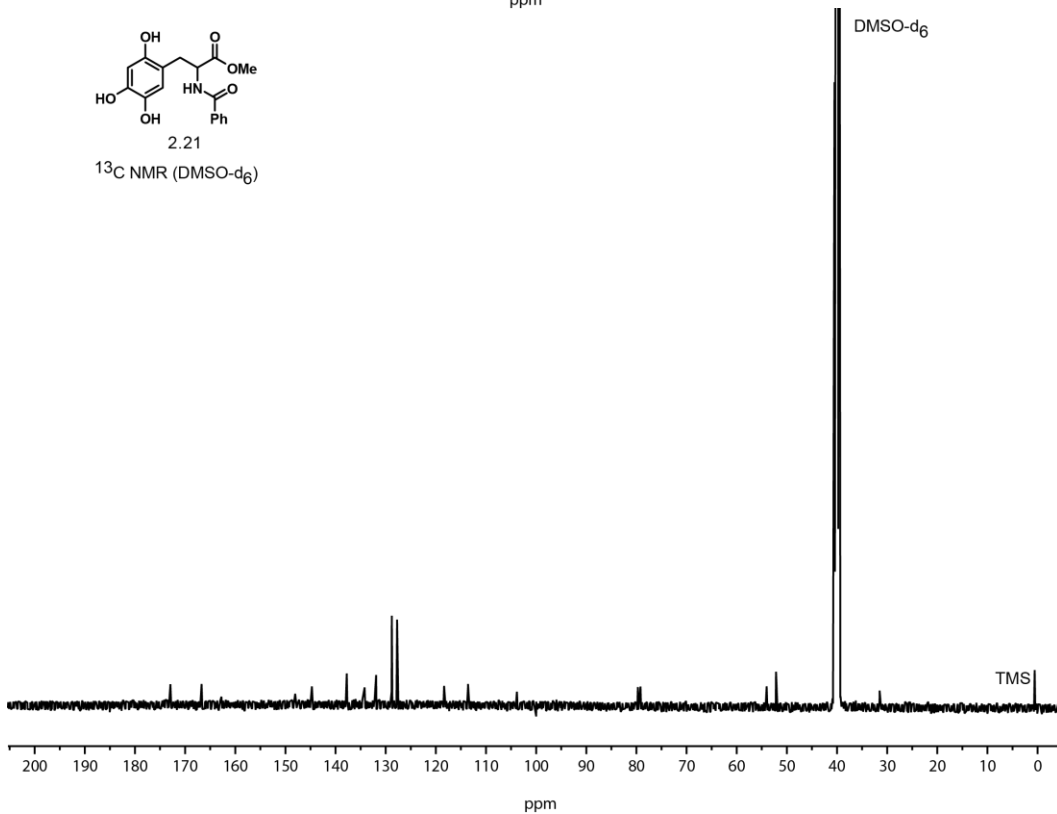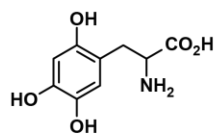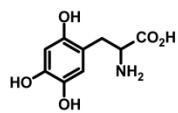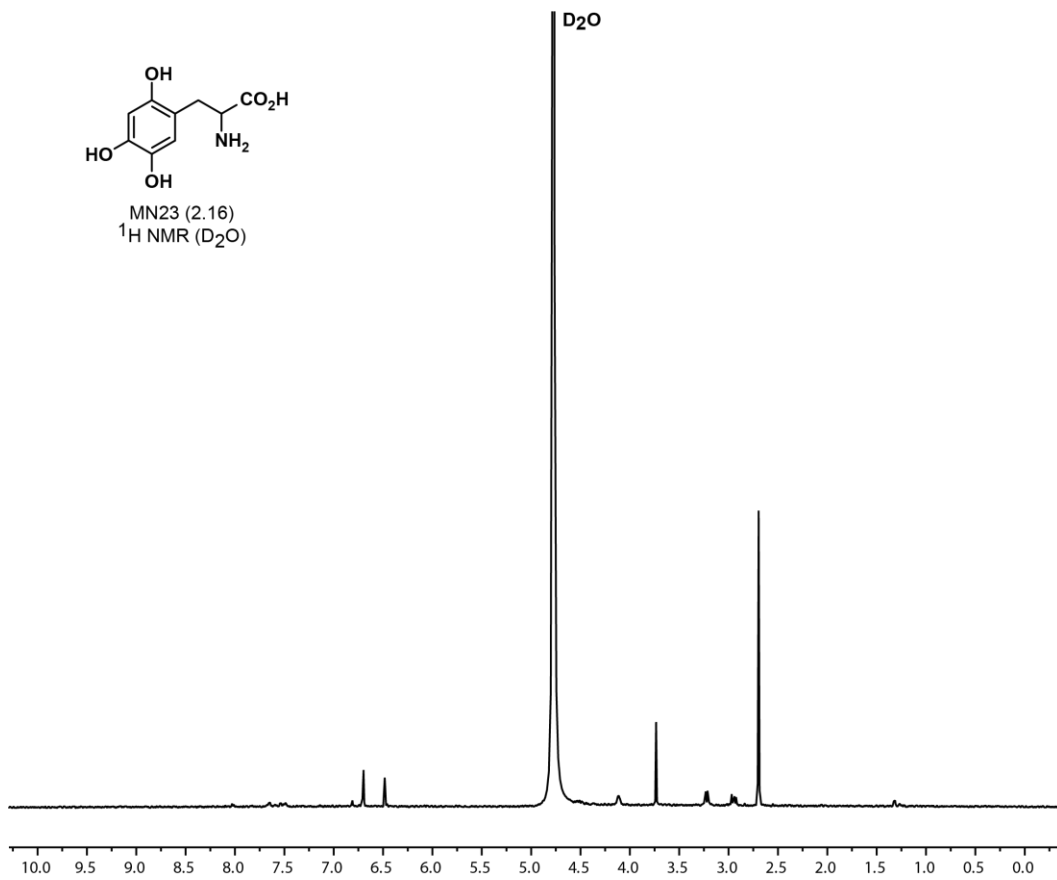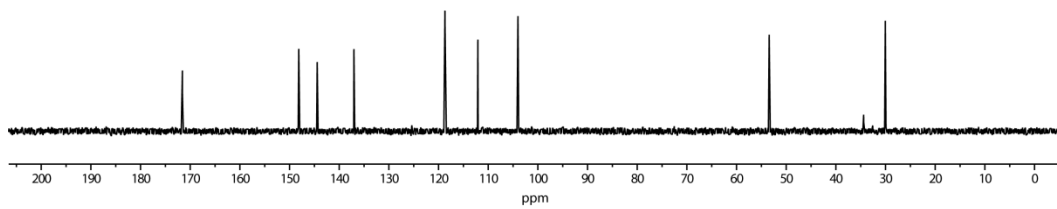
Chapter 3

SMALL MOLECULE APOBEC3G DNA CYTOSINE DEAMINASE INHIBITORS BASED ON A 4-AMINO-1,2,4-TRIAZOLE-3-THIOL SCAFFOLD

3.1 Introduction

Since the discovery of acquired immune deficiency syndrome (AIDS) and the identification of human immunodeficiency virus (HIV), the causative retrovirus of AIDS, a wealth of biochemical and immunological investigation has fuelled the development of more than twenty-five antiretrovirals and the introduction of highly active antiretroviral therapy (HAART).[205,206] Though these therapies have slowed the global AIDS epidemic and drastically prolonged the life expectancy of HIV-1-positive patients, the imminent development of drug resistance and the toxic side effects associated with HAART prompt continued efforts towards the discovery of new therapeutics with unique mechanisms of action.[207]

Research over the past decade has elucidated a previously unknown mechanism of host-virus interaction between a family of retrovirus restriction factors found in human host cells and the virally encoded virion infectivity factor (Vif).[65,85,208] APOBEC3G (apolipoprotein B mRNA editing enzyme, catalytic polypeptide-like 3G; A3G), a ssDNA C-to-U deaminase and the archetypal member of this family, is a potent restrictor of Vif-deficient HIV-1 replication. Wild-type virus, however, uses Vif to nucleate the formation of an E3 ubiquitin ligase complex that degrades A3G and enables virus replication in A3G-expressing cells. The APOBEC3-Vif interaction is therefore essential for HIV-1 infection and provides a novel, and minimally explored, target in HIV-1 drug discovery.

Current models hypothesize that A3G restricts HIV-1 replication by incorporating into budding viral particles by a RNA-Gag interaction, hijacking transport with the particle until a target cell is infected, and inhibiting viral cDNA synthesis via both deamination-independent[79] and deamination-dependent

mechanisms.[65,82-85] Deamination-independent inhibition of HIV-1 replication is predicted to occur through direct A3G interaction with viral genomic RNA, causing physical blockage to HIV-1 reverse transcriptase progression. The prominent mechanism by which A3G restricts Vif-deficient HIV-1 replication, however, is through C-to-U deamination events on minus-strand viral DNA which become immortalized as G-to-A hypermutations in the plus (genomic) strand. Such extensive mutation ultimately renders the virus non-infective.

The potent anti-HIV-1 activity of A3G has recently sparked efforts to discover inhibitors of Vif, agonists of A3G and molecules that mask the A3G-Vif interaction surfaces.[136,144,209-213] Small molecules that antagonize Vif reinstate the innate antiviral activity of A3G by boosting G-to-A hypermutation, accomplishing lethal mutagenesis. Inhibitor design strategies to increase the HIV-1 mutation rate can be defined as *"therapy by hypermutation"* (See Chapter 1.4.3 for a detailed description).[150]

Conversely, strong evidence exists to support the hypothesis that A3G is being exploited by HIV-1 through modulation by Vif. By taking advantage of the pro-mutational capabilities of A3G, HIV-1 can accomplish an advantageous level of sublethal mutation to enable viral fitness.[106,150-152] Sequenced genomes from HIV-1-positive patients support this model by exhibiting considerable A3G-dependant mutation patterns despite the ability of Vif to trigger A3G degradation.[102,214] Thus, genetic variation attributable to A3G likely contributes to the characteristically high mutation rate of HIV-1, its ability to evade immune clearance mechanisms, and its rapid evolution of resistance to antiretroviral therapies. Therefore, A3G-catalyzed mutation may be essential for HIV-1 to achieve its unprecedented level of viral fitness, and current therapies and

vaccination strategies may benefit from dampening A3G activity as HIV-1 evolution would be predicted to slow. Our strategy to reduce HIV-1 mutation by inhibiting A3G can be classified as *"therapy by hypomutation"* (See Chapter 1.4.4 for a detailed description).[150]

We recently described the development of a fluorescence-based, high-throughput screening (HTS) assay that was used to identify small molecule inhibitors of A3G.[1] In our previous study, screening of 1280 pharmacologically active compounds (LOPAC, Sigma) demonstrated the A3G-specific inhibitory capabilities of catechol-containing scaffolds, including our prototype A3G antagonist MN30 (**1.10**; IC_{50} = 9.1 µM, PubChem CID-5353329). Mutational screening, structural analysis, and mass spectrometry identified C321, located proximal to the active site, as the binding site for these catechol-based A3G inhibitors. To identify additional A3G-specific inhibitors with unique chemotypes, we screened over 325,000 compounds (Sanford-Burnham Medical Research Institute, NIH MLPCN collection) utilizing our fluorescence-based A3A/A3G DNA cytosine deamination assay.[215] A class of 4-amino-1,2,4-triazole-3-thiols and structurally related analogues were identified and developed as A3G inhibitors based on MLS-0036803, a HTS hit renamed MN256.0105 (**3.1**) in-house. Scaffolds identical or analogous to **3.1** have been previously investigated for fungicidal,[216] antioxidant,[217] cytotoxic,[218] antimicrobial[218] and anti-osteoarthritic[219] applications.
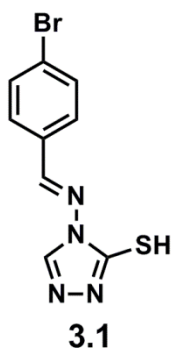
Figure 3.1. Chemical Structure of APOBEC3G Inhibitor MN256.0105 (**3.1**) and the Frequency that the 4-amino-1,2,4-triazole-3-thiol Scaffold was Observed in APOBEC3G Hits from High-throughput Screening.

3.2 Results and Discussion

3.2.1 Synthesis of 4-Amino-1,2,4-Triazole-3-Thiol Analogues.

To elucidate the mechanism of inhibition for the 4-amino-1,2,4-triazole-3-thiol class of screening hits and to reconfirm the original lead molecule, MN256.0105 (**3.1**) was synthesized (Scheme 3.1). 4-amino-1,2,4-triazole-3-thiol (**3.4**) was obtained in high yield by reaction of thiocarbohydrazide (**3.2**) in refluxing aqueous formic acid. Recrystallization from EtOH yielded pure **3.4** in 95% yield. Compound **3.1** was then obtained by condensation of **3.4** with 4-bromobenzaldehyde in excess AcOH in 82% yield. Analogue **3.8** was similarly synthesized in two steps, first by reaction of thiocarbohydrazide with AcOH under refluxing conditions to yield heterocycle **3.5**. The highest yields were accomplished by introducing an empty Dean-Stark trap to remove by distillation excess AcOH upon completion of the reaction, as opposed to the previously reported method of concentration *in vacuo*.[220] Imine formation by reaction with *p*-anisaldehyde under acidic conditions delivered **3.8** (83%, two steps).
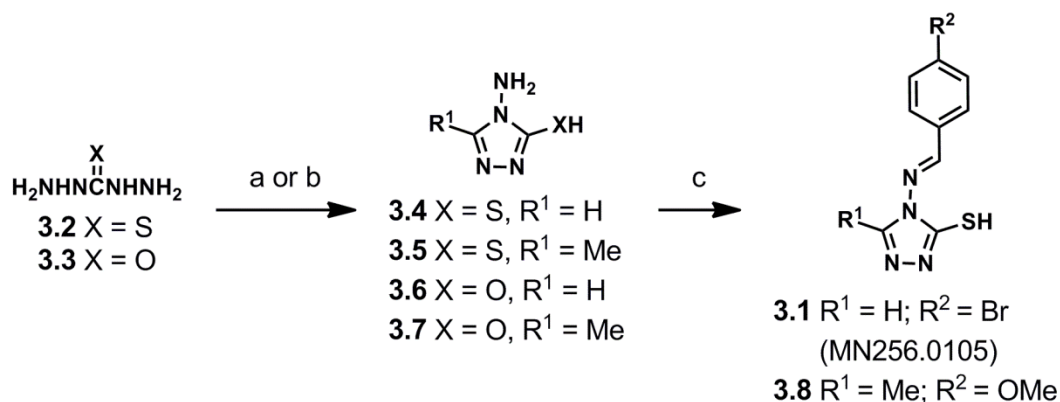
Scheme 3.1. Synthesis of **3.1** and Analogues. *Reagents and conditions:* (a) HCO$_2$H (aq.) or AcOH, reflux (to dryness), 95%-quant. (for **3.4** and **3.5**); (b) (EtO)$_3$CH or (EtO)$_3$CCH$_3$, 60 ^{o}C - reflux, 34-69% (for **3.6** and **3.7**); (c) *p*-MeOC$_6$H$_4$CHO or *p*-BrC$_6$H$_4$CHO, AcOH, reflux, 82-84%.

Chemical modification of the 4-amino-1,2,4-triazole-3-thiol heterocycle (**3.4**) was pursued to evaluate the necessity of the thiol. As shown in Scheme 3.1, the thiol moiety of congeners **3.4** and **3.5** was replaced by a hydroxyl group to deliver **3.6** and **3.7**. These scaffolds were prepared by reacting carbohydrazide with excess triethylorthoformate (**3.6**) or triethylorthoacetate (**3.7**) to achieve the core 4-amino-1,2,4-triazole-3-ol heterocycles in 69% and 34% yields, respectively.

We were also interested in evaluating scaffolds similar to **3.1** that were not subject to imine hydrolysis to evaluate effects of the additional aromatic functionality on A3G inhibitory potency. The synthesis of non-hydrolyzable amide **3.9** was accomplished in moderate yield through treatment of amine **3.5** with benzoyl chloride in refluxing dioxane (Scheme 3.2). We additionally pursued thiol protection methodologies to further gauge the necessity of a free sulfhydryl group for biological potency. For this investigation, we synthesized conjugated thiadiazole **3.10** and *S*-alkylated benzyl analogue **3.11**. Compound **3.10** was

77

prepared by treatment of **3.5** with *p*-methoxybenzonitrile and aqueous H_3PO_4 at elevated temperatures over 5 h (47% yield). Benzyl protection of **3.5** was carried out by reaction with benzyl bromide, in yields consistent with previous reports, to afford compound **3.11**.[221]
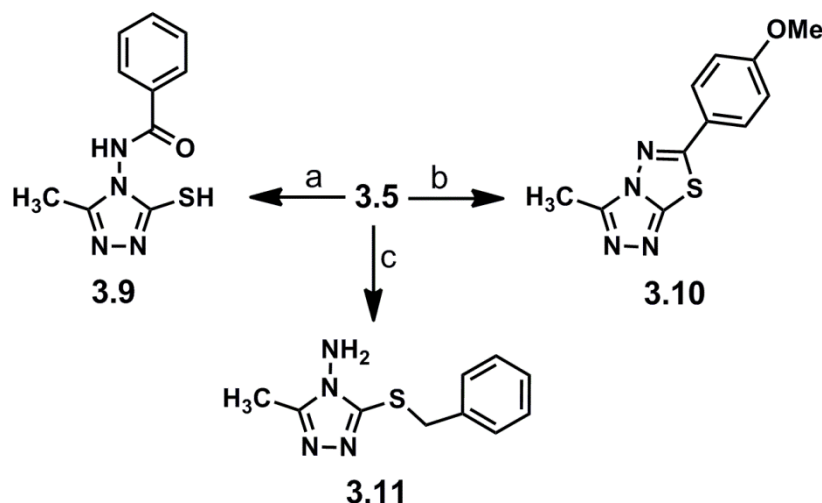
Scheme 3.2. Synthesis of 1,2,4-triazole-3-thiol Analogues. *Reagents and conditions:* (a) BzCl, dioxane, reflux, 44%; (b) *p*-methoxybenzonitrile, H_3PO_4 (aq.), reflux, 47%; (c) BnBr, NaH, DMF, rt, 14%.

3.2.2 Biological Evaluation of Synthetic Analogues

Synthesized small molecules were evaluated for A3G inhibition using our fluorescence-based deamination assay.[1] Using full-length human A3G purified from HEK293T cells and a ssDNA oligonucleotide functionalized with a 5′ 6-FAM fluorophore and a 3′-TAMRA quenching molecule, deamination efficiency was quantified by measured fluorescence. In the absence of inhibitor, deamination of the target cytosine to uracil (C-to-U) is followed by uracil DNA glycosylase-catalyzed excision of U and NaOH-catalyzed phosphodiester backbone cleavage, which releases the 6-FAM fluorophore from the TAMRA quench. Dose-

response curves were generated to determine IC_{50} values for synthesized analogues (Table 3.1).

Synthesized **3.1** exhibited equivalent A3G inhibitory activity to the HTS screened material, verifying results obtained from preliminary A3G inhibition (IC_{50} = 4.3 ± 1.1 µM versus IC_{50} = 2.0 µM, respectively). Structurally related analogue **3.8** (IC_{50} = 3.9 ± 1.2 µM) demonstrated equipotent anti-A3G activity to HTS hit **3.1** (Table 3.1). As a result, we hypothesized that small modifications to the phenyl and triazole rings have little effect on A3G inhibition.

Based on previous work with MN30 (**1.10**),[1] we hypothesized that the thiol functionalities of **3.1** and **3.8** garnered the A3G inhibitory activity. Moreover, the suspected hydrolytic susceptibility of Schiff bases **3.1** and **3.8** under biological conditions prompted us to test the 4-amino-1,2,4-triazole-3-thiol precursors **3.4** and **3.5** as A3G inhibitors. Surprisingly, **3.4** did not display any inhibitory activity at 100 µM concentrations, whereas the related 5-methyl analogue **3.5** (IC_{50} = 6.1 ± 1.1 µM) was found to be nearly equipotent to its parent scaffold **3.8** (IC_{50} = 3.9 ± 1.2 µM). Incorporation of a non-hydrolyzable linker, yielding **3.9**, maintained inhibition (IC_{50} = 8.2 ± 1.2 µM) demonstrating that pendent aromatic functionalities on the exocyclic amine have little effect on the potency of A3G inhibition by molecules of this class.

To demonstrate the necessity of the thiol component of these scaffolds, hydroxyl-substituted analogues **3.6** and **3.7** were tested against purified A3G. No inhibitory activity was detected for either molecule (Table 3.1). Furthermore, evaluation of thiol-alkylated scaffolds **3.10** and **3.11** revealed no A3G inhibition, further demonstrating the necessity of the free thiol.

Table 3.1. APOBEC3G Inhibition (IC$_{50}$) by **3.1** and **3.4**-**3.11**.[a]	
Candidate Inhibitor	IC$_{50}$ (μM)[a]
3.1	4.3 ± 1.1
3.4	No Activity
3.5	6.1 ± 1.1
3.6	No Activity
3.7	No Activity
3.8	3.9 ± 1.2
3.9	8.2 ± 1.2
3.10	No Activity
3.11	No Activity
[a]Performed in triplicate. Values shown are the mean +/- S.D.	

In addition to screening against wild-type A3G, compounds **3.1** and **3.4**-**3.11** were tested for inhibitory activity against the related cytosine deaminase enzyme, APOBEC3A (A3A), to gauge inhibitor specificity. A3A is 65% identical and 73% similar in the A3G C-terminal catalytic domain at the amino acid level. Remarkably, analogues **3.1** and **3.4**-**3.11** all failed to inhibit A3A activity at doses up to 100 μM, in spite of the inherent reactivity of the thiol functionality. To begin querying if molecules of this class can exhibit activity in cells, we screened **3.1**

and **3.4**-**3.11** for inhibitory activity against A3G in HEK293T cell lysates. Unfortunately, no measureable amounts of A3G inhibition were detected for any of the molecules screened. Consequently, the reactive thiol moiety may be unavailable for A3G inhibition in the complex environment of cell lysate.

3.2.3 Reactivity Studies of APOBEC3G Inhibitors with Cysteine-like Substrates

The known reactivity properties of thiols with cysteine residues prompted our evaluation of this scaffold to form disulfide bonds under biological conditions. Amide analogue **3.9**, which contains a free thiol, was dissolved in DMSO, diluted with PBS buffer (pH 7.4) and treated with excess cysteamine. Reaction aliquots were removed at the following time points: 0 min, 30 min, 1 hr and 12 hr and were analyzed by reverse phase HPLC for the presence of new peaks. Complete disappearance of the starting material was observed within 12 h yielding one new product, which was characterized as disulfide **3.12** by mass spectrometry (Figure 3.2). Therefore, molecules of this class that contain free thiols are capable of intercepting other thiols and forming disulfide bonds, which may confer their primary mechanism of enzyme inhibition.
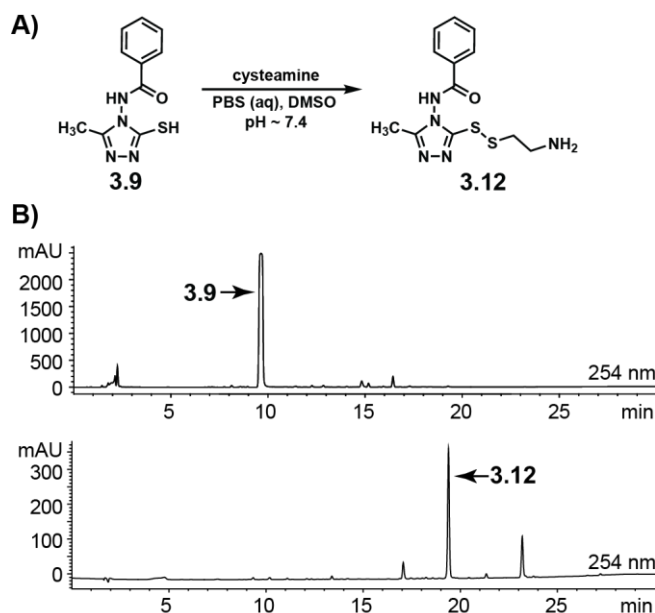
Figure 3.2. Reactivity of **3.9** with Cysteamine. (A) 4-Amino-1,2,4-triazole-3-thiol **3.9** and cysteamine were shaken in aqueous PBS (pH = 7.4) at 37 °C. Aliquots were analyzed by reverse-phase HPLC at t = 0, 30, 60 mins and 12 hr. (B). Reaction at t = 0 min (top) and t = 12 hr (bottom). Peak **3.12** was isolated and characterized by mass spectrometry HRMS-ESI⁺ *m/z* [M+Na⁺] 332.0616 (calc'd); 332.0629 (found).

3.2.4 Mutation Studies Identify C321 as the Inhibitor Binding Site

Since free thiols are required for A3G inhibition by molecules of this class, the surface cysteine residues of A3G were investigated as potential inhibitor binding sites. Previous work has demonstrated that cysteine 321 (C321) of the catalytic A3G domain is an inhibitor binding site for covalent modification by small molecules (Figure 1.10).[1] Employing this methodology, a triple mutant construct A3G-2K3A, which has three surface Cys-to-Ala substitutions (namely C243A, C321A and C356A), and a single amino acid substitution mutant A3G-C321A were tested in parallel with wild type enzyme against thiols **3.1** and **3.8** utilizing the previously described deamination assay.[1] It is important to note that in the

82

context of full-length A3G, these specific substitutions have no effect on localization, deamination, oligomerization or HIV-1 Vif-deficient restriction capabilities.[1,222,223]
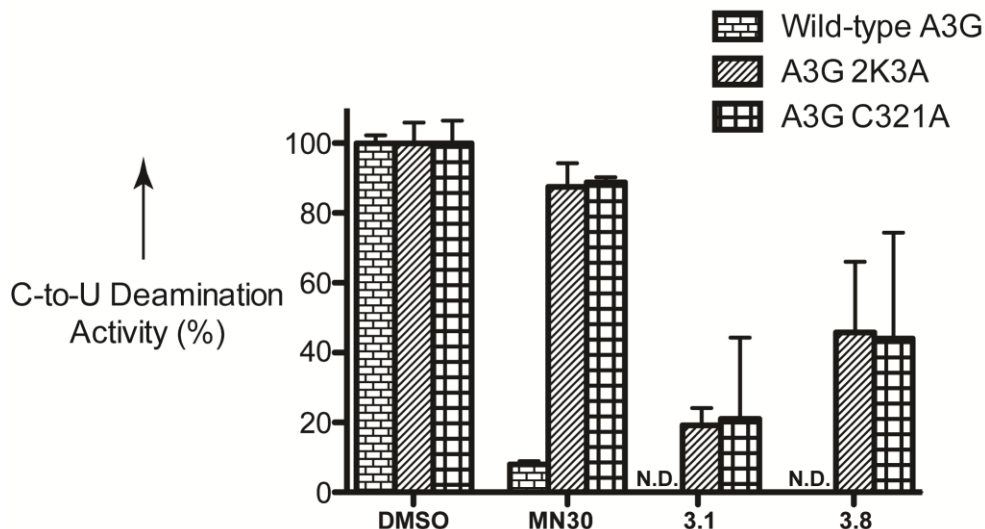
Figure 3.3. Potency of MN30 (**1.10**), **3.1** and **3.8** against Wild-type APOBEC3G and Mutants APOBEC3G-2K3A and APOBEC3G-C321A. The mean and SD of triplicate deaminase assays with 50 µM compound are shown relative to the DMSO only control. (N.D. = Not Detectable).

We found that the mutant enzymes were only partially resistant to compounds **3.1** and **3.8** with recovered deamination efficiency between 19 - 46%. Interestingly, deaminase activity was not fully recovered in comparison to DMSO control or the previously reported catechol-based covalent inhibitor MN30 (**1.10**).[1] Such results imply that these thiol-containing inhibitors may also function, at least in part, through a second inhibitory mechanism. Initial hypotheses derived from the field of transition metal catalysis suggest that the 4-amino-1,2,4-triazole-3-thiol scaffold chelates divalent metals through its thiol and exocyclic amine.[224-227] A3G, which contains a catalytic zinc atom, may therefore suffer a

decrease in deaminase efficiency in the presence of zinc chelating molecules; however, additional experiments are necessary to validate this possibility.

3.3 Conclusion

High-throughput screening and analogue synthesis have identified a class of 4-amino-1,2,4-triazole-3-thiols that inhibit the DNA cytosine deaminase A3G. Counter-screening of the small molecule analogues against related APOBEC3 family member A3A demonstrated marked specificity for A3G inhibition despite the reactivity of the inhibitors to sulfur nucleophiles. Replacement or protection of the thiol moiety of the inhibitors completely abrogated their inhibitory capabilities, providing evidence that a free thiol is a key structural feature of this class of inhibitors. A combination of mutagenesis studies and HPLC assays implicate the inhibitory activity of this class of molecules is partially accomplished through disulfide bond formation to C321, a residue adjacent to the A3G active site. These findings further support our hypothesis that covalent modification to C321 causes conformational change to the A3G protein, where Y315 shifts and sterically blocks substrate DNA cytosines from entering the A3G active site.[24]

Mutant screening potentially implicates a second mechanism of action based on the inability of the C321A mutant to fully recover deamination capabilities in comparison with DMSO control. We hypothesize that the 4-amino-1,2,4-triazole-3-thiol scaffold may engage the catalytic zinc atom in A3G conferring a secondary mechanism of enzyme inhibition, although more evidence is needed to support this theory.

3.4 Experimental Section

General Synthesis Information. Chemical reagents were purchased from Sigma-Aldrich, Alfa Aesar or Acros and used without additional purification. Bulk solvents were from Fisher Scientific and anhydrous solvents were purchased from Sigma-Aldrich. Reactions were performed under an atmosphere of dry N_2 unless otherwise noted. Silica gel chromatography was performed on a Teledyne-Isco Combiflash Rf-200 instrument using Redisep *R*f Gold High Performance silica gel columns (Teledyne-Isco) or self-packed columns with SiliaFlash 60Å silica gel (SiliCycle). HPLC analyses were performed on an Agilent 1200 series instrument equipped with a diode array detector and a Zorbax SB-C18 column (4.6 x 150 mm, 3.5 μm, Agilent Technologies) or a Zorbax SB-AQ column (4.6 x 150 mm, 3.5 μm, Agilent Technologies) for analytical-scale analysis. Compounds used in biological testing were no less than 98% pure as determined by two-wavelength HPLC analysis (254 and 215 nm), except for compounds **3.4** and **3.8**, which were 92% and 93% pure, respectively. Nuclear magnetic resonance (NMR) spectroscopy was performed using a Bruker Avance instrument operating at 400 MHz (for ^{1}H) and 100 MHz (for ^{13}C) at ambient temperature. Chemical shifts are reported in parts per million and normalized to internal solvent peaks or tetramethylsilane (0 ppm). Exchangeable protons (thiols, alcohols and amines) were verified by ^{1}H NMR D_2O exchange experiments. High-resolution mass spectrometry (HRMS) was recorded in positive-ion mode on a Bruker BioTOF II instrument.

4-Amino-1,2,4-triazole-3-thiol (3.4). Prepared as previously described.[228] ^{1}H NMR (DMSO-d$_6$): δ = 13.63 (s, 1H, SH), 8.45 (s, 1H), 5.68 ppm (s, 2H, NH$_2$); ^{13}C NMR (DMSO-d$_6$): δ = 166.0, 142.3 ppm; HRMS-ESI$^+$ *m/z* [M+Na]$^+$ calc'd for C$_2$H$_4$N$_4$S: 139.0054, found: 139.0045.

4-((4-Bromobenzylidene)amino)-1,2,4-triazole-3-thiol (3.1). To a solution of 4-amino-1,2,4-triazole-3-thiol (**3.4**, 0.219 g, 1.89 mmol) in AcOH (8.0 mL) at room temperature was added 4-bromobenzaldehyde (0.349 g, 1.89 mmol). The reaction was then heated to reflux. After 2 h, the reaction was cooled and poured into ice water. The resulting precipitate was collected, washed with water and recrystallized from hot, absolute EtOH to yield compound **3.1** as a pale yellow solid (0.438 g, 82%): ^{1}H NMR (CDCl$_3$): δ = 10.47 (s, 1H), 8.08 (s, 1H), 7.73 (d, *J* = 2.0 Hz, 2H), 7.63 ppm (d, *J* = 2.0 Hz, 2H); ^{13}C NMR (CDCl$_3$): δ = 158.83, 158.78, 140.9, 132.4, 131.2, 130.0, 127.3 ppm; HRMS-ESI$^+$ *m/z* [M+Na]$^+$ calc'd for C$_9$H$_7$BrN$_4$S: 304.9472, found: 304.9468.

4-Amino-5-methyl-1,2,4-triazole-3-thiol (3.5). A mixture of thiocarbohydrazide (**3.2**, 2.60 g, 24.5 mmol) in AcOH (5.0 mL) in a 100 mL round bottom flask was heated to reflux into an empty Dean-Stark trap. Since product formation is kinetically fast, this process served to remove excess acid which enhanced reaction yields. The reaction was allowed to proceed until product formed as a white precipitate and all acid was removed. The residual solid was removed from the flask with water, filtered and recrystallized from hot, aqueous EtOH to yield compound **3.5** as a white powder (3.16 g, 99%): ^{1}H NMR (DMSO-d$_6$): δ = 13.39 (s, 1H, SH), 5.51 (s, 2H, NH$_2$), 2.11 ppm (s, 3H, CH$_3$); ^{13}C NMR (DMSO-d$_6$): δ =

165.37, 149.08, 10.37 ppm; HRMS-ESI$^+$ *m/z* [M+Na]$^+$ calc'd for $C_3H_6N_4S$: 153.0211, found: 153.0213.

4-Amino-1,2,4-triazol-3-ol (3.6). Prepared as previously described.[229] ^{1}H NMR (DMSO-d$_6$): δ = 11.52 (s, 1H, OH), 7.80 (s, 1H), 5.26 ppm (2H, NH$_2$); ^{13}C NMR (DMSO-d$_6$): δ = 154.2, 139.3 ppm; HRMS-ESI$^+$ *m/z* [M+Na]$^+$ calc'd for $C_2H_4N_4O$: 123.0283, found: 123.0292.

4-Amino-5-methyl-1,2,4-triazol-3-ol (3.7). Carbohydrazide (**3.3**, 0.500 g, 5.550 mmol) was suspended in triethylorthoacetate (1 mL), heated from 60 – 90 ^{o}C over 45 min, and then refluxed. After 2 h, the reaction was cooled, concentrated *in vacuo* and the crude solid was recrystallized from hot, absolute EtOH to yield compound **3.7** as a white crystalline solid (0.214 g, 34%): ^{1}H NMR (DMSO-d$_6$): δ = 11.23 (s, 1H, OH), 5.10 (s, 2H, NH$_2$), 2.07 ppm (s, 3H); ^{13}C NMR (DMSO-d$_6$): δ = 154.3, 145.4, 10.7 ppm; HRMS (ESI $^+$) *m/z* [M+H]$^+$ calc'd for $C_3H_6N_4O$: 115.0614, found: 115.0615.

4-((4-Methoxybenzylidene)amino)-5-methyl-1,2,4-triazole-3-thiol (3.8). To a solution of **3.3** (0.100 g, 0.768 mmol) in AcOH (3.5 mL) at room temperature was added *p*-anisaldehyde (93 µL, 0.800 mmol). The reaction was heated to reflux for 2 h, then cooled and poured into ice water. The resulting precipitate was collected and washed with water to yield compound **3.8** as a pale yellow solid (0.160 g, 84%) without further purification: ^{1}H NMR (DMSO-d$_6$): δ = 13.67 (s, 1H), 9.71 (s, 1H), 7.86 (d, *J* = 8.0 Hz, 2H), 7.10 (d, *J* = 8.0 Hz, 2H), 3.85 (s, 3H), 2.32 ppm (s, 3H); ^{13}C NMR (CDCl$_3$): δ = 163.3, 162.4, 161.5, 149.8, 130.8, 125.2,

114.6, 55.6, 11.3 ppm; HRMS-ESI$^+$ *m/z* [M+Na]$^+$ calc'd for $C_{11}H_{12}N_4OS$: 271.0630, found: 271.0617.

***N*-(3-Mercapto-5-methyl-1,2,4-triazol-4-yl)benzamide (3.9).** A solution of **3.3** (0.100 g, 0.770 mmol) in dioxane (5 mL) was treated with benzoyl chloride (100 μL, 0.770 mmol) and heated at reflux for 24 h. The reaction mixture was cooled to rt and concentrated *in vacuo*. SiO$_2$ purification (gradient 40-100% ethyl acetate in hexanes) gave compound **3.9** as a white solid (80.0 mg, 44%): ^{1}H NMR (DMSO-d$_6$): δ = 13.73 (s, 1H, SH), 11.78 (s, 1H, NH), 8.01-7.98 (m, 2H), 7.71-7.57 (m, 3H), 2.20 ppm (s, 3H); ^{13}C NMR (DMSO-d$_6$): δ = 167.0, 165.4, 149.9, 132.9, 130.9, 128.8, 127.9, 10.0 ppm; HRMS-ESI$^+$ *m/z* [M+Na]$^+$ calc'd for $C_{11}H_{11}N_3OS$: 257.0473, found: 257.0288.

6-(4-Methoxyphenyl)-3-methyl-1,2,4-triazolo[3,4-*b*][1,3,4]thiadiazole (3.10). 4-Methoxybenzonitrile (0.100 g, 0.75 mmol) and **3.5** (0.098 g, 0.75 mmol) were suspended in aqueous H_3PO_4 (5 mL) and heated to reflux. After 5 h, the mixture was diluted with an excess of H_2O, neutralized with aqueous NaOH (40% w/v soln) to pH 7-8, and concentrated *in vacuo* to yield compound **3.10** as a pale yellow powder (0.087 g, 47%): ^{1}H NMR (CDCl$_3$): δ = 7.83 (d, *J* = 8.0 Hz, 2H), 7.03 (d, *J* = 8.0 Hz, 2H), 3.90 (s, 3H), 2.76 ppm (s, 3H); ^{13}C NMR (CDCl$_3$): δ = 166.2, 163.2, 153.1, 144.9, 129.0, 122.1, 115.0, 55.8, 10.6 ppm; HRMS-ESI $^+$ *m/z* [M+Na]$^+$ calc'd for $C_{12}H_{11}N_3OS$: 269.0473, found: 269.0468.

3-(Benzylthio)-5-methyl-1,2,4-triazol-4-amine (3.11). Prepared as previously described.[221] ^{1}H NMR (CDCl$_3$): δ = 7.45-7.43 (m, 2H), 7.36-7.30 (m, 3H), 4.60 (s, 2H), 2.37 ppm (s, 3H); ^{13}C NMR (DMSO-d$_6$): δ = 158.7, 152.0, 137.1, 128.7,

127.7, 127.1, 34.4, 10.8 ppm; HRMS-ESI$^+$ m/z [M+H]$^+$ calc'd for $C_{10}H_{12}N_4S$: 221.0861, found: 221.0871.

Expression and Purification of APOBEC3A, APOBEC3G, APOBEC3G 2K3A and APOBEC3G C321A. A3G, A3A, A3G 2K3A and A3G C321A were expressed and purified as previously described.[1]

DNA Deaminase Assay. The DNA deaminase assay was performed as previously described with the ssDNA oligomer 5′-6-FAM-AAA-TAT-TCC-CTA-ATA-GAT-AAT-GTG-A-TAMRA-3′.[1] Deaminase assays with mutant A3G were performed with 50 μM compound, 0.0675 μM A3G, 0.33 μM ssDNA, and excess UDG. None of the synthesized compounds inhibited uracil DNA glycosylase in the context of the in vitro assay.

HPLC Assay for Disulfide Formation. A solution of **3.9** (10.0 mg, 0.040 mmol) in DMSO (100 μL) was diluted with 1x aqueous PBS (5 mL, pH 7.4) and treated with cysteamine (0.684 g, 4.03 mmol, 100 eq). The solution was then shaken at 37 ^{o}C. Aliquots of the reaction mixture were taken at the following time points: 0 min, 30 min, 60 min and 12 h. These reaction aliquots were analyzed by reverse phase analytical HPLC. The HPLC analytical method (Zorbax SB-C18 4.6 x 150 mm, 3.5 μm column, Agilent Technologies; flow rate = 1.0 mL/min) involved isocratic 10% CH_3CN in 0.1% (v/v) aqueous CF_3CO_2H (0 to 2 min), followed by linear gradients of 10-85% CH_3CN (2-24 min) and 85%-95% CH_3CN (24-26 min). The major peak **3.12** (Figure 3.2) was isolated, concentrated in vacuo, and characterized by mass spectrometry. HRMS (ESI$^+$) m/z calc'd for $C_{12}H_{15}N_5OS_2$ [M+Na]$^+$ 332.0616; found 332.0629.

3.5 Spectral Data for Synthesized Compounds

4-((4-bromobenzylidene)amino)-1,2,4-triazole-3-thiol (3.1)
^{1}H NMR (CDCl$_3$):
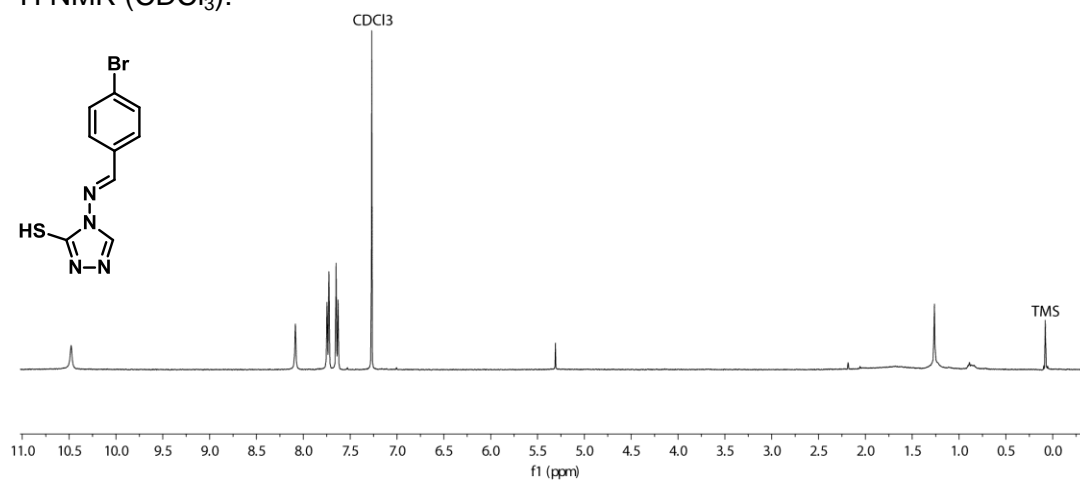
4-((4-bromobenzylidene)amino)-1,2,4-triazole-3-thiol (3.1)
^{13}C NMR (CDCl$_3$):
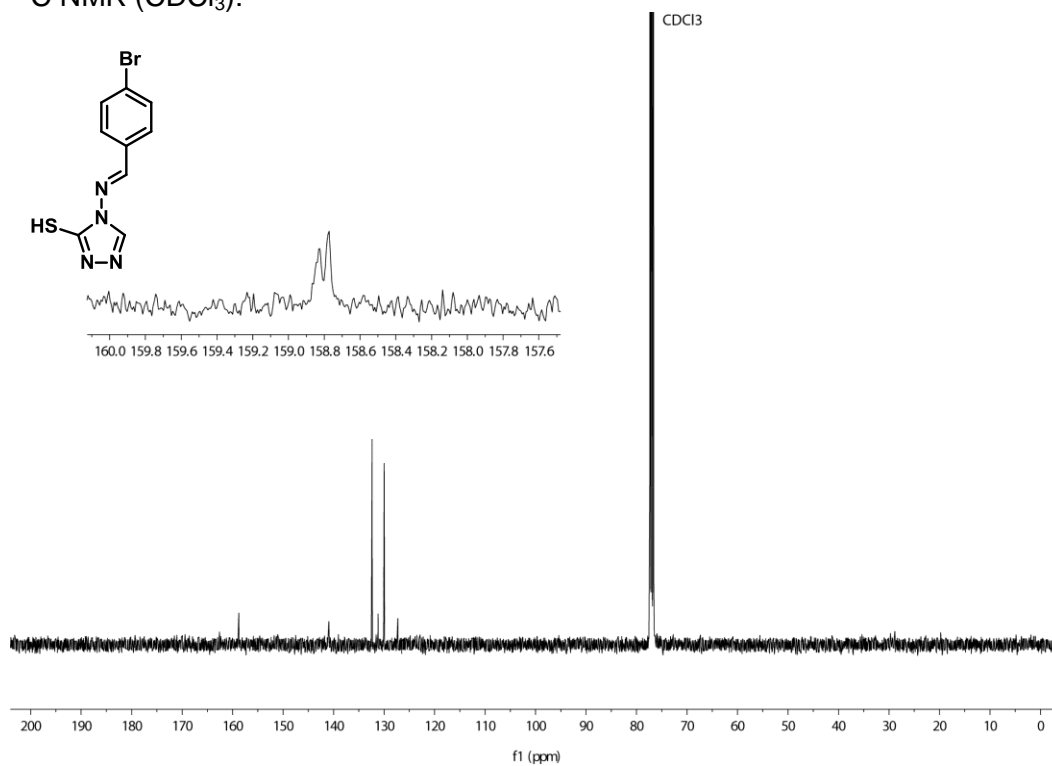
4-amino-1,2,4-triazole-3-thiol (3.4)
^{1}H NMR (DMSO-d_6):

DMSO-d6

TMS

f1 (ppm)
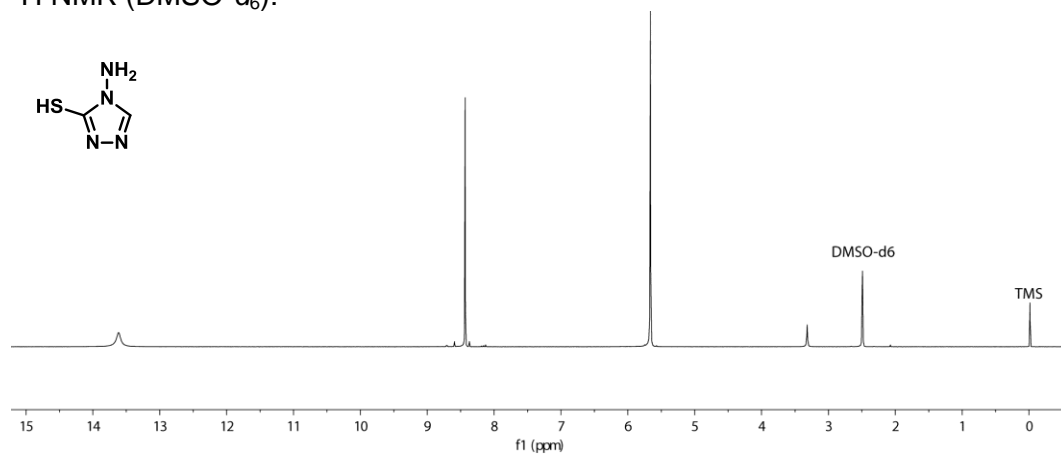
4-amino-1,2,4-triazole-3-thiol (3.4)
^{13}C NMR (DMSO-d_6):

DMSO-d6

f1 (ppm)
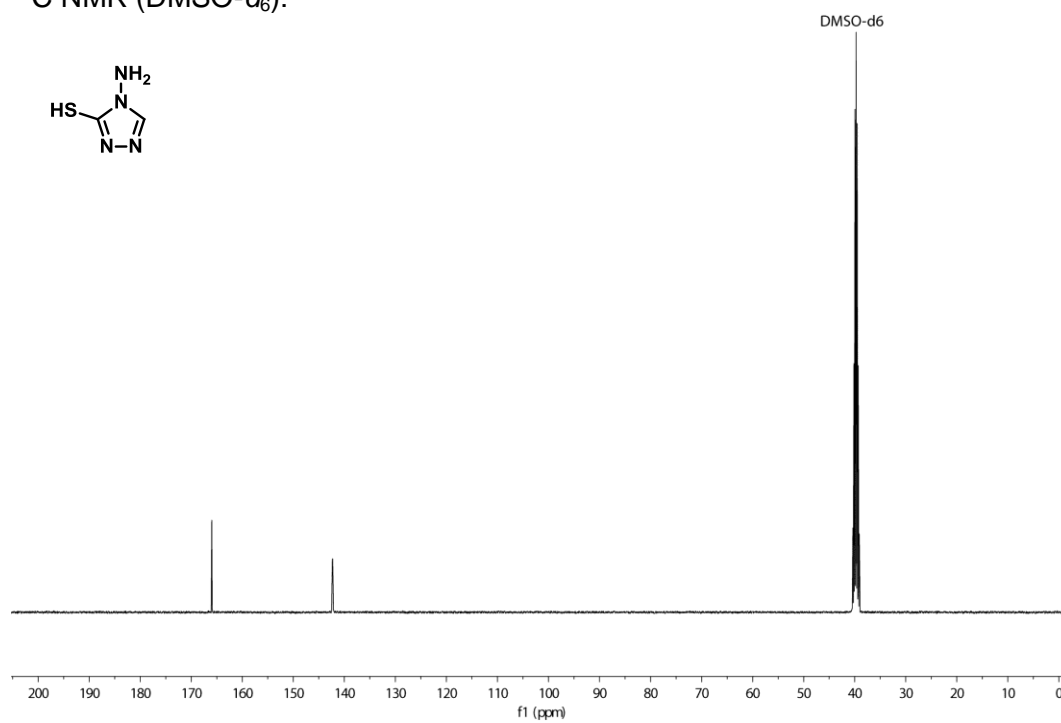
4-amino-5-methyl-1,2,4-triazole-3-thiol (3.5)

^{1}H NMR (DMSO- d_6):
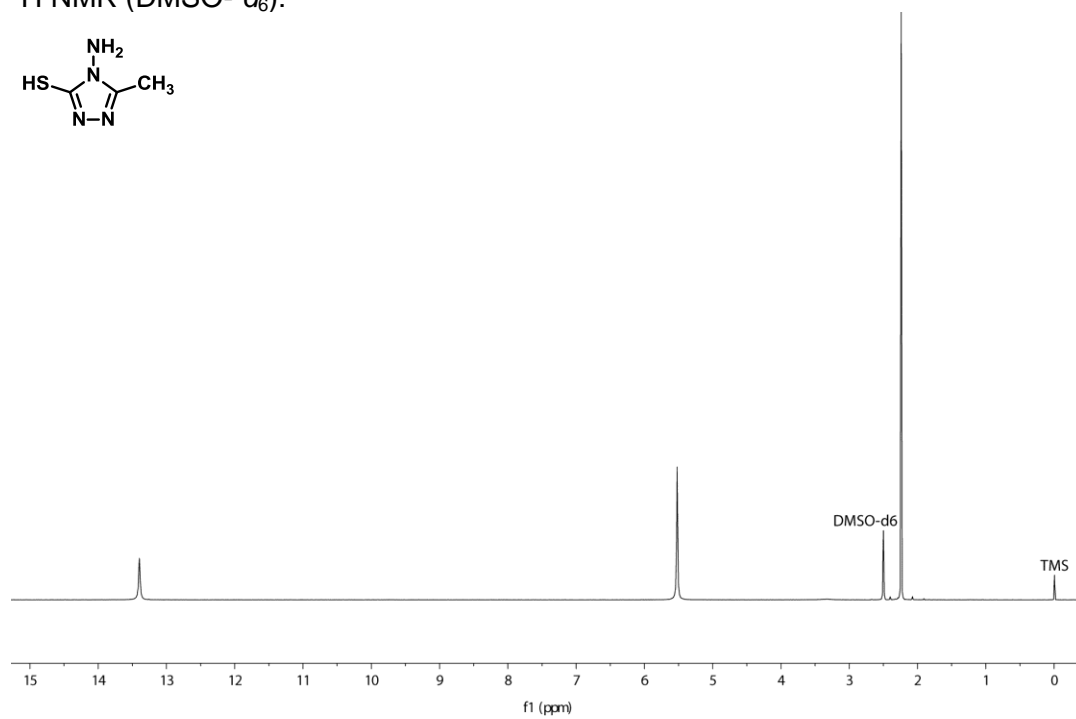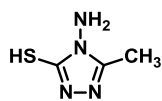
4-amino-5-methyl-1,2,4-triazole-3-thiol (3.5)

^{13}C NMR (DMSO-d_6):

92
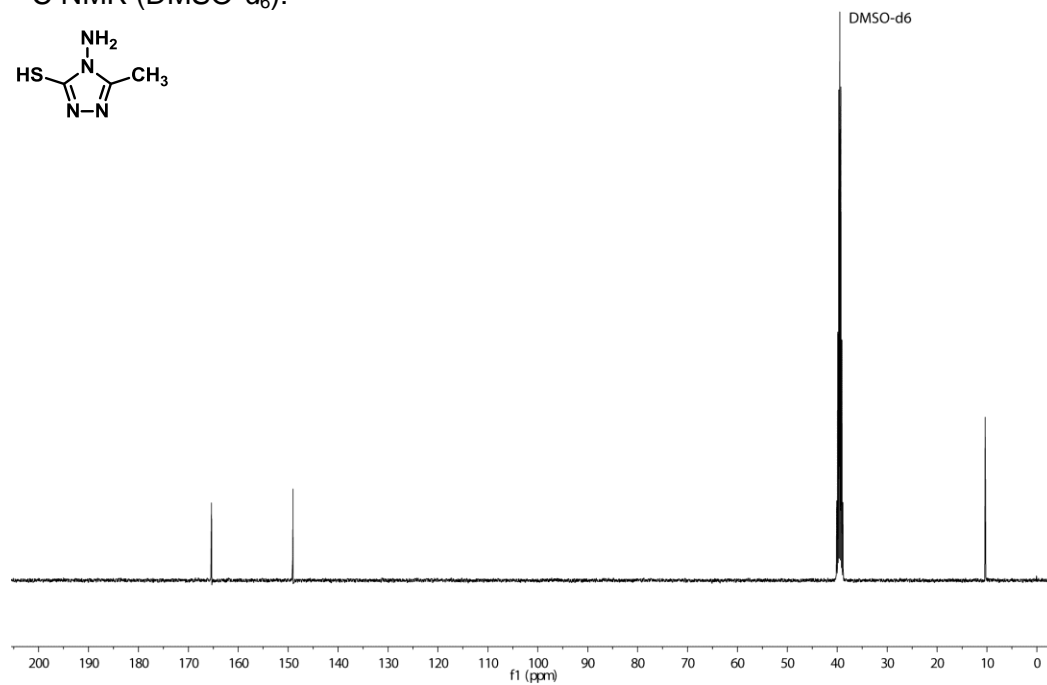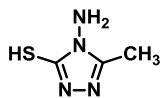
4-amino-1,2,4-triazol-3-ol (3.6)
^{1}H NMR (DMSO-d_6):
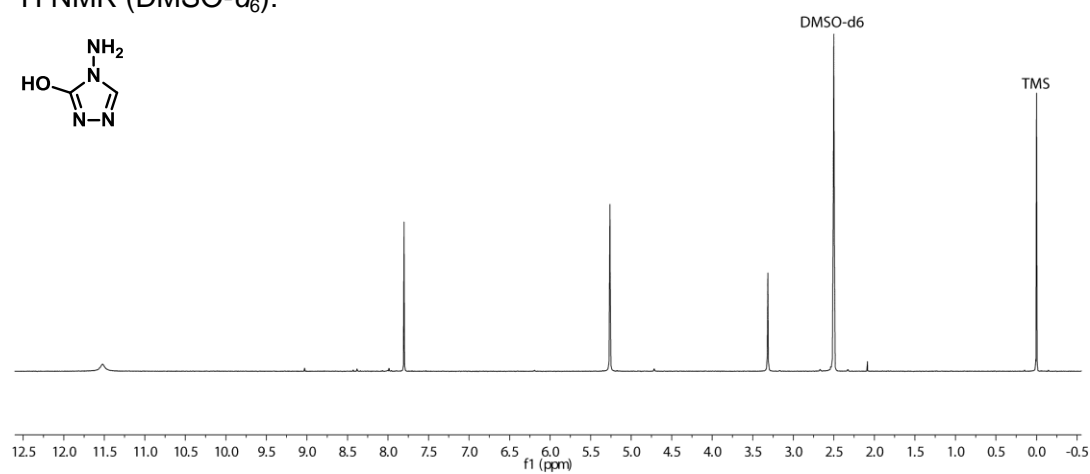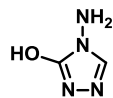
4-amino-1,2,4-triazol-3-ol (3.6)
^{13}C NMR (DMSO-d_6):
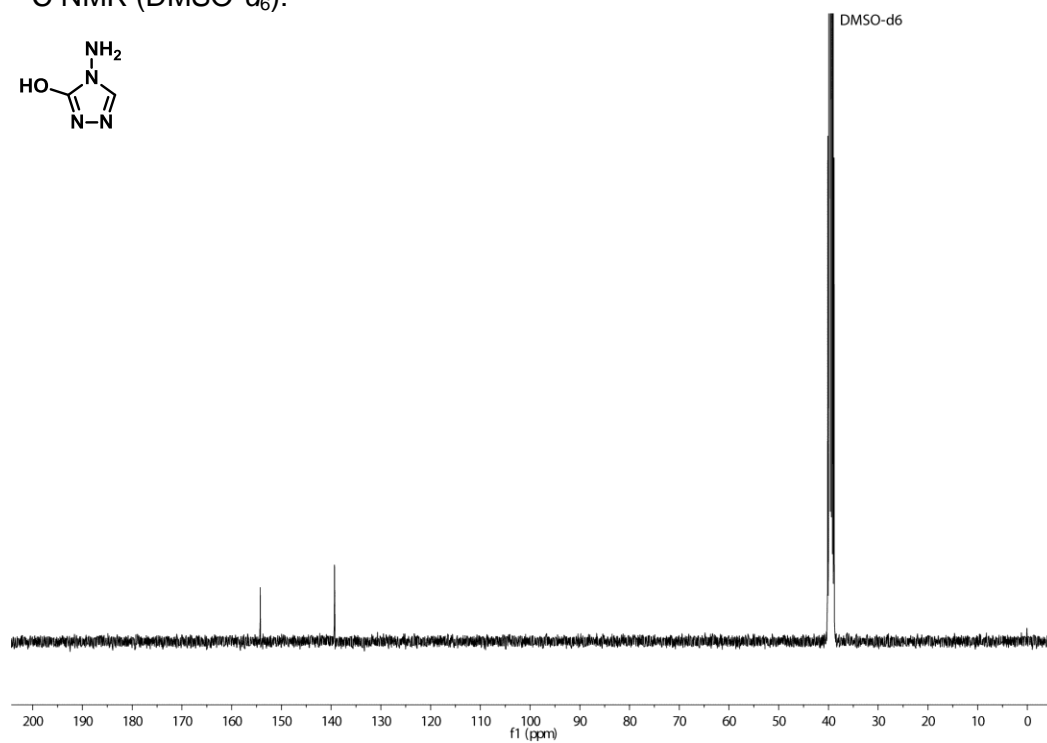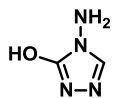
4-amino-5-methyl-1,2,4-triazol-3-ol (3.7)
^{1}H NMR (DMSO-d_6):
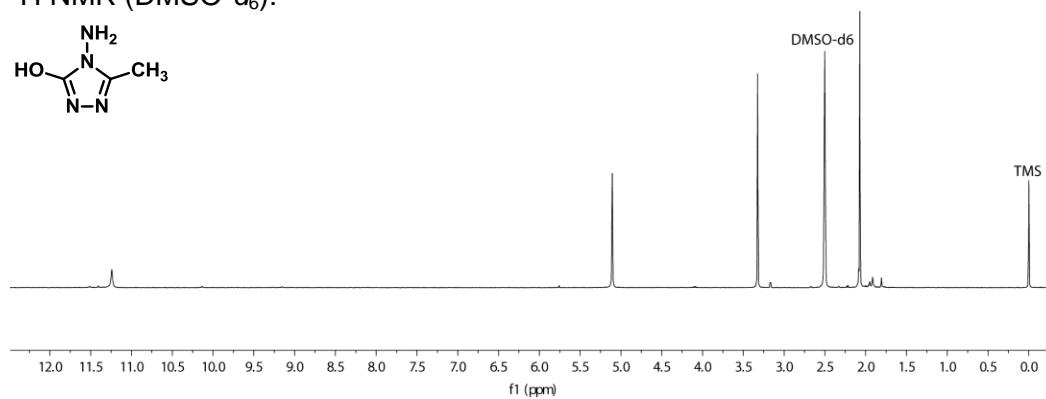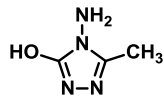
4-amino-5-methyl-1,2,4-triazol-3-ol (3.7)
^{13}C NMR (DMSO-d_6):
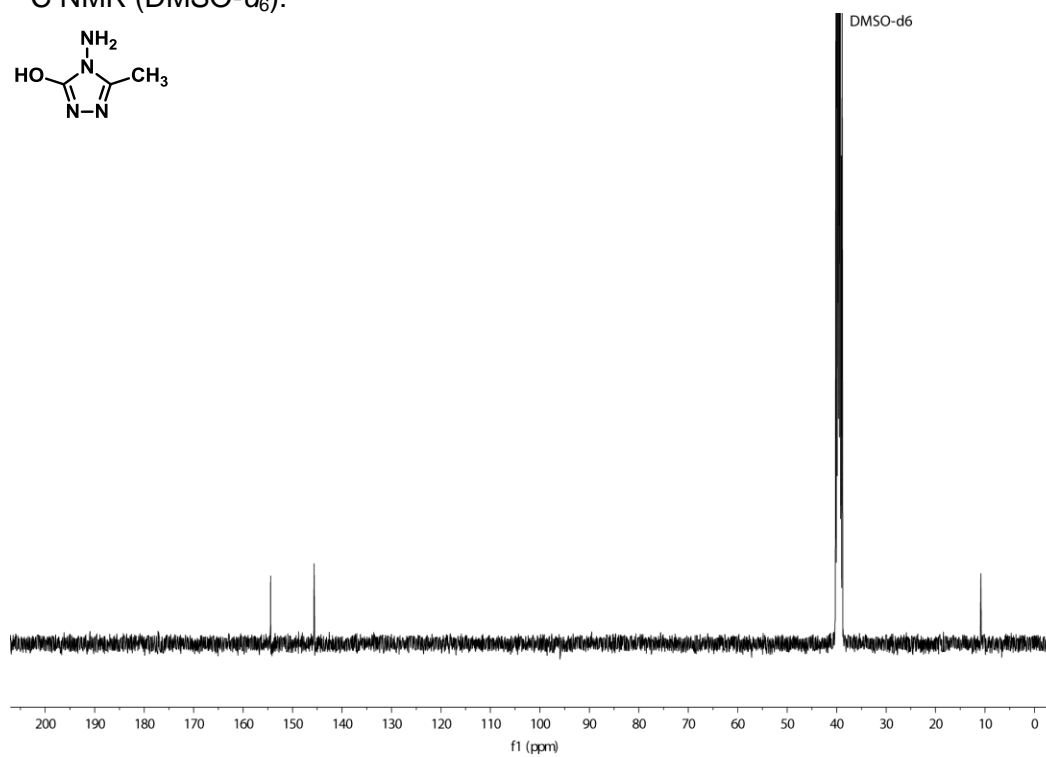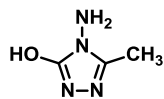
4-((4-methoxybenzylidene)amino)-5-methyl-1,2,4-triazole-3-thiol (3.8)

^{1}H NMR (DMSO-d_6):
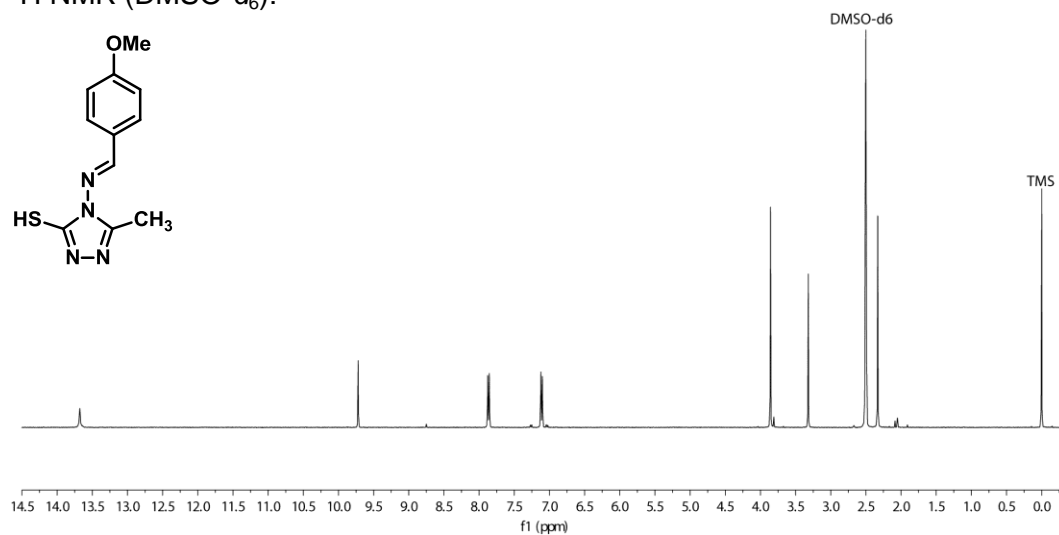
4-((4-methoxybenzylidene)amino)-5-methyl-1,2,4-triazole-3-thiol (3.8)
^{13}C NMR (CDCl$_3$):
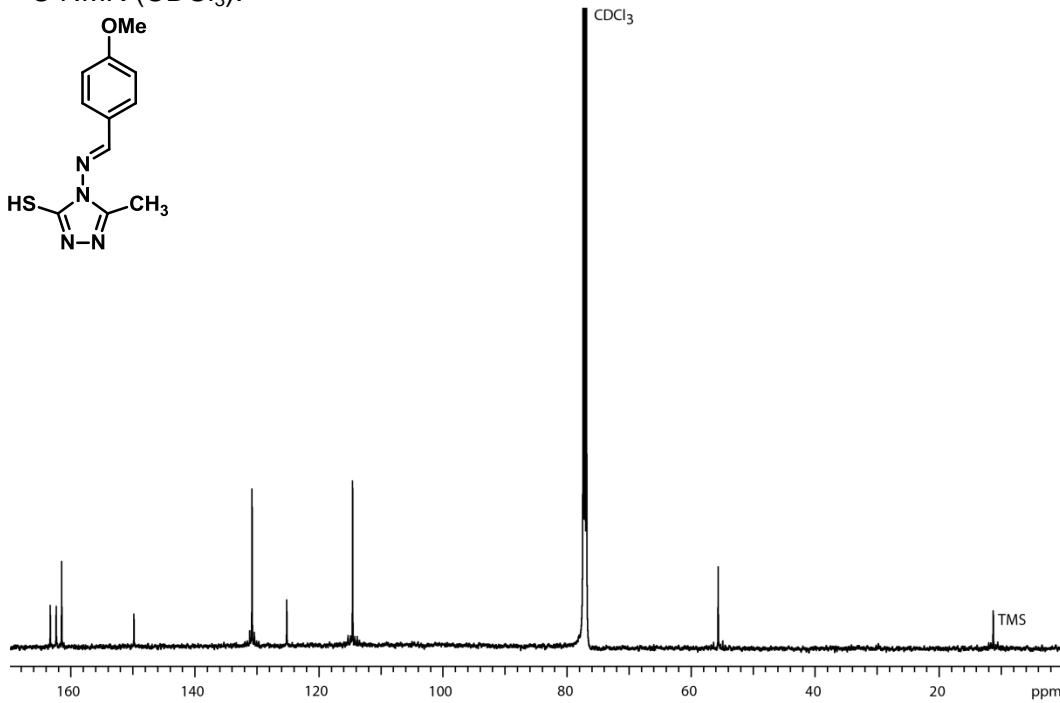
N-(3-mercapto-5-methyl-1,2,4-triazol-4-yl)benzamide (3.9)
^{1}H NMR (DMSO-d_6):
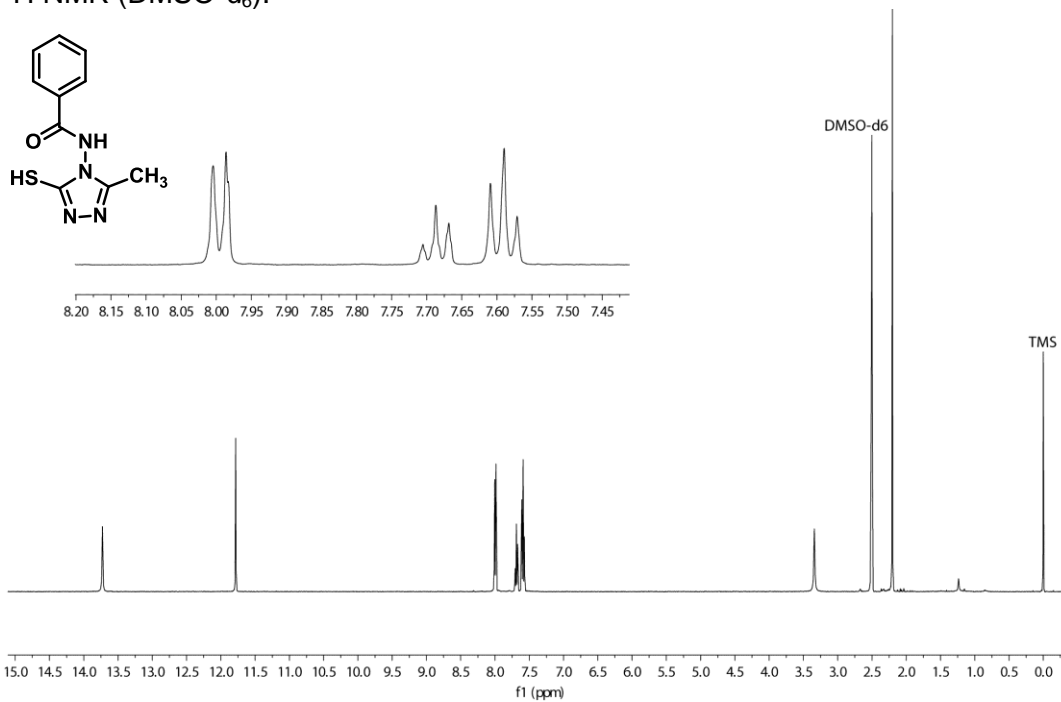
N-(3-mercapto-5-methyl-1,2,4-triazol-4-yl)benzamide (3.9)
^{13}C NMR (DMSO-d_6):
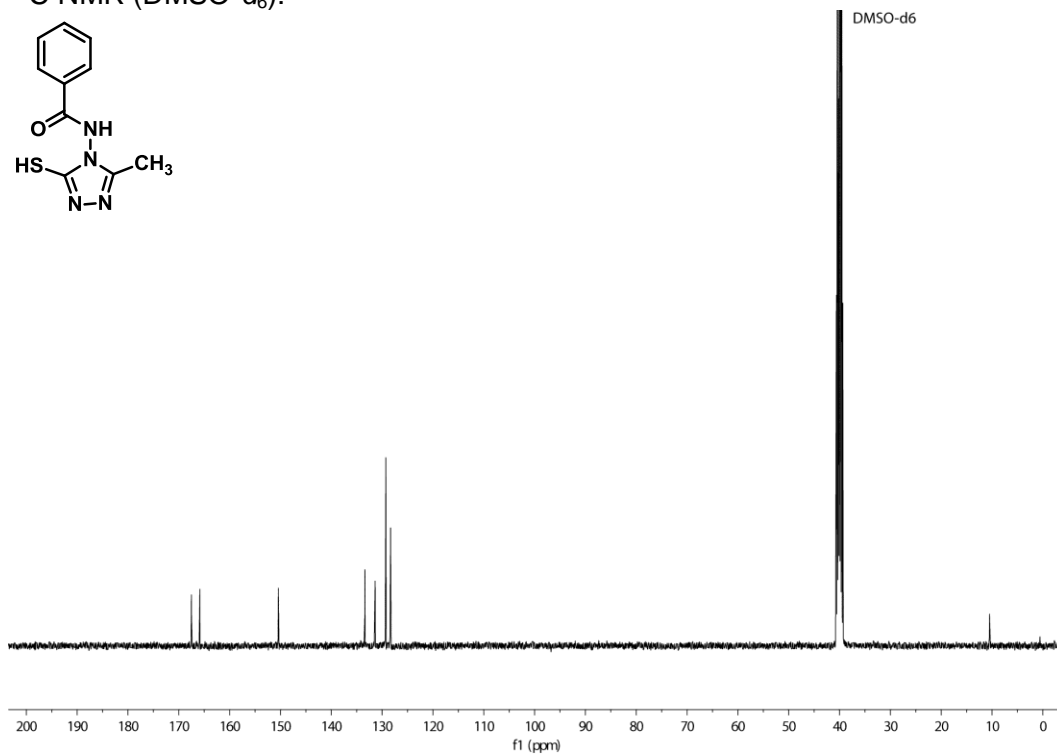
6-(4-methoxyphenyl)-3-methyl-[1,2,4]triazolo[3,4-b][1,3,4]thiadiazole (3.10)
^{1}H NMR (CDCl$_3$):
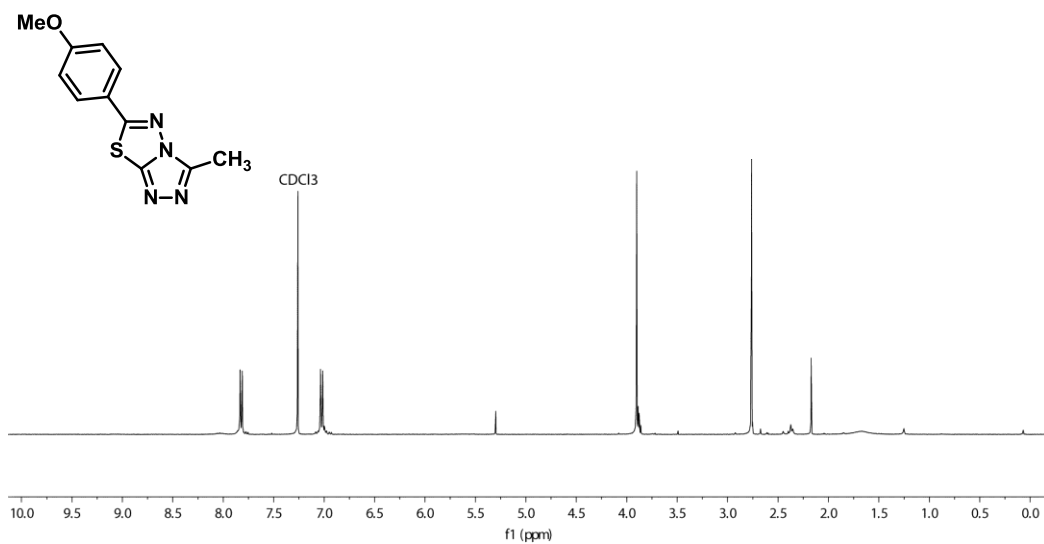
6-(4-methoxyphenyl)-3-methyl-[1,2,4]triazolo[3,4-b][1,3,4]thiadiazole (3.10)
^{13}C NMR (CDCl$_3$):
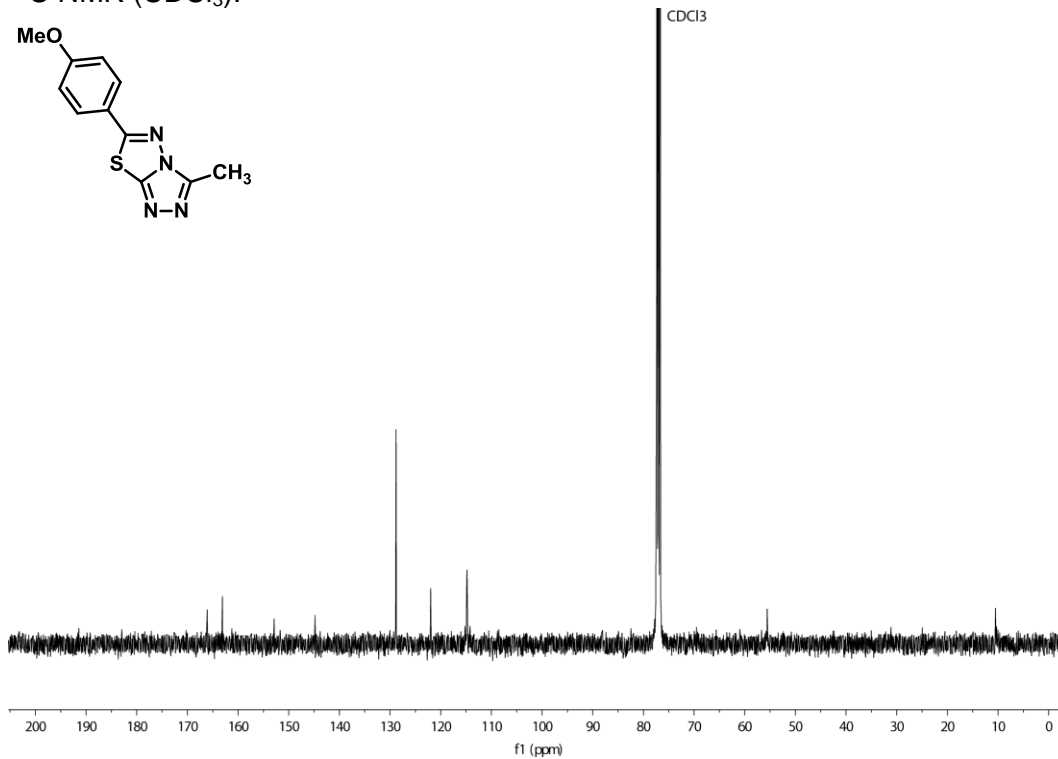
3-(benzylthio)-5-methyl-1,2,4-triazole-4-amine (3.11)
^{1}H NMR (CDCl$_3$):
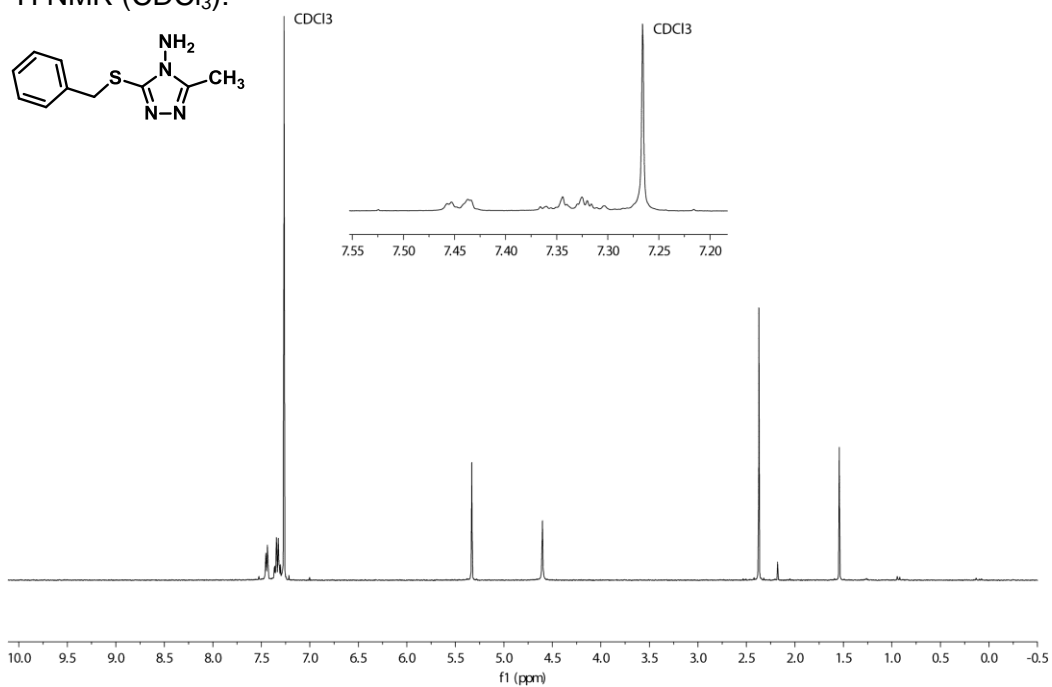
3-(benzylthio)-5-methyl-1,2,4-triazole-4-amine (3.11)
^{13}C NMR (DMSO-d_6):
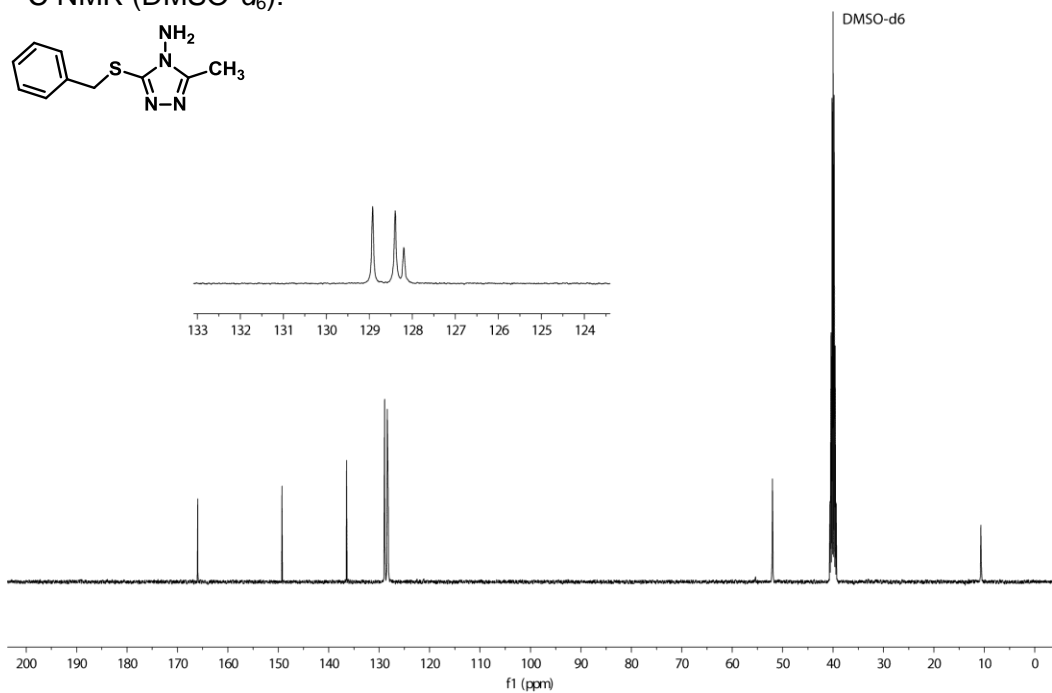
3.6 HPLC Data for Synthesized Compounds

Compounds evaluated biochemically were no less than 98% pure as determined by two-wavelength HPLC analysis (254 and 215 nm), except for compounds **3.4** and **3.8**, which were 92% and 93% pure, respectively. HPLC analyses were performed using one of the following methods as noted:

Method A: Zorbax SB-C18 column (4.6 x 150 mm, 3.5 µm, Agilent Technologies), flow rate = 1.0 mL/min, isocratic 10% CH_3CN in 0.1% (v/v) aqueous CF_3CO_2H (0 to 2 min), followed by linear gradients of 10% to 85% CH_3CN in 0.1% (v/v) aqueous CF_3CO_2H (2 to 24 min) and 85% to 95% CH_3CN in 0.1% (v/v) aqueous CF_3CO_2H (24 to 26 min)

Method B: Zorbax SB-AQ column (4.6 x 150 mm, 3.5 µm, Agilent Technologies), flow rate = 1.0 mL/min, isocratic 0.1% (v/v) aqueous CF_3CO_2H (0 to 5 min), linear gradient of 0% to 80% CH_3CN in 0.1% (v/v) aqueous CF_3CO_2H (5 to 15 min)

4-((4-bromobenzylidene)amino)-*4H*-1,2,4-triazole-3-thiol (3.1) [Method A]
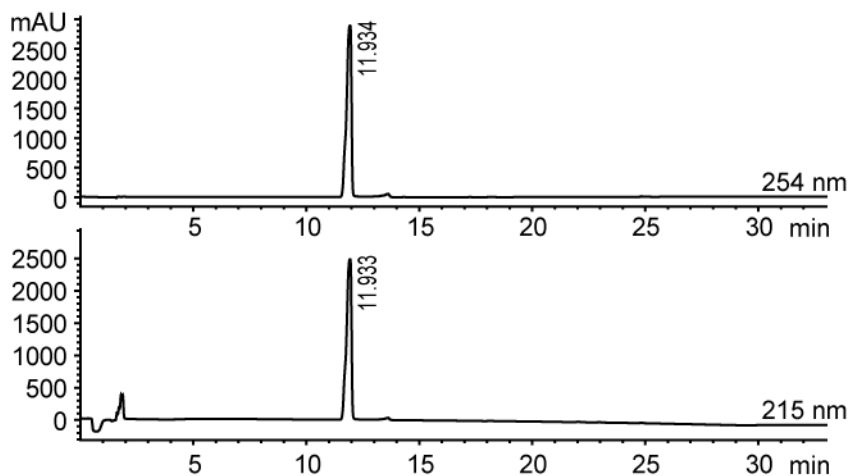
4-amino-*4H*-1,2,4-triazole-3-thiol (3.4) [Method B]
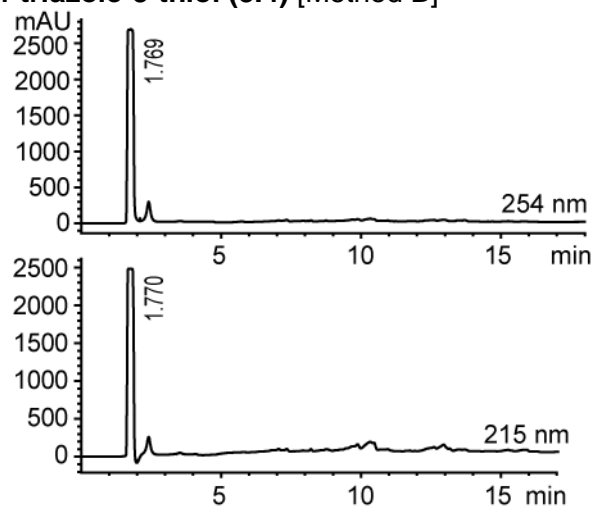
4-amino-5-methyl-1,2,4-triazole-3-thiol (3.5) [Method B]
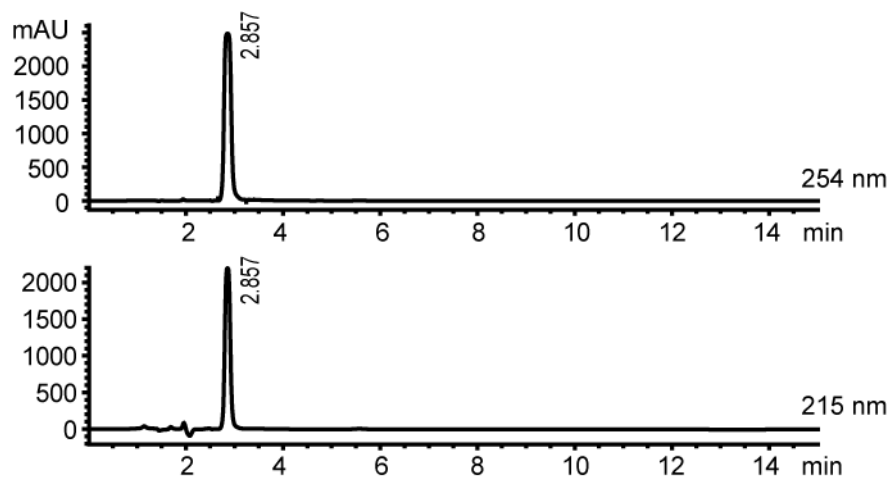
4-amino-*4H*-1,2,4-triazol-3-ol (3.6) [Method B]
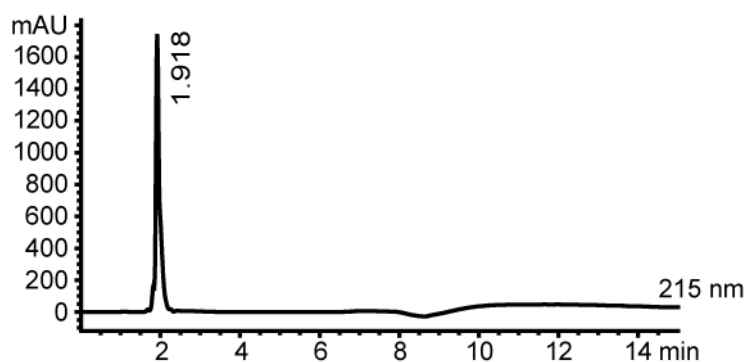
4-amino-5-methyl-1,2,4-triazol-3-ol (3.7) [Method B]
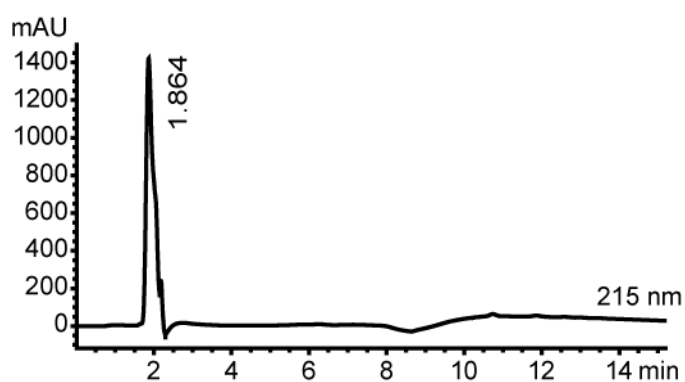
4-((4-methoxybenzylidene)amino)-5-methyl-1,2,4-triazole-3-thiol (3.8)
[Method A]
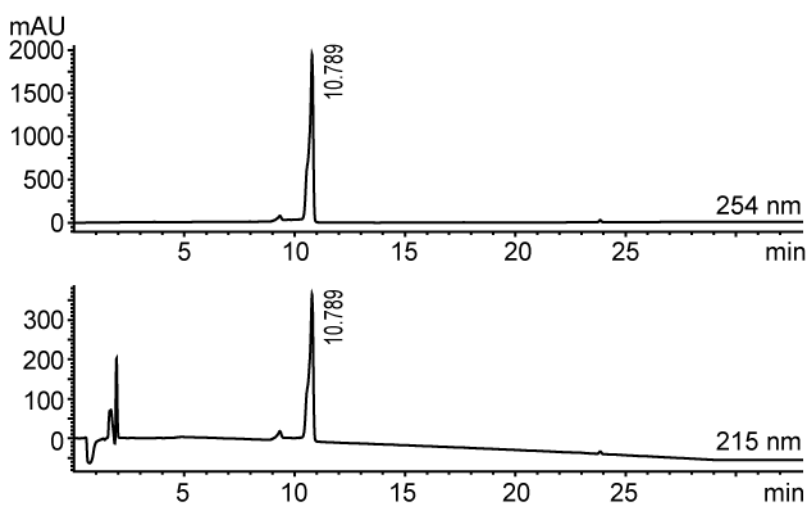
N-(3-mercapto-5-methyl-1,2,4-triazol-4-yl)benzamide (3.9) [Method A]
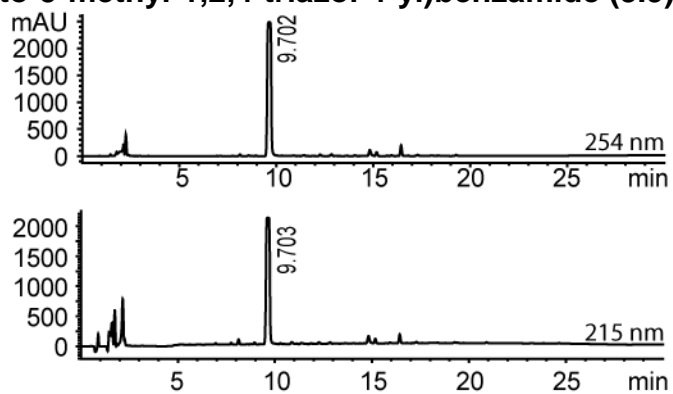
6-(4-methoxyphenyl)-3-methyl-[1,2,4]triazolo[3,4-b][1,3,4]thiadiazole (3.10) [Method A]
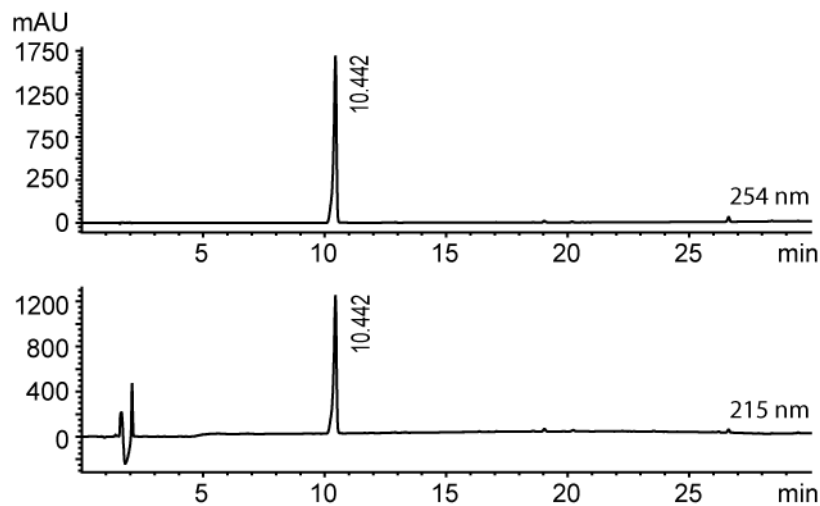
3-(benzylthio)-5-methyl-*4H*-1,2,4-triazole-4-amine (3.11) [Method A]

3.7 Acknowledgements

CHAPTER 4

Oxidative Reactivities of 2-Furylquinolines: Ubiquitous Scaffolds in Common High-Throughput Screening Libraries

4.1 Introduction

The translation of high-throughput screening (HTS) hits to mechanistic probes and lead molecules for drug discovery is often plagued by false positives: compounds that exhibit the desired assay outcome though not as a result of specific interaction with the intended biological target.[230] In 2007, Inglese, Shamu & Guy recommended guidelines for reporting HTS-identified small molecules after recognizing the absence of standards for publishing such discoveries.[192] Included in this commentary is caution for scientists employing HTS to structurally validate their identified small molecules prior to publication, as false positives can not only result in inaccurate data reporting, but their characterization and elimination can burden a drug discovery campaign.[192,231]

Annotations of chemical libraries to identify scaffolds prone to hit in unrelated assays have been performed in recent years. These offending compounds, termed Pan Assay Interference Scaffolds or PAINS, result as a consequence of the physical and chemical properties of the small molecule and/or its interactions with certain components of the HTS assay.[200-203] False positives can arise through various mechanisms including colloidal aggregation, compromised chemical integrity, or inherent reactivity of the small molecule; in addition to organic and/or inorganic impurities in the compound stock solution.[232-238] Maintaining the chemical integrity of small molecule libraries as dimethylsulfoxide (DMSO) stock solutions upon long-term storage and freeze/thaw cycles remains a fundamental concern.[239-241] It is known that a percentage of HTS library members decompose when stored in DMSO, which is the most common solvent employed.[233] A number of decomposition mechanisms

are possible, such as hydrolysis, oxidation, isomerization, and rearrangement reactions. Moreover, compounding factors such as organic (e.g., residual solvent) and inorganic (e.g., salt) impurities may promote decomposition.[233] Herein, we report the decomposition of a seemingly stable HTS scaffold whose substructure is present in 133 of the 329,510 NIH MLPCN library members.

Our laboratories have performed HTS to identify small molecule inhibitors of the DNA cytosine deaminases APOBEC3A (A3A) and APOBEC3G (A3G).[1] The APOBEC3 (apolipoprotein B mRNA editing enzyme, catalytic polypeptide-like 3) family functions *in vivo* to deaminate single-stranded DNA (ssDNA) cytosines to uracils (C-to-U), initiating the protective mechanism of foreign DNA degradation.[242] APOBEC3s, in most cases, play a protective role as an innate immune defense mechanism in cells; however the mutative capacity of A3 enzymes may also contribute to human disease. A3G is predicted to drive human immunodeficiency virus-1 (HIV-1) evolution by enabling a consistent source of sublethal mutation in the HIV-1 genome.[16,105,130] Moreover, the expression of nuclear-localized APOBEC3B (A3B) is up-regulated in over half of primary breast carcinomas, accounting for a large proportion of the mutational load in these tumors.[17] A3B over-expression correlates to a higher overall mutational frequency, and poorer clinical outcomes, such as disease-free and overall survival, in estrogen receptor positive (ER+) breast cancer patients.[17,172] Additionally, A3B over-expression has been implicated in the mutagenesis of bladder, cervical, head and neck, and lung cancers, both adenocarcinoma and squamous, suggesting that A3B-contributed mutation is a common paradigm in cancer mutagenesis.[171,185] Consequently, the identification of small molecule inhibitors of the APOBEC3 enzymes may provide leads that can be further

developed into clinical candidates for suppressing mutation and evolution in HIV-1 and cancer.

Using a previously reported fluorescence-based ssDNA C-to-U deaminase assay, we identified 62 structurally unique dual inhibitors of A3A (92% sequence identity to A3B) and A3G from an HTS of 21,126 small molecules at the University of Minnesota, which included compounds from the following commercial libraries: Sigma LOPAC (LO1280), Tocriscreen, Prestwick Chemical, NIH Clinical Collection and MicroSource Discovery.[1] Compound **4.1** was particularly intriguing because of its low micromolar potency against A3A (IC_{50} = 2.8 μM) and A3G (IC_{50} = 10.8 μM), and its low toxicity against 293T and HeLa cells (>85% cell viability when treated with 50 μM compound after 5 days). We confirmed this observed activity by purchasing **4.1** (Figure 4.1), commercially available from ChemBridge Corporation (#7922691), and subjecting the commercial material to dose response experiments against recombinant A3A and A3G. Purchased **4.1** substantiated our HTS observations demonstrating inhibition of both A3A (IC_{50} = 9.8 μM) and A3G (IC_{50} = 50.3 μM), albeit to a lesser extent.
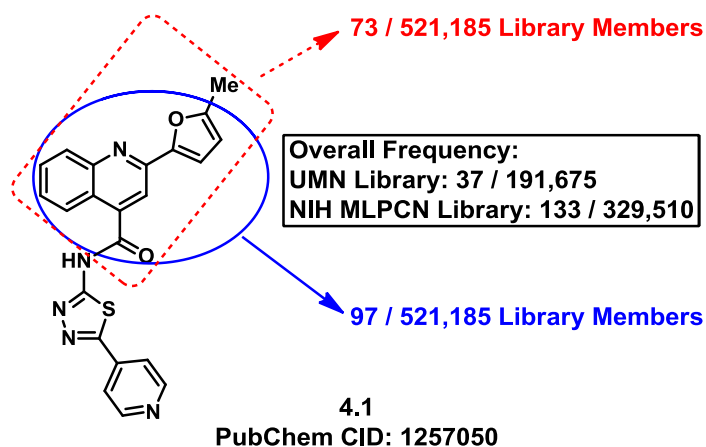
Figure 4.1. Chemical Structure of **4.1** and the Frequency with which the 2-(5-methylfuran-2-yl)quinoline-4-carbonyl (dashed) and the 2-(furan-2-yl)quinoline-4-carbonyl (solid) Substructures occur in the University of Minnesota and the NIH MLPCN Libraries (521,185 total compounds when combined). The boxed text represents the overall frequency of these chemotypes in each individual library. Overlap between the University of Minnesota and NIH MLPCN libraries is <10%.

Quinoline **4.1** is a privileged scaffold as related analogues bearing the 2-furan moiety have been investigated as leads for neurokinin-3 receptor inhibition, and in antimicrobial, antiviral, contraceptive, antitrypanosomal, and anticancer applications, though to the best of our knowledge, none of these molecules have advanced to clinical studies.[243-250] Consistent with this observation, the 2-furylquinoline-4-carbonyl substructure is present in 170 HTS library members available in the University of Minnesota and the NIH MLPCN screening libraries and in many of our own HTS hits (Figure 4.1). As a result of marked A3 inhibition in HTS screening, a low toxicity profile against human cells, and the lack of PAINS warnings, we initiated a structural optimization campaign to refine **4.1** for potency and selectivity.

4.2 Results & Discussion

4.2.1 Synthesis and Enzymatic Assays with 4.1.

In an effort to investigate this scaffold as a potential lead molecule for structure-activity relationship (SAR) studies, we synthesized **4.1** (Scheme 4.1). A short two-step sequence delivered **4.1** in 17% overall yield, which began with the preparation of **4.3**. Pfitzinger-Borsche chemistry was employed by reacting isatin (**4.2**) with 5-acetyl-2-methylfuran under basic conditions to deliver **4.3** in 79% yield.[250] Commercially available **4.4** and carboxylic acid **4.3** were coupled under EDCI·HCl/HOBt conditions to achieve **4.1** in 22% yield. Amine **4.4** can also be synthesized as previously reported.[251]
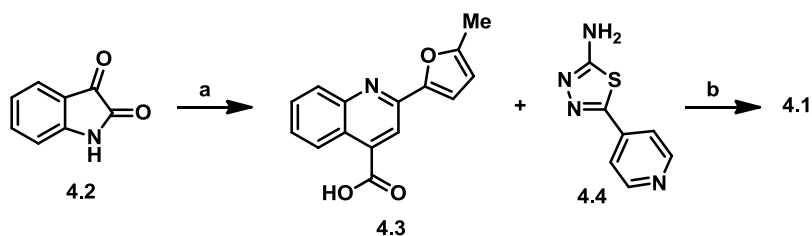
Scheme 4.1. Synthesis of **4.1**. *Reagents and conditions:* (a) 5-acetyl-2-methylfuran, KOH, EtOH, 65 °C to reflux, 79%; (b) EDCI·HCl, HOBt, NMM, DMF, 22%.

Synthetic **4.1** was subsequently evaluated for A3A and A3G inhibition using our previously described fluorescence-based deamination assay.[1,156] However, we were surprised to find that **4.1** exhibited no inhibition of either A3 enzyme when tested in dose response assays up to 200 μM concentrations (Figure 4.2; day 0). To verify our results, the same DMSO stock of **4.1** was re-tested on multiple occasions in the days that followed, and curiously, A3G inhibitory activity was noted, with the magnitude of A3G inhibition paralleling the

age of the DMSO stock solution. A testing schedule that assayed for A3G inhibition at days 3, 21, 38, and 72 demonstrated that the DMSO stock solution of **4.1**, aged in a closed microcentrifuge tube at 20-22 °C (on lab bench), increasingly and incrementally gained A3G inhibitory activity over a period of approximately two months, and as early as three days. Specifically, at 200 μM treatment, the aged stock of **4.1** reduced A3G deamination activity to 82% (3 days), 55% (21 days), 29% (38 days), and 29% (74 days) (Figure 4.2). It is worth noting that although this phenomenon with A3G was consistently reproduced, inhibitory activity against A3A, as seen in the HTS, was never recovered.
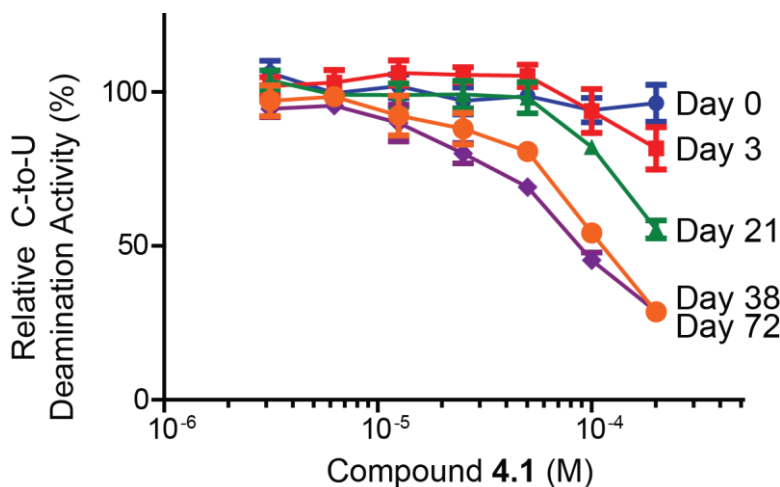
Figure 4.2. Dose Response Assays for APOBEC3G Inhibition by Freshly Synthesized and Solubilized **4.1** at 0, 3, 21, 38 and 72 Days. Data indicates that the stock solution of **4.1** gains A3G inhibitory activity over time. Assays were performed in triplicate and deaminase activity was quantified as previously reported.[18,36] Means ± standard deviations are indicated.

4.2.2 Identification of the Decomposition Products of 4.1

Based on the observed increase in inhibitory activity over time, we proposed that **4.1** decomposes into one or more chemically distinct A3G

110

inhibitors. We first HPLC analyzed a 10 mM stock solution of synthesized **4.1** that was fortuitously dissolved in DMSO and stored in the laboratory for 16 months. This discrete sample primarily existed as a single product (Figure 4.3).
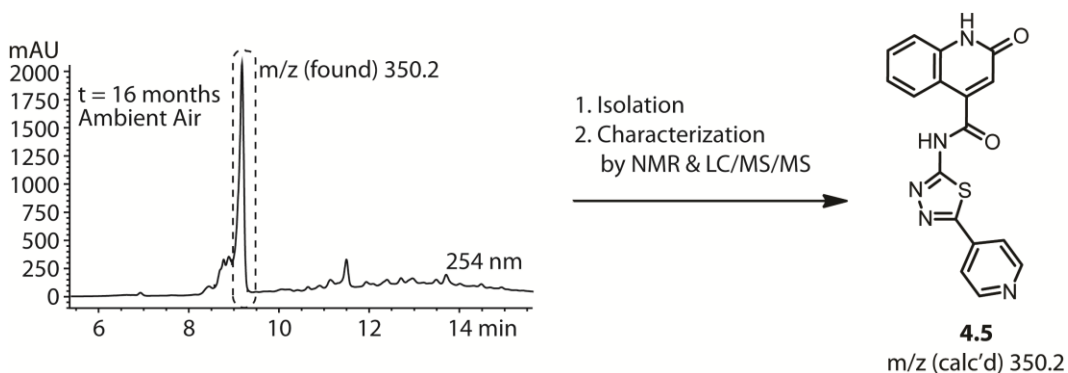
Figure 4.3. Analytical HPLC Analysis of a 10 mM DMSO Stock Solution of **4.1**. After 16 months, **4.1** converted to **4.5** as determined by HPLC isolation and characterization by ^{1}H and ^{13}C NMR and LC-MS/MS.

The major peak was isolated by HPLC, and the decomposition product was identified as **4.5** by ^{1}H and ^{13}C NMR, IR, and LC-MS. Spectroscopic data suggested that **4.5** exists as the more energetically stable lactam,[252-254] which is supported by an IR spectrum that shows a strong C=O vibrational frequency (1771 cm^{-1}) and the notable absence of a strong, broad –OH signal.

To confirm that **4.5** is a decomposition product of **4.1** and that it inhibits A3G, we synthesized **4.5** by coupling amine **4.4** and commercially available 2-hydroxyquinoline-4-carboxylic (**4.6**) acid with PyBOP in 59% yield (Scheme 4.2).[255] Following the isolation and characterization of **4.5**, the purified aliquot was evaluated for A3A and A3G inhibitory activity.
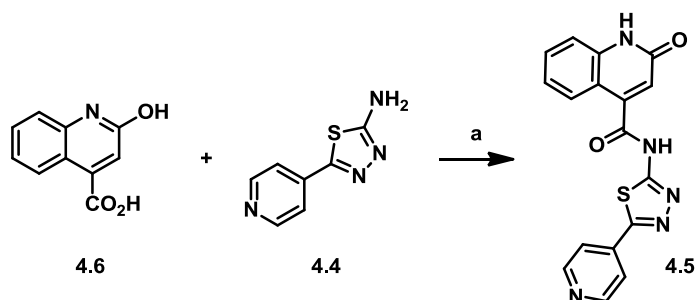
Scheme 4.2. Synthesis of **4.5**. (A) Synthesis of **4.5**. *Reagents and conditions*: (a) PyBOP, NMM, DMF, 59%.

We found that isolated **4.5** reduced A3G-deamination efficiency to 83% at 200 µM, accounting for some of the inhibitory activity associated with the aged stock solution of **4.1** (Figure 4.4A). Biochemical evaluation of synthesized **4.5** revealed a weak A3G inhibitor, reducing deamination efficiency by 50% (±1.5) at 200 µM (Figure 4.4A). LC-MS/MS traces of isolated **4.5** and synthesized **4.5** were identical, thereby confirming the identity of the decomposition product (Figures 4.4B,C). The slight discrepancy between the observed biochemical activities can be accounted for by the small amount of **4.5** (<1 mg) isolated from the aged DMSO stock solution. Inherently, the determined mass of purified **4.5** could reflect a higher probability of error, skewing the concentration of the stock solution, and thus, the calculated percent inhibition.

112
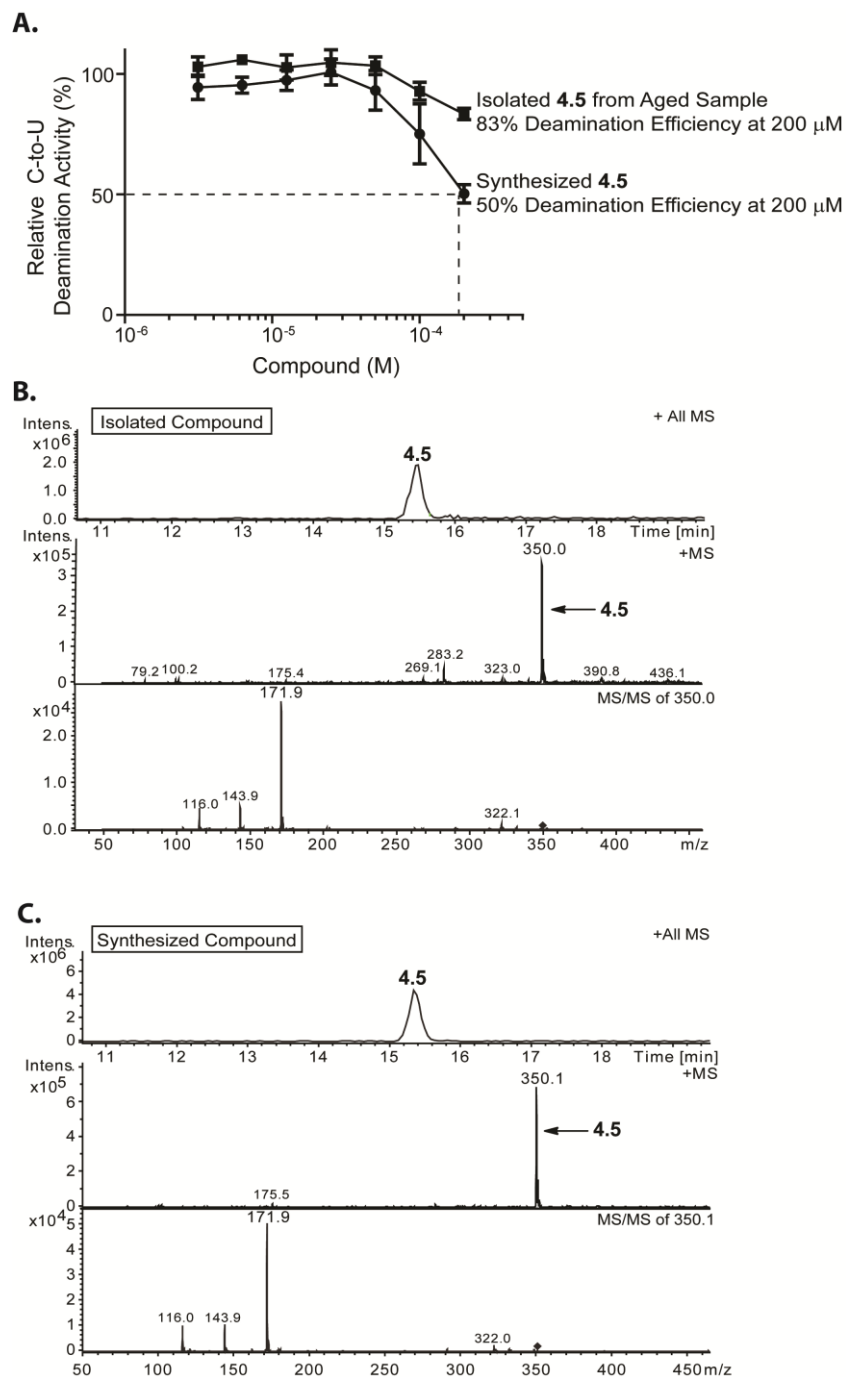
Figure 4.4. Biochemical Evaluation and Characterization of Isolated and Synthesized **4.5**. (A) Dose response assays for A3G inhibition by **4.5** isolated from an aged DMSO stock solution and synthesized **4.5**. Assays were performed in triplicate and deaminase activity was quantified as described previously.[18] Means ± standard deviations are indicated. (B) LC-MS/MS analysis of isolated **4.5** compared to the LC-MS/MS chromatorgram of synthesized **4.5** (C).

Next, analytical HPLC was employed to monitor the decomposition kinetics of **4.1** over the time frame that we observed increasing A3G inhibitory activity (t = 72 days, Figure 4.2). As expected at time 0, **4.1** exists in solution as a pure compound (Figure 4.5A). It was observed that by 21 days, however, notable decomposition of **4.1** had occurred, resulting in a mixture of decomposition products (Figure 4.5B). LC-MS analysis of the aged stock identified the masses of the three prominent peaks as 378.1, 464.1, and 430.1, respectively. The structures corresponding to these three masses were predicted to be oxidative decomposition products **4.7**, **4.8a-4.8b**, and **4.9** (Figure 4.5C), which were confirmed by HPLC isolation and ^{1}H NMR and HRMS driven structural elucidation.
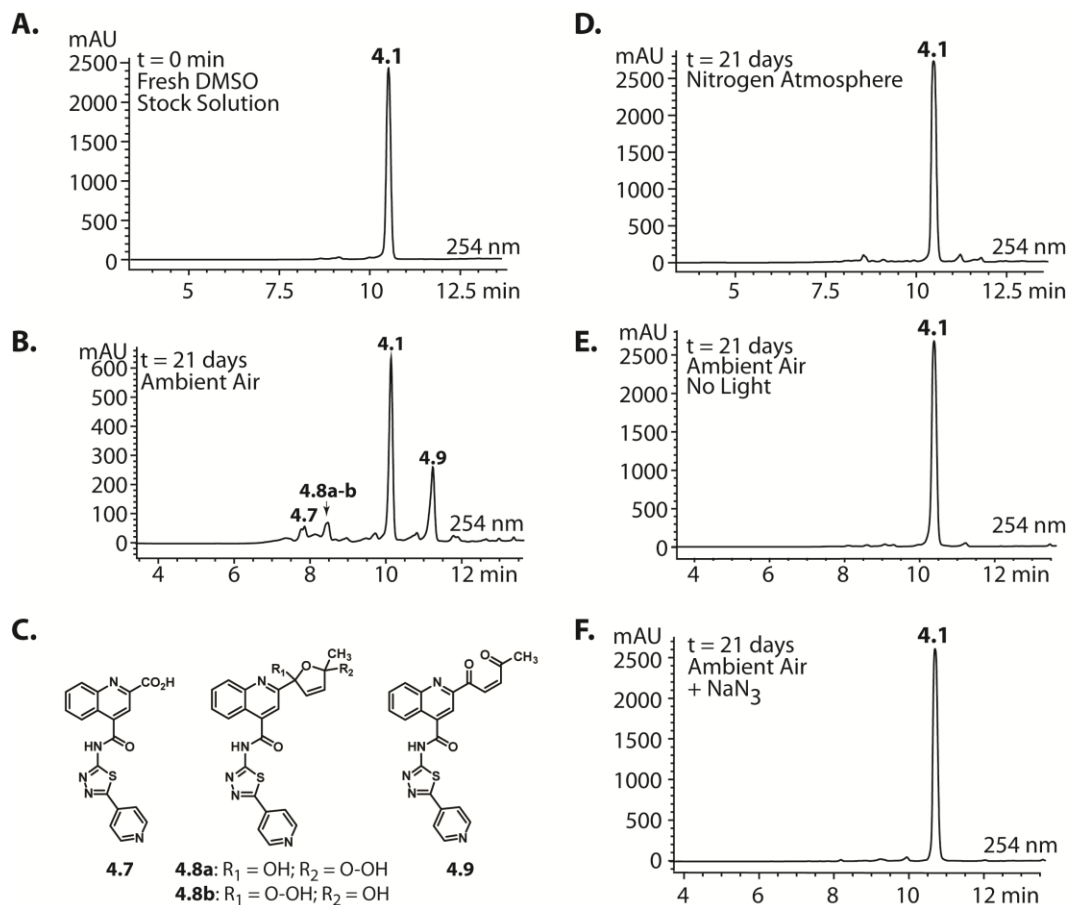
Figure 4.5. Analytical HPLC Analyses of 10 mM DMSO Stocks of **4.1**. (A) Fresh stock solutions of **4.1** are >99% pure as determined by HPLC. (B) After 21 days of gentle shaking in ambient atmosphere at 25 °C, HPLC analysis shows evidence of decomposition through the appearance of multiple new peaks. (C) Compounds **4.7**, **4.8a-4.8b**, and **4.9** can be assigned to the three prominent peaks in the decomposition mixture. These compounds were isolated by HPLC and characterized by LC-MS, ^{1}H NMR, HRMS, and co-injection of the isolated standards with aged samples of **4.1** (t = 21 d). (D) DMSO stocks of **4.1** aged under inert conditions (N₂) exhibit drastically reduced decomposition. (E, F) DMSO stocks of **4.1** aged in the dark or in the presence of NaN₃ exhibit no decomposition.

To verify that the isolated samples were, in fact, decomposition products of **4.1**, aliquots of the isolated samples (as 10 mM DMSO stock solutions) were spiked into a stock solution of **4.1** aged to 21 days. The anticipated enrichment

115

(doubling) of the intensity of decomposition peaks for **4.7**, **4.8a-4.8b**, and **4.9** (Figure 4.5B) was observed (Figure 4.6). Decomposition products **4.7** and **4.9** were also synthesized by $RuO_2 \cdot H_2O/NaIO_4$-catalyzed oxidation of **4.1** to give a 2:1:2 mixture of **4.7**:**4.1**:**4.9**. These compounds were isolated by HPLC and characterized. LC-MS/MS traces of isolated and synthesized **4.7** and isolated and synthesized **4.9** were respectively identical, confirming the identities of these decomposition products (Section 4.7, Figures 4.10, 4.11). Moreover, aliquots of the synthesized compounds (as 10 mM DMSO stock solutions) were spiked into an aged stock of **4.1** at 21 days. Enrichment of the intensities of the appropriate peaks was observed (Figure 4.6).

116
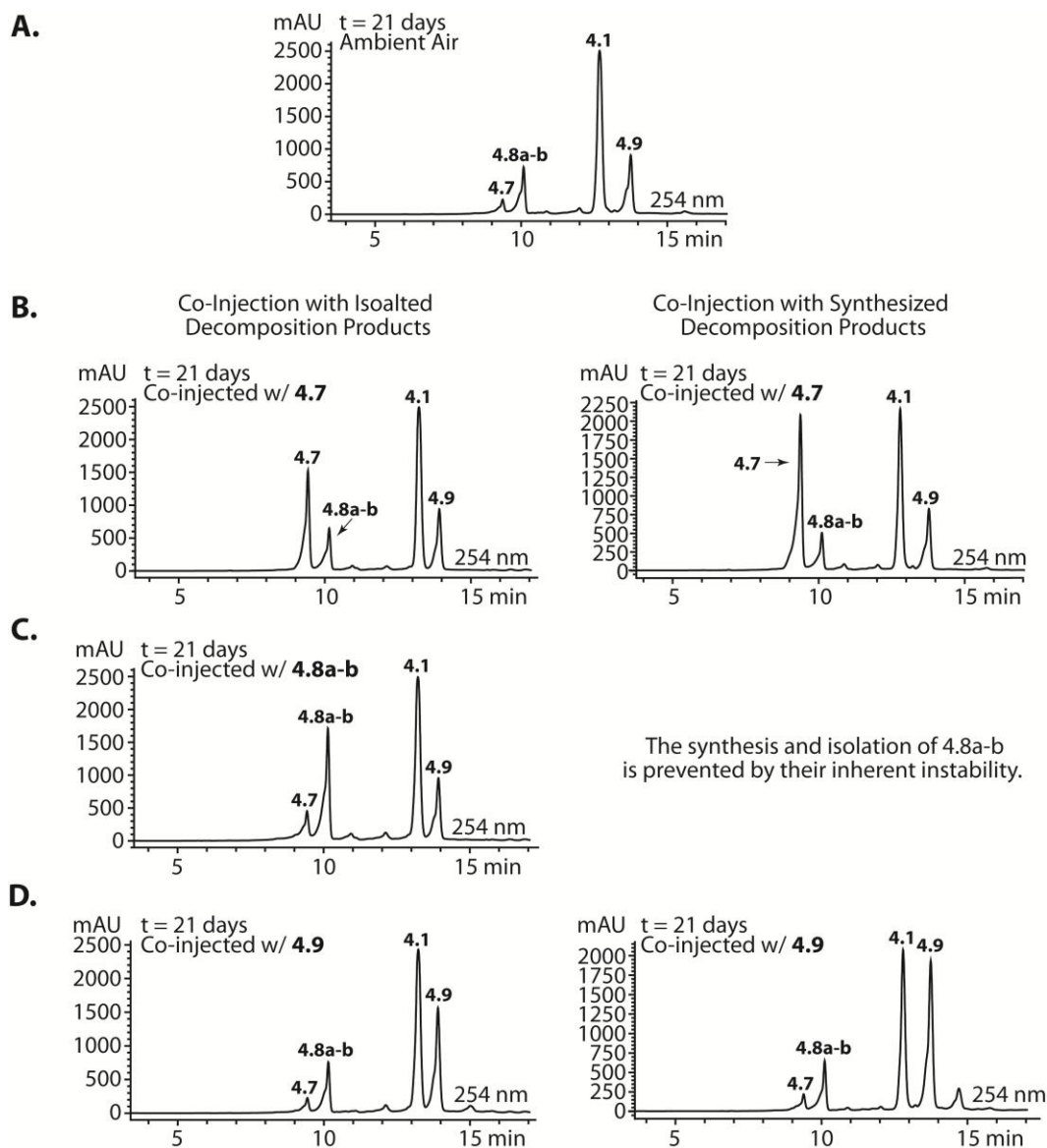
Figure 4.6. Co-Injections of Isolated and Synthesized Decomposition Products **4.7, 4.8a-b,** and **4.9** with Aged **4.1**. Ten mM DMSO stock solutions of **4.1** incubated for 21 days were spiked with 10 mM DMSO stock solutions of standard (either isolated or synthesized **4.7**, **4.8a-4.8b**, or **4.9**) and diluted with biological grade MeOH so that the final concentration of each stock solution was 1 mM. The resulting solutions were analyzed by HPLC.

Biochemical evaluations of synthesized **4.7** and **4.9** identified **4.9** as the most potent A3G inhibitor, with an IC_{50} = 21 ± 4.0 µM (Figure 4.7). Decomposition

117

product **4.7** reduced deamination efficiency to 43% (± 2.8) at 200 µM, exhibiting

activity similar to **4.5**, which reduced deamination efficiency to 50% (±1.5) at 200

µM (Figure 4.4A). A freshly isolated sample of **4.8a-4.8b** was also biochemically

evaluated, but this intermediate exhibited no A3G inhibition. 2-

Hydroxyquinonline-4-carboxylic acid (**4.6**), quinoline-2,4-carboxylic acid, and 5-

(pyridin-4-yl)-1,3,4-thiadiazol-2-amine (**4.4**), which are substructures of the

decomposition products, were also evaluated for A3G inhibitory activity and

found to be inactive (data not shown). Taken together, decomposition product **4.9**

(IC_{50} = 20 ± 4.2 µM for A3G) most closely mirrored the biochemical activity

exhibited by the commercially-available ChemBridge material (IC_{50} = 50.3 µM for

A3G) and in the HTS (IC_{50} = 10.8 µM for A3G).
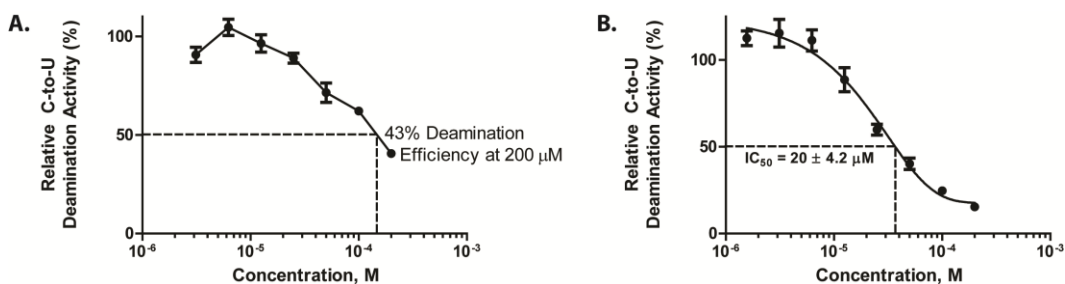
Figure 4.7. Biochemical Evaluation of Synthesized **4.7** and **4.9**. Dose response
assays for A3G inhibition by synthesized **4.7** (A) and **4.9** (B). Assays were
performed in triplicate and deaminase activity was quantified as described
previously.[18] Means ± standard deviations are indicated.

4.2.3 Mechanism of Decomposition.

To elucidate the mechanism by which **4.1** undergoes decomposition to

4.5, **4.7**, **4.8a-4.8b**, and **4.9**, we first performed an analogous aging experiment,

except a saturated N_2 atmosphere was used instead of laboratory air.

Degradation of **4.1** was dramatically slowed under these conditions, supporting an oxidative mechanism of decomposition (Figure 4.5D). Moreover, decomposition was inhibited when DMSO stocks of **4.1** were maintained in the dark or in the presence of $^1O_2$-quenching reagent NaN_3 (Figures 4.5E,F). From these qualitative experiments, we proposed that the decomposition of **4.1** is enabled by the *in situ* generation of $^1O_2$, which is (auto)photosensitized by **4.1**. Additional experiments revealed that decomposition occurs at the same rate regardless of the temperature in which the DMSO stock is stored (-20 °C vs. rt vs. 37 °C; data not shown).
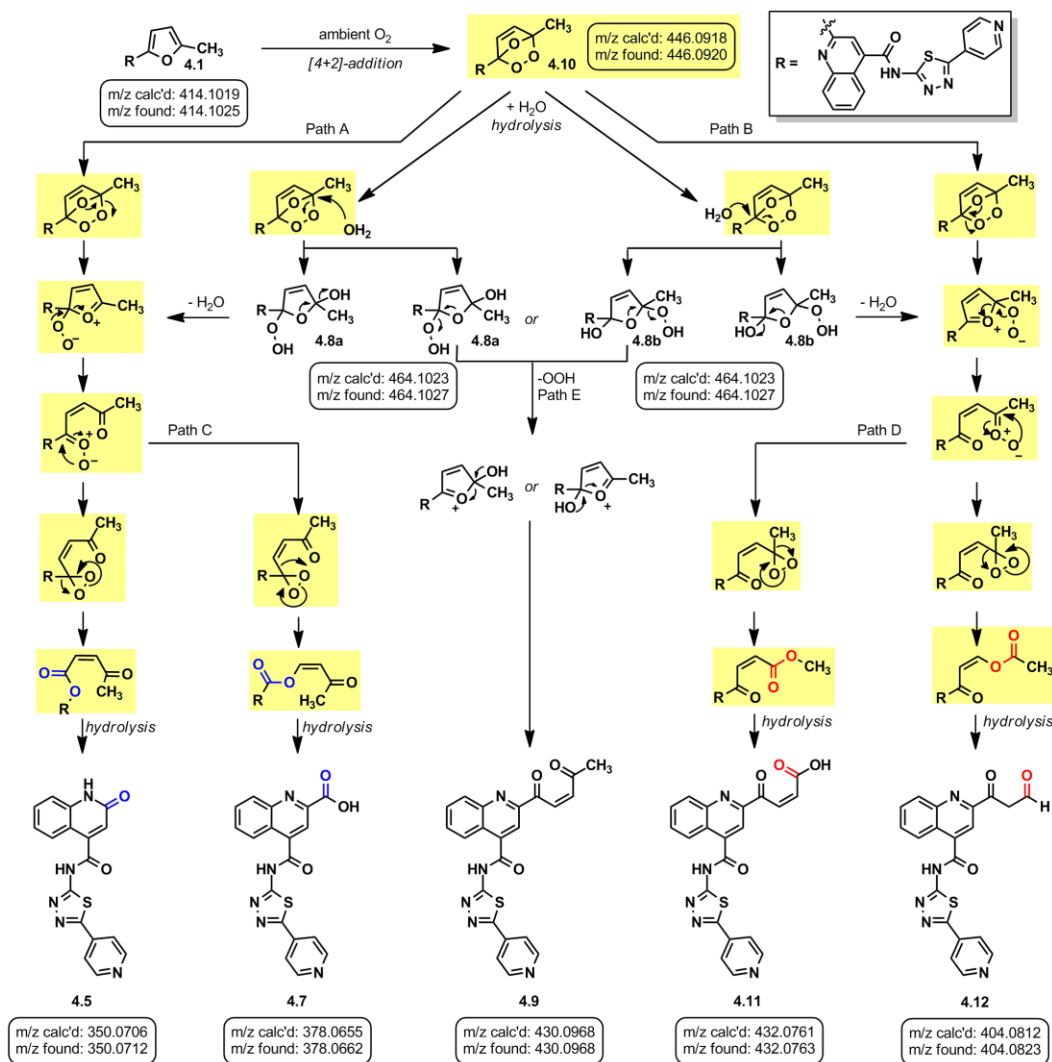
Figure 4.8. Mechanism of **4.1** Decomposition. (A) Proposed mechanistic pathways for oxygen-mediated decomposition of **4.1**. Intermediates highlighted in yellow exhibit m/z [M+H]$^+$ = 446.1, which is observed in the LC-MS analysis.

Singlet oxygen is 22 kcal/mol higher in energy than ground state oxygen and exhibits double bond character as a result of having paired electrons in the same LUMO.[256] Schenck first proposed this [4+2] cycloaddition by hypothesizing that sensitized or auto-sensitized photooxygenations of furans produce endoperoxides.[257] Subsequent work demonstrated that the resulting

endoperoxides can yield dioxirane intermediates (via carbonyl oxides) that further rearrange to give "anomalous ozonolysis" products through an intramolecular Baeyer-Villiger mechanism.[258-260] Evidence for the carbonyl oxide intermediate has been demonstrated through trapping experiments.[261] Baeyer-Villiger oxidation would explain the incorporation of the lactam carbonyl and the carboxylic acid at the 2-position of **4.1**. Based on this previous literature, we propose that the furan of **4.1** undergoes [4+2] cycloaddition with $^1O_2$ to give endoperoxide **4.10**. The endoperoxide can collapse without directional bias to yield carbonyl oxide species that readily convert into dioxirane intermediates. This mechanism is unlikely to be concerted as previous research has demonstrated that carbonyl oxide intermediates are readily intercepted by olefins, sulfides, and ketones.[262] Furthermore, cyclization to the dioxirane resonance is thought to be driven by destabilization of the carbonyl oxide by the enone.[262] The resulting dioxiranes can then undergo Baeyer-Villiger-type rearrangements to produce four penultimate esters that are hydrolyzed in aqueous conditions. Our proposed mechanism could also yield α,β-unsaturated acid **4.11** and aldehyde **4.12**, in addition to, lactam **4.5** and carboxylic acid **4.7**. To account for observed decomposition products **4.8a**, **4.8b**, and **4.9** (Figure 4.5), endoperoxide **4.10** could alternatively be hydrolyzed by H_2O present in the DMSO stock.[263] We propose that the hydrolysis of **4.10** yields peroxides **4.8a** and **4.8b**, which are inherently unstable and can rearrange to enone **4.9** via the loss of -OOH and ring opening (Path E, Figure 4.8)[263] or decomposition products **4.5**, **4.7**, **4.11** and **4.12** through the reversible loss of H_2O and the aforementioned mechanism (Figure 4.8). When isolated by HPLC, 10 mM DMSO stocks of **4.8a/4.8b** exhibited a short shelf life of <48 h. After which, analysis of these

stocks by analytical HPLC displayed primarily **4.7** and **4.9**, which were confirmed by isolation and ^{1}H NMR (data not shown).

LC-MS analysis of DMSO stock solutions of **4.1** aged 38 days under ambient air provided significant experimental support for our proposed mechanism of decomposition. Lactam **4.5** (*m/z* 350.1), carboxylic acid **4.7** (*m/z* 378.1), enone **4.9** (*m/z* 430.1), α,β-unsaturated acid **4.11** (*m/z* 432.1), and aldehyde **4.12** (*m/z* 404.1) were all found in our analysis (Figure 4.8). Furthermore, we also observed masses that correspond to either **4.8a** or **4.8b** (*m/z* 464.1), which would result from hydrolysis of endoperoxide **4.10**. Hydrolysis of the carbonyl oxides or dioxiranes could also yield this same mass (*m/z* 464.1). Additionally, the mass corresponding to $^1O_2$ addition to the furan (*m/z* 446.1) was observed in our sample, which could denote the endoperoxide **4.10**, the carbonyl oxides, the dioxiranes, or the esters (Figure 4.8, possible *m/z* 446.1 intermediates are highlighted in yellow). Aging of a DMSO solution of **4.1** under an atmosphere of [^{18}O]-O_2 was performed to further support that **4.1** reacts with photosensitized molecular oxygen to yield the intermediates reported above. Accordingly, we found incorporation of heavy oxygen into **4.5*** and **4.7*** (*m/z* 352.1 and 380.1 for aging under [^{18}O]-O_2 versus 350.1 and 378.1 for **4.5** and **4.7**, respectively), as well as isotopically-labeled **4.8a*** or **4.8b*** (+4 Daltons) in our analysis.

Similar patterns of decomposition following laboratory aging in DMSO are observed regardless of the sample analysis method (e.g., 4.6 x 150 mm, 3.5 μm C18 column, trifluoroacetic acid modifier versus 0.5 x 150 mm, 5 μm C18 column, trifluoroacetic acid and formic acid eluent modifiers). The addition of formic acid to the eluent was required for mass spectrometry analysis (LC-MS).

However, we do note some minor differences in the relative abundances of the decomposition products as visible in the UV chromatograms between these methods. Given that quantitative measurements of the decomposition products are outside the scope of this investigation, and that the masses of the decomposition products are clearly observed, we employed these HPLC methods interchangeably for sample analysis in additional mechanistic queries.

To further demonstrate that **4.1** decomposes by the proposed cycloaddition-rearrangement sequences, we employed known photochemical conditions to an oxygenated solution of **4.1**.[264] A 10 mM DMSO solution of **4.1** was irradiated with visible light (300 W) under an oxygen-saturated environment (O_2 balloon, 1 atm) in the presence of rose bengal (RB), a photosensitizer. LC-MS analysis of the crude reaction mixture exhibited *m/z* products corresponding to **4.5**, **4.7**, **4.8a-b**, **4.9**, the intermediates with the common *m/z* of 446.1, and related analogues **4.11** and **4.12** (Figure 4.9A). To demonstrate that **4.1** auto-sensitizes its photooxygenation, we also irradiated **4.1** in DMSO using visible light (300 W) in an oxygen-saturated atmosphere (O_2 balloon, 1 atm) that was absent of sensitizer. Surprisingly, we observed more extensive decomposition without addition of photosensitizer (Figure 4.9B). These conditions permitted additional mechanistic work without the long incubation times used previously (e.g., weeks of time, Figure 3) To rule out the potential influence of heat generated by the lamp on the decomposition of **4.1**, and to further provide evidence for oxidative decomposition, an identical experiment was performed under an N_2 atmosphere (balloon, 1 atm). In the absence of oxygen, virtually no decomposition of **4.1** was observed over 9 h, although constantly irradiated (Figure 4.9C).
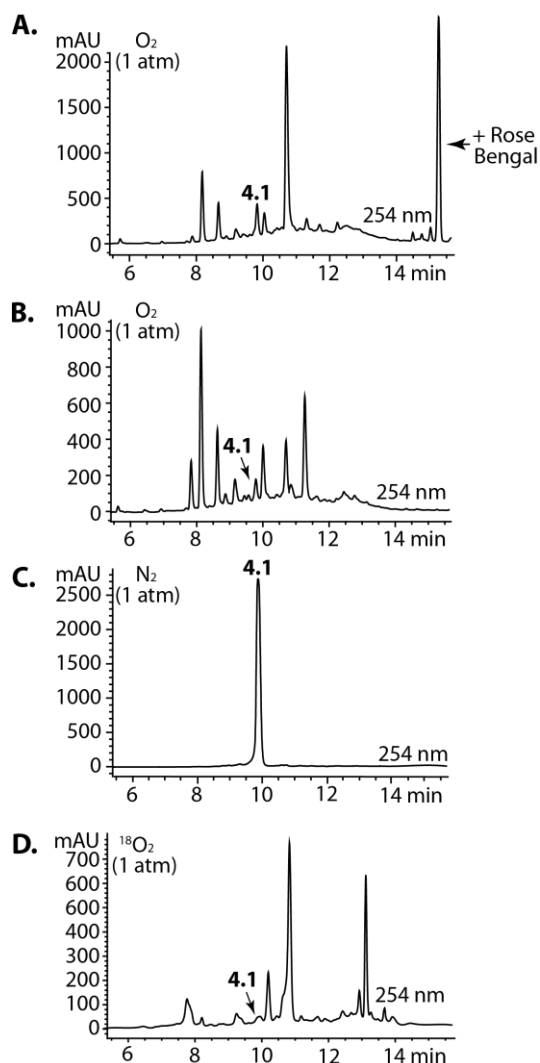
Figure 4.9. Photochemical Decomposition of **4.1**. (A) The decomposition of **4.1** can be achieved in short reactions times (9h vs. 21d) by irradiating DMSO stocks of **4.1** with visible light (300W) in an oxygen saturated atmosphere. (B) Decomposition readily occurs in the absense of photosensitizer. (C) No decomposition occurs under an N_2 atmosphere. (D) Decomposition in the presence of $[^{18}O]\text{-}O_2$. Rose bengal was not added to reactions B – D.

Finally, we observed the incorporation of isotopically labeled $[^{18}O]\text{-}O_2$ by performing this photooxidation in a saturated $^{18}O_2$ environment (balloon, 1 atm; Figure 4.9E). LC-MS analysis revealed incorporation of the isotope, yielding **4.5***

(m/z = 352.1, +2.0 Daltons), **4.7*** (m/z 380.1, +2.0 Daltons), and hydrolysis

products **4.8a*** and/or **4.8b*** (*m/z* 468.1, +4.0 Daltons). Conversely, irradiation of **4.1** in an O_2 environment (balloon, 1 atm) in the presence of $H_2^{18}O$ yielded incorporation of the isotope only as a result of hydrolysis with [^{18}O]-labeled water and no incorporation into any other intermediate.

4.2.4 Mechanistic Determinants.
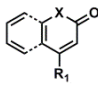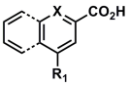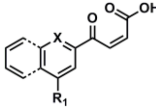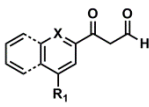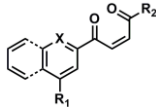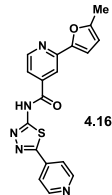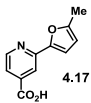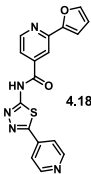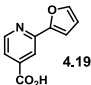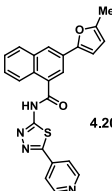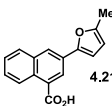
To determine the minimal sub-structure of **4.1** susceptible to this mechanism of decomposition, a series of mechanistic probes was synthesized and subjected to laboratory aging. The designed probes gauged the necessity for a 4-position amide, a methyl furan, a quinoline ring, and a 4-position carbonyl. Accordingly, analogues were studied which contained a free carboxylic acid as opposed to an amide linkage (**4.13**,**4.15**,**4.17**,**4.19**,**4.21**,**4.23**), a furan as opposed to a methyl furan (**4.14**,**4.15**,**4.18**,**4.19**,**4.22**,**4.23**), a pyridyl (**4.16**-**4.19**) or naphthyl ring (**4.20**-**4.23**) in place of the quinoline, or the absence a 4-position substituent (**4.24**,**4.25**). Syntheses were performed according to standard organic transformations. Generally, ring system-furan connections were accomplished under Stille or Suzuki conditions from commercial reagents, and amide bond couplings were accomplished with EDCI·HCl, HOBt, and DIPEA. DMSO stock solutions (10 mM) for the 13 probes were made identically to those prepared for **4.1** and solutions were exposed to laboratory air at 25 °C for 38 days. Aliquots were taken at 0, 2, 7, 21 and 38 days and analyzed by analytical HPLC. Percent decomposition was measured by dividing the ratio of the area under the curve (AUC) of compound over internal standard at day 38 by the ratio at time 0 (Table 4.1). The stock solutions of each compound were also subjected to LC-MS analysis at day 38. The extent of decomposition varied widely across the
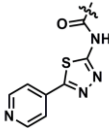
mechanistic probes. The following general trends were observed: (1) a higher degree of decomposition occurred in probes that contained 4-position amide linkages as compared to their free carboxylic acid counterparts, (2) a higher degree of decomposition was observed in probes with methyl functionalized furans in comparison to the non-substituted analogues, (3) probes lacking a 4-position carbonyl exhibited the least decomposition, and (4) the identity of the ring system had little effect on the extent of decomposition. Notable exceptions to these trends were observed, and thus, they must be accepted as only suggestions. For example, quinoline-based probe **4.15**, which is absent of the 4-position amide linkage and methyl-substituted furan, showed more decomposition than probes **4.13** (methyl furan) and **4.14** (amide linkage). Additionally, naphthyl-based probe **4.22** showed extensive decomposition, although it lacked a furan methyl substituent. The percentage parent remaining for probes exhibiting a 4-position carboxylic acid ranged from 69%-92%, for probes exhibiting a 4-position amide linkage from 0-99%, and >99% for probes lacking a 4-position carbonyl. Decomposition was observed for probes based on all three ring systems, with 6-99% parent remaining for the quinoline-based series, 34-99% remaining for the pyridine-based series, and 0-89% for the naphthylene-based series. The most common decomposition products confirmed by LC-MS were the endoperoxide intermediate, the carboxylic acid (analogous to **4.7**), and the enone (analogous to **4.9**). It is important to note that the reported percentages of probe remaining are in the context of 38 d, and that DMSO stocks analyzed at later times points (t = months) exhibited decomposition in every probe (data not shown). Taken together, each of the furan-substituted aromatic

126

systems investigated in this study are prone to oxidative decomposition, albeit to

varying rates.

Table 4.1. Decomposition Study of Substructure Probes of 4.1 in DMSO Solution

Decomposition Products Observed[c,d]

$X = C, N; R_1 = CO_2H,$; $R_2 = CH_3, H$

Probe	Exact Mass	% Parent Remaining ± SD (38 days)[a,b]					
4.1	413.1	6 ± 1	+ 350.1 (350.1)	+ 378.1 (378.1)	+ 432.1 (432.1)	+ 404.1 (404.1)	+ 430.1 (430.1)
4.13	253.1	83 ± 18	+ 190.1 (190.1)	+ 218.1 (218.1)	+ 272.1 (272.1)	-	+ 270.1 (270.1)
4.14	399.1	101 ± 7	+ 350.2 (350.1)	+ 378.2 (378.1)	+[e] 432.2 (432.1)	-	-
4.15	239.1	69 ± 7	+ 190.2 (190.1)	-	+[e] 272.1 (272.1)	-	-

127

			Decomposition Products Observed[c,d]				
Probe	Exact Mass	% Parent Remaining ± SD (38 days)[a,b]					

$X = C, N; R_1 = CO_2H$, ; $R_2 = CH_3, H$

Probe	Exact Mass	% Parent Remaining ± SD (38 days)[a,b]					
4.16	363.1	34 ± 4	-	+ 328.2 (328.0)	-	-	+ 380.2 (380.1)
4.17	203.1	85 ± 8	-	-	-	-	+ 220.1 (220.1)
4.18	349.4	90 ± 12	-	-	+[e] 382.2 (382.1)	-	-
4.19	189.0	92 ± 6	-	-	-	-	-
4.20	412.1	25 ± 1	-	+ 377.2 (377.1)	-	-	+ 429.2 (429.1)
4.21	252.1	82 ± 31	-	-	-	-	+ 269.2 (269.1)

128

Probe	Exact Mass	% Parent Remaining ± SD (38 days)[a,b]	Decomposition Products Observed[c,d]				

X = C, N; R₁ = CO₂H, [structure]; R₂ = CH₃, H

Probe	Exact Mass	% Parent Remaining ± SD (38 days)	Col1	Col2	Col3	Col4	Col5
4.22	399.1	0	-	+ 377.2 (377.1)	+[e] 431.2 (431.1)	+ 403.2 (403.1)	+ 415.1 (415.1)
4.23	238.1	89 ± 8	-	-	+[e] 271.1 (271.0)	+ 243.1 (243.0)	+ 254.1 (254.1)
4.24	209.1	102 ± 12	-	-	-	-	+ 226.2 (226.2)
4.25	195.1	117 ± 16	-	-	+[e] 228.1 (228.1)	-	-
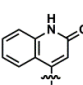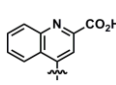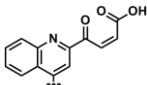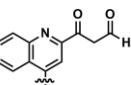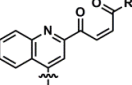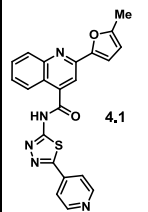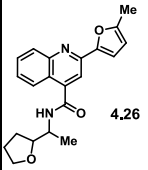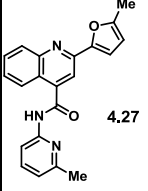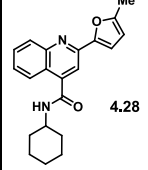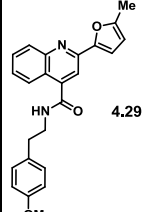
[a]10 mM solutions in DMSO were shaken gently at 25 °C open to the atmosphere. Percent remaining is the mean of three independent experiments. [b]DMSO stock solutions were analyzed by LC-MS on day 38. [c]Decomposition products positively identified are denoted by +, while products not detected are denoted by -. For observed decomposition products, the masses are presented as found mass, then calculated mass in parentheses. Masses were calculated for $[M+H]^+$. [d]The aldehyde decomposition product could also be the enol tautomer. [e]For probes with a non-methylated furan, the α,β-unsaturated acid and $[M+O_2+H]^+$ intermediates (highlighted in yellow in Figure 4.8) have the same MW. The α,β-unsaturated acid is represented in this table as identified; however, the observed m/z may correspond to an $[M+O_2+H]^+$ intermediate.
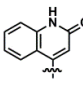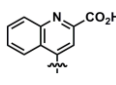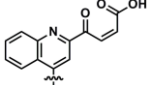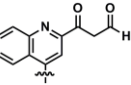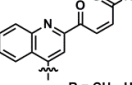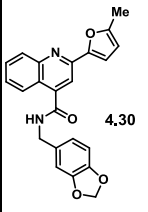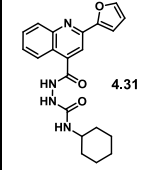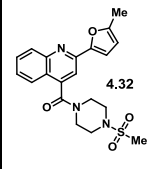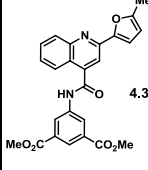
4.2.5 General Applicability of Oxidative Decomposition to Structurally Related HTS Library Scaffolds

Together, the University of Minnesota and the NIH MLPCN screening libraries contain 170 compounds based on this 2-furylquinoline-4-carbonyl substructure. To investigate if other 2-furylquinoline HTS members can

decompose similarly to **4.1**, we purchased eight representative compounds that were present in either the University of Minnesota library or the NIH MLPCN screening collection. DMSO stock solutions (10 mM) for the eight compounds were made identically to those prepared for **4.1** and solutions were exposed to laboratory air at 25 °C for 38 days. Aliquots were taken at 0, 2, 7, 21 and 38 days and analyzed by HPLC. Decomposition was observed in all of the compound stocks as early as 2 days post solvation, and at day 38, the stocks had decomposed between 16 – 81% (Table 4.2). Percent decomposition was calculated as described above. The stock solutions of each compound were subjected to LC-MS analysis, and in each case, peaks corresponding to an oxygen-furan cycloaddition adduct $[M+O_2+H]^+$, the lactam decomposition product (analogous to **4.5**), and the carboxylic acid decomposition product (analogous to **4.7**) were observed. In the majority of experiments, the enone (analogous to **4.9**), the α,β-unsaturated acid (analogous to **4.11**), and the aldehyde (analogous to **4.12**) decomposition products were also observed. Our data suggests that HTS library compounds containing the 2-furylquinoline-4-carbonyl substructure are wholly subject to oxygen-mediated decomposition via the aforementioned mechanism and that this decomposition occurs within a timeframe relevant to HTS screening investigations.

Table 4.2. Decomposition of Furan-Functionalized Quinolines in DMSO Solution

HTS Library Member[a]	PubChem CID	Exact Mass	% Parent Remaining ± SD (38 days)[b,c]	Decomposition Products Observed[d,e]				
								R = CH₃, H
4.1	1257050	413.1	6 ± 1	+ 350.1 (350.1)	+ 378.1 (378.1)	+ 432.1 (432.1)	+ 404.1 (404.1)	+ 430.1 (430.1)
4.26	2965431	350.2	55 ± 4	+ 287.1 (287.1)	+ 315.1 (315.1)	-	+ 341.4 (341.1)	+ 367.2 (367.2)
4.27	845057	343.1	73 ± 8	+ 280.1 (280.1)	+ 308.1 (308.1)	+ 362.1 (362.1)	+ 334.2 (334.1)	+ 360.2 (360.1)
4.28	898877	334.2	54 ± 19	+ 271.1 (271.1)	+ 299.1 (299.1)	+ 353.2 (353.1)	+ 325.2 (325.1)	+ 351.2 (351.2)
4.29	1290240	386.2	84 ± 32	+ 323.1 (323.1)	+ 351.2 (351.1)	+ 405.2 (405.1)	+ 377.2 (377.1)	+ 403.2 (403.2)

131

HTS Library Member[a]	PubChem CID	Exact Mass	% Parent Remaining ± SD (38 days)[b,c]	Decomposition Products Observed[d,e]				
								R = CH$_3$, H
4.30	1257050	413.1	6 ± 1	+ 350.1 (350.1)	+ 378.1 (378.1)	+ 432.1 (432.1)	+ 404.1 (404.1)	+ 430.1 (430.1)
4.31	1295580	378.2	64 ± 19	+ 329.1 (329.1)	+ 357.1 (357.1)	+[f] 411.1 (411.1)	+ 383.1 (383.1)	-
4.32	2220790	399.1	26 ± 4	+ 336.1 (336.1)	+ 364.1 (364.1)	+ 418.1 (418.1)	+ 390.1 (390.1)	+ 416.1 (416.1)
4.33	1000751	444.1	19 ± 10	+ 381.1 (381.1)	+ 409.1 (409.1)	+ 463.1 (463.1)	-	+ 461.1 (461.1)

[a]Available in either the NIH MLPCN collection or the University of Minnesota small molecule collection. [b]10 mM solutions in DMSO were shaken gently at 25 °C open to the atmosphere. Percent remaining is the mean of three independent experiments. [c]DMSO stock solutions were analyzed by LC-MS on day 38. [d]Decomposition products positively identified are denoted by +, while products not detected are denoted by -. For observed decomposition products, the masses are presented as found mass and calculated mass in parentheses. Masses were calculated for [M+H]$^+$. [e]The aldehyde decomposition product could also be the enol tautomer. [f]For probes with a non-methylated furan, the α,β-unsaturated acid and [M+O$_2$+H]$^+$ intermediates (highlighted in yellow in Figure 4) have the same MW. The α,β-unsaturated acid is represented in this table as identified; however, the observed m/z may correspond to an [M+O$_2$+H]$^+$ intermediate.

4.3 Conclusions

In summary, it was found that the chemical integrity of **4.1** was compromised by air oxidation of the furan, yielding intermediates that rearrange

through a Baeyer-Villiger mechanism to products **4.5**, **4.7**, **4.11**, and **4.12**, and via hydrolysis-promoted rearrangement to **4.9**. Oxygen mediated decomposition of the 2-furylquinoline-4-carbonyl moiety appears to occur in chemically analogous scaffolds as demonstrated through the aging of eight randomly selected HTS library compounds. Our observations reinforce the phenomenon that small molecule instability in DMSO continues to plague HTS-based drug discovery efforts. Moreover, the 2-furylquinoline-4-amide substructure should be considered a PAINS scaffold and only prioritized as a drug lead with extensive structural validation. Finally, taking the steps to deconvolute this impure screening hit translated to the discovery of a modestly potent small molecule inhibitor of A3G.

4.4 Experimental Section

General Synthesis Information. Chemical reagents were purchased from commercial sources and used without additional purification. The eight representative 2-furylquinolines (**4.26-4.33**) were purchased from Chembridge Corporation, and confirmed to be >95% by two-wavelength HPLC. Bulk solvents were from Fisher Scientific and anhydrous *N,N'*-dimethylformamide (DMF) was purchased from Sigma-Aldrich. Anhydrous solvents were obtained from an MBraun Solvent Purification system. Reactions were performed under an atmosphere of dry N_2 where noted. Silica gel chromatography was performed on a Teledyne-Isco Combiflash Rf-200 instrument using Redisep *R*f Gold High Performance silica gel columns (Teledyne-Isco) or self-packed columns with SiliaFlash 60Å silica gel (SiliCycle). HPLC analyses were performed on an Agilent 1200 series instrument equipped with a diode array detector and a

Zorbax SB-C18 column (4.6 x 150 mm, 3.5 μm, Agilent Technologies). Compounds used in biochemical testing were no less than 98% pure as determined by two-wavelength HPLC analysis (254 and 215 nm). Nuclear magnetic resonance (NMR) spectroscopy was performed using a Bruker Avance instrument operating at 400 MHz or 500 MHz (for ^{1}H) and 100 MHz (for ^{13}C) at ambient temperature. Chemical shifts are reported in parts per million and normalized to internal solvent peaks or tetramethylsilane (0 ppm). High-resolution mass spectrometry (HRMS) was recorded in positive-ion mode on a Bruker BioTOF II instrument.

2-(5-Methylfuran-2-yl)-*N*-(5-(pyridin-4-yl)-1,3,4-thiadiazol-2-yl)quinoline-4-carboxamide (4.1). To a 0 $^{\circ}$C solution of 2-(5-Methylfuran-2-yl)quinoline-4-carboxylic acid (**4.3**)[250] (101 mg, 0.40 mmol) and pyridine thiadiazole **4.4**[251] (79 mg, 0.44 mmol) in DMF (4 mL) were added EDCI·HCl (86 mg, 0.45 mmol) and HOBt (82 mg, 0.61 mmol), followed by NMM (240 μL). The reaction solution was slowly warmed to room temperature and stirred for 18 h. The resulting solution was poured into sat. aq. NH$_4$Cl (30 mL) and extracted with EtOAc (3 x 30 mL). The combined organic layers were washed with brine (2 x 30 mL), dried over anhydrous Na$_2$SO$_4$, filtered and concentrated. The crude product was purified via SiO$_2$ column chromatography using a gradient of MeOH (0% to 50%) in CH$_2$Cl$_2$ to afford 36 mg (22%) of **4.1** as a yellow solid. IR (neat) 2968 cm^{-1}, 1774 cm^{-1}, 1506 cm^{-1}; ^{1}H NMR (DMSO-d$_6$) δ = 13.82 (s, 1H), 8.77 (dd, *J* = 4.5 Hz, 1.6 Hz, 2H), 8.27 (s, 1H), 8.15 (d, *J* = 8.0 Hz, 1H), 8.09 (d, *J* = 8.0 Hz, 1H), 8.01 (dd, *J* = 4.5 Hz, 1.6 Hz, 2H), 7.83 (ddd, *J* = 8.4 Hz, 7.0 Hz, 1.3Hz, 1H), 7.64 (ddd, *J* = 8.2 Hz, 7.0 Hz, 1.1 Hz, 1H), 7.39 (d, *J* = 3.3 Hz, 1H), 6.40 (dd, *J* = 3.3 Hz, 0.9 Hz,

1H), 2.45 (s, 3H); ^{13}C (DMSO-d$_6$) δ = 165.4, 160.3, 159.8, 154.9, 150.9, 150.8, 147.8, 147.8, 139.0, 137.0, 130.6, 129.1, 127.2, 124.9, 122.4, 120.9, 116.9, 113.1, 109.2, 13.6; HRMS-ESI$^+$ *m/z* [M + H]$^+$ calc'd for C$_{22}$H$_{15}$N$_5$O$_2$S: 414.1025, found: 414.1033.

2-Oxo-*N*-(5-pyridin-4-yl)-1,3,4-thiadiazol-2-yl)-1,2-dihydroquinoline-4-carboxamide (4.5). 2-oxo-1,2-dihydroquinoline-4-carboxylic acid (**4.6**) (50 mg, 0.27 mmol) and PyBOP (156 mg, 0.300 mmol) were placed in a dry flask and dissolved in DMF (1 mL). 2-Amino-5-(4-pyridyl)-1,3,4-thiadiazole (**4.4**, 54 mg, 0.3 mmol) was added followed by NMM (33 µL, 0.30 mmol). The reaction was stirred overnight at room temperature. A light precipitate formed over the course of the reaction. This precipitate was collected via vacuum filtration and dried under vacuum to afford 54 mg (59 %) of **4.5** as a light yellow powder. IR (neat) 3058 cm^{-1}, 2970 cm^{-1}, 1772 cm^{-1}, 1594 cm^{-1}, 1505 cm^{-1}; ^{1}H NMR (DMSO-d$_6$): δ = 13.72 (s, 1H), 12.10 (s, 1H), 8.77 (d, *J* = 8.0 Hz, 2H), 7.99 (d, *J* = 8.0 Hz, 2H), 7.73 (d, *J* = 8.0 Hz, 1H), 7.59 (t, *J* = 8.0 Hz, 1H), 7.40 (d, *J* = 8.0 Hz, 1H), 7.23 (t, *J* = 8.0 Hz, 1H), 6.91 (s, 1H); ^{13}C (DMSO-d$_6$): δ = 165.2, 160.4, 159.7, 150.8, 149.2, 147.5, 142.0, 136.9, 131.6, 128.5, 128.5, 125.2, 122.9, 121.7, 120.9; HRMS-ESI$^+$ *m/z* [M + H]$^+$ calc'd for C$_{17}$H$_{11}$N$_5$O$_2$S: 350.0712, found: 350.0714.

4-((5-(Pyridin-4-yl)-1,3,4-thiadiazol-2-yl)carbamoyl)quinoline-2-carboxylic acid (4.7) and **(Z)-2-(4-oxopent-2-enoyl)-N-(5-(pyridin-4-yl)-1,3,4-thiadiazol-2-yl)quinoline-4-carboxamide (4.9)**. This procedure was adapted from published literature.[265] To a mixture of 2-(5-methylfuran-2-yl)-N-(5-(pyridin-4-yl)-1,3,4-thiadiazol-2-yl)quinoline-4-carboxamide (**4.1**, 250.0 mg, 0.605 mmol) in CCl$_4$/MeCN (6 mL, 1:1, v/v) was added NaIO$_4$ (582.0 mg, 2.721 mmol) in H$_2$O (6

mL) and $RuO_2 \cdot H_2O$ (6.0 mg, 0.048 mmol).The biphasic mixture was stirred vigorously at rt exposed to ambient air. After 16 h, the resulting ppt was removed by filtration and washed with MeOH (5 x 20 mL) to yield a brown powder. Purification of 25 mg crude product was performed on an Agilent 1200 series instrument equipped with a diode array detector and Zorbax SB-C18 column (4.6 x 150 mm, 3.5 µm, Agilent Technologies). The purification method (1 mL/min flow rate) involved isocratic 10% MeCN in ddH_2O (both containing 0.1% TFA; 0 to 2 mins) followed by linear gradients of 10% to 25% MeCN in ddH_2O (both containing 0.1% TFA; 2 to 12 mins), 25-35% MeCN in ddH_2O (both containing 0.1% TFA; 12 to 27 min), 35-90% MeCN in ddH_2O (both containing 0.1% TFA; 27 to 35 min), and isocratic 90% MeCN in ddH_2O (both containing 0.1% TFA; 35-40 mins). Wavelengths monitored = 215 nm and 254 nm. Compound **4.7** (5.0 mg, 29%) was isolated as a pale yellow powder, and compound **4.9** (9.1 mg, 36%) was isolated as a brown powder following lyophilization. (**4.7**) ^{1}H NMR (DMSO-d_6): δ = 13.90 (bs, 1H), 8.77 (d, J = 5.0 Hz, 2H), 8.47 (s, 1H), 8.30 (d, J = 9.5 Hz, 1H), 8.28 (d, J = 8.5 Hz, 1H), 8.01 (d, J = 5.0 Hz, 2H), 7.97 (t, J = 7.5 Hz, 1H), 7.86 (t, J = 7.5 Hz, 1H); HRMS-ESI[+] m/z [M + H][+] calc'd for $C_{17}H_{11}N_5O_2S$: 378.0655, found: 378.0662; (**4.9**) [1]H (DMSO-d_6): δ = 14.00 (bs, 1H), 8.80 (bd, 2H), 8.54 (s, 1H), 8.47 (d, J = 16.5 Hz, 1H), 8.41 (d, J = 8.5 Hz, 1H), 8.36 (d, J = 9.0 Hz, 1H), 8.04 (m, 3H), 7.93 (t, J = 8.0 Hz, 1H), 7.19 (d, J = 16.5 Hz, 1H), 2.56 (s, 3H); HRMS-ESI[+] m/z [M + H][+] calc'd for $C_{17}H_{11}N_5O_2S$: 430.0968, found: 430.0957.

2-(5-Methylfuran-2-yl)quinoline-4-carboxylic acid (**4.13**). Synthesized as previously described.[250] Isolated as a brown powder (79%). ^{1}H NMR (DMSO-d_6)

δ = 8.64 (d, *J* = 11.0 Hz, 1H), 7.87 (d, *J* = 10.5 Hz, 1H), 7.79 (s, 1H), 7.61 (ddd, *J* = 8.5 Hz, 6.0 Hz, 2.0 Hz, 1H), 7.41 (ddd, *J* = 8.5 Hz, 6.5 Hz, 2.0 Hz, 1H), 7.14 (d, *J* = 4.0 Hz, 1H), 6.31 (d, *J* = 4.5 Hz, 1H), 2.42 (s, 3H); LRMS-ESI$^+$ *m/z* [M + H]$^+$ calc'd for C$_{15}$H$_{11}$NO$_3$: 254.1, found: 254.1.

General Procedure for the Coupling of 5-(pyridin-4-yl)-1,3,4-thiadiazol-2-amine to Carboxylic Acids (4.14, 4.16, 4.18, 4.20, 4.22): To a stirred solution of 5-(pyridin-4-yl)-1,3,4-thiadiazol-2-amine (**4.4**, 1 equiv.) in DMF (0.3 M) was added the appropriate carboxylic acid (1 equiv.), EDCI·HCl (1.2 equiv.), HOBt (1.2 equiv.), and NMM (6.0 equiv.), and the reaction was stirred at rt. After 24 h, the DMF was removed in vacuo, and the resulting residue was triturated with MeOH. The ppt was removed by filtration and purified over SiO$_2$ (0% to 30% MeOH in DCM) to yield the desired products.

2-(Furan-2-yl)-N-(5-(pyridin-4-yl)-1,3,4-thiadiazol-2-yl)quinoline-4-carboxamide (4.14). Yellow powder (24%). ^{1}H NMR (DMSO-d$_6$) δ = 13.85 (s, 1H), 8.78 (d, *J* = 4.5 Hz, 2H), 8.35 (s, 1H), 8.19 (d, *J* = 8.5 Hz, 1H), 8.12 (d, *J* = 8.0 Hz, 1H), 8.02 (m, 3H), 7.87 (t, *J* = 7.0 Hz, 1H), 7.68 (t, *J* = 7.5 Hz, 1H), 7.50 (d, *J* = 2.5 Hz, 1H), 6.79 (m, 1H); LRMS-ESI$^+$ *m/z* [M + H]$^+$ calc'd for C$_{21}$H$_{13}$N$_5$O$_2$S: 400.1, found: 400.2.

2-(5-Methylfuran-2-yl)-N-(5-(pyridin-4-yl)-1,3,4-thiadiazol-2-yl)isonicotinamide (4.16). Yellow powder (6%). ^{1}H (DMSO-d$_6$): δ = 13.81 (bs, 1H), 8.77 (m, 3H), 8.31 (s, 1H), 7.97 (d, *J* = 4.2 Hz, 2H), 7.84 (d, *J* = 5.2 Hz, 1H), 7.12 (d, *J* = 3.3 Hz, 1H), 6.34 (d, *J* = 3.3 Hz, 1H), 2.42 (s, 3H); LRMS-ESI$^+$ m/z [M + H]$^+$ calc'd for C$_{18}$H$_{13}$N$_5$O$_2$S: 364.1, found: 364.2.

2-(Furan-2-yl)-N-(5-(pyridin-4-yl)-1,3,4-thiadiazol-2-yl)isonicotinamide (**4.18**).

White powder (9%). ^{1}H (DMSO-d$_6$): δ = 13.77 (bs, 1H), 8.82 (d, J = 5.0 Hz, 1H), 8.76 (d, J = 5.0 Hz, 2H), 8.40 (s, 1H), 7.97 (d, J = 4.5 Hz, 2H), 7.94 (m, 1H), 7.90 (d, J = 5.0 Hz, 1H), 7.23 (d, J = 3.0 Hz, 1H), 6.72 (m, 1H); LRMS-ESI$^+$ m/z [M + H]$^+$ calc'd for C$_{17}$H$_{11}$N$_5$O$_2$S: 350.1, found: 350.2.

3-(5-Methylfuran-2-yl)-N-(5-(pyridin-4-yl)-1,3,4-thiadiazol-2-yl)-1-naphthamide (**4.20**) Yellow powder (12%). ^{1}H (DMSO-d$_6$): δ = 13.57 (bs, 1H), 8.76 (d, J = 5.5 Hz, 2H), 8.45 (m, 1H), 8.34 (m, 1H), 8.28 (m, 1H), 8.21 (d, J = 8.0 Hz, 1H), 8.08 (d, J = 8.5 Hz, 1H), 7.99 (d, J = 5.5 Hz, 2H), 7.60 (m, 2H), 7.09 (d, J = 3.0 Hz, 1H), 6.30 (m, 1H); 2.41 (s, 3H); LRMS-ESI$^+$ m/z [M + H]$^+$ calc'd for C$_{23}$H$_{16}$N$_4$O$_2$S: 413.1, found: 413.2.

3-(Furan-2-yl)-N-(5-(pyridin-4-yl)-1,3,4-thiadiazol-2-yl)-1-naphthamide (**4.22**). Pale yellow powder (7%). ^{1}H (DMSO-d$_6$): δ = 13.61 (bs, 1H), 8.78 (dd, J = 4.5 Hz, 1.5 Hz, 2H), 8.45 (m, 1H), 8.35 (d, J = 1.5 Hz, 1H), 8.24 (dd, J = 6.5 Hz, 2.5 Hz, 1H), 8.12 (dd, J = 6.5 Hz, 2.0 Hz, 1H), 8.01 (dd, J = 4.5 Hz, 1.5 Hz, 2H), 7.89 (d, J = 1.0 Hz, 1H), 7.63 (m, 2H), 7.24 (d, J = 3.0 Hz, 1H), 6.71 (dd, J = 3.5 Hz, 2.0 Hz, 1H); LRMS-ESI$^+$ m/z [M + H]$^+$ calc'd for C$_{22}$H$_{14}$N$_4$O$_2$S: 399.1, found: 399.1.

2-(Furan-2-yl)quinoline-4-carboxylic acid (**4.15**) Synthesized as previously described.[250] Isolated as brown powder (34%). ^{1}H NMR (DMSO-d$_6$) δ = 8.63 (dd, J = 11.0 Hz, 2.0 Hz, 1H), 8.27 (s, 1H), 8.47 (dd, J = 11.0 Hz, 1.0 Hz, 1H), 7.97 (dd, J = 2.5 Hz, 1.0 Hz, 1H), 7.82 (ddd, J = 9.0 Hz, 7.0 Hz, 1.5 Hz, 1H), 7.66 (ddd, J = 9.0 Hz, 7.0 Hz, 1.5 Hz, 1H), 7.44 (dd, J = 4.5 Hz, 1.0 Hz, 1H), 6.75 (dd,

J = 4.0 Hz, 2.0 Hz, 1H); LRMS-ESI$^+$ *m/z* [M + H]$^+$ calc'd for C$_{22}$H$_{15}$N$_5$O$_2$S: 414.1025, found: 414.1033. LRMS-ESI$^+$ *m/z* [M + H]$^+$ calc'd for C$_{14}$H$_9$NO$_3$: 240.1, found: 240.1.

General Procedure for Suzuki Coupling with 5-Methylfuran-2-Boronic Acid Pinocol Ester or Furan-2-Boronic Acid (**4.17, 4.21, 4.23, 4.24**): To a mixture of the appropriate iodine or bromide (1 equiv.) in DMF/H$_2$O (0.08 M, 5/1, v/v) was added boronic acid (1.5 equiv.), and Na$_2$CO$_3$ (1.5 equiv.). The reaction mixture was degassed with bubbling N$_2$ for 10 min, and Pd(PPh$_3$)$_2$Cl$_2$ (5 mol %) was added. The reaction mixture was degassed with bubbling N$_2$ for 10 additional min, and then heated to 95 ^{o}C. After 2h, the reaction was cooled to rt, and the reaction was concentrated onto SiO$_2$. SiO$_2$ purification (0% to 50% MeOH in DCM) provided the desired products.

2-(5-Methylfuran-2-yl)isonicotinic acid (**4.17**). Brown powder (>99%). ^{1}H (CD$_3$OD): δ = 8.47 (d, J = 5.5 Hz, 1H), 8.15 (s, 1H), 7.63 (dd, J = 5.0 Hz, 1.0 Hz, 1H), 6.98 (d, J = 3.0 Hz, 1H), 6.19 (d, J = 3.0 Hz, 1H), 2.39 (s, 3H); LRMS-ESI$^+$ m/z [M + H]$^+$ calc'd for C$_{11}$H$_9$NO$_3$: 204.1, found: 204.1.

3-(5-Methylfuran-2-yl)-1-naphthoic acid (**4.21**). Brown Powder (21%). ^{1}H (CD$_3$OD): δ = 8.80 (m, 1H), 8.42 (m, 1H), 8.25 (m, 1H), 7.92 (dd, J = 5.5 Hz, 3.5 Hz, 1H), 7.52 (m, 2H), 6.81 (d, J = 3.0 Hz, 1H), 6.17 (m, 1H), 2.41 (s, 3H); LRMS-ESI$^+$ m/z [M + H]$^+$ calc'd for C$_{16}$H$_{12}$O$_3$: 253.1, found: 253.1.

3-(Furan-2-yl)-N-(5-(pyridin-4-yl)-1,3,4-thiadiazol-2-yl)-1-naphthamide (**4.23**). Pale yellow powder (48%). ^{1}H (CDCl$_3$): δ = 9.01 (d, J = 8.5 Hz, 1H), 8.67 (m, 1H), 8.36 (m, 1H), 7.94 (d, J = 8.0 Hz, 1H), 7.62 (t, J = 8.0 Hz, 1H), 7.57 (m, 2H), 6.87

(d, J = 3.0 Hz, 1H), 6.56 (dd, J = 3.5 Hz, 2.0 Hz, 1H); LRMS-ESI$^+$ m/z [M + H]$^+$ calc'd for $C_{15}H_{10}O_3$: 239.1, found: 239.1.

2-(5-Methylfuran-2-yl)quinoline (4.24). White powder (48%). ^{1}H (CDCl$_3$): δ = 8.14 (d, J = 9.0 Hz, 1H), 8.12 (d, J = 11 Hz, 1H), 7.79 (d, J = 8.5 Hz, 1H), 7.77 (d, J = 7.0 Hz, 1H), 7.70 (t, J = 7.0 Hz, 1H), 7.48 (t, J = 7.0 Hz, 1H), 7.13 (d, J = 2.5 Hz, 1 Hz, 1H), 6.20 (d, J = 2.0 Hz, 1H), 2.48 (s, 3H); LRMS-ESI$^+$ m/z [M + H]$^+$ calc'd for $C_{14}H_{11}NO$: 210.1, found: 210.1.

General Procedure for Stille Coupling with 2-(tributylstannyl)furan (**4.19**, **4.25**): To a suspension of 2-iodoisonicotinic acid (1 equiv.) and Pd(PPh$_3$)$_2$Cl$_2$ (2 mol %) in anhydrous 1,4-dioxane (0.08 M) was added 2-(tributylstannyl)furan (4.5 equiv.), and the reaction was heated to 90 ^{o}C. After 14 h, the reaction was cooled to rt and the reaction mixture was filtered through a Celite pad. The filtrate was concentrated in vacuo and the resulting residue was triturated with hexanes. The ppt was removed by filtration to yield the desired product.

2-(Furan-2-yl)isonicotinic acid (**4.19**). Tan powder (29%). ^{1}H (CD$_3$OD): δ = 8.54 (d, J = 5.5 Hz, 1H), 8.24 (s, 1H), 7.71 (dd, J = 5.0 Hz, 1.0 Hz, 1H), 7.69 (d, J = 1 Hz, 1H), 7.12 (d, J = 3.5 Hz, 1H), 6.61 (dd, J = 3.5 Hz, 1.5 Hz, 1H); LRMS-ESI$^+$ m/z [M + H]$^+$ calc'd for $C_{10}H_7NO_3$: 190.0, found: 190.1.

2-(Furan-2-yl)quinoline (**4.25**). Tan powder (77%). ^{1}H (CDCl$_3$): δ = 8.16 (d, J = 8.5 Hz, 1H), 8.13 (d, J = 8.5 Hz, 1H), 7.82 (d, J = 8.5 Hz, 1H), 7.78 (d, J = 8.5 Hz, 1H), 7.70 (t, J = 8.5 Hz, 1H), 7.63 (m, 1H), 7.50 (t, J = 8.0 Hz, 1H), 7.22 (d, J = 3.0 Hz, 1H), 6.59 (dd, J = 3.0 Hz, 1.5 Hz, 1H); LRMS-ESI$^+$ m/z [M + H]$^+$ calc'd for $C_{13}H_9NO$: 196.1, found: 196.1.

Expression and Purification of APOBEC3A and APOBEC3G. A3A and A3G were expressed and purified as previously described.[1]

DNA Deaminase Assay. The DNA deaminase assay was performed as previously described with the ssDNA oligomer 5'-6-FAM-AAA-TAT-TCC-CTA-ATA-GAT-AAT-GTG-A-TAMRA-3'.[1] A detailed description of the fluorescence-based deamination assay can be found in the SI, Section I. None of the synthesized compounds inhibited uracil DNA glycosylase in the context of the in vitro assay.

Aging of 4.1 under Ambient Conditions. To a scintillation vial containing **4.1** (62.0 mg, 0.15 mmol) was added DMSO (15 mL). An aliquot (1 mL) was dispensed into a separate scintillation vial and left uncapped, exposed to laboratory air. A second aliquot (1 mL) was transferred to a flame dried scintillation vial under N_2. Aliquots (100 μL at time points 0, 3, 7, 14, and 21 days were diluted with MeCN (0.9 mL) and analyzed on an Agilent 1200 series instrument equipped with a diode array detector and Zorbax SB-C18 column (4.6 x 150 mm, 3.5 μm, Agilent Technologies). The analysis method (1 mL/min flow rate) involved isocratic 10% MeCN in ddH_2O (both containing 0.1% TFA; 0 to 2 mins) followed by linear gradients of 10% to 85% MeCN in ddH_2O (both containing 0.1% TFA; 2 to 24 mins) followed by 85% to 95% MeCN in ddH_2O (both containing 0.1% TFA; 24-26 mins). Wavelengths monitored = 215 nm and 254 nm. The experiment was performed in triplicate. Similar data was obtained for each replicate.

Isolation of 4.5, 4.7, 4.8a-b, and 4.9 from DMSO Stock Solutions of Aged 4.1 (10 mM). Purification was performed on an Agilent 1200 series instrument equipped with a diode array detector and Zorbax SB-C18 column (4.6 x 150 mm, 3.5 µm, Agilent Technologies). The purification method (1 mL/min flow rate) involved isocratic 10% MeCN in ddH$_2$O (both containing 0.1% TFA; 0 to 2 mins) followed by linear gradients of 10% to 25% MeCN in ddH$_2$O (both containing 0.1% TFA; 2 to 12 mins), 25-35% MeCN in ddH$_2$O (both containing 0.1% TFA; 12 to 27 min), 35-90% MeCN in ddH$_2$O (both containing 0.1% TFA; 27 to 35 min), and isocratic 90% MeCN in ddH$_2$O (both containing 0.1% TFA; 35-40 mins). Wavelengths monitored = 215 nm and 254 nm.

Aging of 4.1 under Photochemical Conditions. Rose Bengal (25.0 mg, 0.0242 mmol, 10 mol %) and **4.1** (100.0 mg, 0.242 mmol) were suspended in DMSO (1 mL) and O$_2$ was bubbled into the mixture throughout the course of the reaction. The mixture was irradiated with 300W of visible light. The temperature of the reaction vessel was modulated by a tepid water bath and light was focused on the reaction by surrounding the light bulb and vessel with aluminum foil. After 9 h, an aliquot (4.2 µL) of the reaction mixture was dissolved in MeCN (0.995 mL) and analyzed on an Agilent 1200 series instrument equipped with a diode array detector and Zorbax SB-C18 column (4.6 x 150 mm, 3.5 µm, Agilent Technologies). The analysis method (1 mL/min flow rate) involved isocratic 10% MeCN in ddH$_2$O (both containing 0.1% TFA; 0 to 2 mins) followed by linear gradients of 10% to 50% MeCN in ddH$_2$O (both containing 0.1% TFA; 2 to 10 mins) and 50-95% MeCN in ddH$_2$O (both containing 0.1% TFA; 10 to 12 min), and isocratic 95% MeCN in ddH$_2$O (both containing 0.1% TFA; 12-15 mins).

142

Wavelengths monitored = 215 nm and 254 nm. Once established that **4.1** autosensitizes its own photooxidation, rose bengal was omitted from future mechanistic studies. The identical reaction setup was employed to further probe the mechanism of decomposition and was accomplished by exchanging individual components. Specifically, bubbled oxygen was replaced in one experiment by N_2 and in another by $^{18}O_2$. In the final experiment, 10% (of the total volume) $H_2^{18}O$ was added to the DMSO. For the experiments employing N_2, $^{18}O_2$, and $H_2^{18}O$, three cycles of freeze-pump-thaw were employed to remove any dissolved oxygen in the DMSO. Each of these aging experiments (O_2, N_2, $^{18}O_2$ and $H_2^{18}O$) was performed in triplicate. Similar data was obtained for each replicate.

Aging of Mechanistic Probes and Structurally Analogous 2-furylquinolines. Three 10 mM DMSO stock solutions were prepared for each compound and the three samples were aged over 6 weeks in 1 mL microcentrifuge tubes. The stocks were exposed to laboratory air by piercing the cap of the microcentrifuge tube with a small hole. Aliquots were taken from each sample at time points 0, 2, 21, and 38 days and were diluted with MeCN and analyzed by reverse phase analytical HPLC. Analysis was performed on an Agilent 1200 series instrument equipped with a diode array detector and Zorbax SB-C18 column (4.6 x 150 mm, 3.5 μm, Agilent Technologies). The analysis method (1 mL/min flow rate) involved isocratic 10% MeCN in ddH_2O (both containing 0.1% TFA; 0 to 2 mins) followed by linear gradients of 10% to 50% MeCN in ddH_2O (both containing 0.1% TFA; 2 to 10 mins) and 50-95% MeCN in ddH_2O (both containing 0.1% TFA; 10 to 12 min), and isocratic 95% MeCN in ddH_2O (both containing 0.1% TFA; 12-15 mins).

Wavelengths monitored = 215 nm and 254 nm. To quantify the amount of parent compound remaining, the area under the curve (AUC) of the parent compound was divided by the AUC of an internal standard. Rose bengal (2.5 μM) was used as the internal standard and was added during the MeCN dilution steps immediately before HPLC analysis. Aging experiments were performed in triplicate and values shown are the mean ± standard deviation (calculated in Microsoft Excel). Calibration curves to normalize for injection variances during HPLC analysis were generated for each compound. For all 21 compounds, R^2 > 0.95 (non-linear regression).

Protocol for LC-MS Analysis of Aged compounds. LC-MS analyses were performed on an Agilent 1100 series instrument equipped with an Agilent MSD SL Ion Trap mass spectrometer (positive-ion mode) and a Zorbax SB-C18 column (0.5 x 150 mm, 5 μm, Agilent Technologies). The analysis method (15 μL/min flow rate) involved isocratic 10% MeCN (containing 0.1% TFA) in ddH$_2$O (containing 0.1% HCO$_2$H; 0 to 2 mins) followed by a linear gradient of 10% to 90% MeCN (containing 0.1% TFA) in ddH$_2$O (containing 0.1% HCO$_2$H; 2 to 24 mins), and isocratic 90% MeCN (containing 0.1% TFA) in ddH$_2$O (containing 0.1% HCO$_2$H; 24-26 mins). The column was heated to 40 ^{o}C. Wavelengths monitored = 214 nm and 254 nm.

144

4.5. Spectral Data for the Synthesized and Isolated Compounds

^{1}H NMR (d$_6$-DMSO)

(4.1)

^{13}C NMR (d$_6$-DMSO)

(4.1)

¹H NMR (d₆-DMSO)

(4.5)

¹³C NMR (d₆-DMSO)

(5 **(4.5)**

146

4.7

4.9
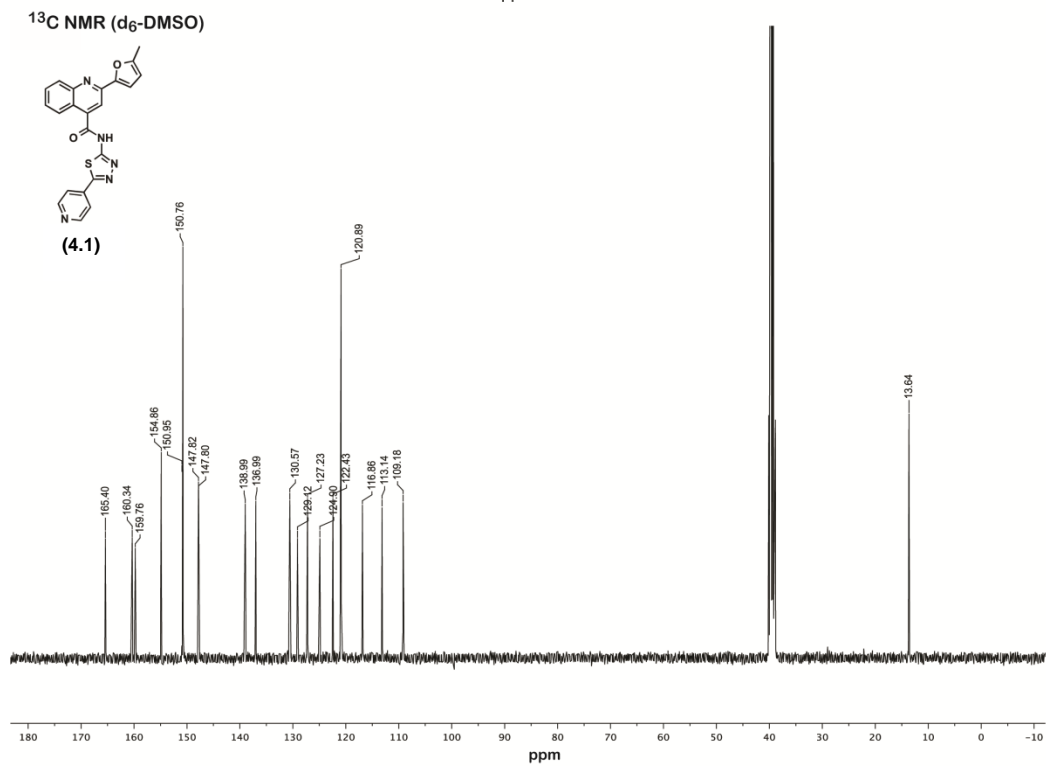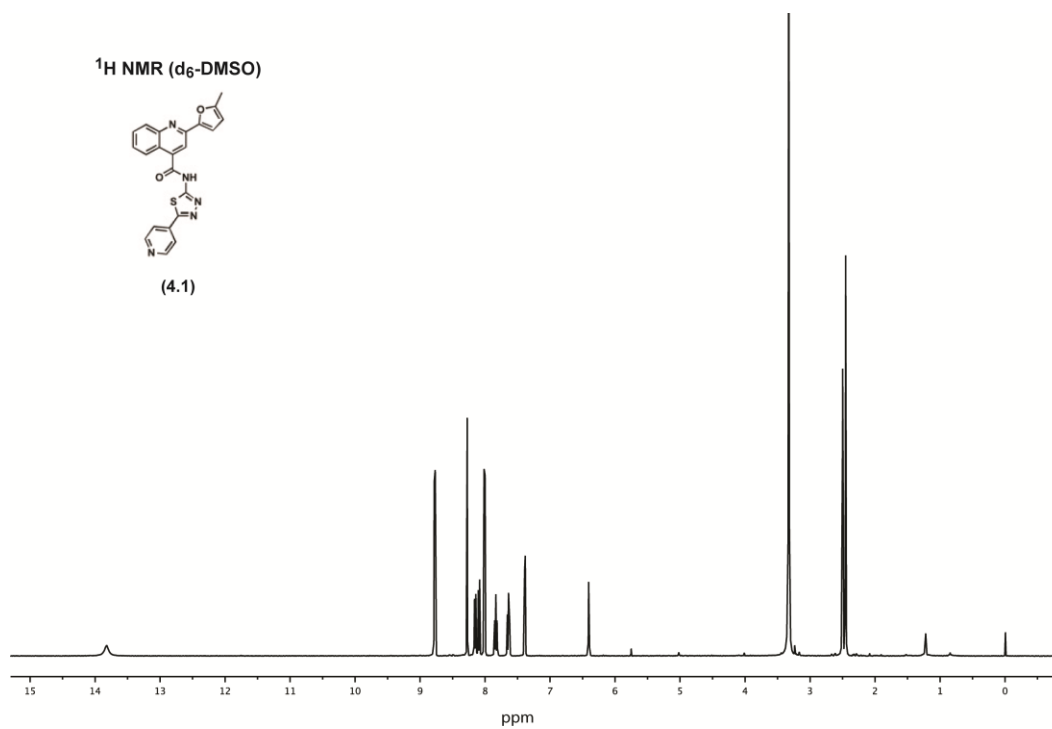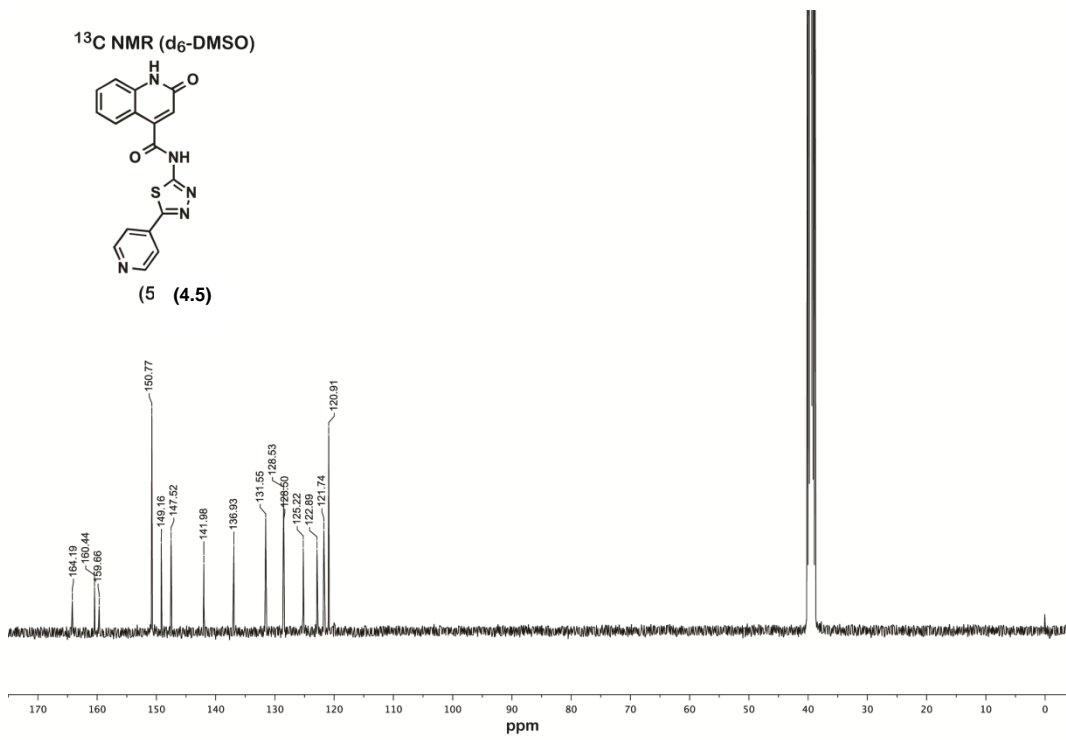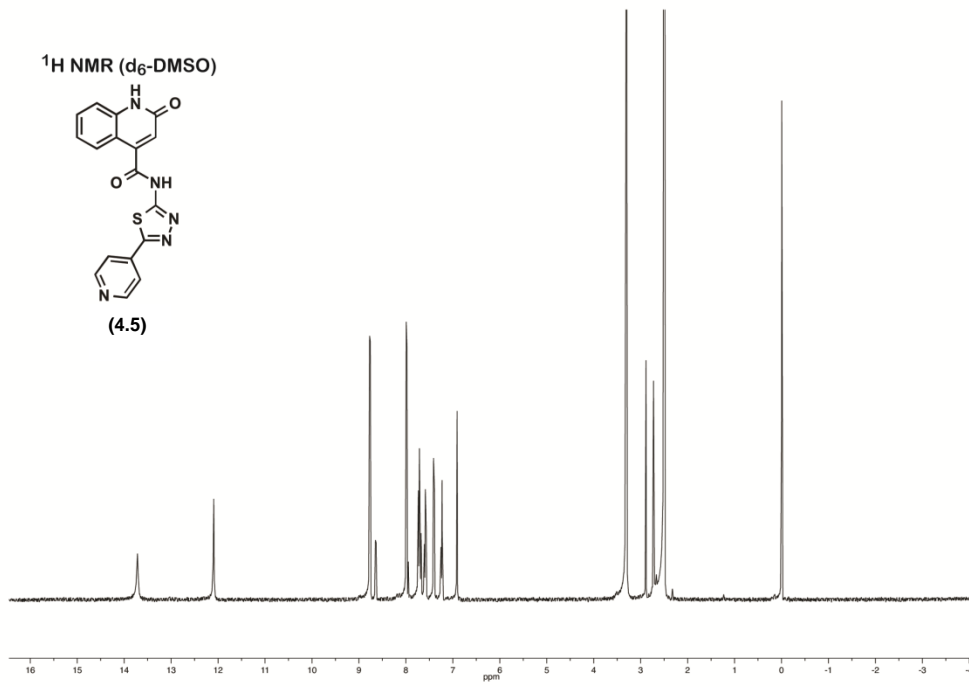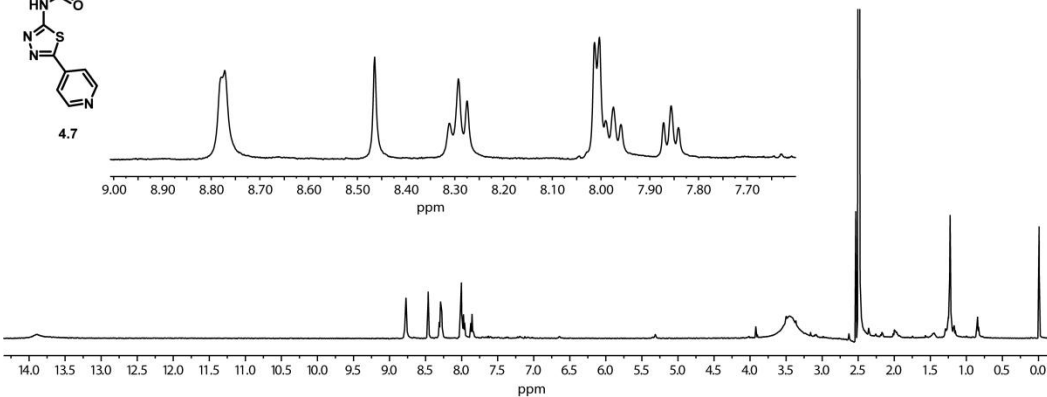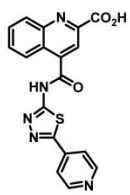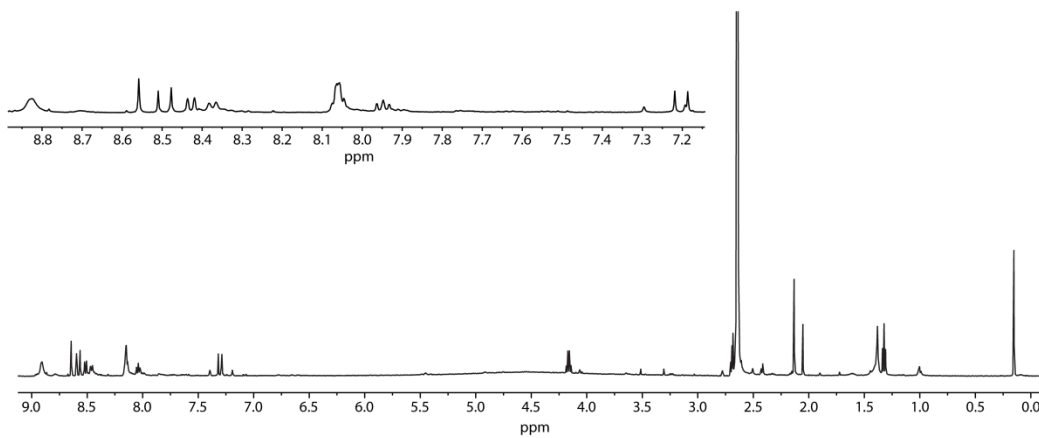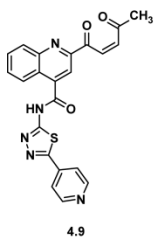
4.6 HPLC Data for Synthesized & Isolated Compounds

General Protocol for HPLC Analysis of Synthesized and Isolated Compounds. DMSO stock solutions of newly synthesized molecules were dissolved in distilled and deionized water (ddH$_2$O) containing trifluoroacetic acid (TFA, 0.1% v/v) and analyzed on an Agilent 1200 series instrument equipped with a diode array detector and Zorbax SB-C18 column (4.6 x 150 mm, 3.5 µm, Agilent Technologies). The analysis method (1 mL/min flow rate) involved isocratic 10% MeCN in ddH$_2$O (both containing 0.1% TFA; 0 to 2 mins) followed by linear gradients of 10% to 85% MeCN in ddH$_2$O (both containing 0.1% TFA; 2 to 24 mins) and 85% to 95% MeCN in ddH$_2$O (both containing 0.1% TFA; 24 to 26 mins). Wavelengths monitored = 215 nm and 254 nm.

Synthesized **4.1**:

Synthesized **4.5**:

148
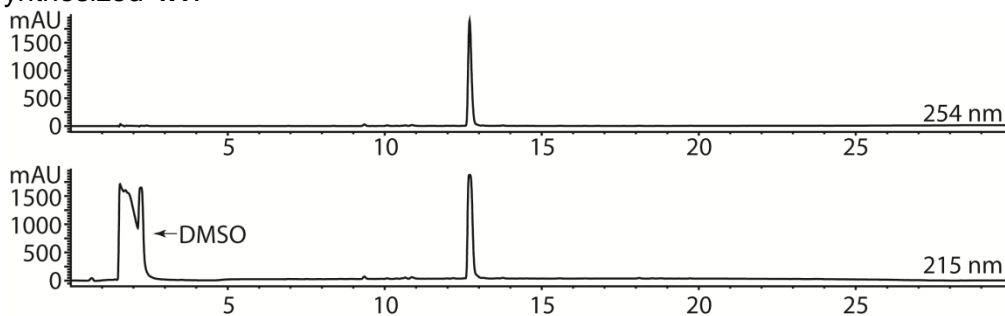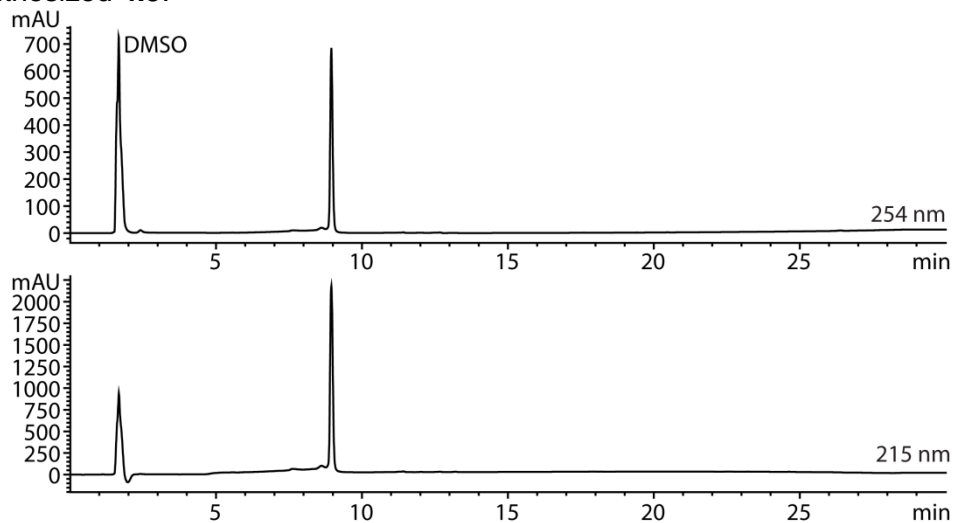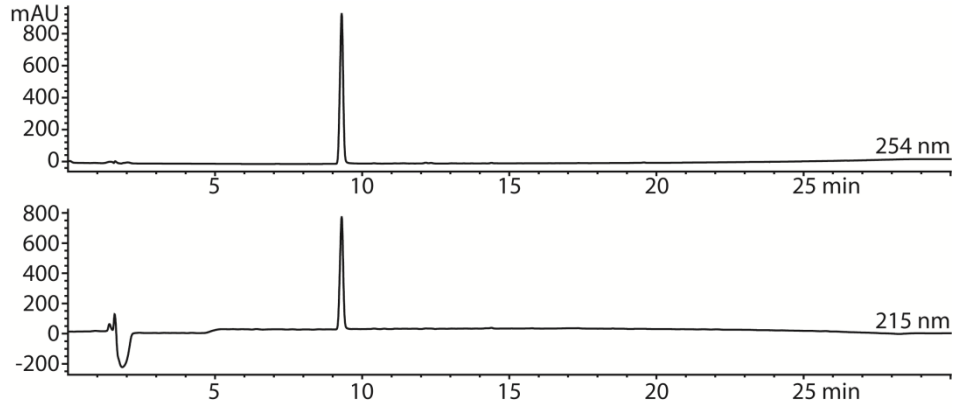
Isolated **4.6**:

Isolated **4.7a-4.7b**:

Isolated **4.8**:

149
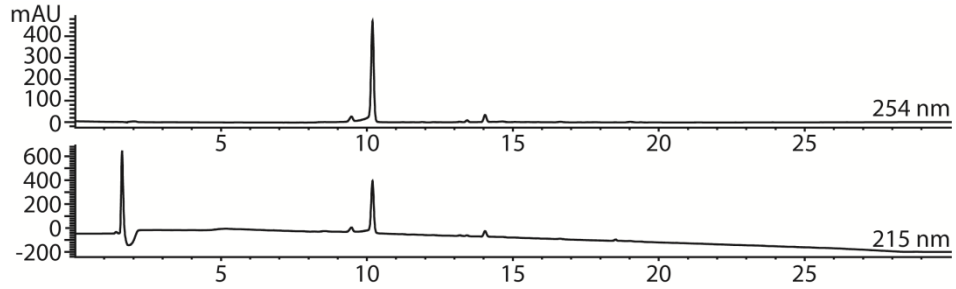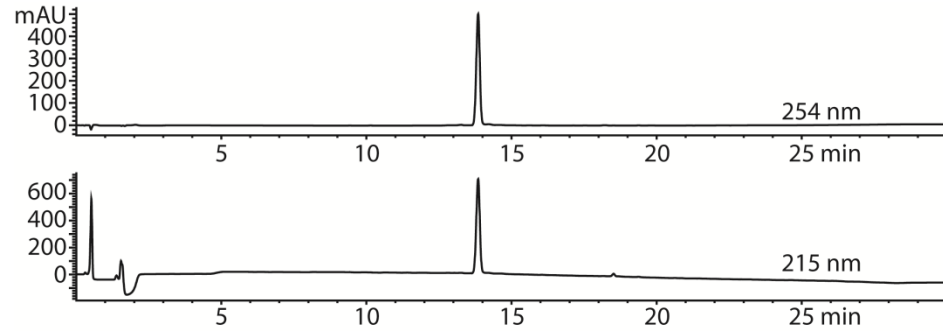
4.7 Synthesis & LC-MS/MS Analysis of Synthesized 4.7 and 4.9
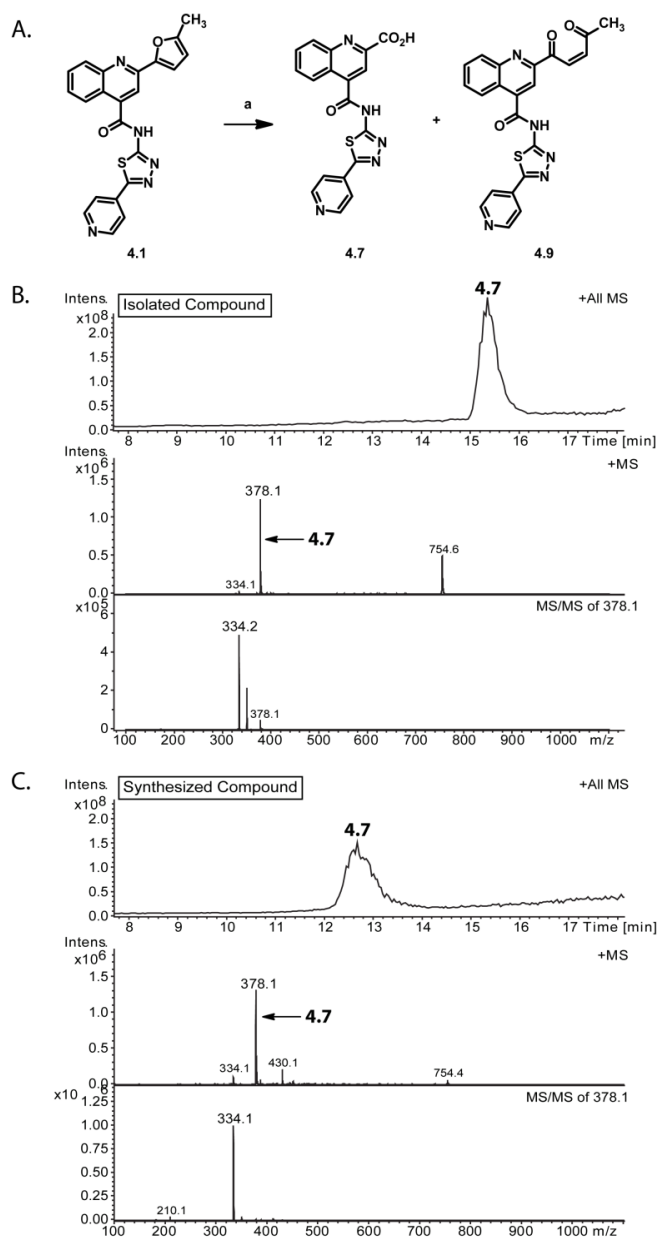
Figure 4.10. Synthesis and Characterization of **4.7**. (A) Synthesis of **4.7**. *Reagents and conditions*: (a) $RuO_2 \cdot H_2O$, $NaIO_4$, $CCl_4/MeCN/H_2O$, 29%[50] (B) LC-MS/MS analysis of isolated **4.7** compared to the LC-MS/MS chromatorgram of synthesized **4.7** (C). The difference in retention time between the isolated and synthesized material is explained by differences in sample preparation. Isolated **4.6** was injected in a $MeCN/H_2O$ solution, while synthesized **4.6** was injected in a DMSO/MeOH solution.
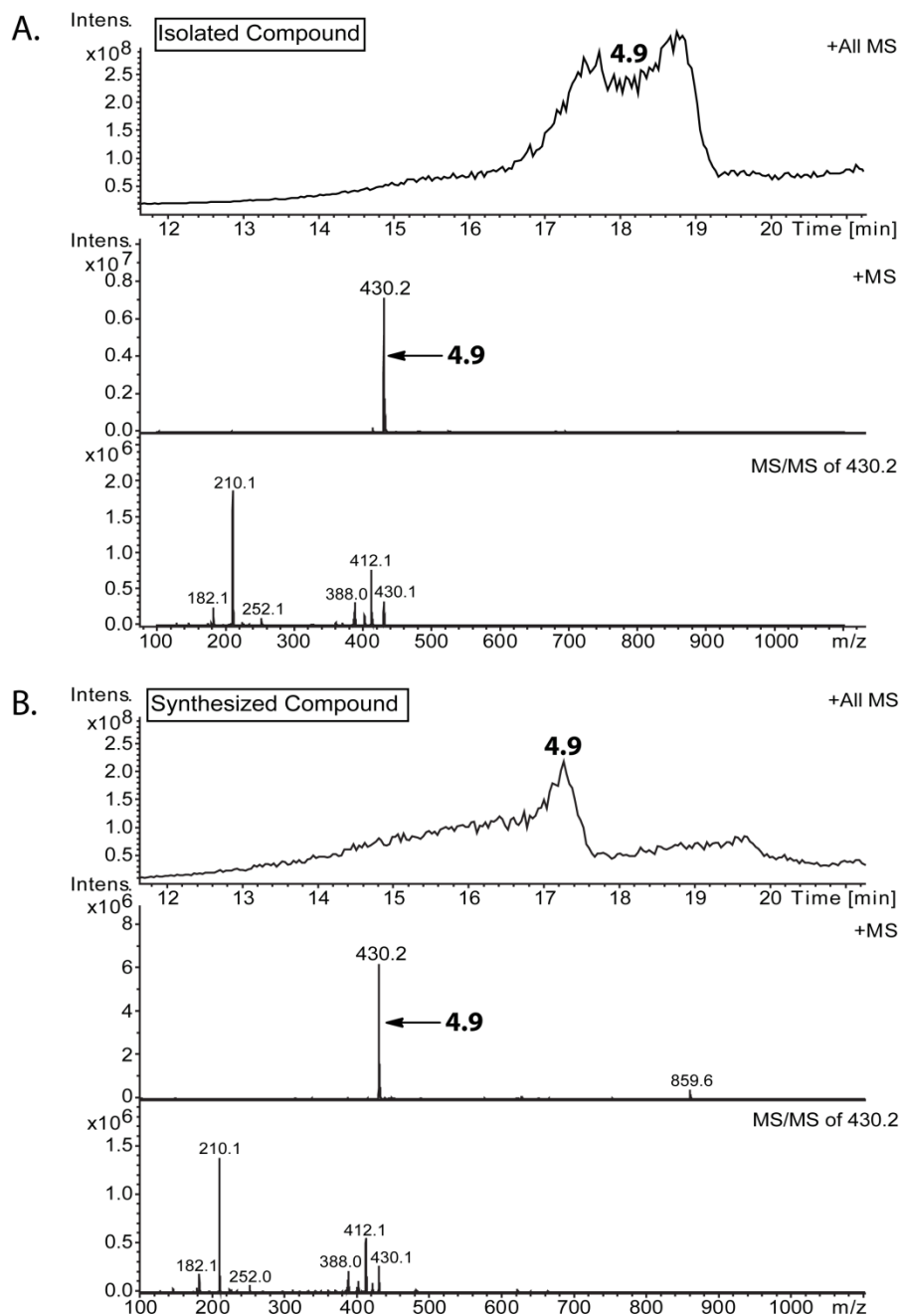
Figure 4.11. LCMS Characterization of **4.9**. The synthesis of **4.9** is shown in Figure 4.10. (A) LC-MS/MS analysis of isolated **4.7** compared to the LC-MS/MS chromatorgram of synthesized **4.9** (B). The difference in retention time between the isolated and synthesized material is explained by differences in sample preparation. Isolated **4.9** was injected in a MeCN/H$_2$O solution, while synthesized **4.9** was injected in a DMSO/MeOH solution.

4.8 High Resolution Mass Spectrum of Aged 4.1 (t = 21 days) as 10 mM DMSO Stock

Figure 4.12. HRMS of **4.1** Incubated for 21 Days.

152

ME03047 #68 RT: 1.00 AV: 1 NL: 2.85E5
T: FTMS + c ESI Full ms [100.00-1000.00]
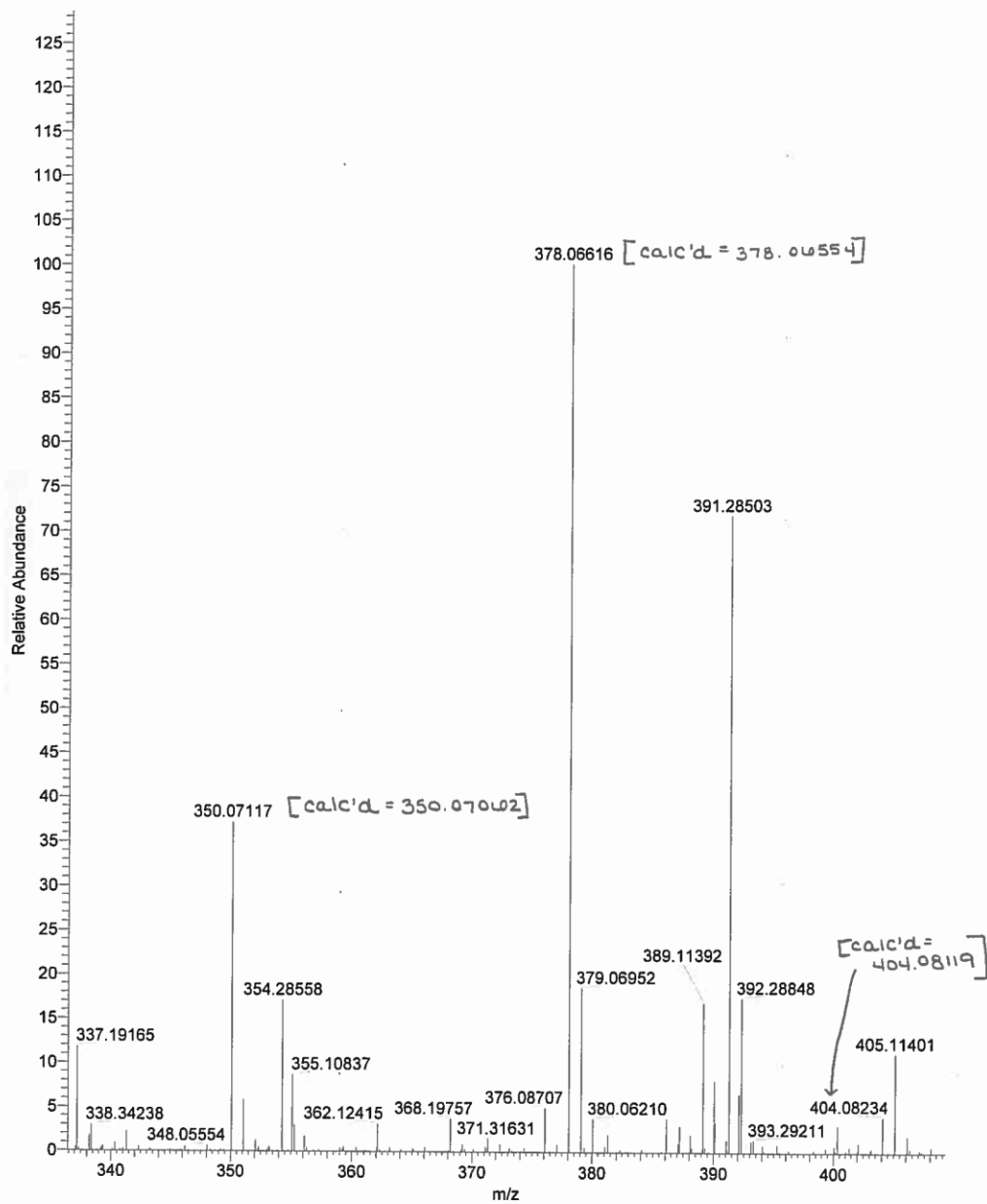
Figure 4.13. Magnified HRMS of **4.1** Incubated for 21 Days. Spectrum from m/z = 335 – 410.

153
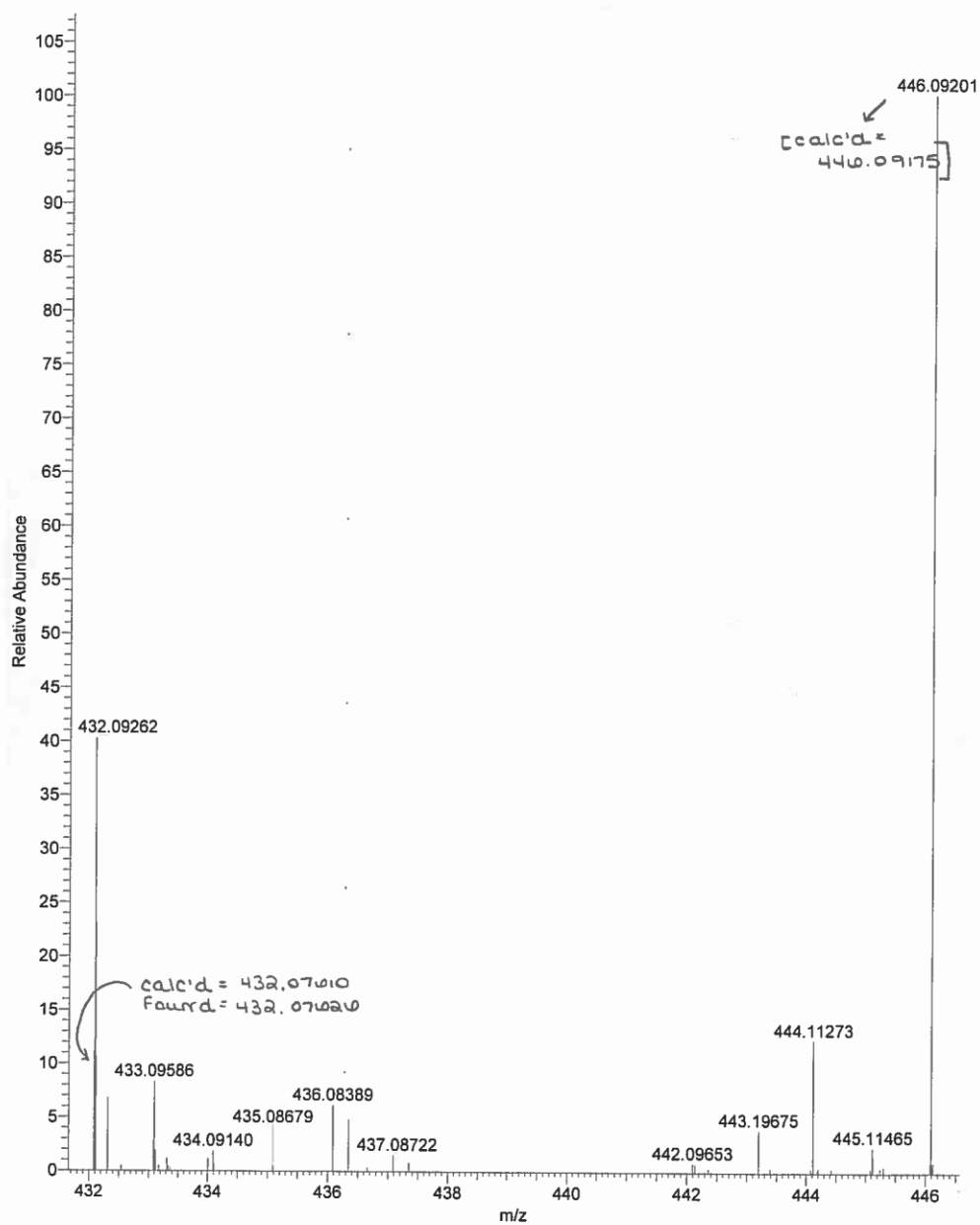
Figure 4.14. Magnified HRMS of **4.1** Incubated for 21 Days. Spectrum from m/z = 430 – 450.

154

4.9 Acknowledgements

Chapter 5

BENZISOTHIAZOLINONE-BASED PROBES OF APOBEC3G STRUCTURE AND FUNCTION

This body of work was conducted in collaboration with Dr. Ming Li, Professor Reuben S. Harris, and Professor Daniel A. Harki.

5.1 Introduction

In recent years, multiple members of the APOBEC3 (apolipoprotein B mRNA editing enzyme, catalytic polypeptide-like) family of ssDNA cytosine-to-uracil (C-to-U) deaminases have emerged as therapeutic targets in HIV-1 and cancer drug discovery.

Specifically, APOBEC3D/F/G and H are human retroviral restriction factors, which can potently inhibit HIV-1 in the absence of viral counter measures. In clinical infection, however, HIV-1 encodes virion infectivity factor (Vif), a viral accessory protein that mediates APOBEC3 expression levels through ubiquitylation and proteasomal degradation.[65,85,208] To accomplish HIV-1 restriction, APOBEC3D/F/G and H incorporate into budding viral particles from HIV-1 infected cells,[69-75] and travel with the particles until an HIV-1 näive cell is reached.[30] Upon fusion of the viral particle to the cell membrane and initiation of reverse transcription, the relevant APOBEC3s inhibit viral replication through deamination dependent[65,82-85] and deamination independent[79-81] mechanisms. Deamination-dependent restriction is accepted as the foremost protective mechanism garnered by the APOBEC3s, and results in extensive C-to-U deamination on the minus-strand cDNA.[50,90-93] APOBEC3 deamination is pre-mutagenic, as the resulting DNA uracils become immortalized as G-to-A hypermutation after viral replication is complete.[88,90-95] If uncontested by Vif, the APOBEC3s can lethally mutagenize the viral genome. For a detailed discussion of the role of APOBEC3s in HIV-1 infection, also see Chapter 1.4.

As a result, a crucial relationship exists between the APOBEC3s and Vif, which ultimately dictates the mutation rate of HIV-1. Moreover, therapies that

target this host-viral interaction may provide the final resolution in accomplishing HIV-1 clearance. Many groups have investigated small molecule inhibitors of Vif, with the goal of restoring the innate antiviral activity of the APOBEC3s, a strategy termed "*therapy by hypermutation*".[136,144,209-213] Strong evidence also exists to support a strategy of "*therapy by hypomutation*," whereby APOBEC3-contributed mutation is required by the virus to achieve an optimum rate of fitness.[106,150-152] In support of this hypothesis, sequenced genomes from HIV-1-positive patients display considerable APOBEC3-dependant mutation patterns, despite the ability of Vif to neutralize the APOBEC3s.[102,214] As a result, mutation attributable to the APOBEC3s likely contributes to the high mutation rate of HIV-1, and thus, its ability to evade immunological and antiretroviral pressures. If APOBEC3-catalyzed mutation is essential for HIV-1 to rapidly evolve, a complimentary therapy that dampens APOBEC3 activity would also slow HIV-1 evolution.[150]

APOBEC3B has recently been implicated in the mutagenesis of breast,[17] ovarian,[158] lung, bladder, head/neck,[163] and cervical cancers.[157,171] The Harris laboratory demonstrated that APOBEC3B is significantly over-expressed in breast cancer cell lines and primary tissues, in comparison to their normal counterparts.[17] APOBEC3B over-expression translates to an elevated overall mutation rate, and the likelihood of pro-cancerous mutations, such as those occurring in the *TP53* and/or *cMyc* genes.[17] Moreover, APOBEC3B over-expression has been clinically shown to correlate with reduced survival rates in breast cancer patients, in comparison to patients that express low levels of APOBEC3B.[172] As mutation is the driving force of cancer initiation, tumor growth, cancer metastasis, and the development of therapeutic resistance, the discovery

of APOBEC3B inhibitors may offer a strategy to reduce the mutation rate and mutation-associated outcomes of cancer.

Extensive efforts over the few last years have yielded the first-in-class inhibitors of the APOBEC3 family.[1,156,190] Strategies, thus far, have relied on the implementation of a fluorescence-based ssDNA deamination assay for high-throughput screening (HTS) of chemical inhibitors against APOBEC3A, APOBEC3B, and APOBEC3G (see Chapter 2 for more details).[1,156,190] The first APOBEC3 inhibitor was achieved by screening the 1280-member Sigma LOPAC library of pharmacologically active compounds. In this effort, MN30 (PubChem CID: 5353329, **1.10**) demonstrated APOBEC3G-specific inhibition, which was accomplished by covalently modifying C321, a residue located proximal to the active site (See Chapter 1.4.4).[1] A molecular model of APOBEC3G inhibition by MN30 (**1.10**) posits that the covalent binding event forces an inhibitory conformational change in nearby Y315.[1] The model suggests that Y315 flips to accommodate MN30 (**1.10**), and as a result, interacts detrimentally with W285, a conserved active site residue.[1] Additionally, an HTS of >325,000 compounds (Sanford-Burnham Medical Research Institute, NIH MLPCN Collection) identified a large class of 1,2,4-trizole-3-thiols, a substructure that ultimately accounted for ~20% of the APOBEC3G-specific screening hits.[156] MN256 (**3.1**), the parent hit, and related analogues are hypothesized to engage C321, analogous to MN30 (**3.1**), as this inhibitor class lost inhibitory potency when tested against an APOBEC3G C321A enzyme mutant.[156]

Despite these early successes, on-going efforts to discover and develop small molecule APOBEC3 inhibitors have been restricted by the lack of structural information regarding ligand binding. Although a number of *apo* X-ray and NMR

structures of the APOBEC3s exist, including structures of APOBEC3A, APOBEC3C, APOBEC3F C-terminal domain (CTD), APOBEC3G CTD, and APOBEC3G N-terminal domain (NTD), none of these structures characterize ligand binding, even to the substrate ssDNA.[1,13,26,48,54-61] To rationally design potent and selective small molecule inhibitors of the APOBEC3s, the next logical step in our inhibitor discovery campaign is to elucidate details of APOBEC3 – ligand interaction.

MN18.0101 (**5.1**)
93% A3G Inhibition
at 10 μM

MN18 (**5.2**)
IC_{50} (A3A) = 31 μM
IC_{50} (A3B CTD) = 11 μM
IC_{50} (A3F CTD) = 5 μM
IC_{50} (A3G) = 2.8 μM
(lysates)
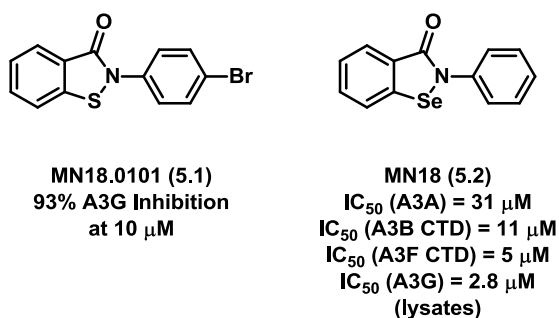
Figure 5.1. Chemical Structures of APOBEC3G Probe Leads MN18.0101 (**5.1**) and MN18 (**5.2**). MN18.0101 (**5.1**) was identified by HTS at Sanford-Burham Medicinal Research Institute and MN18 (**5.2**) was identified by HTS at the University of Minnesota Institute for Therapeutics Discovery & Development (ITDD). The presented biochemical data corresponds to the HTS (**5.1**) or in-house biochemical evaluation of commercially available material (**5.2**). MN18 (**5.2**) has been previously published by the Harki and Harris labs.[1]

By using a class of benzisothiazolinones and structurally related analogues, which were identified via HTS at the Sanford-Burnham Research Institute and University of Minnesota ITDD, we sought to develop HTS hits MN18.0101 (**5.1**) and MN18 (**5.2**), commonly known as ebselen (PubChem CID 3194), into chemical probes of the APOBEC3s (Figure 5.1). Despite being classified as Pan Assay Interference Scaffolds (PAINS),[195,231,266] MN18.0101 (**5.1**) and MN18 (**5.2**) have been previously used as tools to map reactive

cysteines within a protein of interest.[267-269] This is particularly applicable to APOBEC3 drug discovery as the majority of small molecule APOBEC3G inhibitors are cysteine reactive electrophiles, and little is known about their specific binding sites within the enzyme. Compounds with a core benzo[d]isothiazol-3(2H)-one or benzo[d][1,2]selenazol-3(2H)-one have been shown to react covalently with cellular thiols to form heteroatom S-S or S-Se bonds, through ring opening (Figure 5.2).[267-272] An extensive body of literature exists on efforts to develop compounds of this class into therapeutic leads for a multitude of diseases, including antiviral,[268,273-275] antimalarial,[276] anticancer,[277-283] antioxidant,[284] antimicrobial,[285] and anti-osteoarthritic[286] applications.

We envision that MN18.0101 (**5.1**) and MN18 (**5.2**) offer excellent starting points for the design of structural APOBEC3 probes to acquire the first experimental data on protein – ligand binding. Importantly, the MN18 (**5.2**) series is the first that we have studied that not only maintains potent inhibition in cellular lysates, but inhibits all of the evaluated APOBEC3s (APOBEC3A/B/F/G). Thus, by identifying the binding site of MN18 (**5.2**), we may identify a common target for the entire APOBEC3 family.
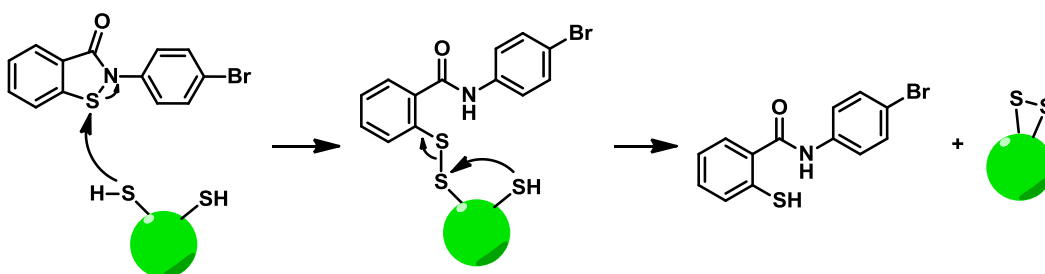
Figure 5.2. Proposed Reaction of Benzisothiazolinones with Biological Cysteines.[270-272] The labile N-S bond is cleaved by a cellular thiol forming a small molecule-protein disulfide adduct. This mechanism of covalent inhibition is

161

reversible under reducing conditions (not shown) or through disufilde exchange. Disulfide exchange with an intramolecular cysteine is depicted in the Figure.

5.2 Synthesis of 5.1

HTS hit **5.1** was synthesized in two steps from commercially available methyl thiosalicylate (**5.3**). The amide intermediate was accomplished through AlMe$_3$-promoted aminolysis, according to the procedure originally published by Weinreb.[287,288] The amide was cyclized to the desired benzisothiazolinone using the hypervalent iodine reagent phenyliodine(III)-bis(trifluoroacetate) (PIFA), which first oxidizes the amide nitrogen to the *N*-acylnitrenium ion, which is an excellent electrophile and readily undergoes intramolecular heterocyclization.[289]
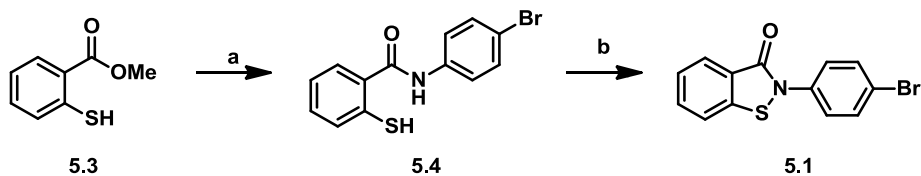
Scheme 5.1. Synthesis of **5.1**. (a) 4-bromoaniline, AlMe$_3$, DCM, 0° to 60° C, 50%; (b) PIFA, DCM, TFA, 0 $^\circ$C, 52%.

5.3 Biochemical Evaluation of 5.1 against a Panel of APOBEC3s

As **5.1** and **5.2** have been previously demonstrated to ring open and bind cellular thiols, we evaluated **5.1** against a panel of previously developed APOBEC3G enzymes. Specifically, the activity of **5.1**, dosed at 50 μM, was analyzed versus wild-type APOBEC3G, triple mutant construct 2K3A,[45] and the single amino acid substitution mutant C321A (Figure 5.3).[45] Previous work to discover small molecule APOBEC3G inhibitors identified C321, a residue within 8 Å of the active site, as the covalent binding site of MN30 (a catechol, **1.10**).[1] C321 is also the proposed binding site of the previously reported inhibitory thiols based on 1,2,4-triazole-3-thiol substructures (see Chapter 3).[156] APOBEC3G 2K3A was previously designed for x-ray crystallography studies and employed in the co-crystallization experiments with MN30 (**1.10**).[1] Importantly, APOBEC3G 2K3A contains three surface Cys-to-Ala substitutions (C243A, C321A, and C356A), which represent the three surface cysteines of APOBEC3G's CTD.

While the previously reported APOBEC3G covalent inhibitors (MN30 [**1.10**], MN256.0102 [**3.8**], MN256.0105 [**3.1**]) lost significant activity against the cysteine mutants, **5.1** maintained nearly equipotent inhibition against APOBEC3G C321A as compared to wild-type enzyme, and lost only ~25% inhibition against 2K3A. Comparatively, the mutant enzymes were more susceptible to **5.1** as compared to the other inhibitor classes. This observation suggests that the benzisothiazolinones target an alternative binding site on the APOBEC3G enzyme. Strengthening this hypothesis, only APOBEC3G contains the proximal cysteine, C321. As MN18 (**5.2**) also potently inhibits the APOBEC3

family (APOBEC3A/B/F/G), there is likely another critical cysteine for enzyme activity.
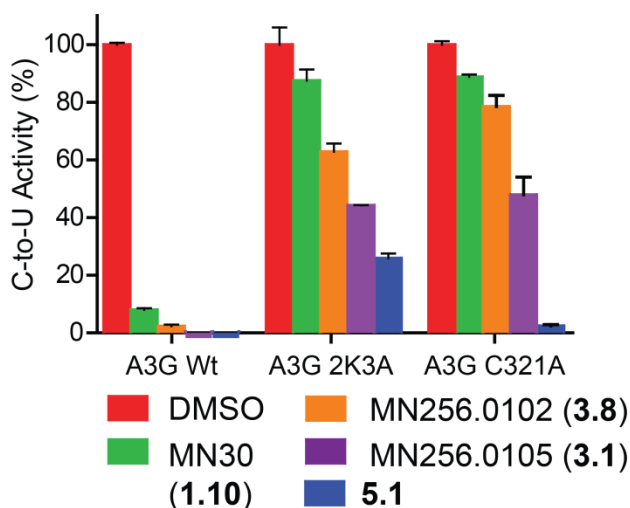
Figure 5.3. Potency of MN30 (**1.10**), MN256.0102 (**3.8**), MN256.0105 (**3.1**), and **5.1** against Wild-type APOBEC3G and APOBEC3G Mutants 2K3A and C321A. The means and SD of triplicate deaminase assays with 50 µM compound are shown relative to the DMSO-only control.

5.4 Compound 5.1 Reacts with Thiols *In Vitro.*

To confirm the reported reactivity of benzisothiazolinones with biologically-relevant nucleophiles, the ability of **5.1** to form covalent adducts was evaluated *in vitro.* APOBEC3G inhibitor **5.1** was incubated with excess cysteine methyl ester (100x) in PBS at pH = 7.4, and aliquots were analyzed at various time points by HPLC (Figure 5.4). A covalent adduct between **5.1** and cysteine methyl ester were observed as early as 30 min post incubation, and by 12 h, complete consumption of **5.1** was observed (Figure 5.4). The proposed adduct is based on previous literature, where mass spectrometry identified adducts to cysteine residues of various proteins with the same compound.[270-272]

164
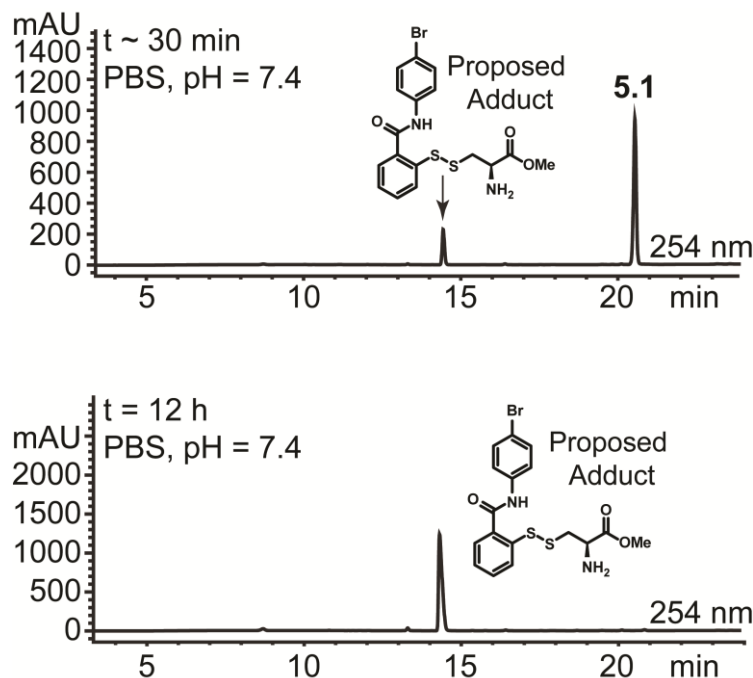
Figure 5.4. Reactivity of **5.1** with Cysteine Methyl Ester. Benzisothiazoline **5.1** and cysteine methyl ester were incubated in aq. PBS (pH = 7.4) at 37 °C. Aliquots were analyzed by reverse-phase HPLC at t ~ 30 min and t = 12 h. Reaction at t = 0 min (top) and t = 12 h (bottom). Complete conversion to a **5.1** – cysteine methyl ester adduct was observed in this experimental time frame. The proposed adduct is the disulfide bond.

5.5 EMSAs Demonstrate 5.1 Inhibits APOBEC3G – ssDNA Binding

In addition to the benzisothiazolinone class likely inhibiting APOBEC3G through a covalent mechanism of action, **5.1** prevents APOBEC3G – ssDNA substrate binding. Electrophoretic mobility shift assays (EMSAs) demonstrated the potent inhibition of substrate binding at the tested 50 μM concentration (Figure 5.5). The effect of **5.1** on APOBEC3G, where no detectable protein – substrate binding was observed, stands in stark contrast to previously published covalent inhibitors. Specifically, the MN256 class of 1,2,4-triazole-3-thiols and MN30 (**1.10**), which are proposed to covalently modify C321, allow APOBEC3G -

ssDNA binding as evidenced by higher molecular weight bands corresponding to DNA – protein complexes. Importantly, the APOBEC3G NTD is hypothesized to be the primary DNA binding domain, which suggests that the benzisothiazolinone family may function as allosteric inhibitors through NTD covalent modification.
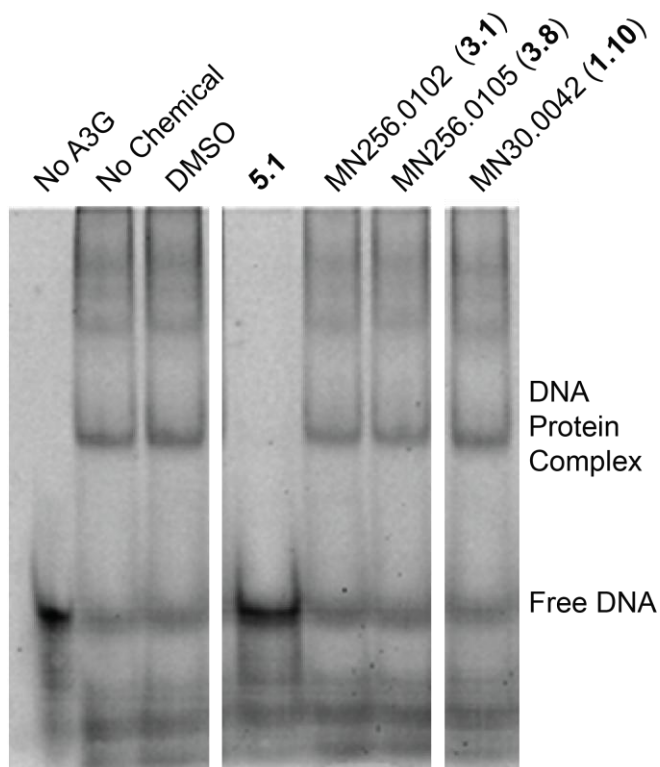
Figure 5.5. Electrophoretic Mobility Shift Assay of **5.1**. In contrast to previously published inhibitors, MN30 (**1.10**)[1] and MN256 (**3.1**),[156] **5.1** potently inhibits protein – ligand binding at 50 μM as evidenced by the distinct free oligo band. Controls for no enzyme, no small molecule, and DMSO are included.
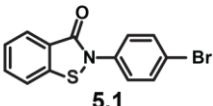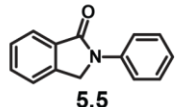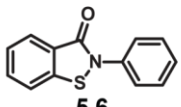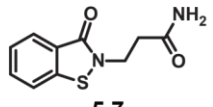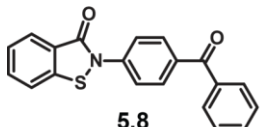
5.6 Synthesis and Biochemical Screening of 5.1-Based Analogues

Structure activity relationship studies on **5.1** have been initiated with the goal of identifying required functionalities and achieving a photoaffinity probe (Table 5.1). Compound **5.5** was purchased commercially, and evaluated to confirm the necessity of the N-S bond. As expected, analogue **5.5** showed no inhibitory activity when tested up to 100 μM. The sulfur analogue of ebselen (sans the 4-bromo) was pursued to evaluate the function of the bromo-substituent. As expected, analogue **5.6** was equipotent to **5.1**. Analogue **5.7** was pursued because a prodrug of this scaffold has been extensively studied as a nucleocapsid inhibitor for anti-HIV-1 drug discovery by the Appella laboratory (NIDDK).[273,290] Interesting, the HIV-1 relevant APOBEC3s, APOBEC3D/F/G/H, were expressed in their experimental model systems; however, the affect of their preclinical candidate on the APOBEC3s has not been investigated. In our hands, analogue **5.7** exhibited a single digit micromolar IC_{50} against APOBEC3G. Taken together, modifications appear to be tolerated off the benzthiazolinone nitrogen, though substituents may be sterically restricted as demonstrated by the benzophenone analogue **5.8**. Unfortunately, analogue **5.8** was designed as a photoaffinity probe of **5.1**, and because it displays no inhibitory activity when test up to 200 μM, others probes will be explored. The synthesis of an aromatic azide is currently underway.

To note, the syntheses of analogues **5.6** and **5.8** were accomplished according to the route described above (Chapter 5.2). Analogue **5.7**, however, was not amendable to AlMe$_3$-mediated aminolysis, so an alternative DIC-

mediated amide bond coupling was employed. PIFA-catalyzed oxidation of intermediate **5.11** gave the desired analogue **5.7.**

Table 5.1. Biochemical Activities of **5.1** Analogues.

Compound	IC$_{50}$ (µM)
5.1	8.0 ± 1.2
5.5	>100
5.6	7
5.7	5
5.8	>100

5.7 Conclusion and Future Work

HTS at the University of Minnesota ITDD and Sanford-Burnham Research Institute identified structural analogues MN18.0101 (**5.1**) and MN18 (**5.2**) as potent inhibitors of the APOBEC3 family. Hit **5.1** demonstrates APOBEC3G-specific activity, inhibiting with an IC$_{50}$ = 8.0 ± 1.2 µM. Hit **5.1**, however, maintains inhibition against APOBEC3G mutants 2K3A and C321A, in contrast to previously reported APOBEC3G-specific inhibitors. Despite their structural similarity, **5.2** exhibited pan APOBEC3 inhibition, with appreciable potencies against APOBEC3A (IC$_{50}$ = 30 µM), APOBEC3B CTD (IC$_{50}$ = 11 µM),

APOBEC3F CTD (IC_{50} = 5 µM), and APOBEC3G (IC_{50} = 2.8 µM) in cell lysates. Preliminary studies with **5.1** demonstrated that molecules of this class readily react with biologically relevant thiols *in vitro*, and potently inhibit APOBEC3G – ssDNA substrate binding. An early SAR library has demonstrated that modifications to the benzisothiazolinone are tolerated up to a certain size. Unfortunately, a first generation attempt to accomplish a MN18.0101-based photoaffinity probe proved unsuccessful, which has prompted second generation studies. We envision that this early work provides a foundation for the elucidation of the MN18 series binding site, which we hypothesize may be a novel target for APOBEC3 inhibition.

5.8 Experimental

General Synthesis Information. Chemical reagents were purchased from commercial sources and used without additional purification. Bulk solvents were from Fisher Scientific and anhydrous *N,N'*-dimethylformamide (DMF) was purchased from Sigma-Aldrich. Anhydrous solvents were obtained from an MBraun Solvent Purification system. Reactions were performed under an atmosphere of dry N_2 where noted. Silica gel chromatography was performed on a Teledyne-Isco Combiflash Rf-200 instrument using Redisep *R*f Gold High Performance silica gel columns (Teledyne-Isco) or self-packed columns with SiliaFlash 60Å silica gel (SiliCycle). HPLC analyses were performed on an Agilent 1200 series instrument equipped with a diode array detector and a Zorbax SB-C18 column (4.6 x 150 mm, 3.5 µm, Agilent Technologies). Compounds used in biological testing were no less than 95% pure as determined by two-wavelength HPLC analysis (254 and 215 nm). Nuclear magnetic

resonance (NMR) spectroscopy was performed using a Bruker Avance instrument operating at 400 MHz or 500 MHz (for ^{1}H) and 100 MHz or 125 MHz (for ^{13}C) at ambient temperature. Chemical shifts are reported in parts per million and normalized to internal solvent peaks or tetramethylsilane (0 ppm).

General Procedure for AlM$_3$ – Catalyzed Aminolysis. To a suspension of amine (1 equiv.) in anhydrous DCM (0.55 M) was added AlMe$_3$ (2 M in hexanes, 1 equiv.) dropwise at 0 ^{o}C. The reaction was allowed to warm to rt, and was stirred until gas evolution ceased. After ~30 min, methyl thiosalicylate (2 equiv.) was added, and the reaction was heated to reflux overnight. After 15 h, the reaction was cooled to rt and quenched carefully with 1 M HCl. The organic layer was separated and the aq. layer was extracted with DCM (3 x 20 mL). The combined organic layers were washed with sat. aq. NaHCO$_3$ (20 mL), ddH$_2$O (20 mL), and brine (20 mL), dried over Na$_2$SO$_4$, and concentrated *in vacuo* to yield the desired amide intermediates (**5.4**, **5.9**, **5.10**) in 31% - 50% yield.
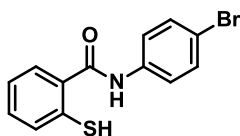
5.4

N-(4-Bromophenyl)-2-mercaptobenzamide (5.4). The crude material was triturated with DCM to yield **5.4** as a yellow solid (50%). ^{1}H NMR (DMSO-d$_6$) δ = 10.57 (bs, 1H), 7.72 (d, 2H, J = 11.1 Hz), 7.63 (d, 1H, J = 9.6 Hz), 7.54 (d, 2H, J = 11.1 Hz), 7.51 (d, 1H, J = 9.8 Hz), 7.37 (t, 1H, J = 9.5 Hz), 7.25 (t, 1H, J = 9.3 Hz); ^{13}C NMR (DMSO-d$_6$) δ = 165.8, 138.2, 136.5, 134.3, 131.7, 131.6, 128.6, 126.4, 126.3, 122.0, 115.7; HRMS-ESI$^+$ m/z [M+Na]$^+$ calc'd for C$_{13}$H$_{10}$BrNOS: 329.9559, found: 329.9552.
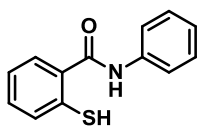
5.9

2-Mercapto-N-phenylbenzamide (5.9). SiO$_2$ purification (gradient 0% to 50% EtOAc in hexanes) gave **5.9** as a white solid (34%). ^{1}H NMR (CDCl$_3$) δ = 10.37 (bs, 1H), 7.73 (d, 2H, J = 7.9 Hz), 7.61 (d, 1H, J = 7.7 Hz), 7.50 (d, 1H, J = 7.9 Hz), 7.35 (m, 3H), 7.25 (t, 1H, J = 7.5 Hz), 7.10 (t, 1H, J = 7.5 Hz); ^{13}C NMR (DMSO-d$_6$) δ = 166.9, 139.5, 134.5, 133.6, 131.0, 131.0, 129.1, 129.0, 125.2, 124.2, 120.4; HRMS-ESI$^+$ m/z [M+Na]$^+$ calc'd for C$_{13}$H$_{11}$NOS: 252.0454, found: 252.0449.
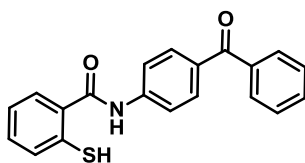
5.10

N-(4-Benzoylphenyl)-2-mercaptobenzamide (5.10). Bright orange powder (31%). ^{1}H NMR (DMSO-d$_6$) δ = 10.93 (s, 1H), 7.96 (d, 2H, *J* = 8.6 Hz), 7.82 (m, 3H), 7.77 (d, 1H, *J* = 8.1 Hz), 7.74 (d, 2H, *J* = 7.1 Hz), 7.67 (t, 1H, *J* = 7.5 Hz), 7.57 (m, 3H), 7.42 (t, 1H, *J* = 7.5 Hz). ^{13}C NMR (DMSO-d$_6$) δ = 194.6, 166.1, 143.0, 137.5, 136.5, 134.3, 132.3, 132.0, 131.8, 131.0, 129.4, 128.7, 128.5, 126.5, 126.4, 119.3; HRMS-ESI$^+$ *m/z* [M+Na]$^+$ calc'd for C$_{20}$H$_{15}$NO$_2$S: 356.0716, found: 356.0700.
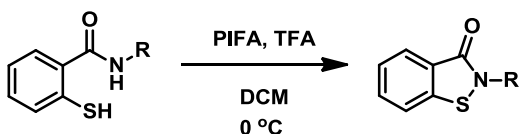
General Procedure for PIFA Oxidation. To a solution of 2-mercapto-N-phenylbenzamide (e.g. **5.4**) and TFA (2 equiv.) in DCM (0.05 M) was added PIFA (1.5 equiv.) at 0 ^{o}C. The reaction was stirred at 0 ^{o}C for 1h, and then the solvent was removed *in vacuo.* SiO$_2$ purification (0% to 50% EtOAc in hexanes) gave the desired benzisothiazolinones (**5.1**, **5.6**, **5.7**, **5.8**) in 35% - 60% yield.

5.1
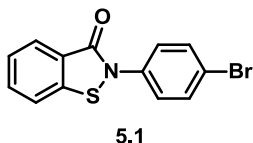
2-(4-Bromophenyl)benzo[d]isothiazol-3(2H)-one (5.1). White solid (52%). ^{1}H NMR (CDCl$_3$) δ = 8.07 (d, 1H, J = 10.3 Hz), 7.96 (d, 1H, J = 9.3 Hz), 7.77 (t, 1H, J = 9.6 Hz), 7.72 (m, 4H), 7.51 (t, 1H, J = 9.5 Hz). ^{13}C NMR (DMSO-d$_6$) δ = 163.3, 139.9, 136.6, 132.8, 132.3, 126.2, 126.1 (3C), 124.2, 122.0, 119.2; HRMS-ESI$^+$ m/z [M+Na]$^+$ calc'd for C$_{13}$H$_8$BrNOS: 327.9402, found: 327.9404.

5.6
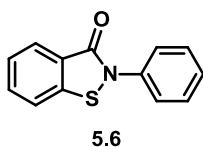
2-Phenylbenzo[d]isothiazol-3(2H)-one (5.6). Pale yellow solid (42%). ^{1}H NMR (CDCl$_3$) δ = 8.09 (d, 1H, J = 7.9 Hz), 7.72 (d, 2H, J = 8.0 Hz), 7.67 (t, 1H, J = 7.6 Hz), 7.59 (d, 1H, J = 8.1 Hz), 7.48 (m, 3H), 7.33 (t, 1H, J = 7.5 Hz). ^{13}C NMR (CDCl$_3$) δ = 164.3, 140.0, 137.4, 132.5, 129.5, 127.4, 127.2, 126.0, 125.0, 124.7, 120.2; HRMS-ESI$^+$ m/z [M+H]$^+$ calc'd for C$_{13}$H$_9$NOS: 228.0478, found: 228.0467.

5.7
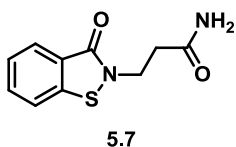
3-(3-Oxobenzo[d]isothiazol-2(3H)-yl)propanamide (5.7). Cream solid (35%). ^{1}H NMR (DMSO-d$_6$) δ = 7.96 (d, 1H, J = 8.1 Hz), 7.85 (d, 1H, J = 7.4 Hz), 7.67 (t, 1H, J = 7.7 Hz), 7.42 (m, 2H), 6.34 (bs, 1H), 4.00 (t, 2H, J = 6.7 Hz), 2.48 (t, 2H, J = 6.6 Hz). ^{13}C NMR (DMSO-d$_6$) δ = 171.5, 164.2, 140.8, 131.7, 125.4, 125.3,

123.9, 121.8, 34.8. Note: One ^{13}C resonance is buried beneath the solvent peaks. HRMS-ESI$^+$ *m/z* [M+H]$^+$ calc'd for $C_{10}H_{10}N_2O_2S$: 223.0536, found: 223.0526.

5.8
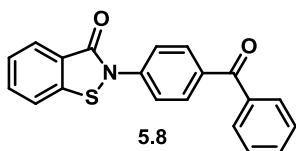
2-(4-Benzoylphenyl)benzo[d]isothiazol-3(2H)-one (5.8). Peach solid (60%). ^1H NMR (CDCl$_3$) δ = 8.14 (d, 1H, *J* = 7.5 Hz), 8.00 (d, 1H, *J* = 7.5 Hz), 7.96 (d, 2H, *J* = 8.5 Hz), 7.91 (t, 1H, *J* = 7.6 Hz), 7.85 (m, 3H), 7.74 (d, 2H, *J* = 8.7 Hz), 7.62 (t, 1H, *J* = 7.4 Hz), 7.52 (t, 2H, *J* = 7.5 Hz). ^{13}C NMR (CDCl$_3$) δ = 195.6, 164.4, 138.1, 137.4, 135.0, 133.8, 132.9, 131.7, 131.6, 130.2, 128.6, 128.2, 127.1, 126.2, 125.5, 100.1; HRMS-ESI$^+$ *m/z* [M+H]$^+$ calc'd for $C_{20}H_{13}NO_2S$: 332.0740, found: 332.0726.

5.11
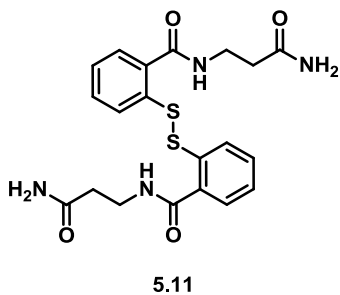
2,2'-Disulfanediylbis(N-(3-amino-3-oxopropyl)benzamide) (5.11). To a solution of 2, 2′-dithiodiobenzoic acid (0.28 g, 0.91 mmol) in THF/isopropanol (9 mL, 7/2, v/v) was added N-hydroxysuccinimide (0.23 g, 2.00 mmol) and DIC (0.29 mL, 1.91 mmol). The solution was stirred at rt, and after 4 h, the resulting ppt was removed by filtration. The solid was immediately taken up in DMF (2.3

mL), and to this solution was added 3-aminopropanamide (0.25 g, 2.01 mmol) and Et_3N (0.13 mL, 0.19 mmol). The reaction was stirred at rt overnight. After 12 h, the DMF was removed *in vacuo*, and the residue was washed with hot EtOH (20% aq.) to yield 0.18 g (45%) of **5.11** as a white solid. This intermediated was used without further purification. ^{1}H NMR (DMSO-d_6) δ = 8.65 (t, 2H, J = 5.7 Hz), 7.63 (d, 4H, J = 6.4 Hz), 7.45 (t, 2H, J = 7.5 Hz), 7.39 (bs, 2H), 7.29 (t, 2H, J = 7.5 Hz), 6.86 (bs, 2H), 3.45 (q, 4H, J = 7.3 Hz), 2.39 (t, 4H, J = 7.3 Hz). ^{13}C NMR (DMSO-d_6) δ = 172.4, 166.8, 136.7, 133.7, 131.1, 127.9, 125.9, 125.6, 36.0, 34.8; HRMS-ESI[+] *m/z* [M+H][+] calc'd for $C_{20}H_{22}N_4O_4S_2$: 447.1155, found: 447.1137.

Expression and Purification of APOBEC3A, APOBEC3G, APOBEC3G 2K3A and APOBEC3G C321A. A3G, A3A, A3G 2K3A and A3G C321A were expressed and purified as previously described.[1]

DNA Deaminase Assay. The DNA deaminase assay was performed as previously described with the ssDNA oligomer 5'-6-FAM-AAA-TAT-TCC-CTA-ATA-GAT-AAT-GTG-A-TAMRA-3'.[1] Deaminase assays with mutant A3G were performed with 50 µM compound, 0.0675 µM A3G, 0.33 µM ssDNA, and excess UDG. None of the synthesized compounds inhibited uracil DNA glycosylase in the context of the in vitro assay.

HPLC Assay for Disulfide Formation. A solution of **5.1** (10.0 mg, 0.040 mmol) in DMSO (100 µL) was diluted with 1x aqueous PBS (5 mL, pH 7.4) and treated with cysteine methyl ester (0.684 g, 4.03 mmol, 100 eq). The solution was then shaken at 37 °C. Aliquots of the reaction mixture were taken at the following time

points: 0 min, 30 min, 60 min and 12 h. These reaction aliquots were analyzed by reverse phase analytical HPLC. The HPLC analytical method (Zorbax SB-C18 4.6 x 150 mm, 3.5 µm column, Agilent Technologies; flow rate = 1.0 mL/min) involved isocratic 10% CH_3CN in 0.1% (v/v) aqueous CF_3CO_2H (0 to 2 min), followed by linear gradients of 10-85% CH_3CN (2-24 min) and 85%-95% CH_3CN (24-26 min).

5.9 NMR Spectra of Synthesized Compounds
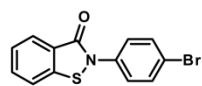
5.1
^{1}H NMR (DMSO-d$_6$)

5.1
^{13}C NMR (DMSO-d$_6$)

5.4
^{1}H NMR (DMSO-d$_6$)

5.4
^{1}H NMR (DMSO-d$_6$)

178

5.6

1H NMR (CDCl3)

CDCl3

10.0 9.5 9.0 8.5 8.0 7.5 7.0 6.5 6.0 5.5 5.0 4.5 4.0 3.5 3.0 2.5 2.0 1.5 1.0 0.5 0.0
ppm

CDCl3

5.6

13C NMR (CDCl3)

200 190 180 170 160 150 140 130 120 110 100 90 80 70 60 50 40 30 20 10 0
ppm

5.7

^{1}H NMR (DMSO-d$_6$)

DMSO-d$_6$

TMS

H$_2$O

5.7

^{13}C NMR (DMSO-d$_6$)

DMSO-d$_6$

180
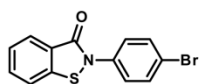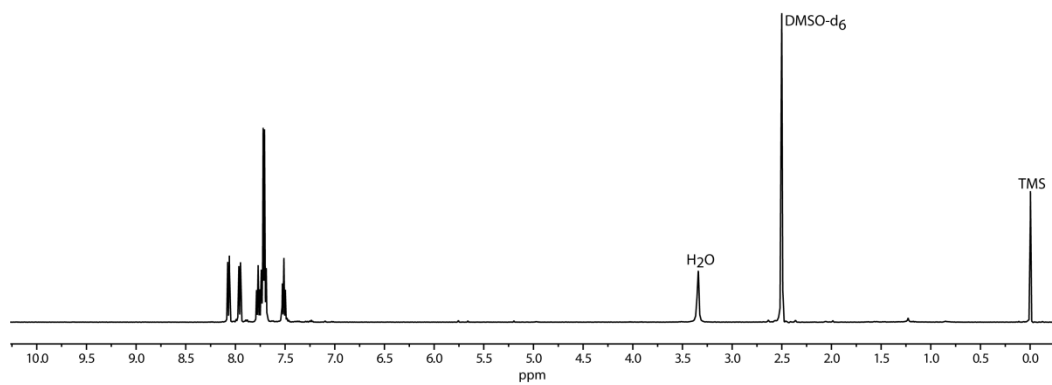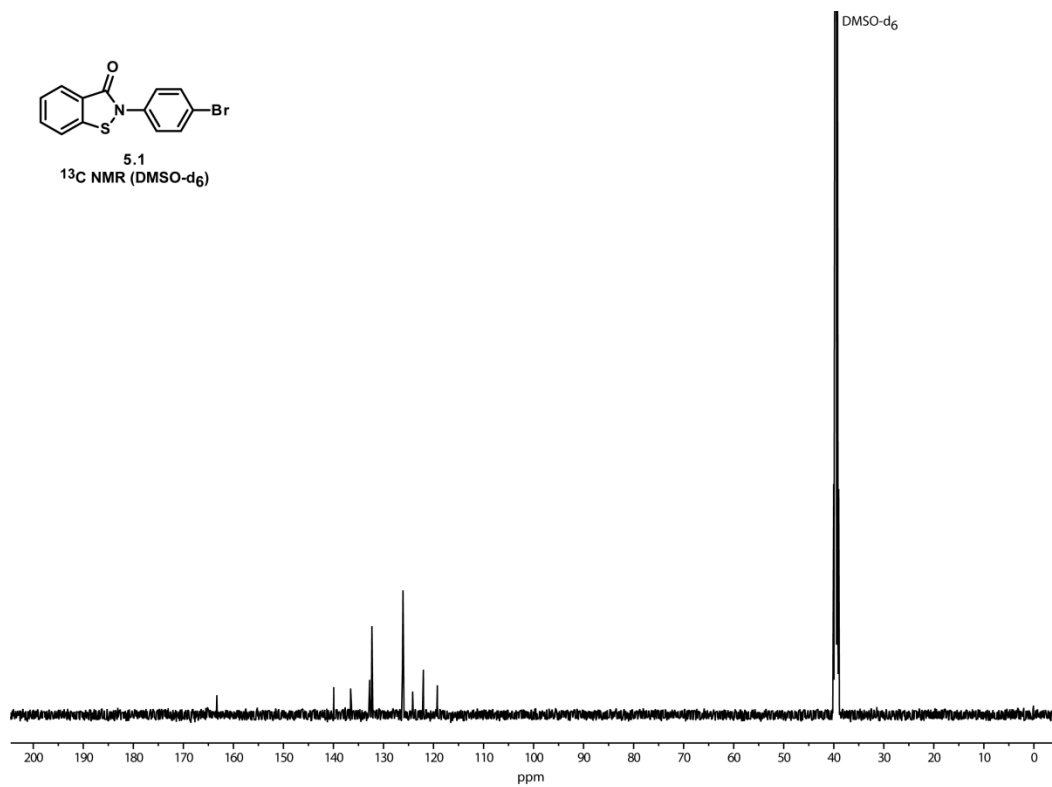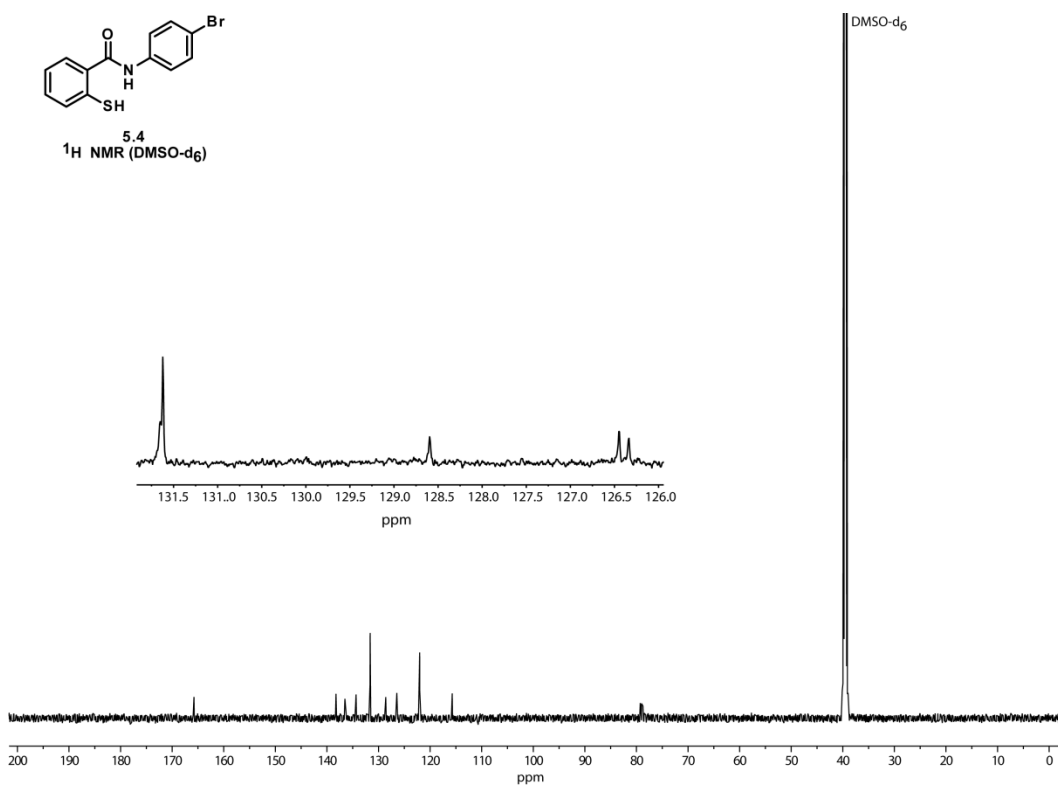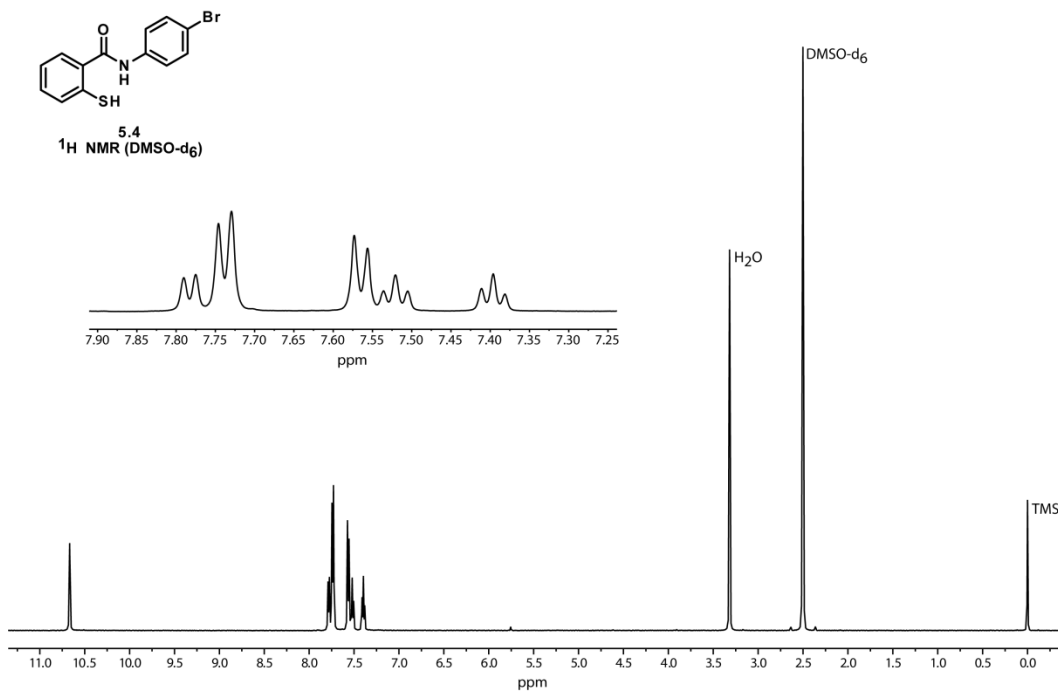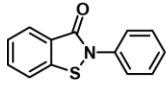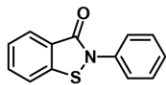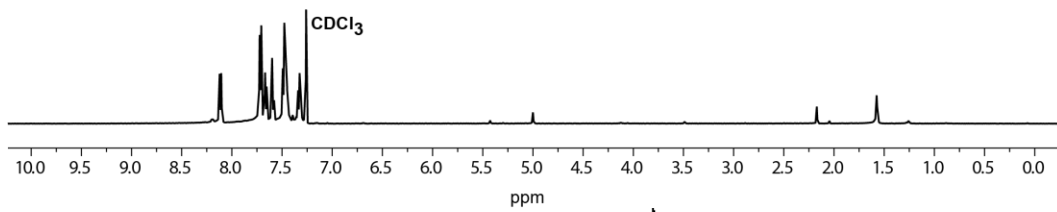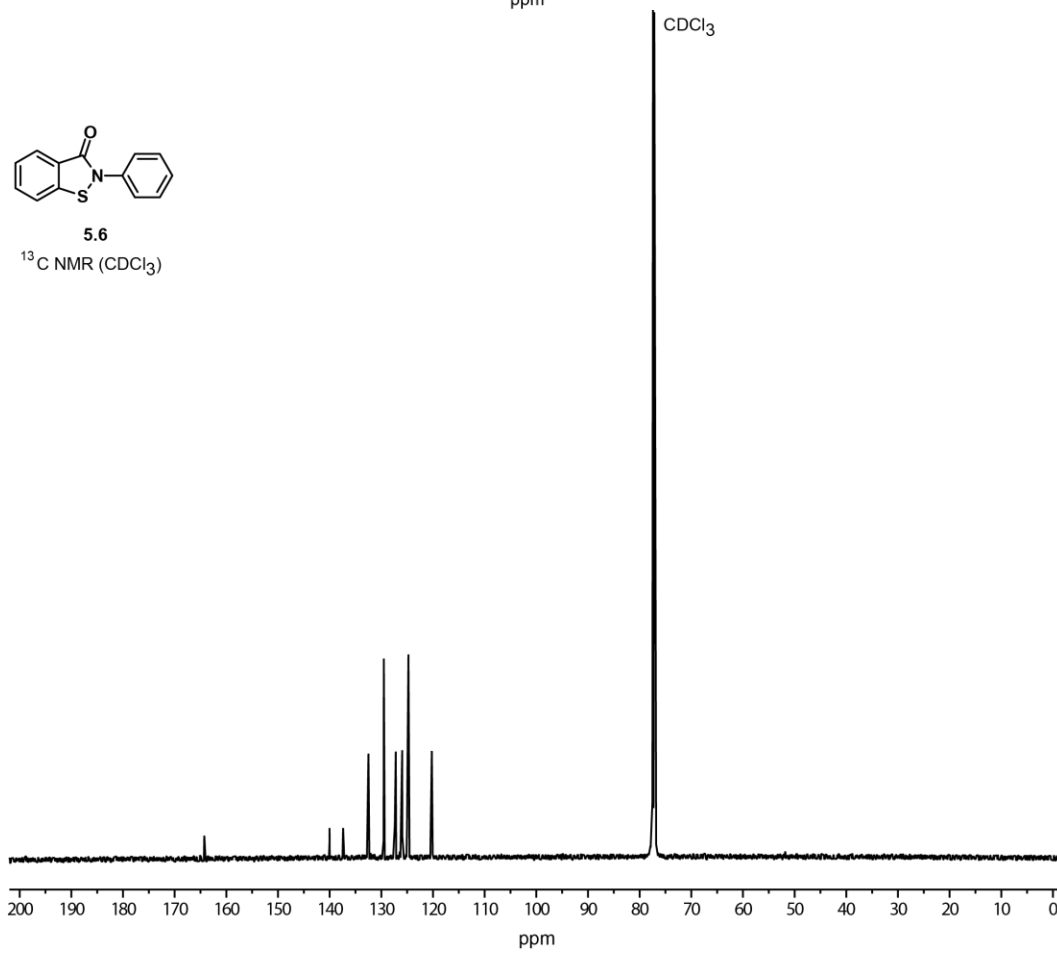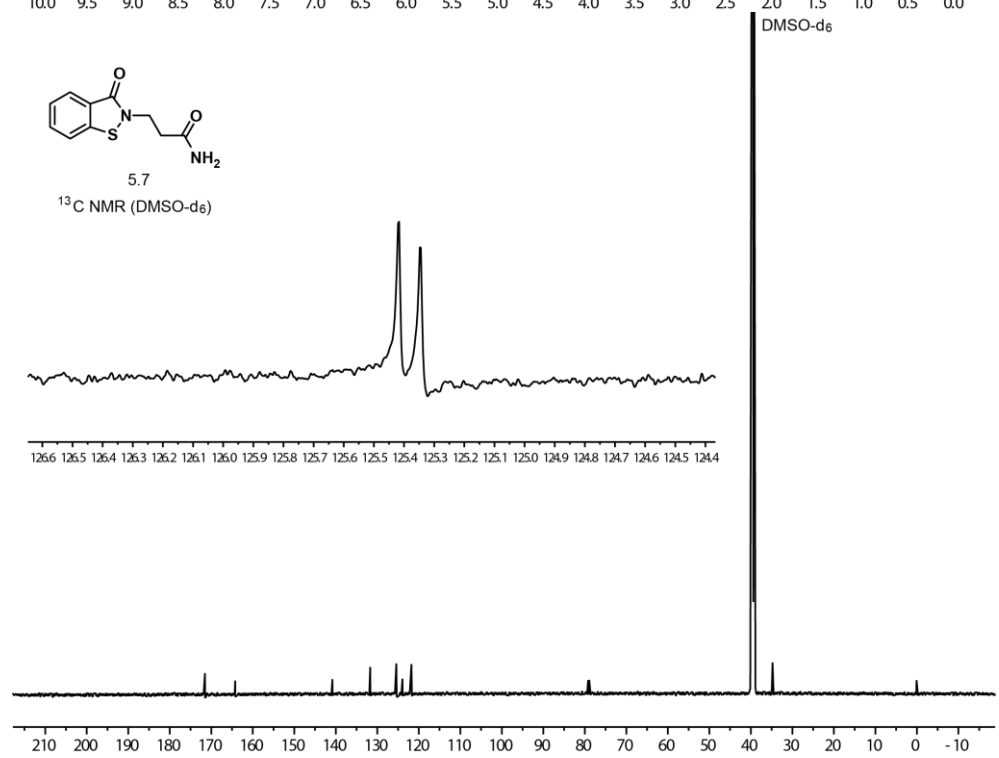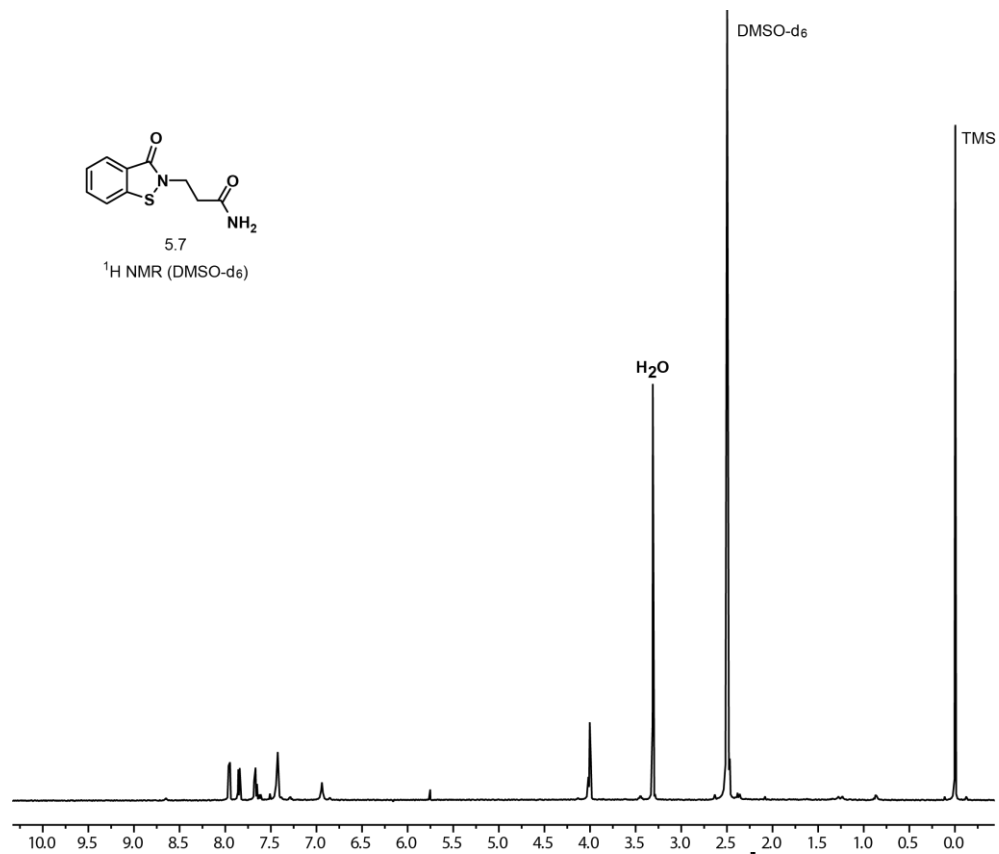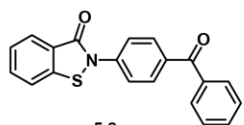
5.8

^{1}H NMR (CDCl$_3$)

5.8

^{13}C NMR (CDCl$_3$)

181
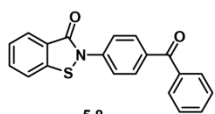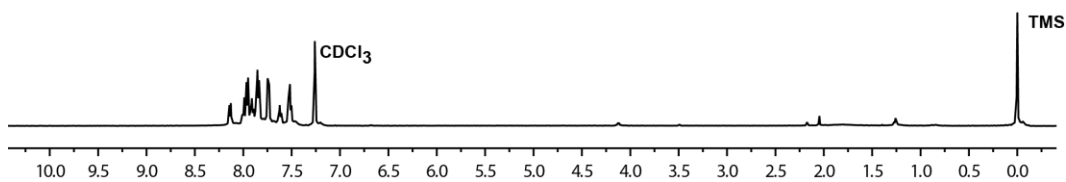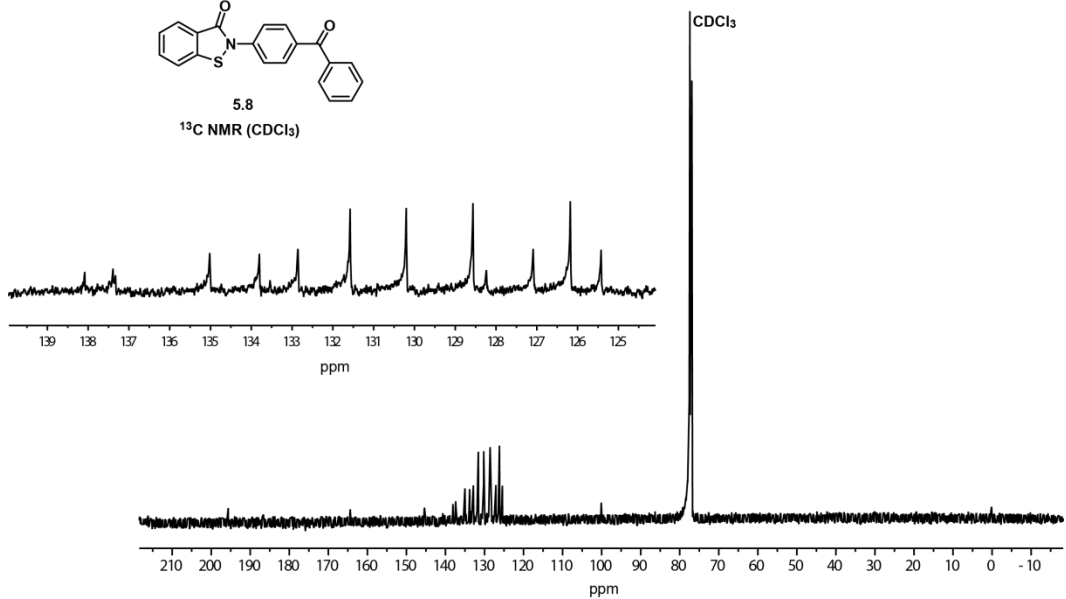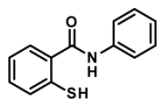
5.9
^{1}H NMR (DMSO-d$_6$)

5.9
^{13}C NMR (DMSO-d$_6$)

182
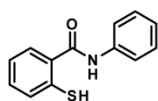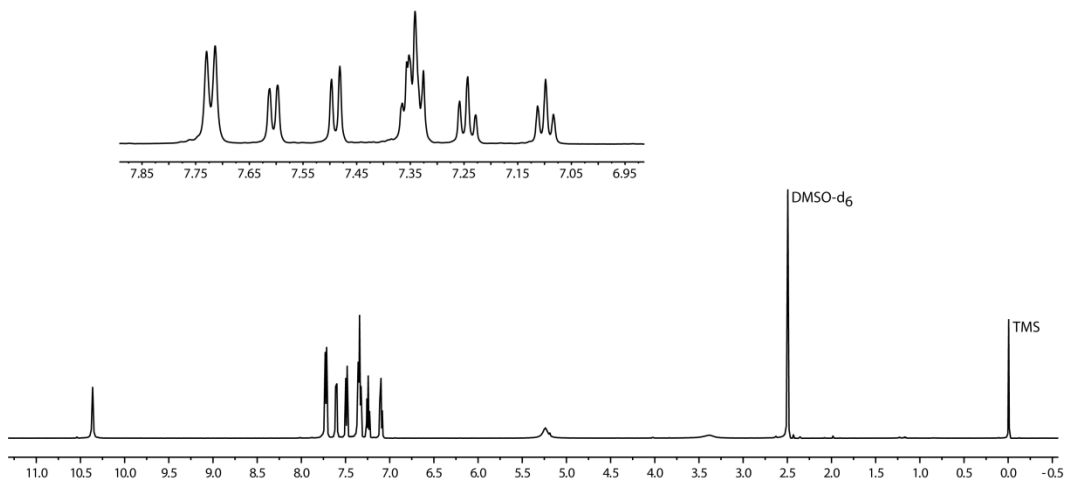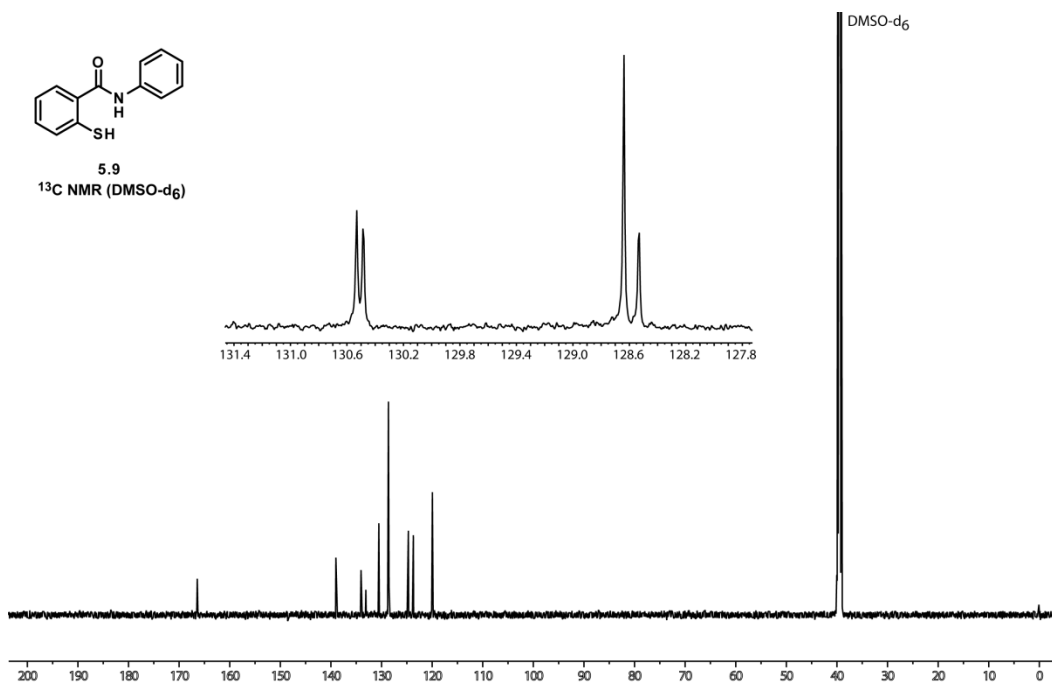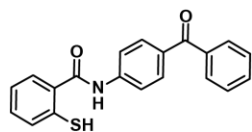
5.10

^{1}H NMR (DMSO-d$_6$)

5.10

^{13}C NMR (DMSO-d$_6$)

183

5.11
¹H NMR (DMSO-d₆)

5.11
¹H NMR (DMSO-d₆)

184
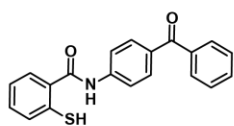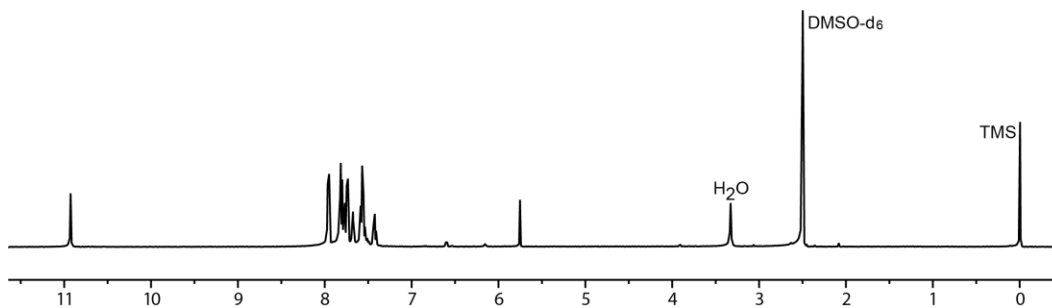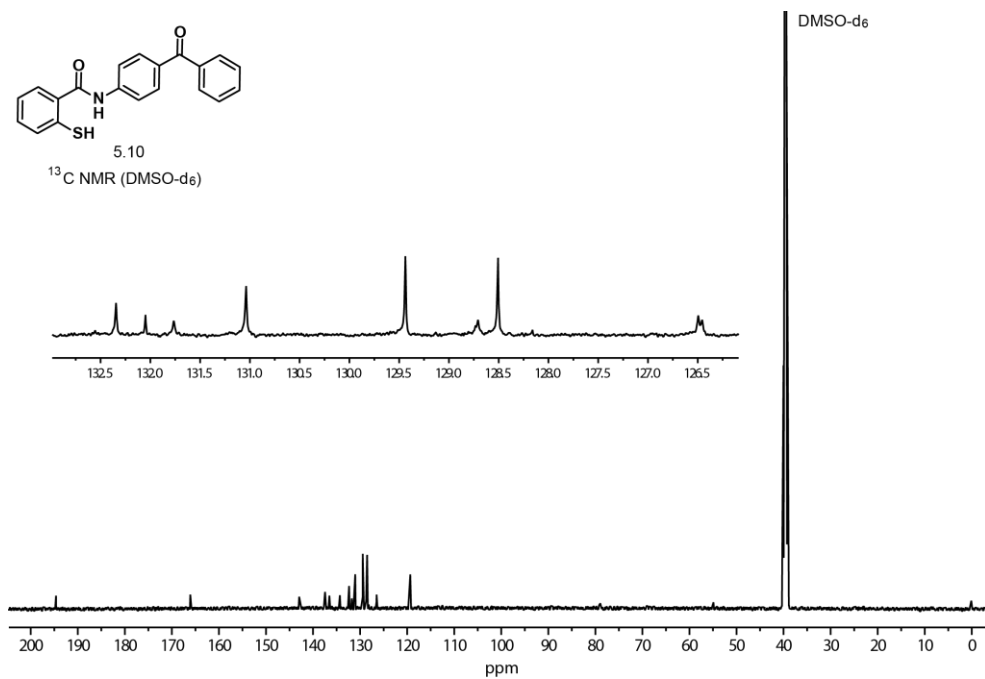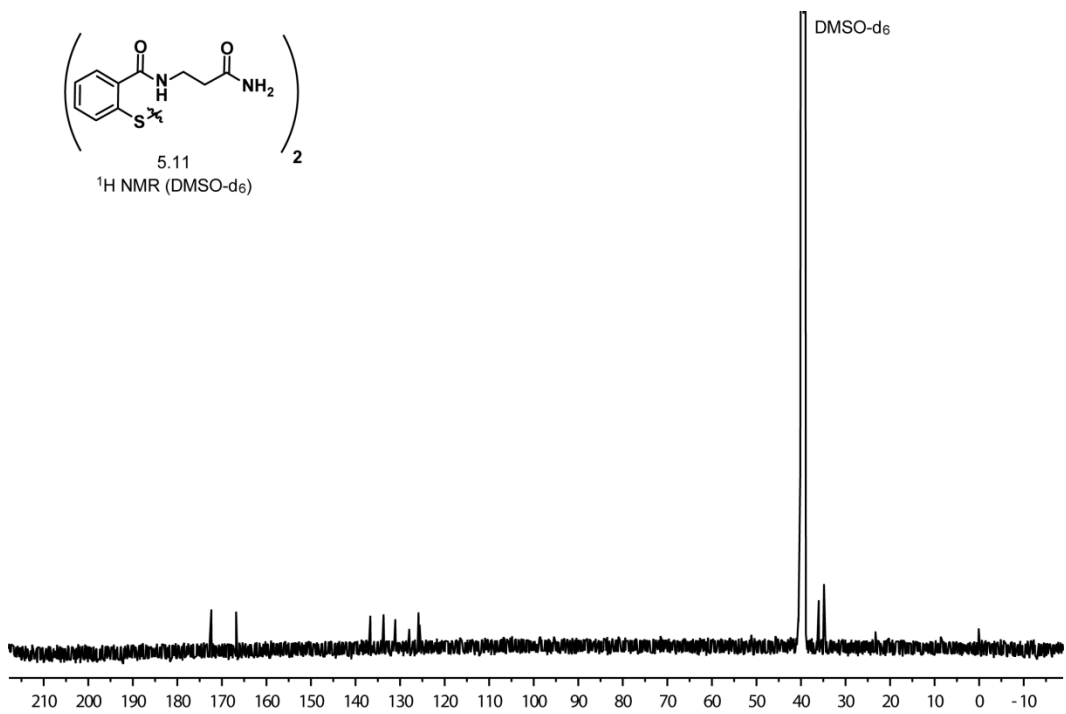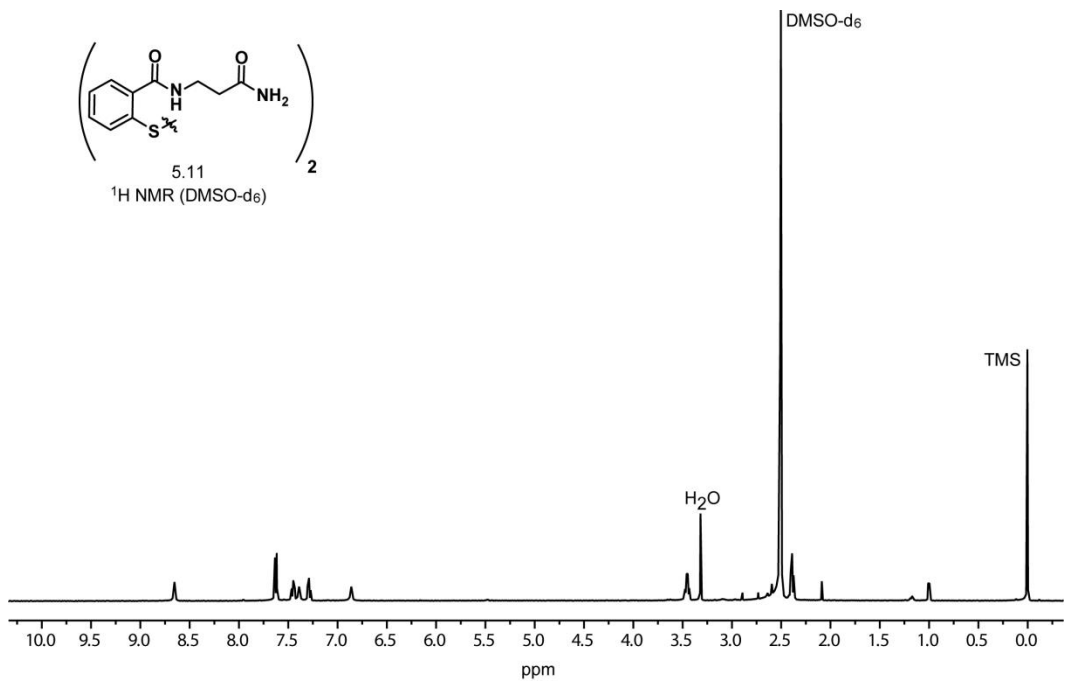
Bibliography

1.   Li, M.; Shandilya, S. M.; Carpenter, M. A.; Rathore, A.; Brown, W. L.; Perkins, A. L.; Harki, D. A.; Solberg, J.; Hook, D. J.; Pandey, K. K.; Parniak, M. A.; Johnson, J. R.; Krogan, N. J.; Somasundaran, M.; Ali, A.; Schiffer, C. A.; Harris, R. S. First-in-class small molecule inhibitors of the single-strand DNA cytosine deaminase APOBEC3G. *ACS Chem. Biol.* **2012**, *7*, 506-517.

2.   Muramatsu, M.; Kinoshita, K.; Fagarasan, S.; Yamada, S.; Shinkai, Y.; Honjo, T. Class switch recombination and hypermutation require activation-induced cytidine deaminase (AID), a potential RNA editing enzyme. *Cell* **2000**, *102*, 553-563.

3.   Muramatsu, M.; Sankaranand, V. S.; Anant, S.; Sugai, M.; Kinoshita, K.; Davidson, N. O.; Honjo, T. Specific expression of activation-induced cytidine deaminase (AID), a novel member of the RNA-editing deaminase family in germinal center B cells. *J. Biol. Chem.* **1999**, *274*, 18470-18476.

4.   Di Noia, J.; Neuberger, M. S. Altering the pathway of immunoglobulin hypermutation by inhibiting uracil-DNA glycosylase. *Nature* **2002**, *419*, 43-48.

5.   Petersen-Mahrt, S. K.; Harris, R. S.; Neuberger, M. S. AID mutates E-coli suggesting a DNA deamination mechanism for antibody diversification. *Nature* **2002**, *418*, 99-103.

6.   Longerich, S.; Basu, U.; Alt, F.; Storb, U. AID in somatic hypermutation and class switch recombination. *Curr. Opin. Immunol.* **2006**, *18*, 164-174.

7.   Di Noia, J. M.; Neuberger, M. S. Molecular mechanisms of antibody somatic hypermutation. *Annu. Rev. Biochem.* **2007**, *76*, 1-22.

8.   Conticello, S. G. The AID/APOBEC family of nucleic acid mutators. *Genome Biol.* **2008**, *9*, 229.

9.   Chan, L. Apolipoprotein B, the major protein component of triglyceride-rich and low density lipoproteins. *J. Biol. Chem.* **1992**, *267*, 25621-25624.

10.   Jarmuz, A.; Chester, A.; Bayliss, J.; Gisbourne, J.; Dunham, I.; Scott, J.; Navaratnam, N. An anthropoid-specific locus of orphan C to U RNA-editing enzymes on chromosome 22. *Genomics* **2002**, *79*, 285-296.

11.   LaRue, R. S.; Andresdottir, V.; Blanchard, Y.; Conticello, S. G.; Derse, D.; Emerman, M.; Greene, W. C.; Jonsson, S. R.; Landau, N. R.; Lochelt, M.; Malik, H. S.; Malim, M. H.; Munk, C.; O'Brien, S. J.; Pathak, V. K.; Strebel, K.; Wain-Hobson, S.; Yu, X. F.; Yuhki, N.; Harris, R. S. Guidelines for naming nonprimate APOBEC3 genes and proteins. *J. Virol.* **2009**, *83*, 494-497.

12.   LaRue, R. S.; Jonsson, S. R.; Silverstein, K. A.; Lajoie, M.; Bertrand, D.; El-Mabrouk, N.; Hotzel, I.; Andresdottir, V.; Smith, T. P.; Harris, R. S. The artiodactyl APOBEC3 innate immune repertoire shows evidence for a multi-functional domain organization that existed in the ancestor of placental mammals. *BMC Mol. Biol.* **2008**, *9*, 104.

13.   Chen, K. M.; Harjes, E.; Gross, P. J.; Fahmy, A.; Lu, Y.; Shindo, K.; Harris, R. S.; Matsuo, H. Structure of the DNA deaminase domain of the HIV-1 restriction factor APOBEC3G. *Nature* **2008**, *452*, 116-119.

14.   Hultquist, J. F.; Lengyel, J. A.; Refsland, E. W.; LaRue, R. S.; Lackey, L.; Brown, W. L.; Harris, R. S. Human and Rhesus APOBEC3D, APOBEC3F, APOBEC3G, and APOBEC3H Demonstrate a Conserved Capacity To Restrict Vif-Deficient HIV-1. *J. Virol.* **2011**, *85*, 11220-11234.

15.   Koning, F. A.; Newman, E. N.; Kim, E. Y.; Kunstman, K. J.; Wolinsky, S. M.; Malim, M. H. Defining APOBEC3 expression patterns in human tissues and hematopoietic cell subsets. *J. Virol.* **2009**, *83*, 9474-9485.

16.   Refsland, E. W.; Stenglein, M. D.; Shindo, K.; Albin, J. S.; Brown, W. L.; Harris, R. S. Quantitative profiling of the full APOBEC3 mRNA repertoire in lymphocytes and tissues: implications for HIV-1 restriction. *Nucleic Acids Res.* **2010**, *38*, 4274-4284.

17.   Burns, M. B.; Lackey, L.; Carpenter, M. A.; Rathore, A.; Land, A. M.; Leonard, B.; Refsland, E. W.; Kotandeniya, D.; Tretyakova, N.; Nikas, J. B.; Yee, D.; Temiz, N. A.; Donohue, D. E.; McDougle, R. M.; Brown, W. L.; Law, E. K.; Harris, R. S. APOBEC3B is an enzymatic source of mutation in breast cancer. *Nature* **2013**, *494*, 366-370.

18.   Swirski, F. K.; Nahrendorf, M.; Etzrodt, M.; Wildgruber, M.; Cortez-Retamozo, V.; Panizzi, P.; Figueiredo, J. L.; Kohler, R. H.; Chudnovskiy, A.; Waterman, P.; Aikawa, E.; Mempel, T. R.; Libby, P.; Weissleder, R.; Pittet, M. J. Identification of splenic reservoir monocytes and their deployment to inflammatory sites. *Science* **2009**, *325*, 612-616.

19.   Stenglein, M. D.; Burns, M. B.; Li, M.; Lengyel, J.; Harris, R. S. APOBEC3 proteins mediate the clearance of foreign DNA from human cells. *Nat. Struct. Mol. Biol.* **2010**, *17*, 222-229.

20.   Peng, G.; Lei, K. J.; Jin, W.; Greenwell-Wild, T.; Wahl, S. M. Induction of APOBEC3 family proteins, a defensive maneuver underlying interferon-induced anti-HIV-1 activity. *J. Exp. Med.* **2006**, *203*, 41-46.

21.   Daniele, R. P.; Dauber, J. H.; Altose, M. D.; Rowlands, D. T., Jr.; Gorenberg, D. J. Lymphocyte studies in asymptomatic cigarette smokers. A comparison between lung and peripheral blood. *Am. Rev. Respir. Dis.* **1977**, *116*, 997-1005.

22.   Weisberg, S. P.; McCann, D.; Desai, M.; Rosenbaum, M.; Leibel, R. L.; Ferrante, A. W., Jr. Obesity is associated with macrophage accumulation in adipose tissue. *J. Clin. Invest.* **2003**, *112*, 1796-1808.

23.   Harris, R. S.; Petersen-Mahrt, S. K.; Neuberger, M. S. RNA editing enzyme APOBEC1 and some of its homologs can act as DNA mutators. *Mol. Cell* **2002**, *10*, 1247-1253.

24.   Aydin, H.; Taylor, M. W.; Lee, J. E. Structure-guided analysis of the human APOBEC3-HIV restrictome. *Structure* **2014**, *22*, 668-684.

25.   Desimmie, B. A.; Delviks-Frankenberrry, K. A.; Burdick, R. C.; Qi, D.; Izumi, T.; Pathak, V. K. Multiple APOBEC3 restriction factors for HIV-1 and one Vif to rule them all. *J. Mol. Biol.* **2014**, *426*, 1220-1245.

26.   Feng, Y.; Baig, T. T.; Love, R. P.; Chelico, L. Suppression of APOBEC3-mediated restriction of HIV-1 by Vif. *Front. Microbiol.* **2014**, *5*, 1-23.

27.   Imahashi, M.; Izumi, T.; Watanabe, D.; Imamura, J.; Matsuoka, K.; Ode, H.; Masaoka, T.; Sato, K.; Kaneko, N.; Ichikawa, S.; Koyanagi, Y.; Takaori-Kondo, A.; Utsumi, M.; Yokomaku, Y.; Shirasaka, T.; Sugiura, W.; Iwatani, Y.;

Naoe, T. Lack of association between intact/deletion polymorphisms of the APOBEC3B gene and HIV-1 risk. *PLoS One* **2014**, *9*, e92861.

28.   Malim, M. H.; Bieniasz, P. D. HIV Restriction Factors and Mechanisms of Evasion. *Cold Spring Harb. Perspect. Med.* **2012**, *2*, a006940.

29.   Strebel, K. HIV Accessory Proteins versus Host Restriction Factors. *Curr. Opin. Virol.* **2013**, *3*, 692-699.

30.   Refsland, E. W.; Harris, R. S. The APOBEC3 family of retroelement restriction factors. *Curr. Top. Microbiol. Immunol.* **2013**, *371*, 1-27.

31.   Wedekind, J. E.; Dance, G. S.; Sowden, M. P.; Smith, H. C. Messenger RNA editing in mammals: new members of the APOBEC family seeking roles in the family business. *Trends Genet.* **2003**, *19*, 207-216.

32.   Liddament, M. T.; Brown, W. L.; Schumacher, A. J.; Harris, R. S. APOBEC3F properties and hypermutation preferences indicate activity against HIV-1 in vivo. *Curr. Biol.* **2004**, *14*, 1385-1391.

33.   Conticello, S. G.; Thomas, C. J.; Petersen-Mahrt, S. K.; Neuberger, M. S. Evolution of the AID/APOBEC family of polynucleotide (deoxy)cytidine deaminases. *Mol. Biol. Evol.* **2005**, *22*, 367-377.

34.   Betts, L.; Xiang, S.; Short, S. A.; Wolfenden, R.; Carter, C. W., Jr. Cytidine deaminase. The 2.3 A crystal structure of an enzyme: transition-state analog complex. *J. Mol. Biol.* **1994**, *235*, 635-656.

35.   Johansson, E.; Mejlhede, N.; Neuhard, J.; Larsen, S. Crystal structure of the tetrameric cytidine deaminase from Bacillus subtilis at 2.0 A resolution. *Biochemistry* **2002**, *41*, 2563-2570.

36.   Ko, T. P.; Lin, J. J.; Hu, C. Y.; Hsu, Y. H.; Wang, A. H.; Liaw, S. H. Crystal structure of yeast cytosine deaminase. Insights into enzyme mechanism and evolution. *J. Biol. Chem.* **2003**, *278*, 19111-19117.

37.   Xie, K.; Sowden, M. P.; Dance, G. S.; Torelli, A. T.; Smith, H. C.; Wedekind, J. E. The structure of a yeast RNA-editing deaminase provides insight into the fold and function of activation-induced deaminase and APOBEC-1. *Proc. Natl. Acad. Sci. U. S. A.* **2004**, *101*, 8114-8119.
188

38.   Ireton, G. C.; Black, M. E.; Stoddard, B. L. The 1.14 A crystal structure of yeast cytosine deaminase: evolution of nucleotide salvage enzymes and implications for genetic chemotherapy. *Structure* **2003**, *11*, 961-972.

39.   Harjes, S.; Solomon, W. C.; Li, M.; Chen, K. M.; Harjes, E.; Harris, R. S.; Matsuo, H. Impact of H216 on the DNA binding and catalytic activities of the HIV restriction factor APOBEC3G. *J. Virol.* **2013**, *87*, 7008-7014.

40.   Nabel, C. S.; Lee, J. W.; Wang, L. C.; Kohli, R. M. Nucleic acid determinants for selective deamination of DNA over RNA by activation-induced deaminase. *Proc. Natl. Acad. Sci. U. S. A.* **2013**, *110*, 14225-14230.

41.   Cohen, R. M.; Wolfenden, R. Cytidine deaminase from Escherichia coli. Purification, properties and inhibition by the potential transition state analog 3,4,5,6-tetrahydrouridine. *J. Biol. Chem.* **1971**, *246*, 7561-7565.

42.   Wolfenden, R.; Kati, W. M. Testing the limits of protein-ligand binding discrimination with transition-state analogue inhibitors. *Acc. of Chem. Res.* **1991**, *24*, 209-215.

43.   Carpenter, M. A.; Rajagurubandara, E.; Wijesinghe, P.; Bhagwat, A. S. Determinants of sequence-specificity within human AID and APOBEC3G. *DNA repair* **2010**, *9*, 579-587.

44.   Rathore, A.; Carpenter, M. A.; Demir, O.; Ikeda, T.; Li, M.; Shaban, N. M.; Law, E. K.; Anokhin, D.; Brown, W. L.; Amaro, R. E.; Harris, R. S. The local dinucleotide preference of APOBEC3G can be altered from 5'-CC to 5'-TC by a single amino acid substitution. *J. Mol. Biol.* **2013**, *425*, 4442-4454.

45.   Wang, M.; Rada, C.; Neuberger, M. S. Altering the spectrum of immunoglobulin V gene somatic hypermutation by modifying the active site of AID. *J. Exp. Med* **2010**, *207*, 141-153.

46.   Kohli, R. M.; Maul, R. W.; Guminski, A. F.; McClure, R. L.; Gajula, K. S.; Saribasak, H.; McMahon, M. A.; Siliciano, R. F.; Gearhart, P. J.; Stivers, J. T. Local sequence targeting in the AID/APOBEC family differentially impacts retroviral restriction and antibody diversification. *J. Biol. Chem.* **2010**, *285*, 40956-40964.

47.   Kohli, R. M.; Abrams, S. R.; Gajula, K. S.; Maul, R. W.; Gearhart, P. J.; Stivers, J. T. A portable hot spot recognition loop transfers sequence preferences from APOBEC family members to activation-induced cytidine deaminase. *J. Biol. Chem.* **2009**, *284*, 22898-22904.

48.   Holden, L. G.; Prochnow, C.; Chang, Y. P.; Bransteitter, R.; Chelico, L.; Sen, U.; Stevens, R. C.; Goodman, M. F.; Chen, X. S. Crystal structure of the anti-viral APOBEC3G catalytic domain and functional implications. *Nature* **2008**, *456*, 121-124.

49.   Conticello, S. G.; Langlois, M. A.; Yang, Z.; Neuberger, M. S. DNA deamination in immunity: AID in the context of its APOBEC relatives. *Adv. Immunol.* **2007**, *94*, 37-73.

50.   Yu, Q.; Konig, R.; Pillai, S.; Chiles, K.; Kearney, M.; Palmer, S.; Richman, D.; Coffin, J. M.; Landau, N. R. Single-strand specificity of APOBEC3G accounts for minus-strand deamination of the HIV genome. *Nat. Struct. Mol. Biol.* **2004**, *11*, 435-442.

51.   Rausch, J. W.; Chelico, L.; Goodman, M. F.; Le Grice, S. F. Dissecting APOBEC3G substrate specificity by nucleoside analog interference. *J. Biol. Chem.* **2009**, *284*, 7047-7058.

52.   Holtz, C. M.; Sadler, H. A.; Mansky, L. M. APOBEC3G cytosine deamination hotspots are defined by both sequence context and single-stranded DNA secondary structure. *Nucleic Acids Res.* **2013**, *41*, 6139-6148.

53.   Iwatani, Y.; Takeuchi, H.; Strebel, K.; Levin, J. G. Biochemical activities of highly purified, catalytically active human APOBEC3G: correlation with antiviral effect. *J. Virol.* **2006**, *80*, 5992-6002.

54.   Bohn, M.-F.; Shandilya, Shivender M. D.; Albin, John S.; Kouno, T.; Anderson, Brett D.; McDougle, Rebecca M.; Carpenter, Michael A.; Rathore, A.; Evans, L.; Davis, Ahkillah N.; Zhang, J.; Lu, Y.; Somasundaran, M.; Matsuo, H.; Harris, Reuben S.; Schiffer, Celia A. Crystal Structure of the DNA Cytosine Deaminase APOBEC3F: The Catalytically Active and HIV-1 Vif-Binding Domain. *Structure* **2013**, *21*, 1042-1050.

55.   Byeon, I. J.; Ahn, J.; Mitra, M.; Byeon, C. H.; Hercik, K.; Hritz, J.; Charlton, L. M.; Levin, J. G.; Gronenborn, A. M. NMR structure of human

restriction factor APOBEC3A reveals substrate binding and enzyme specificity. *Nat. Commun.* **2013**, *4*, 1890.

56. Kitamura, S.; Ode, H.; Nakashima, M.; Imahashi, M.; Naganawa, Y.; Kurosawa, T.; Yokomaku, Y.; Yamane, T.; Watanabe, N.; Suzuki, A.; Sugiura, W.; Iwatani, Y. The APOBEC3C crystal structure and the interface for HIV-1 Vif binding. *Nat. Struct. Mol. Biol.* **2012**, *19*, 1005-1010.

57. Shandilya, S. M.; Nalam, M. N.; Nalivaika, E. A.; Gross, P. J.; Valesano, J. C.; Shindo, K.; Li, M.; Munson, M.; Royer, W. E.; Harjes, E.; Kono, T.; Matsuo, H.; Harris, R. S.; Somasundaran, M.; Schiffer, C. A. Crystal structure of the APOBEC3G catalytic domain reveals potential oligomerization interfaces. *Structure* **2010**, *18*, 28-38.

58. Shandilya, S. M.; Bohn, M. F.; Schiffer, C. A. A computational analysis of the structural determinants of APOBEC3's catalytic activity and vulnerability to HIV-1 Vif. *Virology* **2014**, *471-473*, 105-116.

59. Siu, K. K.; Sultana, A.; Azimi, F. C.; Lee, J. E. Structural determinants of HIV-1 Vif susceptibility and DNA binding in APOBEC3F. *Nat. Commun.* **2013**, *4*, 2593.

60. Salter, J. D.; Morales, G. A.; Smith, H. C. Structural insights for HIV-1 therapeutic strategies targeting Vif. *Trends Biochem. Sci.* **2014**, *39*, 373-380.

61. Furukawa, A.; Nagata, T.; Matsugami, A.; Habu, Y.; Sugiyama, R.; Hayashi, F.; Kobayashi, N.; Yokoyama, S.; Takaku, H.; Katahira, M. Structure, interaction and real-time monitoring of the enzymatic reaction of wild-type APOBEC3G. *EMBO J.* **2009**, *28*, 440-451.

62. Harris, R. S.; Dudley, J. P. APOBECs and virus restriction. *Virology* **2015**, *479-480*, 131-145.

63. Hultquist, J. F.; Harris, R. S. Leveraging APOBEC3 proteins to alter the HIV mutation rate and combat AIDS. *Future Virol.* **2009**, *4*, 605-619.

64. Harris, R. S.; Hultquist, J. F.; Evans, D. T. The restriction factors of human immunodeficiency virus. *J. Biol. Chem.* **2012**, *287*, 40875-40883.

65.   Malim, M. H.; Emerman, M. HIV-1 Accessory Proteins—Ensuring Viral Survival in a Hostile Environment. *Cell Host Microbe* **2008**, *3*, 388-398.

66.   Fletcher, A. J.; Towers, G. J. Inhibition of retroviral replication by members of the TRIM protein family. *Curr. Top. Microbiol. Immunol.* **2013**, *371*, 29-66.

67.   Neil, S. J. The antiviral activities of tetherin. *Curr. Top. Microbiol. Immunol.* **2013**, *371*, 67-104.

68.   Sharkey, M. Restriction of retroviral infection of macrophages. *Curr. Top. Microbiol. Immunol.* **2013**, *371*, 105-122.

69.   Alce, T. M.; Popik, W. APOBEC3G is incorporated into virus-like particles by a direct interaction with HIV-1 Gag nucleocapsid protein. *J. Biol. Chem.* **2004**, *279*, 34083-34086.

70.   Luo, K.; Liu, B.; Xiao, Z.; Yu, Y.; Yu, X.; Gorelick, R.; Yu, X. F. Amino-terminal region of the human immunodeficiency virus type 1 nucleocapsid is required for human APOBEC3G packaging. *J. Virol.* **2004**, *78*, 11841-11852.

71.   Schafer, A.; Bogerd, H. P.; Cullen, B. R. Specific packaging of APOBEC3G into HIV-1 virions is mediated by the nucleocapsid domain of the gag polyprotein precursor. *Virology* **2004**, *328*, 163-168.

72.   Svarovskaia, E. S.; Xu, H.; Mbisa, J. L.; Barr, R.; Gorelick, R. J.; Ono, A.; Freed, E. O.; Hu, W. S.; Pathak, V. K. Human apolipoprotein B mRNA-editing enzyme-catalytic polypeptide-like 3G (APOBEC3G) is incorporated into HIV-1 virions through interactions with viral and nonviral RNAs. *J. Biol. Chem.* **2004**, *279,* 35822-35828.

73.   Khan, M. A.; Kao, S.; Miyagi, E.; Takeuchi, H.; Goila-Gaur, R.; Opi, S.; Gipson, C. L.; Parslow, T. G.; Ly, H.; Strebel, K. Viral RNA is required for the association of APOBEC3G with human immunodeficiency virus type 1 nucleoprotein complexes. *J. Virol.* **2005**, *79*, 5870-5874.

74.   Burnett, A.; Spearman, P. APOBEC3G multimers are recruited to the plasma membrane for packaging into human immunodeficiency virus type 1 virus-like particles in an RNA-dependent process requiring the NC basic linker. *J. Virol.* **2007**, *81*, 5000-5013.

75.   Bogerd, H. P.; Cullen, B. R. Single-stranded RNA facilitates nucleocapsid: APOBEC3G complex formation. *RNA* **2008**, *14*, 1228-1236.

76.   Hache, G.; Liddament, M. T.; Harris, R. S. The retroviral hypermutation specificity of APOBEC3F and APOBEC3G is governed by the C-terminal DNA cytosine deaminase domain. *J. Biol. Chem.* **2005**, *280*, 10920-10924.

77.   Martin, K. L.; Johnson, M.; D'Aquila, R. T. APOBEC3G complexes decrease human immunodeficiency virus type 1 production. *J. Virol.* **2011**, *85*, 9314-9326.

78.   Song, C.; Sutton, L.; Johnson, M. E.; D'Aquila, R. T.; Donahue, J. P. Signals in APOBEC3F N-terminal and C-terminal deaminase domains each contribute to encapsidation in HIV-1 virions and are both required for HIV-1 restriction. *J. Biol. Chem.* **2012**, *287*, 16965-16974.

79.   Bishop, K. N.; Verma, M.; Kim, E.-Y.; Wolinsky, S. M.; Malim, M. H. APOBEC3G Inhibits Elongation of HIV-1 Reverse Transcripts. *PLoS Pathog.* **2008**, *4*, e1000231.

80.   Newman, E. N.; Holmes, R. K.; Craig, H. M.; Klein, K. C.; Lingappa, J. R.; Malim, M. H.; Sheehy, A. M. Antiviral function of APOBEC3G can be dissociated from cytidine deaminase activity. *Curr. Biol.* **2005**, *15*, 166-170.

81.   Iwatani, Y.; Chan, D. S.; Wang, F.; Maynard, K. S.; Sugiura, W.; Gronenborn, A. M.; Rouzina, I.; Williams, M. C.; Musier-Forsyth, K.; Levin, J. G. Deaminase-independent inhibition of HIV-1 reverse transcription by APOBEC3G. *Nucleic Acids Res.* **2007**, *35*, 7096-7108.

82.   Schumacher, A. J.; Hache, G.; Macduff, D. A.; Brown, W. L.; Harris, R. S. The DNA deaminase activity of human APOBEC3G is required for Ty1, MusD, and human immunodeficiency virus type 1 restriction. *J. Virol.* **2008**, *82*, 2652-2660.

83.   Miyagi, E.; Opi, S.; Takeuchi, H.; Khan, M.; Goila-Gaur, R.; Kao, S.; Strebel, K. Enzymatically active APOBEC3G is required for efficient inhibition of human immunodeficiency virus type 1. *J. Virol.* **2007**, *81*, 13346-13353.

84.   Browne, E. P.; Allers, C.; Landau, N. R. Restriction of HIV-1 by APOBEC3G is cytidine deaminase-dependent. *Virology* **2009**, *387*, 313-321.

85.   Albin, J. S.; Harris, R. S. Interactions of host APOBEC3 restriction factors with HIV-1 in vivo: implications for therapeutics. *Expert Rev. Mol. Med.* **2010**, *12*.

86.   Bishop, K. N.; Holmes, R. K.; Malim, M. H. Antiviral potency of APOBEC proteins does not correlate with cytidine deamination. *J. Virol.* **2006**, *80*, 8450-8458.

87.   Opi, S.; Takeuchi, H.; Kao, S.; Khan, M. A.; Miyagi, E.; Goila-Gaur, R.; Iwatani, Y.; Levin, J. G.; Strebel, K. Monomeric APOBEC3G is catalytically active and has antiviral activity. *J. Virol.* **2006**, *80*, 4673-4682.

88.   Mbisa, J. L.; Barr, R.; Thomas, J. A.; Vandegraaff, N.; Dorweiler, I. J.; Svarovskaia, E. S.; Brown, W. L.; Mansky, L. M.; Gorelick, R. J.; Harris, R. S.; Engelman, A.; Pathak, V. K. Human immunodeficiency virus type 1 cDNAs produced in the presence of APOBEC3G exhibit defects in plus-strand DNA transfer and integration. *J. Virol.* **2007**, *81*, 7099-7110.

89.   Bishop, K. N.; Verma, M.; Kim, E. Y.; Wolinsky, S. M.; Malim, M. H. APOBEC3G inhibits elongation of HIV-1 reverse transcripts. *PLoS Pathog.* **2008**, *4*, e1000231.

90.   Harris, R. S.; Bishop, K. N.; Sheehy, A. M.; Craig, H. M.; Petersen-Mahrt, S. K.; Watt, I. N.; Neuberger, M. S.; Malim, M. H. DNA determination mediates innate immunity to retroviral infection. *Cell* **2003**, *113*, 803-809.

91.   Lecossier, D.; Bouchonnet, F.; Clavel, F.; Hance, A. J. Hypermutation of HIV-1 DNA in the absence of the Vif protein. *Science* **2003**, *300*, 1112.

92.   Mangeat, B.; Turelli, P.; Caron, G.; Friedli, M.; Perrin, L.; Trono, D. Broad antiretroviral defence by human APOBEC3G through lethal editing of nascent reverse transcripts. *Nature* **2003**, *424*, 99-103.

93.   Zhang, H.; Yang, B.; Pomerantz, R. J.; Zhang, C.; Arunachalam, S. C.; Gao, L. The cytidine deaminase CEM15 induces hypermutation in newly synthesized HIV-1 DNA. *Nature* **2003**, *424*, 94-98.

94. Kaiser, S. M.; Emerman, M. Uracil DNA glycosylase is dispensable for human immunodeficiency virus type 1 replication and does not contribute to the antiviral effects of the cytidine deaminase Apobec3G. *J. Virol.* **2006**, *80*, 875-882.

95. Yang, B.; Chen, K.; Zhang, C.; Huang, S.; Zhang, H. Virion-associated uracil DNA glycosylase-2 and apurinic/apyrimidinic endonuclease are involved in the degradation of APOBEC3G-edited nascent HIV-1 DNA. *J. Biol. Chem.* **2007**, *282*, 11667-11675.

96. Schumacher, A. J.; Hache, G.; MacDuff, D. A.; Brown, W. L.; Harris, R. S. The DNA deaminase activity of human APOBEC3G is required for Ty1, MusD, and human immunodeficiency virus type 1 restriction. *J. Virol.* **2008**, *82*, 2652-2660.

97. Bishop, K. N.; Holmes, R. K.; Sheehy, A. M.; Davidson, N. O.; Cho, S. J.; Malim, M. H. Cytidine deamination of retroviral DNA by diverse APOBEC proteins. *Curr. Biol.* **2004**, *14*, 1392-1396.

98. Fitzgibbon, J. E.; Mazar, S.; Dubin, D. T. A new type of G-->A hypermutation affecting human immunodeficiency virus. *AIDS Res. Hum. Retroviruses* **1993**, *9*, 833-838.

99. Janini, M.; Rogers, M.; Birx, D. R.; McCutchan, F. E. Human immunodeficiency virus type 1 DNA sequences genetically damaged by hypermutation are often abundant in patient peripheral blood mononuclear cells and may be generated during near-simultaneous infection and activation of CD4(+) T cells. *J. Virol.* **2001**, *75*, 7973-7986.

100. Caride, E.; Brindeiro, R. M.; Kallas, E. G.; de Sa, C. A.; Eyer-Silva, W. A.; Machado, E.; Tanuri, A. Sexual transmission of HIV-1 isolate showing G-->A hypermutation. *J. Clin. Virol.* **2002**, *23*, 179-189.

101. Kieffer, T. L.; Kwon, P.; Nettles, R. E.; Han, Y.; Ray, S. C.; Siliciano, R. F. G-->A hypermutation in protease and reverse transcriptase regions of human immunodeficiency virus type 1 residing in resting CD4+ T cells in vivo. *J. Virol.* **2005**, *79*, 1975-1980.

102. Pace, C.; Keller, J.; Nolan, D.; James, I.; Gaudieri, S.; Moore, C.; Mallal, S. Population level analysis of human immunodeficiency virus type 1

hypermutation and its relationship with APOBEC3G and vif genetic variation. *J. Virol.* **2006**, *80*, 9259-9269.

103.   Gandhi, S. K.; Siliciano, J. D.; Bailey, J. R.; Siliciano, R. F.; Blankson, J. N. Role of APOBEC3G/F-mediated hypermutation in the control of human immunodeficiency virus type 1 in elite suppressors. *J. Virol.* **2008**, *82*, 3125-3130.

104.   Land, A. M.; Ball, T. B.; Luo, M.; Pilon, R.; Sandstrom, P.; Embree, J. E.; Wachihi, C.; Kimani, J.; Plummer, F. A. Human immunodeficiency virus (HIV) type 1 proviral hypermutation correlates with CD4 count in HIV-infected women from Kenya. *J. Virol.* **2008**, *82*, 8172-8182.

105.   Albin, J. S.; Harris, R. S. Interactions of host APOBEC3 restriction factors with HIV-1 in vivo: implications for therapeutics. *Expert Rev. Mol. Med.* **2010**, *12*, e4.

106.   Haché, G.; Mansky, L. M.; Harris, R. S. Human APOBEC3 proteins, retrovirus restriction, and HIV drug resistance. *AIDS Rev.* **2006**, *8*, 148-157.

107.   Loeb, L. A.; Essigmann, J. M.; Kazazi, F.; Zhang, J.; Rose, K. D.; Mullins, J. I. Lethal mutagenesis of HIV with mutagenic nucleoside analogs. *Proc. Natl. Acad. Sci. U. S. A.* **1999**, *96*, 1492-1497.

108.   Strebel, K.; Daugherty, D.; Clouse, K.; Cohen, D.; Folks, T.; Martin, M. A. The HIV 'A' (sor) gene product is essential for virus infectivity. *Nature* **1987**, *328*, 728-730.

109.   Gabuzda, D. H.; Lawrence, K.; Langhoff, E.; Terwilliger, E.; Dorfman, T.; Haseltine, W. A.; Sodroski, J. Role of vif in replication of human immunodeficiency virus type 1 in CD4+ T lymphocytes. *J. Virol.* **1992**, *66*, 6489-6495.

110.   Fisher, A. G.; Ensoli, B.; Ivanoff, L.; Chamberlain, M.; Petteway, S.; Ratner, L.; Gallo, R. C.; Wong-Staal, F. The sor gene of HIV-1 is required for efficient virus transmission in vitro. *Science* **1987**, *237*, 888-893.

111. Sheehy, A. M.; Gaddis, N. C.; Choi, J. D.; Malim, M. H. Isolation of a human gene that inhibits HIV-1 infection and is suppressed by the viral Vif protein. *Nature* **2002**, *418*, 646-650.

112. Kan, N. C.; Franchini, G.; Wong-Staal, F.; DuBois, G. C.; Robey, W. G.; Lautenberger, J. A.; Papas, T. S. Identification of HTLV-III/LAV sor gene product and detection of antibodies in human sera. *Science* **1986**, *231*, 1553-1555.

113. Lee, T. H.; Coligan, J. E.; Allan, J. S.; McLane, M. F.; Groopman, J. E.; Essex, M. A new HTLV-III/LAV protein encoded by a gene found in cytopathic retroviruses. *Science* **1986**, *231*, 1546-1549.

114. Sodroski, J.; Goh, W. C.; Rosen, C.; Tartar, A.; Portetelle, D.; Burny, A.; Haseltine, W. Replicative and cytopathic potential of HTLV-III/LAV with sor gene deletions. *Science* **1986**, *231*, 1549-1553.

115. von Schwedler, U.; Song, J.; Aiken, C.; Trono, D. Vif is crucial for human immunodeficiency virus type 1 proviral DNA synthesis in infected cells. *J. Virol.* **1993**, *67*, 4945-4955.

116. Conticello, S. G.; Harris, R. S.; Neuberger, M. S. The Vif protein of HIV triggers degradation of the human antiretroviral DNA deaminase APOBEC3G. *Curr. Biol.* **2003**, *13*, 2009-2013.

117. Marin, M.; Rose, K. M.; Kozak, S. L.; Kabat, D. HIV-1 Vif protein binds the editing enzyme APOBEC3G and induces its degradation. *Nat. Med.* **2003**, *9*, 1398-1403.

118. Sheehy, A. M.; Gaddis, N. C.; Malim, M. H. The antiretroviral enzyme APOBEC3G is degraded by the proteasome in response to HIV-1 Vif. *Nat. Med.* **2003**, *9*, 1404-1407.

119. Yu, X.; Yu, Y.; Liu, B.; Luo, K.; Kong, W.; Mao, P.; Yu, X. F. Induction of APOBEC3G ubiquitination and degradation by an HIV-1 Vif-Cul5-SCF complex. *Science* **2003**, *302*, 1056-1060.

120. Mehle, A.; Strack, B.; Ancuta, P.; Zhang, C.; McPike, M.; Gabuzda, D. Vif overcomes the innate antiviral activity of APOBEC3G by

promoting its degradation in the ubiquitin-proteasome pathway. *J. Biol. Chem.* **2004**, *279*, 7792-7798.

121. Jager, S.; Kim, D. Y.; Hultquist, J. F.; Shindo, K.; LaRue, R. S.; Kwon, E.; Li, M.; Anderson, B. D.; Yen, L.; Stanley, D.; Mahon, C.; Kane, J.; Franks-Skiba, K.; Cimermancic, P.; Burlingame, A.; Sali, A.; Craik, C. S.; Harris, R. S.; Gross, J. D.; Krogan, N. J. Vif hijacks CBF-beta to degrade APOBEC3G and promote HIV-1 infection. *Nature* **2012**, *481*, 371-375.

122. Guo, Y.; Dong, L.; Qiu, X.; Wang, Y.; Zhang, B.; Liu, H.; Yu, Y.; Zang, Y.; Yang, M.; Huang, Z. Structural basis for hijacking CBF-beta and CUL5 E3 ligase complex by HIV-1 Vif. *Nature* **2014**, *505*, 229-233.

123. Mariani, R.; Chen, D.; Schrofelbauer, B.; Navarro, F.; Konig, R.; Bollman, B.; Munk, C.; Nymark-McMahon, H.; Landau, N. R. Species-specific exclusion of APOBEC3G from HIV-1 virions by Vif. *Cell* **2003**, *114*, 21-31.

124. Stopak, K.; de Noronha, C.; Yonemoto, W.; Greene, W. C. HIV-1 Vif blocks the antiviral activity of APOBEC3G by impairing both its translation and intracellular stability. *Mol. Cell* **2003**, *12*, 591-601.

125. Kao, S.; Miyagi, E.; Khan, M. A.; Takeuchi, H.; Opi, S.; Goila-Gaur, R.; Strebel, K. Production of infectious human immunodeficiency virus type 1 does not require depletion of APOBEC3G from virus-producing cells. *Retrovirology* **2004**, *1*, 27.

126. Santa-Marta, M.; da Silva, F. A.; Fonseca, A. M.; Goncalves, J. HIV-1 Vif can directly inhibit apolipoprotein B mRNA-editing enzyme catalytic polypeptide-like 3G-mediated cytidine deamination by using a single amino acid interaction and without protein degradation. *J. Biol. Chem.* **2005**, *280*, 8765-8775.

127. Opi, S.; Kao, S.; Goila-Gaur, R.; Khan, M. A.; Miyagi, E.; Takeuchi, H.; Strebel, K. Human immunodeficiency virus type 1 Vif inhibits packaging and antiviral activity of a degradation-resistant APOBEC3G variant. *J. Virol.* **2007**, *81*, 8236-8246.

128. Goila-Gaur, R.; Khan, M. A.; Miyagi, E.; Kao, S.; Opi, S.; Takeuchi, H.; Strebel, K. HIV-1 Vif promotes the formation of high molecular mass APOBEC3G complexes. *Virology* **2008**, *372*, 136-146.

129.   Britan-Rosich, E.; Nowarski, R.; Kotler, M. Multifaceted counter-APOBEC3G mechanisms employed by HIV-1 Vif. *J. Mol. Biol.* **2011**, *410*, 1065-1076.

130.   Harris, R. S. Enhancing immunity to HIV through APOBEC. *Nat. Biotechnol.* **2008**, *26*, 1089-1090.

131.   Bonnac, L. F.; Mansky, L. M.; Patterson, S. E. Structure-activity relationships and design of viral mutagens and application to lethal mutagenesis. *J. Med. Chem.* **2013**, *56*, 9403-9414.

132.   Nathans, R.; Cao, H.; Sharova, N.; Ali, A.; Sharkey, M.; Stranska, R.; Stevenson, M.; Rana, T. M. Small-molecule inhibition of HIV-1 Vif. *Nat Biotechnol.* **2008**, *26*, 1187-1192.

133.   Barnor, J. S.; Miyano-Kurosaki, N.; Yamaguchi, K.; Sakamoto, A.; Ishikawa, K.; Inagaki, Y.; Yamamoto, N.; Osei-Kwasi, M.; Ofori-Adjei, D.; Takaku, H. Intracellular expression of antisense RNA transcripts complementary to the human immunodeficiency virus type-1 vif gene inhibits viral replication in infected T-lymphoblastoid cells. *Biochem. Biophys. Res. Commun.* **2004**, *320*, 544-550.

134.   Barnor, J. S.; Miyano-Kurosaki, N.; Yamaguchi, K.; Abumi, Y.; Ishikawa, K.; Yamamoto, N. Lentiviral-mediated delivery of combined HIV-1 decoy TAR and Vif siRNA as a single RNA molecule that cleaves to inhibit HIV-1 in transduced cells. *Nucleos. Nucleot. Nucl.* **2005**, *24*, 431-434.

135.   Ali, A.; Wang, J.; Nathans, R. S.; Cao, H.; Sharova, N.; Stevenson, M.; Rana, T. M. Synthesis and structure-activity relationship studies of HIV-1 virion infectivity factor (Vif) inhibitors that block viral replication. *ChemMedChem* **2012**, *7*, 1217-1229.

136.   Mohammed, I.; Parai, M. K.; Jiang, X.; Sharova, N.; Singh, G.; Stevenson, M.; Rana, T. M. SAR and Lead Optimization of an HIV-1 Vif-APOBEC3G Axis Inhibitor. *ACS Med. Chem. Lett.* **2012**, *3*, 465-469.

137.   Cen, S.; Peng, Z. G.; Li, X. Y.; Li, Z. R.; Ma, J.; Wang, Y. M.; Fan, B.; You, X. F.; Wang, Y. P.; Liu, F.; Shao, R. G.; Zhao, L. X.; Yu, L.; Jiang, J. D. Small molecular compounds inhibit HIV-1 replication through specifically stabilizing APOBEC3G. *J. Biol. Chem.* **2010**, *285*, 16546-16552.

138.   Matsui, M.; Shindo, K.; Izumi, T.; Io, K.; Shinohara, M.; Komano, J.; Kobayashi, M.; Kadowaki, N.; Harris, R. S.; Takaori-Kondo, A. Small molecules that inhibit Vif-induced degradation of APOBEC3G. *Virol. J.* **2014**, *11*, 122.

139.   Pan, T.; He, X.; Chen, B.; Chen, H.; Geng, G.; Luo, H.; Zhang, H.; Bai, C. Development of benzimidazole derivatives to inhibit HIV-1 replication through protecting APOBEC3G protein. *Eur. J. Med. Chem.* **2015**, *95*, 500-513.

140.   Zhou, M.; Luo, H.; Li, R.; Ding, Z. Exploring the binding mode of HIV-1 Vif inhibitors by blind docking, molecular dynamics and MM/GBSA. *RSC Adv.* **2013**, *3*, 22532-22543.

141.   Lv, W.; Liu, Z.; Jin, H.; Yu, X.; Zhang, L. Three-dimensional structure of HIV-1 VIF constructed by comparative modeling and the function characterization analyzed by molecular dynamics simulation. *Org. Biomol. Chem* **2007**, *5*, 617-626.

142.   Zuo, T.; Liu, D.; Lv, W.; Wang, X.; Wang, J.; Lv, M.; Huang, W.; Wu, J.; Zhang, H.; Jin, H.; Zhang, L.; Kong, W.; Yu, X. Small-molecule inhibition of human immunodeficiency virus type 1 replication by targeting the interaction between Vif and ElonginC. *J. Virol.* **2012**, *86*, 5497-5507.

143.   Huang, W.; Zuo, T.; Jin, H.; Liu, Z.; Yang, Z.; Yu, X.; Zhang, L. Design, synthesis and biological evaluation of indolizine derivatives as HIV-1 VIF-ElonginC interaction inhibitors. *Mol. Divers.* **2013**, *17*, 221-243.

144.   Smith, J. L.; Bu, W.; Burdick, R. C.; Pathak, V. K. Multiple ways of targeting APOBEC3-virion infectivity factor interactions for anti-HIV-1 drug development. *Trends Pharmacol. Sci.* **2009**, *30*, 638-646.

145.   Ejima, T.; Hirota, M.; Mizukami, T.; Otsuka, M.; Fujita, M. An anti-HIV-1 compound that increases steady-state expression of apoplipoprotein B mRNA-editing enzyme-catalytic polypeptide-like 3G. *Int. J. Mol. Med.* **2011**, *28*, 613-616.

146.   Fujita, M.; Otsuka, M.; Sugiura, Y. Metal-chelating inhibitors of a zinc finger protein HIV-EP1. Remarkable potentiation of inhibitory activity by introduction of SH groups. *J. Med. Chem.* **1996**, *39*, 503-507.

147.   Otsuka, M.; Fujita, M.; Sugiura, Y.; Yamamoto, T.; Inoue, J.; Maekawa, T.; Ishii, S. Synthetic inhibitors of regulatory proteins involved in the signaling pathway of the replication of human immunodeficiency virus 1. *Bioorg. Med. Chem.* **1997**, *5*, 205-215.

148.   Kim, E. Y.; Bhattacharya, T.; Kunstman, K.; Swantek, P.; Koning, F. A.; Malim, M. H.; Wolinsky, S. M. Human APOBEC3G-mediated editing can promote HIV-1 sequence diversification and accelerate adaptation to selective pressure. *J. Virol.* **2010**, *84*, 10402-10405.

149.   Mulder, L. C.; Harari, A.; Simon, V. Cytidine deamination induced HIV-1 drug resistance. *Proc. Natl. Acad. Sci. U. S. A.* **2008**, *105*, 5501-5506.

150.   Harris, R. S. Enhancing immunity to HIV through APOBEC. *Nat. Biotechnol.* **2008**, *26*, 1089-1090.

151.   Sadler, H. A.; Stenglein, M. D.; Harris, R. S.; Mansky, L. M. APOBEC3G Contributes to HIV-1 Variation through Sublethal Mutagenesis. *J. Virol.* **2010**, *84*, 7396-7404.

152.   Mulder, L. C. F.; Harari, A.; Simon, V. Cytidine deamination induced HIV-1 drug resistance. *Proc. Natl. Acad. Sci. U. S. A.* **2008**, *105*, 5501-5506.

153.   Berkhout, B.; de Ronde, A. APOBEC3G versus reverse transcriptase in the generation of HIV-1 drug-resistance mutations. *AIDS* **2004**, *18*, 1861-1863.

154.   Jern, P.; Russell, R. A.; Pathak, V. K.; Coffin, J. M. Likely role of APOBEC3G-mediated G-to-A mutations in HIV-1 evolution and drug resistance. *PLoS Pathog.* **2009**, *5*, e1000367.

155.   Pillai, S. K.; Wong, J. K.; Barbour, J. D. Turning up the volume on mutational pressure: is more of a good thing always better? (A case study of HIV-1 Vif and APOBEC3). *Retrovirology* **2008**, *5*, 26.

156.   Olson, M. E.; Li, M.; Harris, R. S.; Harki, D. A. Small-molecule APOBEC3G DNA cytosine deaminase inhibitors based on a 4-amino-1,2,4-triazole-3-thiol scaffold. *ChemMedChem* **2013**, *8*, 112-117.

157.   Greenman, C.; Stephens, P.; Smith, R.; Dalgliesh, G. L.; Hunter, C.; Bignell, G.; Davies, H.; Teague, J.; Butler, A.; Edkins, S.; O'Meara, S.; Vastrik, I.; Schmidt, E. E.; Avis, T.; Barthorpe, S.; Bhamra, G.; Buck, G.; Choudhury, B.; Clements, J.; Cole, J.; Dicks, E.; Forbes, S.; Gray, K.; Halliday, K.; Harrison, R.; Hills, K.; Hinton, J.; Jenkinson, A.; Jones, D.; Menzies, A.; Mironenko, T.; Perry, J.; Raine, K.; Richardson, D.; Shepherd, R.; Small, A.; Tofts, C.; Varian, J.; Webb, T.; West, S.; Widaa, S.; Yates, A.; Cahill, D. P.; Louis, D. N.; Goldstraw, P.; Nicholson, A. G.; Brasseur, F.; Looijenga, L.; Weber, B. L.; Chiew, Y.-E.; deFazio, A.; Greaves, M. F.; Green, A. R.; Campbell, P.; Birney, E.; Easton, D. F.; Chenevix-Trench, G.; Tan, M.-H.; Khoo, S. K.; Teh, B. T.; Yuen, S. T.; Leung, S. Y.; Wooster, R.; Futreal, P. A.; Stratton, M. R. Patterns of somatic mutation in human cancer genomes. *Nature* **2007**, *446*, 153-158.

158.   Jones, S.; Wang, T. L.; Shih Ie, M.; Mao, T. L.; Nakayama, K.; Roden, R.; Glas, R.; Slamon, D.; Diaz, L. A., Jr.; Vogelstein, B.; Kinzler, K. W.; Velculescu, V. E.; Papadopoulos, N. Frequent mutations of chromatin remodeling gene ARID1A in ovarian clear cell carcinoma. *Science* **2010**, *330*, 228-231.

159.   Nik-Zainal, S.; Alexandrov, L. B.; Wedge, D. C.; Van Loo, P.; Greenman, C. D.; Raine, K.; Jones, D.; Hinton, J.; Marshall, J.; Stebbings, L. A.; Menzies, A.; Martin, S.; Leung, K.; Chen, L.; Leroy, C.; Ramakrishna, M.; Rance, R.; Lau, K. W.; Mudie, L. J.; Varela, I.; McBride, D. J.; Bignell, G. R.; Cooke, S. L.; Shlien, A.; Gamble, J.; Whitmore, I.; Maddison, M.; Tarpey, P. S.; Davies, H. R.; Papaemmanuil, E.; Stephens, P. J.; McLaren, S.; Butler, A. P.; Teague, J. W.; Jonsson, G.; Garber, J. E.; Silver, D.; Miron, P.; Fatima, A.; Boyault, S.; Langerod, A.; Tutt, A.; Martens, J. W. M.; Aparicio, S. A. J. R.; Borg, A.; Salomon, A. V.; Thomas, G.; Borresen-Dale, A.-L.; Richardson, A. L.; Neuberger, M. S.; Futreal, P. A.; Campbell, P. J.; Stratton, M. R.; Int Canc Genome, C. Mutational Processes Molding the Genomes of 21 Breast Cancers. *Cell* **2012**, *149*, 979-993.

160.   Parsons, D. W.; Li, M.; Zhang, X.; Jones, S.; Leary, R. J.; Lin, J. C.; Boca, S. M.; Carter, H.; Samayoa, J.; Bettegowda, C.; Gallia, G. L.; Jallo, G. I.; Binder, Z. A.; Nikolsky, Y.; Hartigan, J.; Smith, D. R.; Gerhard, D. S.; Fults, D. W.; VandenBerg, S.; Berger, M. S.; Marie, S. K.; Shinjo, S. M.; Clara, C.; Phillips, P. C.; Minturn, J. E.; Biegel, J. A.; Judkins, A. R.; Resnick, A. C.; Storm, P. B.; Curran, T.; He, Y.; Rasheed, B. A.; Friedman, H. S.; Keir, S. T.; McLendon, R.; Northcott, P. A.; Taylor, M. D.; Burger, P. C.; Riggins, G. J.; Karchin, R.; Parmigiani, G.; Bigner, D. D.; Yan, H.; Papadopoulos, N.; Vogelstein, B.; Kinzler, K. W.; Velculescu, V. E. The genetic landscape of the childhood cancer medulloblastoma. *Science* **2011**, *331*, 435-439.

161.   Sjoeblom, T.; Jones, S.; Wood, L. D.; Parsons, D. W.; Lin, J.; Barber, T. D.; Mandelker, D.; Leary, R. J.; Ptak, J.; Silliman, N.; Szabo, S.; Buckhaults, P.; Farrell, C.; Meeh, P.; Markowitz, S. D.; Willis, J.; Dawson, D.;

Willson, J. K. V.; Gazdar, A. F.; Hartigan, J.; Wu, L.; Liu, C.; Parmigiani, G.; Park, B. H.; Bachman, K. E.; Papadopoulos, N.; Vogelstein, B.; Kinzler, K. W.; Velculescu, V. E. The consensus coding sequences of human breast and colorectal cancers. *Science* **2006**, *314*, 268-274.

162.   Stephens, P. J.; Tarpey, P. S.; Davies, H.; Van Loo, P.; Greenman, C.; Wedge, D. C.; Nik-Zainal, S.; Martin, S.; Varela, I.; Bignell, G. R.; Yates, L. R.; Papaemmanuil, E.; Beare, D.; Butler, A.; Cheverton, A.; Gamble, J.; Hinton, J.; Jia, M.; Jayakumar, A.; Jones, D.; Latimer, C.; Lau, K. W.; McLaren, S.; McBride, D. J.; Menzies, A.; Mudie, L.; Raine, K.; Rad, R.; Chapman, M. S.; Teague, J.; Easton, D.; Langerod, A.; Lee, M. T. M.; Shen, C.-Y.; Tee, B. T. K.; Huimin, B. W.; Broeks, A.; Vargas, A. C.; Turashvili, G.; Martens, J.; Fatima, A.; Miron, P.; Chin, S.-F.; Thomas, G.; Boyault, S.; Mariani, O.; Lakhani, S. R.; van de Vijver, M.; Van 'tVeer, L.; Foekens, J.; Desmedt, C.; Sotiriou, C.; Tutt, A.; Caldas, C.; Reis-Filho, J. S.; Aparicio, S. A. J. R.; Salomon, A. V.; Borresen-Dale, A.-L.; Richardson, A. L.; Campbell, P. J.; Futreal, P. A.; Stratton, M. R.; Osbreac The landscape of cancer genes and mutational processes in breast cancer. *Nature* **2012**, *486*, 400-404.

163.   Stransky, N.; Egloff, A. M.; Tward, A. D.; Kostic, A. D.; Cibulskis, K.; Sivachenko, A.; Kryukov, G. V.; Lawrence, M. S.; Sougnez, C.; McKenna, A.; Shefler, E.; Ramos, A. H.; Stojanov, P.; Carter, S. L.; Voet, D.; Cortes, M. L.; Auclair, D.; Berger, M. F.; Saksena, G.; Guiducci, C.; Onofrio, R. C.; Parkin, M.; Romkes, M.; Weissfeld, J. L.; Seethala, R. R.; Wang, L.; Rangel-Escareno, C.; Fernandez-Lopez, J. C.; Hidalgo-Miranda, A.; Melendez-Zajgla, J.; Winckler, W.; Ardlie, K.; Gabriel, S. B.; Meyerson, M.; Lander, E. S.; Getz, G.; Golub, T. R.; Garraway, L. A.; Grandis, J. R. The mutational landscape of head and neck squamous cell carcinoma. *Science* **2011**, *333*, 1157-1160.

164.   Berger, M. F.; Lawrence, M. S.; Demichelis, F.; Drier, Y.; Cibulskis, K.; Sivachenko, A. Y.; Sboner, A.; Esgueva, R.; Pflueger, D.; Sougnez, C.; Onofrio, R.; Carter, S. L.; Park, K.; Habegger, L.; Ambrogio, L.; Fennell, T.; Parkin, M.; Saksena, G.; Voet, D.; Ramos, A. H.; Pugh, T. J.; Wilkinson, J.; Fisher, S.; Winckler, W.; Mahan, S.; Ardlie, K.; Baldwin, J.; Simons, J. W.; Kitabayashi, N.; MacDonald, T. Y.; Kantoff, P. W.; Chin, L.; Gabriel, S. B.; Gerstein, M. B.; Golub, T. R.; Meyerson, M.; Tewari, A.; Lander, E. S.; Getz, G.; Rubin, M. A.; Garraway, L. A. The genomic complexity of primary human prostate cancer. *Nature* **2011**, *470*, 214-220.

165.   Kumar, A.; White, T. A.; MacKenzie, A. P.; Clegg, N.; Lee, C.; Dumpit, R. F.; Coleman, I.; Ng, S. B.; Salipante, S. J.; Rieder, M. J.; Nickerson, D. A.; Corey, E.; Lange, P. H.; Morrissey, C.; Vessella, R. L.; Nelson, P. S.; Shendure, J. Exome sequencing identifies a spectrum of mutation frequencies in advanced and lethal prostate cancers. *Proc. Natl. Acad. Sci. U. S. A.* **2011**, *108*, 17087-17092.

166.   Gostissa, M.; Yan, C. T.; Bianco, J. M.; Cogne, M.; Pinaud, E.; Alt, F. W. Long-range oncogenic activation of Igh-c-myc translocations by the Igh 3 ' regulatory region. *Nature* **2009**, *462*, 803-807.

167.   Takizawa, M.; Tolarova, H.; Li, Z.; Dubois, W.; Lim, S.; Callen, E.; Franco, S.; Mosaico, M.; Feigenbaum, L.; Alt, F. W.; Nussenzweig, A.; Potter, M.; Casellas, R. AID expression levels determine the extent of cMyc oncogenic translocations and the incidence of B cell tumor development. *J. Exp. Med.* **2008**, *205*, 1949-1957.

168.   Pavri, R.; Nussenzweig, M. C. AID targeting in antibody diversity. *Adv. Immunol.* **2011**, *110*, 1-26.

169.   Yamanaka, S.; Balestra, M. E.; Ferrell, L. D.; Fan, J.; Arnold, K. S.; Taylor, S.; Taylor, J. M.; Innerarity, T. L. Apolipoprotein B mRNA-editing protein induces hepatocellular carcinoma and dysplasia in transgenic animals. *Proc. Natl. Acad. Sci. U. S. A.* **1995**, *92*, 8483-8487.

170.   Stenglein, M. D.; Harris, R. S. APOBEC3B and APOBEC3F inhibit L1 retrotransposition by a DNA deamination-independent mechanism. *J. Biol. Chem.* **2006**, *281*, 16837-16841.

171.   Burns, M. B.; Temiz, N. A.; Harris, R. S. Evidence for APOBEC3B mutagenesis in multiple human cancers. *Nat. Genet.* **2013**, *45*, 977-983.

172.   Sieuwerts, A. M.; Willis, S.; Burns, M. B.; Look, M. P.; Meijer-Van Gelder, M. E.; Schlicker, A.; Heideman, M. R.; Jacobs, H.; Wessels, L.; Leyland-Jones, B.; Gray, K. P.; Foekens, J. A.; Harris, R. S.; Martens, J. W. Elevated APOBEC3B correlates with poor outcomes for estrogen-receptor-positive breast cancers. *Horm. Canc.* **2014**, *5*, 405-413.

173.   Cescon, D. W.; Haibe-Kains, B.; Mak, T. W. APOBEC3B expression in breast cancer reflects cellular proliferation, while a deletion polymorphism is associated with immune activation. *Proc. Natl. Acad. Sci. U. S. A.* **2015**, *112*, 2841-2846.

174.   Taylor, B. J.; Nik-Zainal, S.; Wu, Y. L.; Stebbings, L. A.; Raine, K.; Campbell, P. J.; Rada, C.; Stratton, M. R.; Neuberger, M. S. DNA deaminases induce break-associated mutation showers with implication of APOBEC3B and 3A in breast cancer kataegis. *eLife* **2013**, *2*, e00534.

175. Chan, K.; Resnick, M. A.; Gordenin, D. A. The choice of nucleotide inserted opposite abasic sites formed within chromosomal DNA reveals the polymerase activities participating in translesion DNA synthesis. *DNA repair* **2013**, *12*, 878-889.

176. Leonard, B.; Hart, S. N.; Burns, M. B.; Carpenter, M. A.; Temiz, N. A.; Rathore, A.; Vogel, R. I.; Nikas, J. B.; Law, E. K.; Brown, W. L.; Li, Y.; Zhang, Y.; Maurer, M. J.; Oberg, A. L.; Cunningham, J. M.; Shridhar, V.; Bell, D. A.; April, C.; Bentley, D.; Bibikova, M.; Cheetham, R. K.; Fan, J. B.; Grocock, R.; Humphray, S.; Kingsbury, Z.; Peden, J.; Chien, J.; Swisher, E. M.; Hartmann, L. C.; Kalli, K. R.; Goode, E. L.; Sicotte, H.; Kaufmann, S. H.; Harris, R. S. APOBEC3B upregulation and genomic mutation patterns in serous ovarian carcinoma. *Cancer Res.* **2013**, *73*, 7222-7231.

177. Harris, R. S. Molecular mechanism and clinical impact of APOBEC3B-catalyzed mutagenesis in breast cancer. *Breast Cancer Res.* **2015**, *17*, 1-10.

178. Kunkel, T. A.; Diaz, M. Enzymatic cytosine deamination: friend and foe. *Mol. Cell* **2002**, *10*, 962-963.

179. Beale, R. C.; Petersen-Mahrt, S. K.; Watt, I. N.; Harris, R. S.; Rada, C.; Neuberger, M. S. Comparison of the differential context-dependence of DNA deamination by APOBEC enzymes: correlation with mutation spectra in vivo. *J. Mol. Biol.* **2004**, *337*, 585-596.

180. Schumacher, A. J.; Nissley, D. V.; Harris, R. S. APOBEC3G hypermutates genomic DNA and inhibits Ty1 retrotransposition in yeast. *Proc. Natl. Acad. Sci. U. S. A.* **2005**, *102*, 9854-9859.

181. Wood, L. D.; Parsons, D. W.; Jones, S.; Lin, J.; Sjoblom, T.; Leary, R. J.; Shen, D.; Boca, S. M.; Barber, T.; Ptak, J.; Silliman, N.; Szabo, S.; Dezso, Z.; Ustyanksky, V.; Nikolskaya, T.; Nikolsky, Y.; Karchin, R.; Wilson, P. A.; Kaminker, J. S.; Zhang, Z.; Croshaw, R.; Willis, J.; Dawson, D.; Shipitsin, M.; Willson, J. K.; Sukumar, S.; Polyak, K.; Park, B. H.; Pethiyagoda, C. L.; Pant, P. V.; Ballinger, D. G.; Sparks, A. B.; Hartigan, J.; Smith, D. R.; Suh, E.; Papadopoulos, N.; Buckhaults, P.; Markowitz, S. D.; Parmigiani, G.; Kinzler, K. W.; Velculescu, V. E.; Vogelstein, B. The genomic landscapes of human breast and colorectal cancers. *Science* **2007**, *318*, 1108-1113.

182. Saraconi, G.; Severi, F.; Sala, C.; Mattiuz, G.; Conticello, S. G. The RNA editing enzyme APOBEC1 induces somatic mutations and a

compatible mutational signature is present in esophageal adenocarcinomas. *Genome Biol.* **2014**, *15*, 1-10.

183.   Hanahan, D.; Weinberg, R. A. Hallmarks of cancer: the next generation. *Cell* **2011**, *144*, 646-674.

184.   Lawrence, M. S.; Stojanov, P.; Polak, P.; Kryukov, G. V.; Cibulskis, K.; Sivachenko, A.; Carter, S. L.; Stewart, C.; Mermel, C. H.; Roberts, S. A.; Kiezun, A.; Hammerman, P. S.; McKenna, A.; Drier, Y.; Zou, L.; Ramos, A. H.; Pugh, T. J.; Stransky, N.; Helman, E.; Kim, J.; Sougnez, C.; Ambrogio, L.; Nickerson, E.; Shefler, E.; Cortes, M. L.; Auclair, D.; Saksena, G.; Voet, D.; Noble, M.; DiCara, D.; Lin, P.; Lichtenstein, L.; Heiman, D. I.; Fennell, T.; Imielinski, M.; Hernandez, B.; Hodis, E.; Baca, S.; Dulak, A. M.; Lohr, J.; Landau, D. A.; Wu, C. J.; Melendez-Zajgla, J.; Hidalgo-Miranda, A.; Koren, A.; McCarroll, S. A.; Mora, J.; Lee, R. S.; Crompton, B.; Onofrio, R.; Parkin, M.; Winckler, W.; Ardlie, K.; Gabriel, S. B.; Roberts, C. W.; Biegel, J. A.; Stegmaier, K.; Bass, A. J.; Garraway, L. A.; Meyerson, M.; Golub, T. R.; Gordenin, D. A.; Sunyaev, S.; Lander, E. S.; Getz, G. Mutational heterogeneity in cancer and the search for new cancer-associated genes. *Nature* **2013**, *499*, 214-218.

185.   Roberts, S. A.; Lawrence, M. S.; Klimczak, L. J.; Grimm, S. A.; Fargo, D.; Stojanov, P.; Kiezun, A.; Kryukov, G. V.; Carter, S. L.; Saksena, G.; Harris, S.; Shah, R. R.; Resnick, M. A.; Getz, G.; Gordenin, D. A. An APOBEC cytidine deaminase mutagenesis pattern is widespread in human cancers. *Nat. Genet.* **2013**, *45*, 970-976.

186.   Alexandrov, L. B.; Nik-Zainal, S.; Wedge, D. C.; Aparicio, S. A.; Behjati, S.; Biankin, A. V.; Bignell, G. R.; Bolli, N.; Borg, A.; Borresen-Dale, A. L.; Boyault, S.; Burkhardt, B.; Butler, A. P.; Caldas, C.; Davies, H. R.; Desmedt, C.; Eils, R.; Eyfjord, J. E.; Foekens, J. A.; Greaves, M.; Hosoda, F.; Hutter, B.; Ilicic, T.; Imbeaud, S.; Imielinski, M.; Jager, N.; Jones, D. T.; Jones, D.; Knappskog, S.; Kool, M.; Lakhani, S. R.; Lopez-Otin, C.; Martin, S.; Munshi, N. C.; Nakamura, H.; Northcott, P. A.; Pajic, M.; Papaemmanuil, E.; Paradiso, A.; Pearson, J. V.; Puente, X. S.; Raine, K.; Ramakrishna, M.; Richardson, A. L.; Richter, J.; Rosenstiel, P.; Schlesner, M.; Schumacher, T. N.; Span, P. N.; Teague, J. W.; Totoki, Y.; Tutt, A. N.; Valdes-Mas, R.; van Buuren, M. M.; van 't Veer, L.; Vincent-Salomon, A.; Waddell, N.; Yates, L. R.; Zucman-Rossi, J.; Futreal, P. A.; McDermott, U.; Lichter, P.; Meyerson, M.; Grimmond, S. M.; Siebert, R.; Campo, E.; Shibata, T.; Pfister, S. M.; Campbell, P. J.; Stratton, M. R. Signatures of mutational processes in human cancer. *Nature* **2013**, *500*, 415-421.

187.   Henderson, S.; Chakravarthy, A.; Su, X.; Boshoff, C.; Fenton, T. R. APOBEC-mediated cytosine deamination links PIK3CA helical domain

mutations to human papillomavirus-driven tumor development. *Cell Rep.* **2014**, *7*, 1833-1841.

188.   Cancer Genome Atlas Research Network; Comprehensive molecular characterization of urothelial bladder carcinoma. *Nature* **2014**, *507*, 315-322.

189.   Kidd, J. M.; Newman, T. L.; Tuzun, E.; Kaul, R.; Eichler, E. E. Population stratification of a common APOBEC gene deletion polymorphism. *PLoS genetics* **2007**, *3*, e63.

190.   Olson, M. E.; Abate-Pella, D.; Perkins, A. L.; Li, M.; Carpenter, M. A.; Rathore, A.; Harris, R. S.; Harki, D. A. Oxidative Reactivities of 2-Furylquinolines: Ubiquitous Scaffolds in Common High-Throughput Screening Libraries. *J. Med. Chem.* **2015**, *58*, 7419-7430.

191.   Thielen, B. K.; Klein, K. C.; Walker, L. W.; Rieck, M.; Buckner, J. H.; Tomblingson, G. W.; Lingappa, J. R. T cells contain an RNase-insensitive inhibitor of APOBEC3G deaminase activity. *PLoS Pathog.* **2007**, *3*, 1320-1334.

192.   Inglese, J.; Shamu, C. E.; Guy, R. K. Reporting data from high-throughput screening of small-molecule libraries. *Nat. Chem. Biol.* **2007**, *3*, 438-441.

193.   Glickman, J. F. In *Assay Guidance Manual*; Sittampalam, G. S., Coussens, N. P., Nelson, H., Arkin, M., Auld, D., Austin, C., Bejcek, B., Glicksman, M., Inglese, J., Iversen, P. W., Li, Z., McGee, J., McManus, O., Minor, L., Napper, A., Peltier, J. M., Riss, T., Trask, O. J., Jr., Weidner, J., Eds. Bethesda MD, 2004.

194.   Acker, M. G.; Auld, D. S. Considerations for the design and reporting of enzyme assays in high-throughput screening applications. *Perspect. Sci.* **2014**, *1*, 56-73.

195.   Baell, J. B.; Holloway, G. A. New substructure filters for removal of pan assay interference compounds (PAINS) from screening libraries and for their exclusion in bioassays. *J. Med. Chem.* **2010**, *53*, 2719-2740.

196. Cordes, M.; Jacques, O.; Köttgen, A.; Jasper, C.; Boudebous, H.; Giese, B. Development of a Model System for the Study of Long Distance Electron Transfer in Peptides. *Adv. Synth. Catal.* **2008**, *350*, 1053-1062.

197. Kim, K.; Parang, K.; Lau, O. D.; Cole, P. A. Tyrosine analogues as alternative substrates for protein tyrosine kinase Csk: insights into substrate selectivity and catalytic mechanism. *Bioorg. Med. Chem.* **2000**, *8*, 1263-1268.

198. Bautista, F. M.; Campelo, J. M.; Garcia, A.; Luna, D.; Marinas, J. M.; Romero, A. A. Study on dry-media microwave azalactone synthesis on different supported KF catalysts: influence of textural and acid-base properties of supports. *J. Chem. Soc. Perkin Trans. 2* **2002**, 227-234.

199. Takagi, M.; Yamamoto, K. Carbamate-directed stereoselective hydrogenation and kinetic resolution of N-protected α-(α-aminoalkyl)acrylates. *Tetrahedron* **1991**, *47*, 8869-8882.

200. Baell, J. B.; Holloway, G. A. New substructure filters for removal of pan assay interference compounds (PAINS) from screening libraries and for their exclusion in bioassays. *J. Med. Chem.* **2010**, *53*, 2719-2740.

201. Dahlin, J. L.; Nissink, J. W.; Strasser, J. M.; Francis, S.; Higgins, L.; Zhou, H.; Zhang, Z.; Walters, M. A. PAINS in the assay: chemical mechanisms of assay interference and promiscuous enzymatic inhibition observed during a sulfhydryl-scavenging HTS. *J. Med. Chem.* **2015**, *58*, 2091-2113.

202. Hussain, J.; Harper, G.; Blaxill, Z.; Areri, I.; Saremi-Yarahmadi, F.; Pickett, S.; Sidebottom, P. In *International Conference on Chemical Structures* Noordwijkerhout, The Netherlands, 2008, p 58-59.

203. Baell, J.; Walters, M. A. Chemistry: Chemical con artists foil drug discovery. *Nature* **2014**, *513*, 481-483.

204. Shlyakhtenko, L. S.; Lushnikov, A. Y.; Li, M.; Lackey, L.; Harris, R. S.; Lyubchenko, Y. L. Atomic force microscopy studies provide direct evidence for dimerization of the HIV restriction factor APOBEC3G. *J. Biol. Chem.* **2011**, *286*, 3387-3395.

205.   Mehellou, Y.; De Clercq, E. Twenty-Six Years of Anti-HIV Drug Discovery: Where Do We Stand and Where Do We Go? *J. Med. Chem.* **2010**, *53*, 521-538.

206.   Thompson, M. A.; Aberg, J. A.; Cahn, P.; Montaner, J. S.; Rizzardini, G.; Telenti, A.; Gatell, J. M.; Gunthard, H. F.; Hammer, S. M.; Hirsch, M. S.; Jacobsen, D. M.; Reiss, P.; Richman, D. D.; Volberding, P. A.; Yeni, P.; Schooley, R. T. Antiretroviral treatment of adult HIV infection: 2010 recommendations of the International AIDS Society-USA panel. *JAMA* **2010**, *304*, 321-333.

207.   Volberding, P. A.; Deeks, S. G. Antiretroviral therapy and management of HIV infection. *Lancet* **2010**, *376*, 49-62.

208.   Hultquist, J. F.; Lengyel, J. A.; Refsland, E. W.; LaRue, R. S.; Lackey, L.; Brown, W. L.; Harris, R. S. Human and rhesus APOBEC3D, APOBEC3F, APOBEC3G, and APOBEC3H demonstrate a conserved capacity to restrict Vif-deficient HIV-1. *J. Virol.* **2011**, *85*, 11220-11234.

209.   Xiao, Z.; Ehrlich, E.; Luo, K.; Xiong, Y.; Yu, X.-F. Zinc chelation inhibits HIV Vif activity and liberates antiviral function of the cytidine deaminase APOBEC3G. *FASEB J.* **2007**, *21*, 217-222.

210.   Nathans, R.; Cao, H.; Sharova, N.; Ali, A.; Sharkey, M.; Stranska, R.; Stevenson, M.; Rana, T. M. Small-molecule inhibition of HIV-1 Vif. *Nat. Biotechnol.* **2008**, *26*, 1187-1192.

211.   Cen, S.; Peng, Z.-G.; Li, X.-Y.; Li, Z.-R.; Ma, J.; Wang, Y.-M.; Fan, B.; You, X.-F.; Wang, Y.-P.; Liu, F.; Shao, R.-G.; Zhao, L.-X.; Yu, L.; Jiang, J.-D. Small Molecular Compounds Inhibit HIV-1 Replication through Specifically Stabilizing APOBEC3G. *J. Biol. Chem.* **2010**, *285*, 16546-16552.

212.   Ejima, T.; Hirota, M.; Mizukami, T.; Otsuka, M.; Fujita, M. An anti-HIV-1 compound that increases steady-state expression of apoplipoprotein B mRNA-editing enzyme-catalytic polypeptide-like 3G. *Int. J. Mol. Med.* **2011**, *28*, 613-616.

213.   Ali, A.; Wang, J.; Nathans, R. S.; Cao, H.; Sharova, N.; Stevenson, M.; Rana, T. M. Synthesis and Structure–Activity Relationship Studies of HIV-1 Virion Infectivity Factor (Vif) Inhibitors that Block Viral Replication. *ChemMedChem* **2012**, *7*, 1217-1229.

214. Wood, N.; Bhattacharya, T.; Keele, B. F.; Giorgi, E.; Liu, M.; Gaschen, B.; Daniels, M.; Ferrari, G.; Haynes, B. F.; McMichael, A.; Shaw, G. M.; Hahn, B. H.; Korber, B.; Seoighe, C. HIV Evolution in Early Infection: Selection Pressures, Patterns of Insertion and Deletion, and the Impact of APOBEC. *PLoS Pathog.* **2009**, *5*, e1000414.

215. Li, M.; Harris, R. S. *Manuscript in Preparation*.

216. Sun, X.; Tao, Y.; Liu, Y.; Jia, Y.; Chen, B. Synthesis and Biological Activities of 4,5-Dihydro-3-methyl-4-amino-1,2,4-triazole-5-thione Schiff Bases. *Acta Chim. Sinica* **2008**, *66*, 234-238.

217. Demchenko, A. M.; Yanchenko, V. O.; Smolskiy, O. S.; Aheyev, V. O.; Lozynskiy, M. O. *Farmatsevtichnii Zhurnal (Kiev)* **2004**, 68.

218. Badr, S. M.; Barwa, R. M. Synthesis of some new [1,2,4]triazolo[3,4-b][1,3,4]thiadiazines and [1,2,4]triazolo[3,4-b][1,3,4] thiadiazoles starting from 5-nitro-2-furoic acid and evaluation of their antimicrobial activity. *Bioorg. Med. Chem.* **2011**, *19*, 4506-4512.

219. Maingot, L.; Leroux, F.; Landry, V.; Dumont, J.; Nagase, H.; Villoutreix, B.; Sperandio, O.; Deprez-Poulain, R.; Deprez, B. New non-hydroxamic ADAMTS-5 inhibitors based on the 1,2,4-triazole-3-thiol scaffold. *Bioorg. Med. Chem. Lett.* **2010**, *20*, 6213-6216.

220. Eweiss, N. F.; Bahajaj, A. A.; Elsherbini, E. A. Synthesis of heterocycles. Part VI. Synthesis and antimicrobial activity of some 4-amino-5-aryl-1,2,4-triazole-3-thiones and their derivatives. *J. Heterocycl. Chem.* **1986**, *23*, 1451-1458.

221. Cartwright, D. D. J.; Clark, B. A. J.; McNab, H. Gas-phase pyrolysis of 4-amino-3-allylthio-1,2,4-triazoles: a new route to [1,3]thiazolo[3,2-b][1,2,4]triazoles. *J. Chem. Soc., Perkin Trans. 1* **2001**, 424-428.

222. Harjes, E.; Gross, P. J.; Chen, K.-M.; Lu, Y.; Shindo, K.; Nowarski, R.; Gross, J. D.; Kotler, M.; Harris, R. S.; Matsuo, H. An Extended Structure of the APOBEC3G Catalytic Domain Suggests a Unique Holoenzyme Model. *J. Mol. Biol.* **2009**, *389*, 819-832.

223.   Shandilya, S. M. D.; Nalam, M. N. L.; Nalivaika, E. A.; Gross, P. J.; Valesano, J. C.; Shindo, K.; Li, M.; Munson, M.; Royer, W. E.; Harjes, E.; Kono, T.; Matsuo, H.; Harris, R. S.; Somasundaran, M.; Schiffer, C. A. Crystal Structure of the APOBEC3G Catalytic Domain Reveals Potential Oligomerization Interfaces. *Structure* **2010**, *18*, 28-38.

224.   Singh, K.; Singh, D. P.; Barwa, M. S.; Tyagi, P.; Mirza, Y. Antibacterial Co(II), Ni(II), Cu(II) and Zn(II) Complexes of Schiff bases Derived from Fluorobenzaldehyde and Triazoles*. *J. Enzym. Inhib. Med. Ch.* **2006**, *21*, 557-562.

225.   Singh, K.; Singh, D. P.; Barwa, M. S.; Tyagi, P.; Mirza, Y. Some bivalent metal complexes of Schiff bases containing N and S donor atoms†. *J. Enzym. Inhib. Med. Ch.* **2006**, *21*, 749-755.

226.   Tabatabaee, M.; Ghassemzadeh, M.; Sadeghi, A.; Shahriary, M.; Neumüller, B.; Rothenberger, A. Synthesis, Characterization and X-ray Structures of AMTT-Type Schiff bases and two CuI Complexes (AMTT= 4-amino-5-methyl-2H-1,2,4-triazole-3(4H)-thione). *Z. Anorg. Allg. Chem.* **2009**, *635*, 120-124.

227.   Ghassemzadeh, M.; Tabatabaee, M.; Soleimani, S.; Neumüller, B. Synthesis, Characterization and Crystal Structures of new 1,2,4-Triazole based Schiff-bases and their Copper(I) Complexes. *Z. Anorg. Allg. Chem.* **2005**, *631*, 1871-1876.

228.   McCarrick, R. M.; Eltzroth, M. J.; Squattrito, P. J. Coordination geometries of bis(4-amino-3-alkyl-1,2,4-triazole-5-thione) complexes of first-row transition metals: crystal structures of complexes with propyl and hydrogen in the 3-position. Relationship to the 3-methyl and 3-ethyl analogs. *Inorg. Chim. Acta.* **2000**, *311*, 95-105.

229.   Zhang, J.; Zhang, T.; Yu, K. Preparation and Structure Characterization of 4-Amino-1,2,4-triazol-5-one Hydrate. *Chem. Heterocycl. Compd.* **2003**, *39*, 461-466.

230.   Bibette, J. Gaining confidence in high-throughput screening. *Proc. Natl. Acad. Sci. U.S.A.* **2012**, *109*, 649-650.

231.   Baell, J. B. Observations on screening-based research and some concerning trends in the literature. *Future Med. Chem.* **2010**, *2*, 1529-1546.

232.   Feng, B. Y.; Simeonov, A.; Jadhav, A.; Babaoglu, K.; Inglese, J.; Shoichet, B. K.; Austin, C. P. A high-throughput screen for aggregation-based inhibition in a large compound library. *J. Med. Chem.* **2007**, *50*, 2385-2390.

233.   Zitha-Bovens, E.; Maas, P.; Wife, D.; Tijhuis, J.; Hu, Q. N.; Kleinoder, T.; Gasteiger, J. COMDECOM: predicting the lifetime of screening compounds in DMSO solution. *J. Biomol. Screen* **2009**, *14*, 557-565.

234.   Chen, A.; Zhao, X.; Mercer, L.; Su, C.; Zalameda, L.; Liu, Y.; Lembke, A.; Eastwood, H.; Dang, S.; Oung, T.; Xia, X.; Young, S. W.; Xiao, S.; McCarter, J. D. Assessment of the Integrity of Compounds Stored in Assay-Ready Plates Using a Kinase Sentinel Assay. *Comb. Chem. High T. Scr.* **2013**, *16*, 644-651.

235.   Hermann, J. C.; Chen, Y.; Wartchow, C.; Menke, J.; Gao, L.; Gleason, S. K.; Haynes, N.-E.; Scott, N.; Petersen, A.; Gabriel, S.; Vu, B.; George, K. M.; Narayanan, A.; Li, S. H.; Qian, H.; Beatini, N.; Niu, L.; Gan, Q.-F. Metal Impurities Cause False Positives in High-Throughput Screening Campaigns. *ACS Med. Chem. Lett.* **2012**, *4*, 197-200.

236.   Johnston, P. A. Redox cycling compounds generate H2O2 in HTS buffers containing strong reducing reagents—real hits or promiscuous artifacts? *Curr. Opin. Cell Biol.* **2011**, *15*, 174-182.

237.   Soares, K. M.; Blackmon, N.; Shun, T. Y.; Shinde, S. N.; Takyi, H. K.; Wipf, P.; Lazo, J. S.; Johnston, P. A. Profiling the NIH Small Molecule Repository for compounds that generate H2O2 by redox cycling in reducing environments. *Assay Drug Dev. Technol.* **2010**, *8*, 152-174.

238.   Rishton, G. M. Reactive compounds and in vitro false positive in HTS. *Drug Discov. Today* **1997**, *2*, 382-384.

239.   Kozikowski, B. A.; Burt, T. M.; Tirey, D. A.; Williams, L. E.; Kuzmak, B. R.; Stanton, D. T.; Morand, K. L.; Nelson, S. L. The effect of freeze/thaw cycles on the stability of compounds in DMSO. *J. Biomol. Screen* **2003**, *8*, 210-215.

240.   Kozikowski, B. A.; Burt, T. M.; Tirey, D. A.; Williams, L. E.; Kuzmak, B. R.; Stanton, D. T.; Morand, K. L.; Nelson, S. L. The effect of room-temperature storage on the stability of compounds in DMSO. *J. Biomol. Screen* **2003**, *8*, 205-209.

241. Blaxill, Z.; Holland-Crimmin, S.; Lifely, R. Stability through the ages: the GSK experience. *J Biomol. Screen.* **2009**, *14*, 547-556.

242. Stenglein, M. D.; Burns, M. B.; Li, M.; Lengyel, J.; Harris, R. S. APOBEC3 proteins mediate the clearance of foreign DNA from human cells. *Nat. Struct. Mol. Biol.* **2010**, *17*, 222-229.

243. Giardina, G. A. M.; Sarau, H. M.; Farina, C.; Medhurst, A. D.; Grugni, M.; Raveglia, L. F.; Schmidt, D. B.; Rigolio, R.; Luttmann, M.; Vecchietti, V.; Hay, D. W. P. Discovery of a novel class of selective non-peptide antagonists for the human neurokinin-3 receptor. 1. Identification of the 4-quinolinecarboxamide framework. *J. Med. Chem.* **1997**, *40*, 1794-1807.

244. Strigacova, J.; Hudecova, D.; Varecka, L.; Lasikova, A.; Vegh, D. Some biological properties of new quinoline-4-carboxylic acid and quinoline-4-carboxamide derivatives. *Folia Microbiol.* **2000**, *45*, 305-309.

245. Cai, X.; Zhang, J.; Chen, M.; Wu, Y.; Wang, X.; Chen, J.; Shen, X.; Qu, D.; Jiang, H. The effect of the potential PhoQ histidine kinase inhibitors on Shigella flexneri virulence. *PLoS One* **2011**, *6*, e23100.

246. Shankerrao, S. B., Y. D.; Mety, S. S. Synthesis, antioxidant, and antibacterial studies of phenolic esters and amides of 2-(1-benzofuran-2-yl) quinoline-4-carboxylic acid. *Med. Chem. Res.* **2013**, *22*, 1163-1171.

247. Spinks, D.; Shanks, E. J.; Cleghorn, L. A.; McElroy, S.; Jones, D.; James, D.; Fairlamb, A. H.; Frearson, J. A.; Wyatt, P. G.; Gilbert, I. H. Investigation of trypanothione reductase as a drug target in Trypanosoma brucei. *ChemMedChem* **2009**, *4*, 2060-2069.

248. Matsuno, K.; Masuda, Y.; Uehara, Y.; Sato, H.; Muroya, A.; Takahashi, O.; Yokotagawa, T.; Furuya, T.; Okawara, T.; Otsuka, M.; Ogo, N.; Ashizawa, T.; Oshita, C.; Tai, S.; Ishii, H.; Akiyama, Y.; Asai, A. Identification of a new series of STAT3 inhibitors by virtual screening. *ACS Med. Chem. Lett.* **2010**, *1*, 371-375.

249. Lack, N. A.; Axerio-Cilies, P.; Tavassoli, P.; Han, F. Q.; Chan, K. H.; Feau, C.; LeBlanc, E.; Guns, E. T.; Guy, R. K.; Rennie, P. S.; Cherkasov, A. Targeting the binding function 3 (BF3) site of the human androgen receptor through virtual screening. *J. Med. Chem.* **2011**, *54*, 8563-8573.

250.   Ghodsi, R.; Zarghi, A.; Daraei, B.; Hedayati, M. Design, synthesis and biological evaluation of new 2,3-diarylquinoline derivatives as selective cyclooxygenase-2 inhibitors. *Bioorg. Med. Chem.* **2010**, *18*, 1029-1033.

251.   Yu, P.; Hu, J.; Zhou, T.-Y.; Wang, P.; Xu, Y.-H. Synthesis, insecticidal evaluation of novel 1,3,4-thiadiazole chrysanthemamide derivatives formed by an EDCI/HOBt condensation. *J. Chem. Res.* **2011**, *35*, 703-706.

252.   Mirek, J.; Sygula, A. Semiempirical MNDO and UV Absorption Studies on Tautomerism of 2-Quinolones. *Z. Naturforsch. Pt. A* **1982**, *37A*, 1276-1283.

253.   Galstyan, G.; Knapp, E. W. Computations of 36 tautomer/isomer equilibria of different lactams. *J. Phys. Chem. A* **2012**, *116*, 6885-6893.

254.   Gerega, A.; Lapinski, L.; Nowak, M. J.; Furmanchuk, A.; Leszczynski, J. Systematic effect of benzo-annelation on oxo-hydroxy tautomerism of heterocyclic compounds. Experimental matrix-isolation and theoretical study. *J. Phys. Chem. A* **2007**, *111*, 4934-4943.

255.   Kaila, N.; Janz, K.; DeBernardo, S.; Bedard, P. W.; Camphausen, R. T.; Tam, S.; Tsao, D. H.; Keith, J. C., Jr.; Nickerson-Nutter, C.; Shilling, A.; Young-Sciame, R.; Wang, Q. Synthesis and biological evaluation of quinoline salicylic acids as P-selectin antagonists. *J. Med. Chem.* **2007**, *50*, 21-39.

256.   Foote, C. S.; Wexler, S.; Ando, W.; Higgins, R. Chemistry of singlet oxygen. IV. Oxygenations with hypochlorite-hydrogen peroxide. *J. Am. Chem. Soc.* **1968**, *90*, 975-981.

257.   Schenck, G. O. Colloquium am 26. Juni 1944. *Angew. Chem.* **1944**, *57*, 101-102.

258.   Criegee, R. Mechanism of ozonolysis. *Angew. Chem.* **1975**, *14*, 746-752.

259.   Wasserman, H. H.; Liberles, A. Formation of epoxides in the pyrrole and furan series by photooxidation. *J. Am. Chem. Soc.* **1960**, *82*, 2086-2086.

260. Bailey, P. S. *Ozonation in Organic Chemistry*; Academic Press: New York, 1978; Vol. 1.

261. Matsuura, T.; Saito, I. *Photochemistry of Heterocyclic Compounds*; Wiley: New York, 1976.

262. Adam, W.; Rodriguez, A. On the question of carbonyl oxide intermediates in the oxygen transfer by furan endoperoxides and bicyclic ozonides: intramolecular trapping experiments. *Tetrahedron Lett.* **1981**, *22*, 3509-3512.

263. Graziano, M. L.; Lesce, M. R.; Scarpati, R. Photosensitized oxidation of furans. Part 1. Synthesis and properties of furan endo-peroxides. *J. Chem. Soc., Perkin Trans. 1* **1980**, 1955-1959.

264. Dufraisse, C.; Ecary, S. Photooxidation on the cyclopentane ring: photooxydi-phenylisobenzofuran. *C. R. Acad. Sci. Paris* **1946**, *233*, 735-737.

265. Palacios, F.; Alonso, C.; Amezua, P.; Rubiales, G. Synthesis of Aza Polycyclic Compounds Derived from Pyrrolidine, Indolizidine, and Indole via Intramolecular Diels−Alder Cycloadditions of Neutral 2-Azadienes. *J. Org. Chem.* **2002**, *67*, 1941-1946.

266. Baell, J.; Walters, M. A. Chemistry: Chemical con artists foil drug discovery. *Nature* **2014**, *513*, 481-483.

267. Lieberman, O. J.; Orr, M. W.; Wang, Y.; Lee, V. T. High-Throughput Screening Using the Differential Radial Capillary Action of Ligand Assay Identifies Ebselen As an Inhibitor of Diguanylate Cyclases. *ACS Chem. Biol.* **2014**, *9*, 183-192.

268. Mukherjee, S.; Weiner, W. S.; Schroeder, C. E.; Simpson, D. S.; Hanson, A. M.; Sweeney, N. L.; Marvin, R. K.; Ndjomou, J.; Kolli, R.; Isailovic, D.; Schoenen, F. J.; Frick, D. N. Ebselen Inhibits Hepatitis C Virus NS3 Helicase Binding to Nucleic Acid and Prevents Viral Replication. *ACS Chem. Biol.* **2014**, *9*, 2393-2403.

269. Favrot, L.; Grzegorzewicz, A. E.; Lajiness, D. H.; Marvin, R. K.; Boucau, J.; Isailovic, D.; Jackson, M.; Ronning, D. R. Mechanism of inhibition of

Mycobacterium tuberculosis antigen 85 by ebselen. *Nat. Commun.* **2013**, *4*, 2748.

270. Xu, K.; Zhang, Y.; Tang, B.; Laskin, J.; Roach, P. J.; Chen, H. Study of highly selective and efficient thiol derivatization using selenium reagents by mass spectrometry. *Anal. Chem.* **2010**, *82*, 6926-6932.

271. Mugesh, G.; du Mont, W. W.; Sies, H. Chemistry of biologically important synthetic organoselenium compounds. *Chem. Rev.* **2001**, *101*, 2125-2179.

272. Sarma, B. K.; Mugesh, G. Glutathione peroxidase (GPx)-like antioxidant activity of the organoselenium drug ebselen: unexpected complications with thiol exchange reactions. *J. Am. Chem. Soc.* **2005**, *127*, 11477-11485.

273. Turpin, J. A.; Song, Y.; Inman, J. K.; Huang, M.; Wallqvist, A.; Maynard, A.; Covell, D. G.; Rice, W. G.; Appella, E. Synthesis and biological properties of novel pyridinioalkanoyl thiolesters (PATE) as anti-HIV-1 agents that target the viral nucleocapsid protein zinc fingers. *J. Med. Chem.* **1999**, *42*, 67-86.

274. Domagala, J. M.; Gogliotti, R.; Sanchez, J. P.; Stier, M. A.; Musa, K.; Song, Y.; Loo, J.; Reily, M.; Tummino, P.; Harvey, P.; Hupe, D.; Sharmeen, L.; Mack, D.; Scholten, J.; Saunders, J.; McQuade, T. 2,2'-Dithiobisbenzamides and 2-benzisothiazolones, two new classes of antiretroviral agents: SAR and mechanistic considerations. *Drug Des. Discov.* **1997**, *15*, 49-61.

275. Tummino, P. J.; Harvey, P. J.; McQuade, T.; Domagala, J.; Gogliotti, R.; Sanchez, J.; Song, Y.; Hupe, D. The human immunodeficiency virus type 1 (HIV-1) nucleocapsid protein zinc ejection activity of disulfide benzamides and benzisothiazolones: correlation with anti-HIV and virucidal activities. *Antimicrob. Agents Chemother.* **1997**, *41*, 394-400.

276. Harris, M. T.; Walker, D. M.; Drew, M. E.; Mitchell, W. G.; Dao, K.; Schroeder, C. E.; Flaherty, D. P.; Weiner, W. S.; Golden, J. E.; Morris, J. C. Interrogating a hexokinase-selected small-molecule library for inhibitors of Plasmodium falciparum hexokinase. *Antimicrob. Agents Chemother.* **2013**, *57*, 3731-3737.

277. Liu, D.; Tian, Z.; Yan, Z.; Wu, L.; Ma, Y.; Wang, Q.; Liu, W.; Zhou, H.; Yang, C. Design, synthesis and evaluation of 1,2-benzisothiazol-3-one

derivatives as potent caspase-3 inhibitors. *Bioorg. Med. Chem.* **2013**, *21*, 2960-2967.

278.   Qin, J.; Xie, P.; Ventocilla, C.; Zhou, G.; Vultur, A.; Chen, Q.; Liu, Q.; Herlyn, M.; Winkler, J.; Marmorstein, R. Identification of a novel family of BRAF(V600E) inhibitors. *J. Med. Chem.* **2012**, *55*, 5220-5230.

279.   Lack, N. A.; Axerio-Cilies, P.; Tavassoli, P.; Han, F. Q.; Chan, K. H.; Feau, C.; LeBlanc, E.; Guns, E. T.; Guy, R. K.; Rennie, P. S.; Cherkasov, A. Targeting the binding function 3 (BF3) site of the human androgen receptor through virtual screening. *J. Med. Chem.* **2011**, *54*, 8563-8573.

280.   Jorgensen, W. L.; Trofimov, A.; Du, X.; Hare, A. A.; Leng, L.; Bucala, R. Benzisothiazolones as modulators of macrophage migration inhibitory factor. *Bioorg. Med. Chem. Lett.* **2011**, *21*, 4545-4549.

281.   Furdas, S. D.; Shekfeh, S.; Bissinger, E. M.; Wagner, J. M.; Schlimme, S.; Valkov, V.; Hendzel, M.; Jung, M.; Sippl, W. Synthesis and biological testing of novel pyridoisothiazolones as histone acetyltransferase inhibitors. *Bioorg. Med. Chem.* **2011**, *19*, 3678-3689.

282.   Brahemi, G.; Kona, F. R.; Fiasella, A.; Buac, D.; Soukupova, J.; Brancale, A.; Burger, A. M.; Westwell, A. D. Exploring the structural requirements for inhibition of the ubiquitin E3 ligase breast cancer associated protein 2 (BCA2) as a treatment for breast cancer. *J. Med. Chem.* **2010**, *53*, 2757-2765.

283.   Cournia, Z.; Leng, L.; Gandavadi, S.; Du, X.; Bucala, R.; Jorgensen, W. L. Discovery of human macrophage migration inhibitory factor (MIF)-CD74 antagonists via virtual screening. *J. Med. Chem.* **2009**, *52*, 416-424.

284.   Smith, S. M.; Min, J.; Ganesh, T.; Diebold, B.; Kawahara, T.; Zhu, Y.; McCoy, J.; Sun, A.; Snyder, J. P.; Fu, H.; Du, Y.; Lewis, I.; Lambeth, J. D. Ebselen and congeners inhibit NADPH oxidase 2-dependent superoxide generation by interrupting the binding of regulatory subunits. *Chem. Biol.* **2012**, *19*, 752-763.

285.   Vasan, M.; Neres, J.; Williams, J.; Wilson, D. J.; Teitelbaum, A. M.; Remmel, R. P.; Aldrich, C. C. Inhibitors of the salicylate synthase (MbtI) from Mycobacterium tuberculosis discovered by high-throughput screening. *ChemMedChem* **2010**, *5*, 2079-2087.

286. Bravo, Y.; Teriete, P.; Dhanya, R. P.; Dahl, R.; Lee, P. S.; Kiffer-Moreira, T.; Ganji, S. R.; Sergienko, E.; Smith, L. H.; Farquharson, C.; Millan, J. L.; Cosford, N. D. Design, synthesis and evaluation of benzoisothiazolones as selective inhibitors of PHOSPHO1. *Bioorg. Med. Chem. Lett.* **2014**, *24*, 4308-4311.

287. Levin, J. I.; Turos, E.; Weinreb, S. M. An Alternative Procedure for the Aluminum-Mediated Conversion of Esters to Amides. *Synth. Commun.* **1982**, *12*, 989-993.

288. Novak, A.; Humphreys, L. D.; Walker, M. D.; Woodward, S. Amide bond formation using an air-stable source of AlMe3. *Tetrahedron Lett.* **2006**, *47*, 5767-5769.

289. Correa, A.; Tellitu, I.; Dominguez, E.; SanMartin, R. Novel alternative for the N-S bond formation and its application to the synthesis of benzisothiazol-3-ones. *Org. Lett.* **2006**, *8*, 4811-4813.

290. Miller Jenkins, L. M.; Ott, D. E.; Hayashi, R.; Coren, L. V.; Wang, D.; Xu, Q.; Schito, M. L.; Inman, J. K.; Appella, D. H.; Appella, E. Small-molecule inactivation of HIV-1 NCp7 by repetitive intracellular acyl transfer. *Nat. Chem. Biol.* **2010**, *6*, 887-889.

Appendix A

**DEVELOPMENT OF A HPLC ASSAY TO QUANTIFY L-XMP TO L-GMP
CONVERSION BY GUANOSINE MONOPHOSPHATE SYNTHETASE**

This work has been published by John Wiley & Sons:
Struntz, N. B.; Hu, T.; White, B. R.; Olson, M. E.; Harki, D. A. "Inhibition of
Guanosine Monophosphate Synthetase by the Substrate Enantiomer L-XMP"
ChemBioChem **2012**, *13*, 2517-2520.

In this work, M.E.O. was responsible for developing the HPLC method to
calculate the kinetic parameters of GMPS.

A.1 Overview

Guanosine monophosphate synthetase (GMPS) functions in *de novo* nucleoside biosynthesis in prokaryotes and eukaryotes to convert xanthosine 5′-monphosphate (XMP) to guanosine 5′-monophosphate (GMP) as shown in Scheme A.1.[1,2]
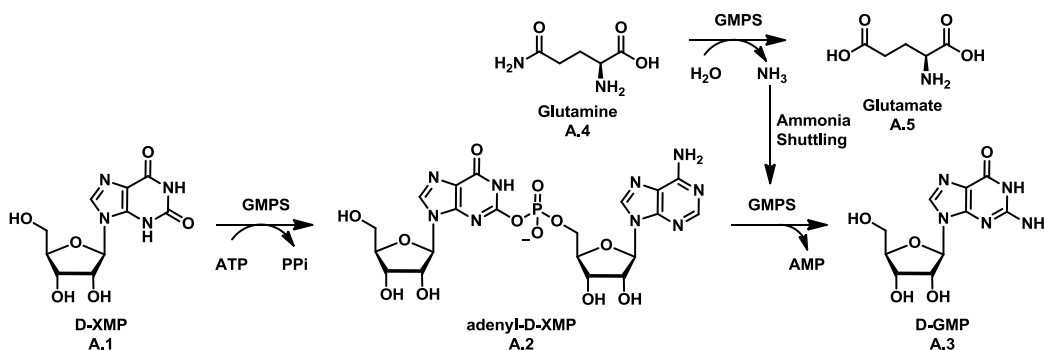
Scheme A.1. Enzymatic Reaction Catalyzed by GMPS. D-XMP is adenylated by ATP in the synthetase active site, which activates the nucleobase for nucleophilic attack and triggers the hydrolysis of glutamine in the amidotransferase active site. D-GMP is finally synthesized through aminolysis of **A.2** by ammonia.[1-6]

GMPS contains two active sites, which are separated by approximately 30 Å, to hydrolyze glutamine and aminate D-XMP (**A.1**). Specifically, glutamine (**A.4**) is hydrolyzed in the amidotransferase active site generating ammonia, which acts as the nucleophile in the subsequent amination of D-XMP (**A.1**). A large conformational change likely occurs to shuttle the nucleophilic ammonia to the synthetase active site, where D-XMP (**A.1**) has been previously adenylated by ATP to yield adenyl-D-XMP (**A.2**).[3,4] Adenylation of D-XMP (**A.1**) activates the nucleobase for the ensuing aminolysis and is thought to signal the start of

220

glutamine hydrolysis.[1-6] D-GMP (**A.3**) is accomplished through aminolysis by ammonia.

The Harki Lab was interested in characterizing the enantioselectivity of GMPS; as previously, the development of mirror-image L-enantiomer nucleosides has been a successful strategy in the development of clinically-approved antiviral therapeutics.[7-10] As one example, L-nucleoside lamivudine (2′,3′-dideoxy-3′-thiacytidine, 3TC) inhibits HIV-1 replication by taking advantage of the loose enantioselectivity of HIV-1 RT.[11] While the relaxed enantioselectivities of viral enzymes are well known,[12,13] many of the key enzymes in nucleoside biosynthesis have not been characterized for their enantioselective preferences. Importantly, characterization of GMPS enantioselectivity could offer a novel target in anticancer and/or antibiotic drug design as inhibitors of nucleotide biosynthesis exhibit anti-proliferative, antibacterial, and immunosuppressive effects.[14-16] Moreover, the crystal structure of *Escherichia coli* (*E. coli*) GMPS exhibits a large solvent accessible synthetase active site,[3] and previous studies have demonstrated that non-natural D-XMP analogues function as substrates and/or inhibitors of GMPS.[17,18] Accordingly, the Harki lab hypothesized that L-XMP would be accommodated in the GMPS synthetase active site, and function as an inhibitor or substrate of enzyme function.

A.2 Results

E. coli GMPS was over-expressed and purified, and L-XMP was synthesized in four steps from 1-*O*-acetyl-2,3,5-tri-*O*-benzoyl-β-L-ribofuranoside, which can accomplished from L-arabinose according to published methods.[19] A

reverse phase HPLC method was developed to separate the components of the enzymatic reaction, and an assay was employed to quantitate the enzymatic reaction products. In brief, GMPS was incubated with a substrate, D-XMP (control) or L-XMP, and NH$_4$OAc (ammonia source). The reaction was terminated at various time points by the addition of ethylenediaminetetraacetic acid (EDTA). After quenching the reaction, protein was removed by a molecular weight spin-column (30 kDa), and the enzymatic reaction products were analyzed by HPLC. In the presence of GMPS, L-XMP was turned over to L-GMP, demonstrating that GMPS can catalyze the aminolysis of the non-natural enantiomer (Figure A.1).
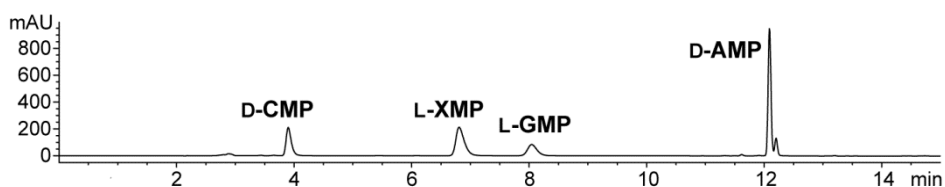
Figure A.1. HPLC Analysis of L-XMP Conversion to L-GMP by GMPS. D-CMP was employed as an external standard to quantify the amount of L-GMP produced per experiment. D-AMP is the byproduct of the reaction.

D-CMP was spiked into the reaction as an external standard, and a calibration curve was prepared by mixing known concentrations of GMP and D-CMP, then measuring their relative ratios at 260 nm. The ratio of GMP to D-CMP in subsequent experiments was then used to quantify the amount of GMP produced in the enzymatic reaction. Quantification was accomplished by fitting the GMP/D-CMP ratios into the slope-intercept equation of the predetermined calibration plot. With these values, GMP production as a function of time could be measured, yielding initial velocity values for GMP production at various XMP

222

concentrations. The measured initial velocities were fitted to the Michaelis-Menton equation and analyzed by non-linear regression to determine the K_m and V_{max} of the reaction.

The apparent K_m value for D-XMP was 35.3 µM, which was in accordance was previously reported values (29 µM and 166 µM) for *E. coli* GMPS.[20,21] Analysis of L-XMP revealed an apparent K_m value of 316.7 µM, 10x that of the natural substrate. The turnover number (k_{cat}) for D-XMP was determined to be 4.8×10^{-2} s^{-1}, which was also in accordance with literature values (9.4×10^{-2} s^{-1}).[20] For L-XMP, the k_{cat} was determined to be 3.2×10^{-6} s^{-1}, a 15,000-fold difference. As a result, the specific activity (k_{cat}/K_m) of L-XMP was 140,000-fold lower than the natural enantiomer (1.4×10^{-3} µM^{-1}s^{-1} for D-XMP versus 1.0×10^{-8} µM^{-1}s^{-1}). The determined kinetic parameters were confirmed by a known continuous UV spectrophotometric assay, and suggested that L-XMP also inhibits GMPS.[20,22] Inhibition of GMPS by L-XMP was confirmed through competition experiments. In brief, addition of fixed concentrations of inhibitor to a variety of D-XMP concentrations, followed by UV-visible analysis enabled the determination of K_i values. L-XMP and two previously reported GMPS inhibitors, decoyinine (uncompetitive)[1] and mizoribine (competitive), were analyzed. Decoyinine exhibited a K_i value of 54.1 µM; mizoribine, a K_i value of 1.8 µM, and L-XMP, a K_i value of 7.5 µM. The K_i values for the positive controls were similar to previously reported values at 26 µM[23] and 10 µM[15], respectively. This result shows that L-XMP is at least as potent, or may be slightly better than known GMPS inhibitors.

Finally, to compare the binding of D-XMP and L-XMP in the GMPS active site, docking studies into the crystal structure of *E. coli* GMPS (PDB: 1GPM[3])

were performed. It was observed that although the large size of the GMPS active side readily accommodates both the natural and non-natural substrates, the ribose sugar of L-XMP occupied a drastically different position and lost many of the molecular interactions observed with docked D-XMP. These interactions likely influence the rate of enzyme turnover and enzyme efficiency.

A.3 Conclusion

In this study, GMPS was found to both turnover and be inhibited by the enantiomer of its natural substrate, D-XMP. Thus, the synthesis and study of L-XMP highlights the promiscuous substrate preferences of GMPS, and implies that other nucleoside biosynthesis enzymes may behave similarly. Moreover, the identification of L-XMP as a novel inhibitor of GMPS and preliminary molecular modeling studies provide a foundation for future inhibitor design.

A.4 Experimental

An Agilent 1200 series instrument equipped with a diode array detector and a Zorbax SB-AQ column (4.6 x 150 mm, 3.5 µm, Agilent Technologies) at 22 °C was used for analysis. The mobile phase comprised aqueous triethylammonium acetate buffer (TEAA, 20 mM, pH = 6, 0 to 5 min), followed by 0 to 50% CH₃CN in TEAA buffer (5 to 15 min) at a flow-rate 1.0 mL/min.

A.5 Acknowledgements

A.6 References

1.	Nakamura, J.; Lou, L. Biochemical characterization of human GMP synthetase. *J. Biol. Chem.* **1995**, *270*, 7347-7353.

2.	Nakamura, J.; Straub, K.; Wu, J.; Lou, L. The glutamine hydrolysis function of human GMP synthetase. Identification of an essential active site cysteine. *J. Biol. Chem.* **1995**, *270*, 23450-23455.

3.	Tesmer, J. J. G.; Klem, T. J.; Deras, M. L.; Davisson, V. J.; Smith, J. L. The crystal structure of GMP synthetase reveals a novel catalytic triad and is a structural paradigm for two enzyme families. *Nat. Struct. Biol.* **1996**, *3*, 74-86.

4.	Tesmer, J. J. G.; Stemmler, T. L.; Penner-Hahn, J. E.; Davisson, V. J.; Smith, J. L. Preliminary X-ray analysis of Escherichia coli GMP synthetase: determination of anomalous scattering factors for a cysteinyl mercury derivative. *Proteins Struct. Funct. Genet.* **1994**, *18*, 394-403.

5.   Chittur, S. V.; Klem, T. J.; Shafer, C. M.; Davisson, V. J. Mechanism for acivicin inactivation of triad glutamine amidotransferases. *Biochemistry* **2001**, *40*, 876-887.

6.   von der Saal, W.; Crysler, C. S.; Villafranca, J. J. Positional isotope exchange and kinetic experiments with Escherichia coli guanosine-5'-monophosphate synthetase. *Biochemistry* **1985**, *24*, 5343-5350.

7.   Spadari, S.; Maga, G.; Verri, A.; Focher, F. Molecular basis for the antiviral and anticancer activities of unnatural L-beta-nucleosides. *Expert Opin. Invest. Drugs* **1998**, *7*, 1285-1300.

8.   Zemlicka, J. Enantioselectivity of the antiviral effects of nucleoside analogues. *Pharmacol. Ther.* **2000**, *85*, 251-266.

9.   Mathe, C.; Gosselin, G. L-nucleoside enantiomers as antivirals drugs: a mini-review. *Antiviral Res.* **2006**, *71*, 276-281.

10.   Maury, G. The enantioselectivity of enzymes involved in current antiviral therapy using nucleoside analogues: a new strategy? *Antiviral Chem. Chemother.* **2000**, *11*, 165-189.

11.   Gray, N. M.; Marr, C. L.; Penn, C. R.; Cameron, J. M.; Bethell, R. C. The intracellular phosphorylation of (-)-2'-deoxy-3'-thiacytidine (3TC) and the incorporation of 3TC 5'-monophosphate into DNA by HIV-1 reverse transcriptase and human DNA polymerase gamma. *Biochem. Pharm.* **1995**, *50*, 1043-1051.

12.   Verri, A.; Montecucco, A.; Gosselin, G.; Boudou, V.; Imbach, J. L.; Spadari, S.; Focher, F. L-ATP is recognized by some cellular and viral enzymes: does chance drive enzymic enantioselectivity? *Biochem. J.* **1999**, *337 (Pt 3)*, 585-590.

13.   Focher, F.; Spadari, S.; Maga, G. Antivirals at the mirror: the lack of stereospecificity of some viral and human enzymes offers novel opportunities in antiviral drug development. *Curr. Drug Targets Infect. Disord.* **2003**, *3*, 41-53.

14.   Ishikawa, H. Mizoribine and mycophenolate mofetil. *Curr. Med. Chem.* **1999**, *6*, 575-597.

15.   Kusumi, T.; Tsuda, M.; Katsunuma, T.; Yamamura, M. Dual inhibitory effect of bredinin. *Cell Biochem. Fun.* **1989**, *7*, 201-204.

16.   Christopherson, R. I.; Lyons, S. D.; Wilson, P. K. Inhibitors of de novo nucleotide biosynthesis as drugs. *Acc. Chem. Res.* **2002**, *35*, 961-971.

17.   Spector, T. Studies with GMP synthetase from Ehrlich ascites cells. Purification, properties, and interactions with nucleotide analogs. *J. Biol. Chem.* **1975**, *250*, 7372-7376.

18.   Salaski, E. J.; Maag, H. GMP Synthetase: Synthesis and Biological Evaluation of a Stable Analog of the Proposed AMP-XMP Reaction Intermediate. *Synlett* **1999**, *1999*, 897-900.

19.   Forsman, J. J.; Warna, J.; Murzin, D. Y.; Leino, R. Reaction kinetics and mechanism of acid-catalyzed anomerization of 1-O-acetyl-2,3,5-tri-O-benzoyl-L-ribofuranose. *Carbohydr. Res.* **2009**, *344*, 1102-1109.

20.   Sakamoto, N. GMP synthetase (Escherichia coli). *Methods Enzymol.* **1978**, *51*, 213-218.

21.   Abbott, J. L.; Newell, J. M.; Lightcap, C. M.; Olanich, M. E.; Loughlin, D. T.; Weller, M. A.; Lam, G.; Pollack, S.; Patton, W. A. The effects of removing the GAT domain from E. coli GMP synthetase. *Protein J.* **2006**, *25*, 483-491.

22.   Bhat, J. Y.; Shastri, B. G.; Balaram, H. Kinetic and biochemical characterization of Plasmodium falciparum GMP synthetase. *Biochem. J.* **2008**, *409*, 263-273.

23.   Spector, T.; Jones, T. E.; Krenitsky, T. A.; Harvey, R. J. Guanosine monophosphate synthetase from Ehrlich ascites cells. Multiple inhibition by pyrophosphate and nucleosides. *Biochim. Biophys. Acta Enzymol.* **1976**, *452*, 597-607.

Appendix B

EPI-001 is a Thiol Reactive Inhibitor of Androgen Sensitive and Castration Resistant Prostate Cancer

In this work, M.E.O developed an HPLC assay and then utilized it to characterize EPI-001:thiol reactivity *in vitro*.

B.1 Overview

Prostate cancer is the most commonly diagnosed cancer in men in the United States with 220,800 new cases predicted for 2015, a number that accounts for 26% of all newly diagnosed cancers in men.[1] Moreover, prostate cancer is the second leading cause of cancer death in US men, with 27,540 deaths predicted for 2015.[1] Current treatments for prostate cancer rely on the inhibition of androgen receptor (AR) activation.[2] The AR is a steroid hormone receptor and transcription factor that functions to promote cell proliferation and survival of both normal and cancerous prostate tissues.[3,4] Moreover, the AR is required for prostate cancer disease progression. Therapies aimed at inhibiting AR activation block androgen production or the binding of stimulatory androgens to the AR. However, the current arsenal of prostate cancer therapies inevitably fails as a result of therapeutic resistance.[5] The foremost mechanism of drug resistance development is mutation to or deletion of the ligand binding domain (LBD) in the AR. Importantly, castration resistance prostate cancers remain dependent on AR signaling, as treatment with second generation androgen deprivation therapies, enzalutamide[6-8] and abiraterone,[9] increase the overall survival of patients. However, resistance to these therapies frequently occurs as a result of AR reactivation mechanisms.[10-14] As a result, there is a grave need to discover therapeutics that inhibit AR through non-LBD surfaces and maintain inhibition in castration resistant prostate cancers.[15-17]

EPI-001 (**B.1**), a bisphenol A diglycidyl ether analogue, was identified as a covalent inhibitor of the AR NH_2-terminal domain (NTD), although the exact binding site in this intrinsically unstructured domain was not elucidated (Figure

B.1).[18,19] EPI-001 (**B.1**) inhibited both androgen sensitive and castration resistant prostate cancers *in vitro* and *in vivo*.[18,19] In this work, the mechanism by which EPI-001 (**B.1**) inhibits the AR NTD and prostate cancer growth was interrogated.
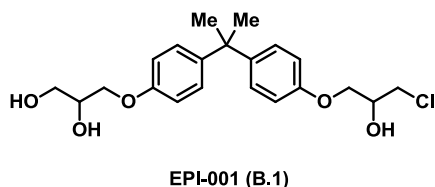
EPI-001 (B.1)

Figure B.1. Chemical Structure of EPI-001 (**B.1**).

B.2 EPI-001 (B.1) Exhibits Multilevel Inhibitory Effects on AR in Prostate Cancer

Transcriptional Activation Units 1 and 5 (TAU1, TAU5) in the NTD are responsible for AR-mediated transcription.[20,21] This is an important detail because constitutively active AR splice variant proteins in castration resistant prostate cancer contain the AR NTD and central DNA binding domain (DBD), but lack the LBD.[16,17] As EPI-001 (**B.1**) was shown to inhibit the AR NTD in previous reports, the effect of EPI-001 on the individual AR TAUs was interrogated by the Dehm laboratory at the University of Minnesota. AR transcriptional activity was measured using an AR[Gal4] hybrid where the AR DBD was replaced with the yeast Gal4 DBD. In all cell lines tested, EPI-001 (**B.1**) inhibited the transcriptional activity of the AR NTD-Gal4 hybrid. In 293T fibroblasts, EPI-001 (**B.1**) potently inhibited both of the individual Gal4-TAU constructs (TAU1 and TAU5). These data demonstrated that inhibition by EPI-001 (**B.1**) was not specific to a discrete AR TAU, and indicated two possible scenarios: 1. EPI-001 binds and inhibits both AR TAUs, or 2. EPI-001 has a cellular target that affects the transcriptional activities of TAU1 and TAU5.

230

It was also observed that treatment of prostate cancer cell lines with EPI-001 (**B.1**) consistently reduced AR mRNA and protein expression levels. This reduction was independent of the proteasome and did not result from decreased mRNA stability. As a result, EPI-001 (**B.1**) is hypothesized to inhibit transcription of the AR gene. Moreover, reduced AR expression correlated with retarded cell growth in both androgen sensitive and castration resistance prostate cancer cell lines. Taken together, inhibition of AR expression is likely an important mechanism of EPI-001 (**B.1**)-mediated prostate cancer inhibition, highlighting the fact that EPI-001 has a second cellular target, in addition to the AR NTD.

Interestingly, bisphenol A diglycidyl ether (BADGE, **B.2**), a structural analogue of EPI-001 (**B.2**), has been previously reported as a selective inhibitor of peroxisome proliferator-activated receptor-gamma (PPARγ).[22-24] PPARγ also plays an important role in prostate development and maintenance,[25] and importantly, agonists of PPARγ, such as troglitazone, inhibit AR synthesis and prostate cancer proliferation *in vitro* and *in vivo.*[26-28] When evaluated for PPARγ modulation, EPI-001 (**B.1**) demonstrated cell line dependent PPARγ agonism/antagonism and a dose-dependent reduction in AR protein expression, respectively similar to the positive controls troglitazone and BADGE (**B.2**). Finally, knockdown studies of PPARγ demonstrated that EPI-001 (**B.1**)-mediated inhibition of AR transcriptional activity is dependent on PPARγ expression.
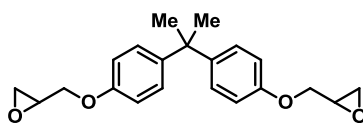
BADGE (B.2)

Figure B.2. Chemical Structure of BADGE (**B.2**).

B.3 EPI-001 Forms Covalent Adducts with Thiols *In Vitro*

The *in vitro* experiments discussed above suggest that the effects of EPI-001 (**B.1**) on the AR and PPARγ pathways are complex and multileveled. The inherent reactivity of this small molecule likely results from its electrophilic nature. Chlorohydrins, such as the moiety in EPI-001 (**B.1**), have been previously demonstrated to interconvert to electrophilic epoxides in aqueous solution.[29] The related analogue BADGE (**B.2**), which contains two such epoxides, has been shown to readily undergo nucleophilic attack in solution.[30] Moreover, BADGE (**B.2**) has been characterized as an endocrine system toxin, highlighting its reactivity in biological systems.[31,32]

B.3A Development of an HPLC Assay

EPI-001 was incubated in aq. PBS / DMSO (10:1) at 37 $^{\circ}$C and analyzed for the percent EPI-001 remaining at 30 min and 12 h (Scheme B.1). Percent remaining was quantified using a previously prepared calibration curve. Specifically, known concentrations of an external standard and EPI-001 were mixed to measure their relative ratios at 254 nm. Rose bengal (RB) was used as the external standard in these assays. In stability experiments, the ratio of EPI-

001 to RB over time was used to quantify the amount of EPI-001 remaining in the

aq. solution.

Scheme B.1. HPLC Assay for EPI-001 Stability. Conditions: EPI-001 was shaken at 37 $^{\circ}$C in aq. PBS / DMSO (~10:1) at pH = 2.4, 7.4, and 9.4. The reactions were analyzed by reverse-phase HPLC at t ~30 min and t = 12 h for the appearance of epoxide. The percent EPI-001 remaining at these time points was quantified.

This assay was also applied to the gauge the reactivity of EPI-001 (**B.1**) with thiols *in vitro.* In these experiments, one of the following thiols: reduced L-glutathione, 2-mercaptoethanol, or cysteamine, was incubated in aq. PBS under reducing conditions (TCEP·HCl), and the solution was adjusted to the desired pH (2.4, 7.4, or 9.4). EPI-001 (**B.1**) or **B.3** were added and aliquots of the reaction were analyzed immediately (t ~30 min) and at 12 h. Percent EPI-001 remaining in the presence of a nucleophilic thiol was quantified as described above. Multiple pH's were interrogated to determine the effect of the environment on EPI-001's reactivity.

B.3B Stability and Reactivity Studies of EPI-001 (B.1) and B.3

Reverse phase HPLC was employed to probe whether EPI-001 (**B.1**) could interconvert to a BADGE-like mono-epoxide (**B.3**) in aqueous solution. EPI-001 (**B.1**) was incubated under acidic, neutral, and basic conditions, and after 12 hours, the epoxide was observed at neutral and basic pH (Figure B.3B). Percent EPI-001 (**B.1**) remaining was measured by comparing the ratio of the area under

233

the curve (AUC) of EPI-001 over internal standard at 30 min to the ratio at 12 h. After 12 hours, 91% and 87% EPI-001 (**B.1**) remained at pH 7.4 and 9.4, respectively. The identity of the mono-epoxide (**B.3**) was confirmed by co-injection with commercial **B.3** and LCMS analysis (Figure B.3C).
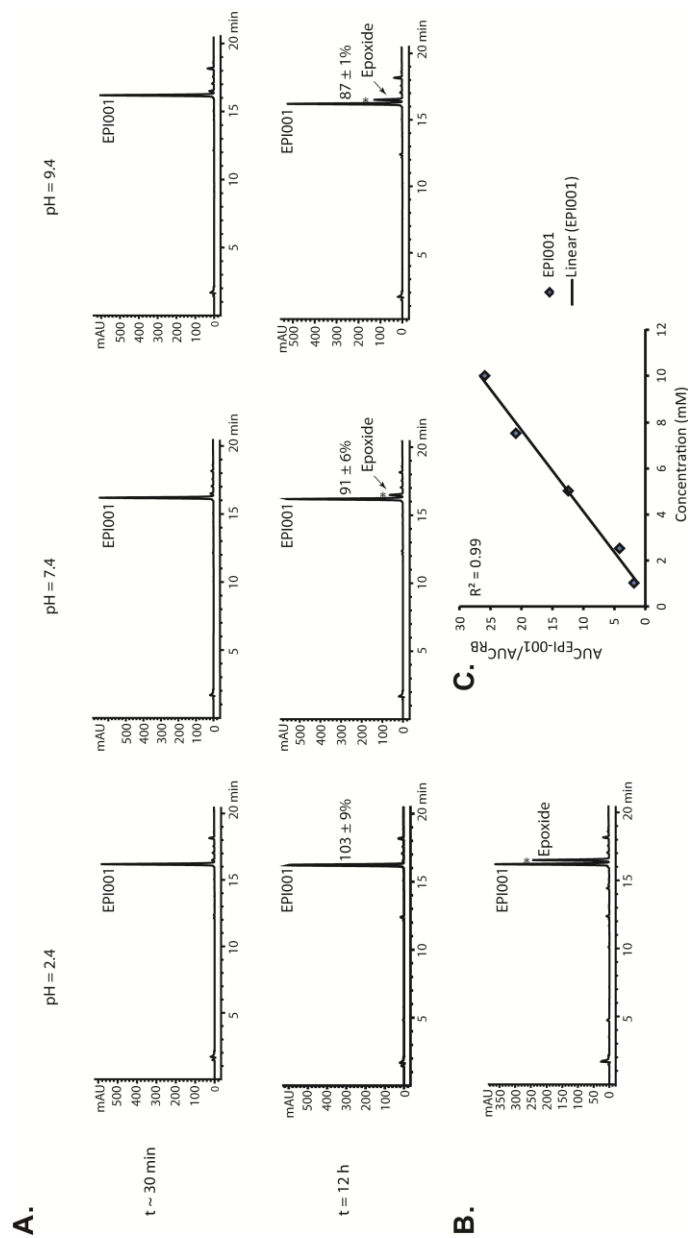
Figure B.3. EPI-001 Stability in Aqueous Solution. (A) At t ~ 30 min, > 99% EPI-001 remains under acid, neutral and basic environments (top). At t = 12 h, the generation of epoxide was observed at pH = 7.4 and pH = 9.4. The reaction mixtures were analyzed by LCMS confirming the presence of epoxide; *m/z* [M+H$^+$] 359.2 (calc'd); 359.0 (found). (B) A solution of EPI-001 in aq. PBS / DMSO incubated for 12 h at pH = 9.4 was spiked with 12 μL of 8.5 mM epoxide in DMSO. The co-injection of this compound standard brought about a doubling of the epoxide peak. (C) A calibration curve was generated to normalize for injection variances during HPLC analysis.

235

EPI-001 (**B.2**) has been hypothesized to inhibit the AR NTD through covalent modification of an unknown binding site.[19] Analogous to the reactivity of BADGE, it was posited that EPI-001 (**B.2**) reacts with an essential nucleophilic side chain in the NTD.[19] A previous study interrogated whether EPI-001 could react promiscuously with nucleophilic thiols *in vitro*, but found no evidence of non-specific reactivity.[19] Based on our observation that EPI-001 (**B.1**) can interconvert to **B.3** under strict pH control, we evaluated the reactivity of EPI-001 with glutathione, 2-mercaptoethanol, and cysteamine under these conditions. As expected, no EPI-001:thiol adducts were observed under acidic conditions (Figure B.4). This observation correlated with our previous study that found that EPI-001 mono-epoxide (**B.3**) was not generated at pH = 2.4. A trace amount of thiol adduct formation was observed between EPI-001 (**B.1**) and glutathione at pH = 7.4, and strikingly, nearly complete conversion to the thiol adduct was observed under basic conditions (Figure B.4, Compound **B.4**). Similarly, a trace amount of thiol adduct formation was observed between EPI-001 (**B.1**) and 2-mercaptoethanol at pH = 7.4, and complete conversion was observed at pH = 9.4 (Figure B.4, Compound **B.5**). No thiol adduct formation was observed between EPI-001 (**B.1**) and cysteamine at neutral pH, but like the other thiol nucleophiles, nearly full conversion to the EPI-001:cysteamine adduct was observed under basic conditions (Figure B.4, Compound **B.6**) In each experiment, the identity of the EPI-001:thiol adduct was confirmed by mass spectrometry (Figure B.5). HPLC chromatograms of the reactions at 30 min are also provided (Figure B.6). The reactivity of mono-epoxide **B.3** towards nucleophilic thiols glutathione, 2-mercaptoethanol, and cysteamine was also investigated. After 12 h, **B.3** had

236

reacted readily with each of the probed thiols, even under acidic conditions (Figure B.7). HPLC chromatograms of the reactions at 30 min are also provided (Figure B.8). Background HPLC chromatograms of the three nucleophilic thiols incubated for 12 h are depicted in Figure B.9.

Collectively, these *in vitro* studies convey that EPI-001 (**B.1**) can interconvert to the reactive mono-epoxide (**B.3**) at neutral and basic pH, and the mono-epoxide is readily alkylated by nucleophilic attack under aqueous conditions. These results suggest that EPI-001 is a general electrophile with the propensity to react with any number of cellular targets under local pH influence.
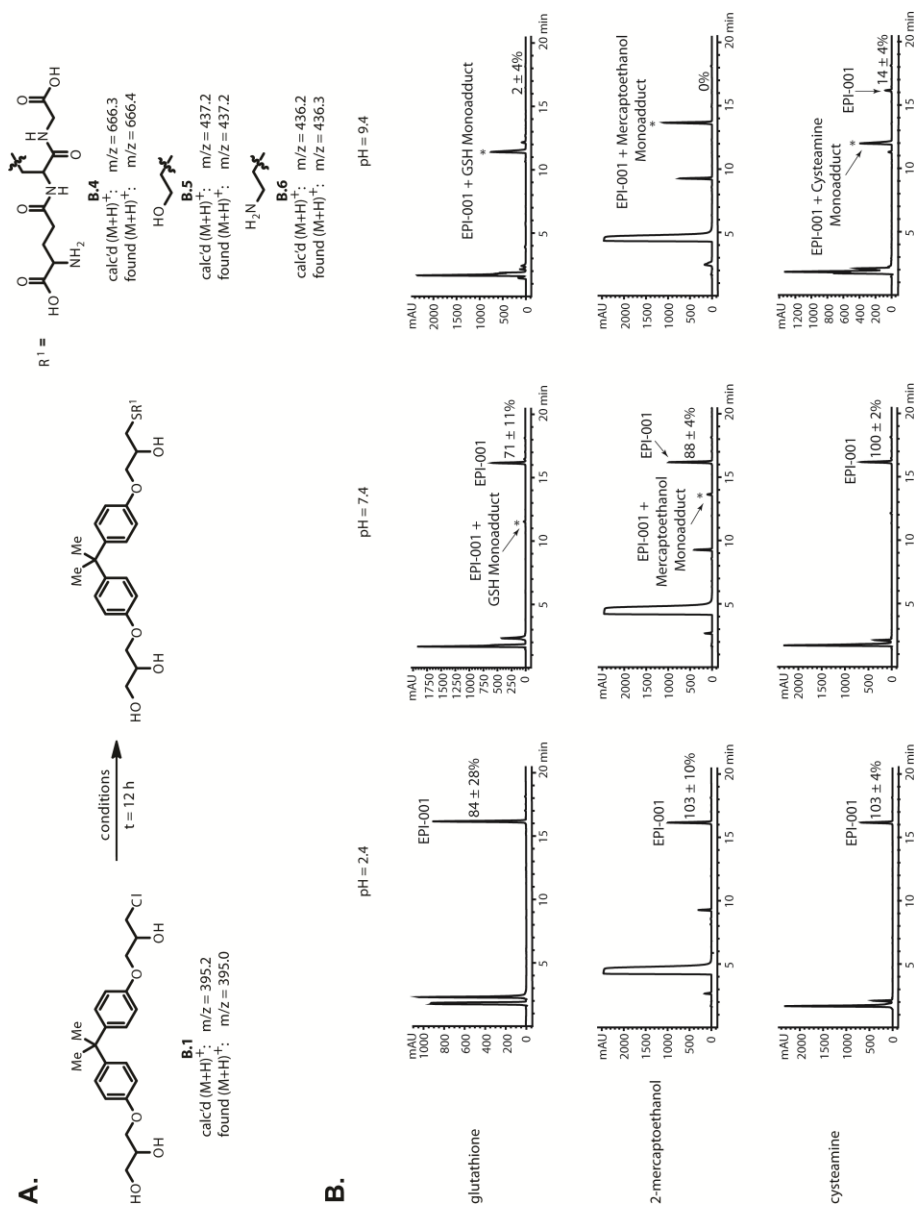
Figure B.4. Reactivity of EPI-001 with Thiols at t = 12 h. (**B.1**) with Biologically-Relevant Thiols (A) Solutions of EPI-001 and thiol in aq. PBS / DMSO (~10:1) at pH's 2.4, 7.4, and 9.4, respectively. (B) At 12 h, a GSH/EPI-001 monoadduct was observed at pH = 7.4 and pH = 9.4. A monoadduct of 2-mercaptoethanol and EPI-001 was similarly observed at pH = 7.4 and 9.4; while a cysteamine/EPI-001 monoadduct was observed only at pH = 9.4. New peaks in the course of the reaction are denoted by an asterisk. Experiments were performed in triplicate and values shown are the mean ± standard deviation. The reaction mixtures were also analyzed by LCMS confirming the presence of EPI-001 adducts.

238
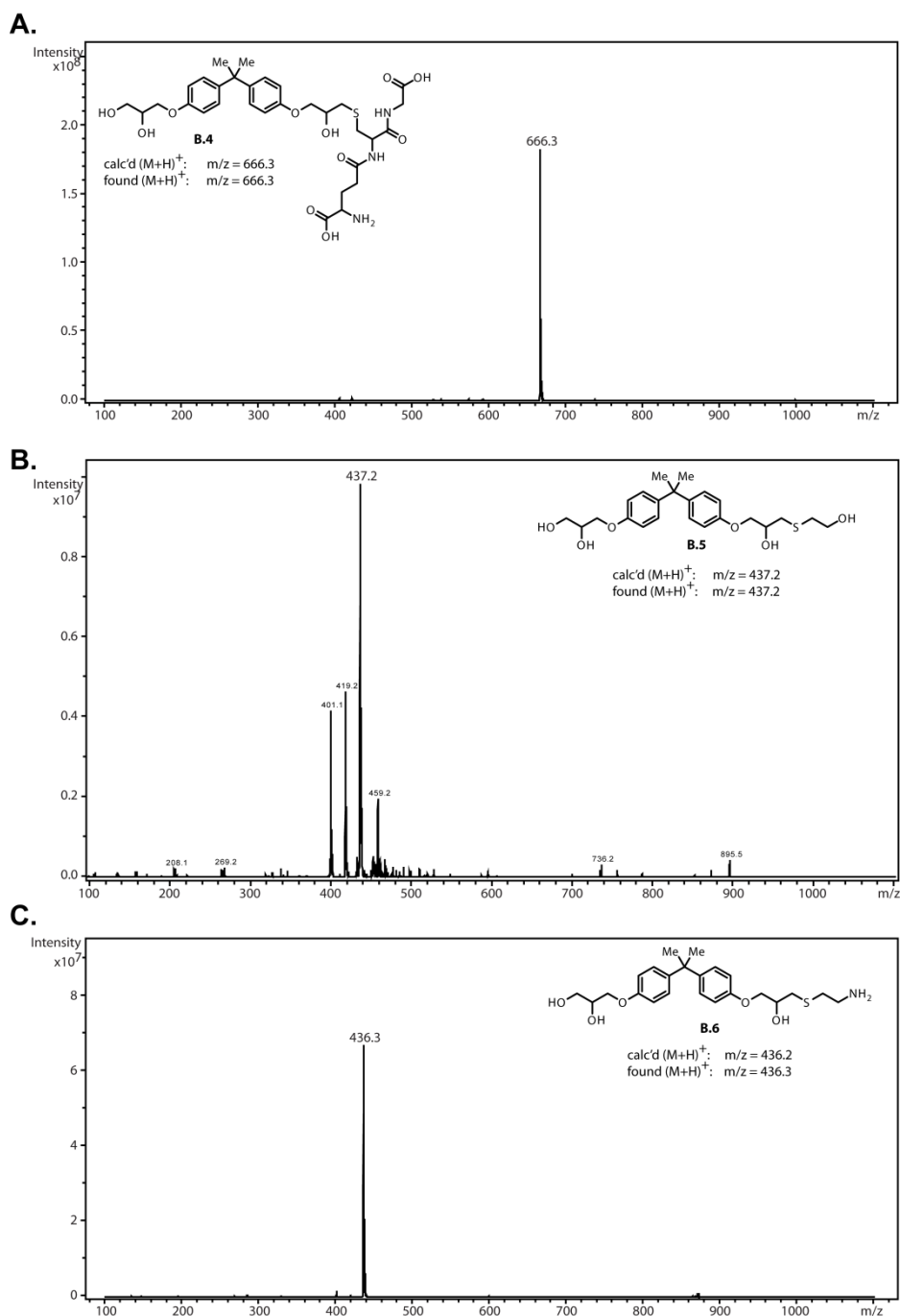
Figure B.5. Mass Chromatograms of EPI-001 (**B.1**) – Thiol Adducts (A) Mass spectrum of the monoadduct of GSH and EPI-001; *m/z* [M+H⁺] 666.3 (calc'd); 666.3 (found). (B) Mass spectrum of the monoadduct of 2-mercaptoethanol and EPI-001; *m/z* [M+H⁺] 437.2 (calc'd); 437.2 (found). (C) Mass spectrum of the monoadduct of cysteamine and EPI-001; *m/z* [M+H⁺] 436.2 (calc'd); 436.3 (found).

239
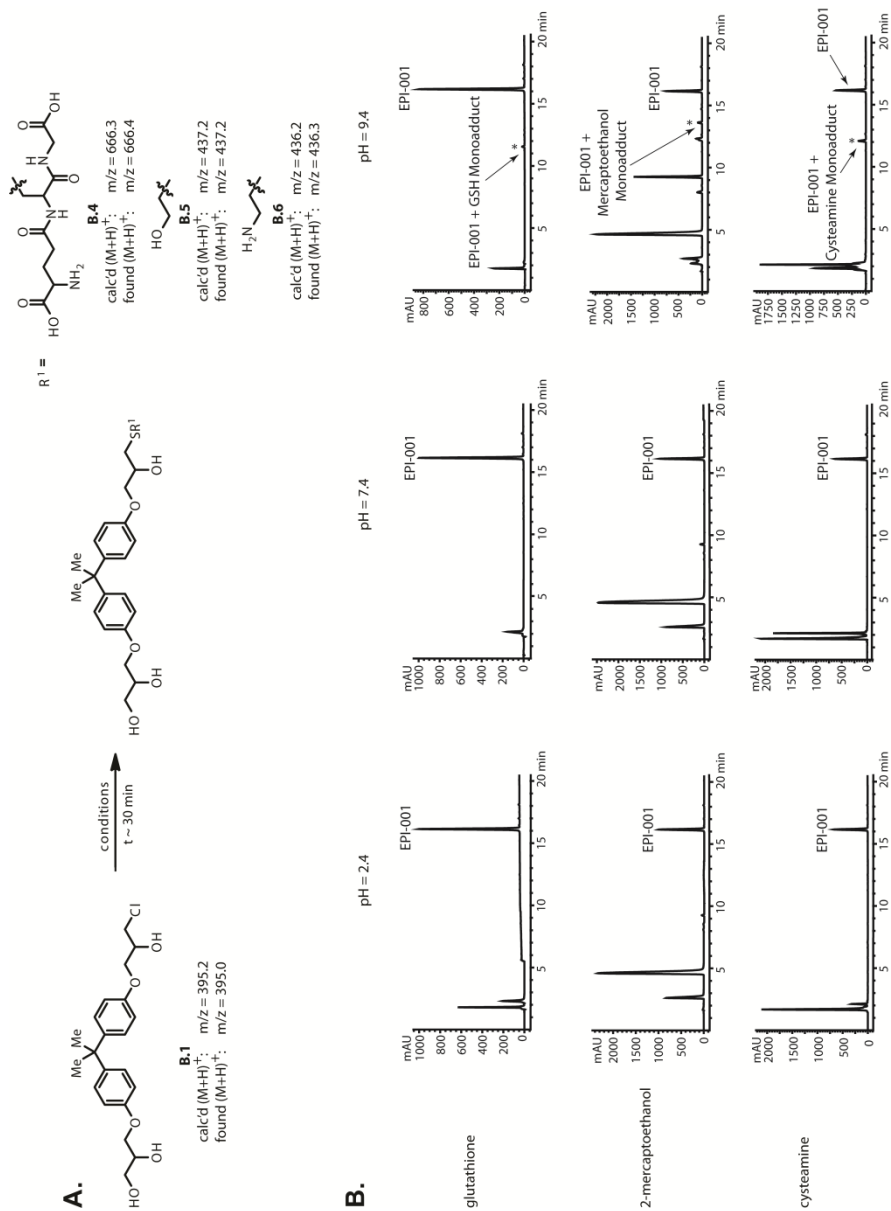
Figure B.6. Reactivity of EPI-001 towards Thiols at t ~ 30 min. (A) Solutions of EPI-001 and thiol in aq. PBS / DMSO (~10:1) at pH's 2.4, 7.4, and 9.4, respectively. (B) At t ~ 30 min, EPI-001 adducts were only observed under strongly basic conditions (pH=9.4). Under such conditions, EPI-001 exhibits reactivity with each of the three thiols. New peaks in the course of the reaction are denoted by an asterisk. Experiments were performed in triplicate, and the identities of the mono-adducts were confirmed by LCMS.

240

B.4 Conclusions

　　EPI-001 (**B.1**) was found to exhibit promiscuous biological effects in the context of prostate cancer. Specifically, EPI-001 (**B.1**) inhibited the transcriptional activity of AR TAU1 and TAU5, and reduced endogenous AR mRNA levels and AR protein expression. Moreover, EPI-001 (**B.1**) modulated peroxisome proliferator-activated receptor-gamma (PPARγ) activity. As a result, this study suggests that the AR NTD is unlikely to be the only biological target of EPI-001 (**B.1**). To explain this lack of specificity, *in vitro* thiol reactivity experiments demonstrated that EPI-001 (**B.1**) is modified by thiols under neutral and basic pH. Our findings suggest that EPI-001 (**B.1**) may alkylate any accessible nucleophilic residue within a suitably basic binding pocket. This study highlights the need to optimize the chemical structure of EPI-001 before undertaking expensive and resource-demanding preclinical development efforts.

B.5 Experimental

General. 2-Mercaptoethanol, cysteamine, and rose bengal were purchased from Sigma-Aldrich, and reduced glutathione and tris(2-carboxyethyl)phosphine hydrochloride salt (TCEP·HCl) were purchased from Alfa Aesar. All chemicals were used without additional purification.

Thiol Reactivity Assay:[33] A solution of thiol (10 equiv.) and TCEP·HCl (100 µL of a 0.5 M DMSO stock soln.) in 1x aqueous PBS (5 mL) was adjusted to the desired pH (2.4, 7.4, or 9.4) using either aqueous HCl (6 M) or NaOH (6 M) as determined by a pH meter (Thermo Scientific Orion 3 Star). Reduced L-

glutathione, 2-mercaptoethanol, and cysteamine, were used as thiols in this assay. To a solution of the appropriate thiol (170 μL) was added either EPI-001 (**B.1**) or **B.3** (1 equiv.; both compounds were solubilized as 50 mM DMSO stock solutions). The total composition of DMSO did not exceed 7.5% in any experiment and the ratio of thiol to EPI-001 (**B.1**)/**B.3** was 10:1. *Note: This order of addition is key to achieving the appropriate pH environment for the reaction as the addition of reduced L-glutathione and TCEP acidify neutral solutions and cysteamine basifies neutral solutions.* Aliquots of reactions were analyzed immediately (t ~30 min) following initial mixing by reverse phase HPLC and LCMS. Reactions were gently shaken at 37 ^{o}C for 12 h, then analyzed again using HPLC and LCMS. Reactions were conducted in 2 mL clear screw cap glass vials (Agilent Technologies). *Note: Thirty minutes was the earliest time point that could be collected after adding EPI-001, mixing, and injecting an aliquot onto the HPLC.* The HPLC analytical method (Zorbax SB-C18 4.6 x 150 mm, 3.5 μm column, Agilent Technologies; flow rate = 1.0 mL/min) involved isocratic 10% CH_3CN in 0.1% (v/v) aqueous CF_3CO_2H (0 to 2 min), followed by linear gradients of 10-85% CH_3CN (2-24 min) and 85%-95% CH_3CN (24-26 min). LCMS analyses were performed on an Agilent 1100 series instrument equipped with an Agilent MSD SL Ion Trap mass spectrometer (positive-ion mode) and a Zorbax SB-C18 column (0.5 x 150 mm, 5 μm, Agilent Technologies). The analysis method (15 μL/min flow rate) involved isocratic 10% MeCN (containing 0.1% TFA) in ddH$_2$O (containing 0.1% HCO$_2$H; 0 to 2 mins) followed by a linear gradient of 10% to 90% MeCN (containing 0.1% TFA) in ddH$_2$O (containing 0.1% HCO$_2$H; 2 to 24 mins), and isocratic 90% MeCN (containing 0.1% TFA) in ddH$_2$O (containing 0.1% HCO$_2$H; 24-26 mins). The column was heated to 40 ^{o}C.

Wavelength monitored = 254 nm for all experiments unless otherwise noted. LCMS analysis was performed on crude reaction mixtures. To account for injection variances, the area under the curve (AUC) of the parent compound was divided by the AUC of an internal standard. Dividing this ratio at t = 12 h by the ratio at t ~ 30 min gave percent parent remaining. Rose bengal (7.5 μM) was used as the internal standard and was added immediately before HPLC analysis Experiments were performed in triplicate and values shown are the mean ± standard deviation (calculated in Microsoft Excel).

B.6 HPLC Chromatograms of B.3 Thiol Reactivity.

Figure B.7. Reactivity of **B.3** with Biologically-Relevant Thiols at t ~30 min. (A) Solutions of **B.3** and thiol in aq. PBS / DMSO (~10:1) at pH's 2.4, 7.4, and 9.4, respectively. (B) At t ~ 30 min, a GSH/**B.3** mono-adduct was observed only under basic conditions (pH = 9.4). A 2-mercaptoethanol/**B.3** mono-adduct was observed at pH = 7.4, and at pH = 9.4, **B.3** was completely consumed by 2-mercaptoethanol. At 30 min, no cysteamine:**B.3** adducts were observed. New peaks appearing in the course of the reaction are denoted by an asterisk.
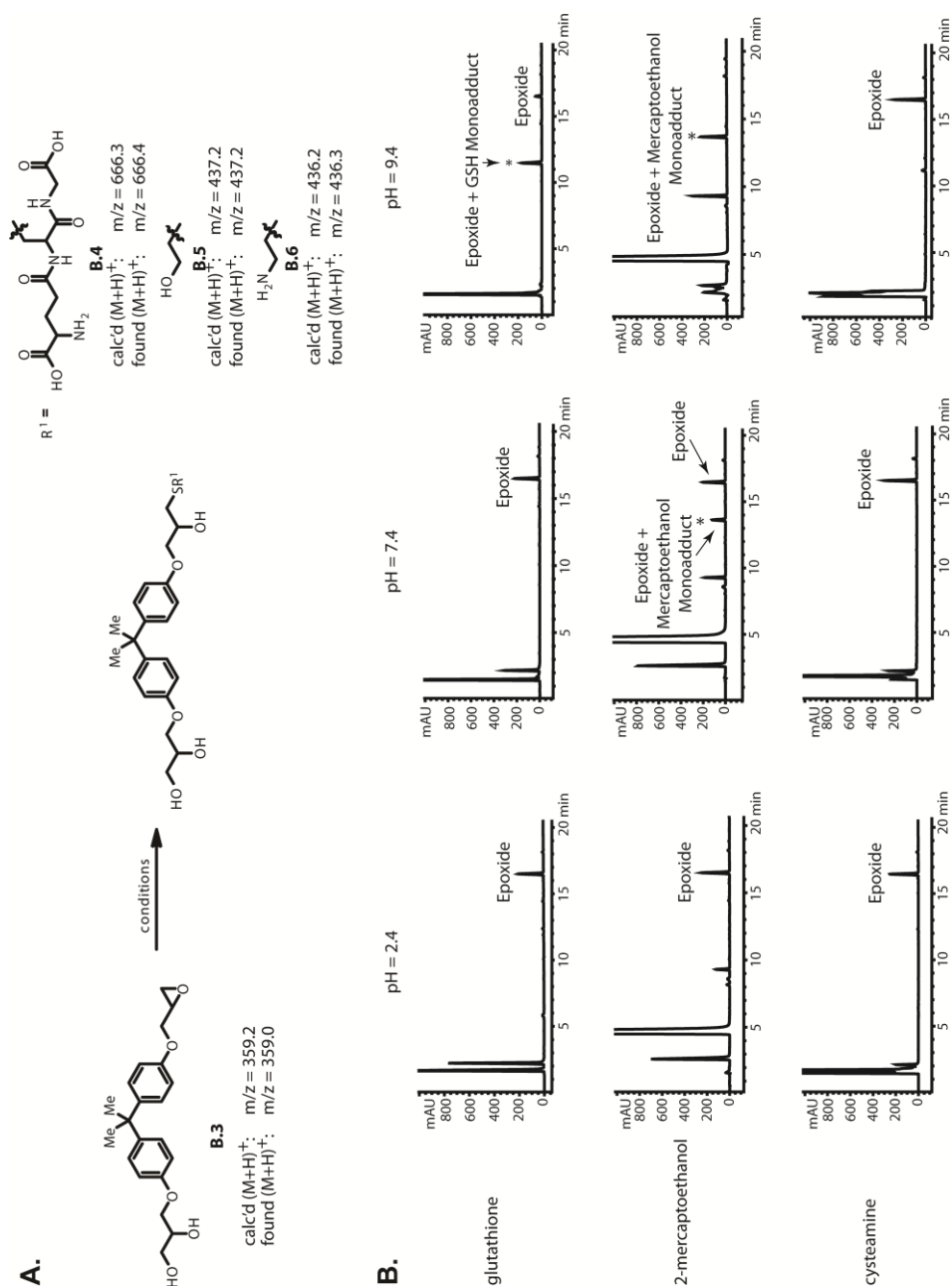
244
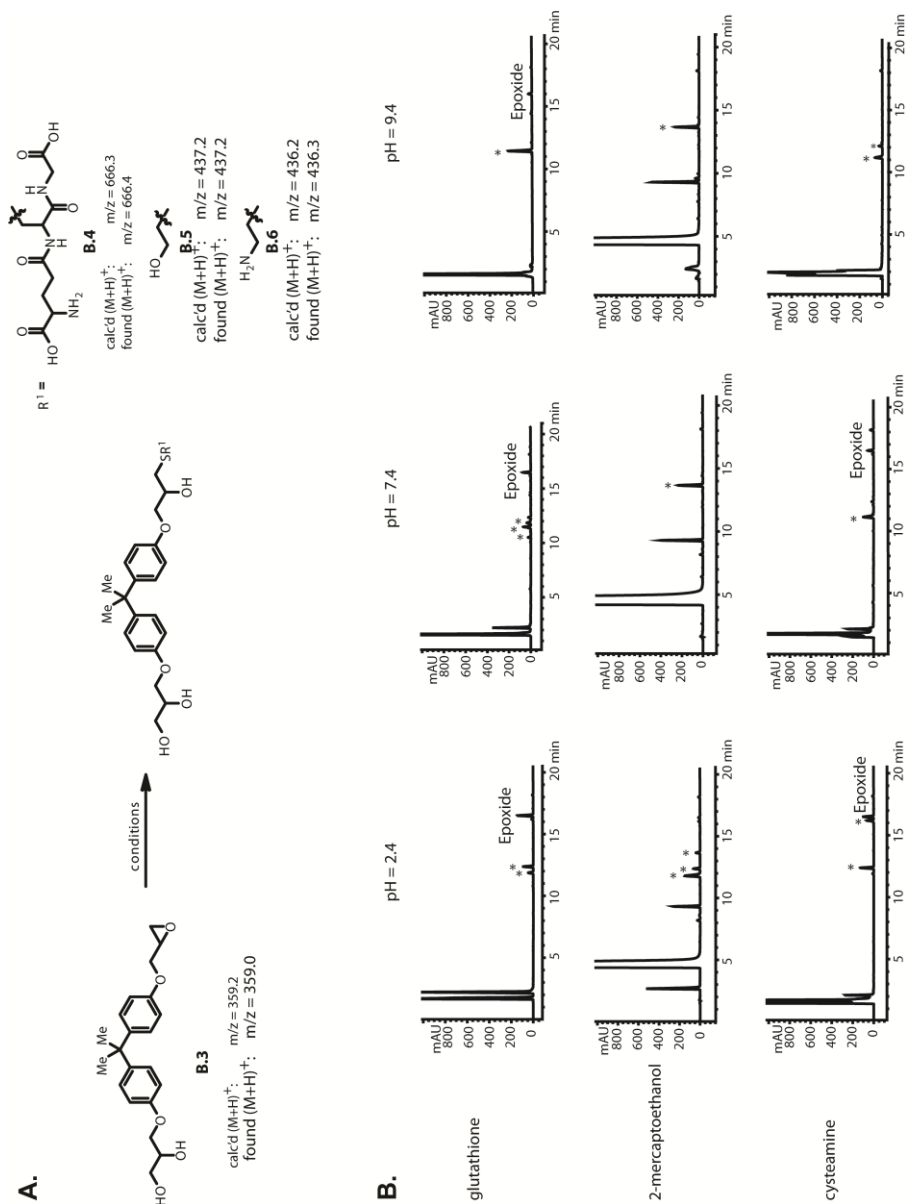
Figure B.8. Reactivity of **B.3** with Biologically-Relevant Thiols at t = 12 h. (A) Solutions of **B.3** and thiol in aq. PBS / DMSO (~10:1) at pH's 2.4, 7.4, and 9.4, respectively. (C) At t = 12 h, the enhanced reactivity of **B.3** under all conditions (acidic, neutral, basic) is clearly evident. A multitude of new peaks (many are thiol adducts) were observed and are denoted by asterisks.

B.7 Control HPLC Chromatograms of Thiol Background

Figure B.9. Control HPLC Chromatograms of Thiol Background. (A) Solutions of the three thiols (GSH, 2-mercaptoethanol, cysteamine) in aq. PBS / DMSO (~10:1) at pH's 2.4, 7.4, and 9.4, respectively. The reactions were analyzed by HPLC at t ~30 min and t = 12 h to accomplish background traces. The traces at t = 12 h are shown.

B.8 Acknowledgements

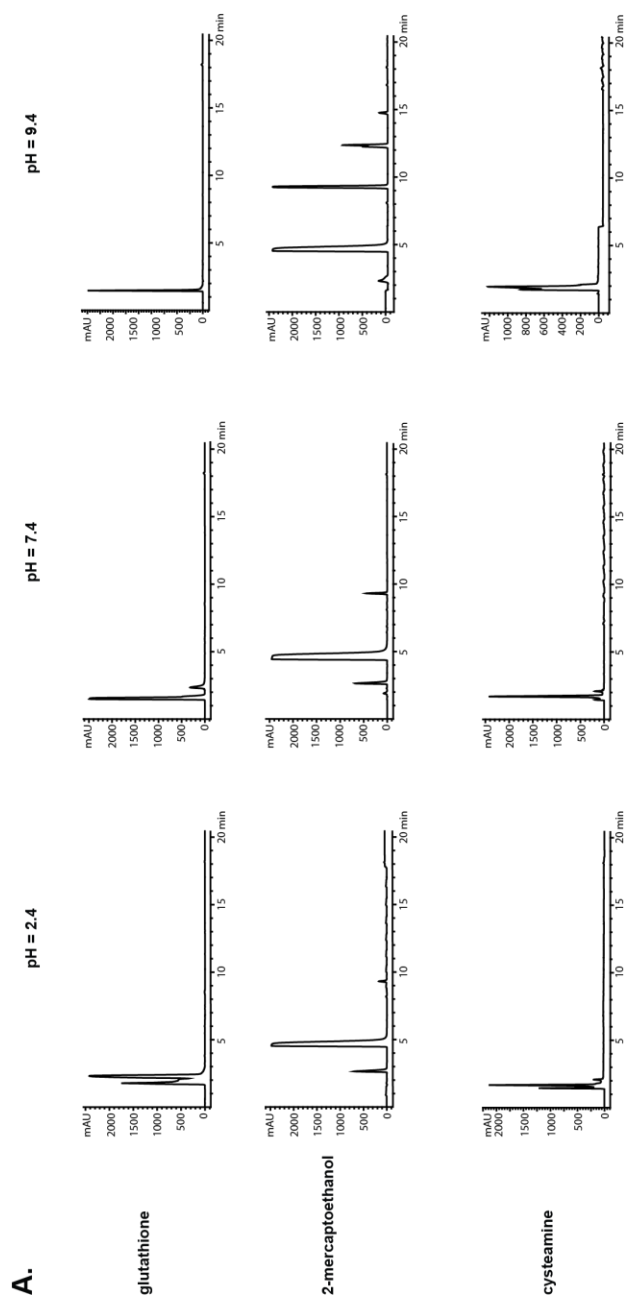**B.9 References**

1.   Siegel, R. L.; Miller, K. D.; Jemal, A. Cancer statistics, 2015. *CA Cancer J. Clin.* **2015**, *65*, 5-29.

2.   Helsen, C.; Van den Broeck, T.; Voet, A.; Prekovic, S.; Van Poppel, H.; Joniau, S.; Claessens, F. Androgen receptor antagonists for prostate cancer therapy. *Endocr. Relat. Cancer* **2014**, *21*, T105-118.

3.   Barfeld, S. J.; Itkonen, H. M.; Urbanucci, A.; Mills, I. G. Androgen-regulated metabolism and biosynthesis in prostate cancer. *Endocr. Relat. Cancer* **2014**, *21*, T57-66.

4.   Culig, Z.; Santer, F. R. Androgen receptor signaling in prostate cancer. *Cancer Metastasis Rev.* **2014**, *33*, 413-427.

5.   Petrylak, D. P. Current state of castration-resistant prostate cancer. *Am. J. Manag. Care* **2013**, *19*, s358-365.

6.   Scher, H. I.; Fizazi, K.; Saad, F.; Taplin, M. E.; Sternberg, C. N.; Miller, K.; de Wit, R.; Mulders, P.; Chi, K. N.; Shore, N. D.; Armstrong, A. J.; Flaig, T. W.; Flechon, A.; Mainwaring, P.; Fleming, M.; Hainsworth, J. D.; Hirmand, M.; Selby, B.; Seely, L.; de Bono, J. S. Increased survival with enzalutamide in prostate cancer after chemotherapy. *N. Engl. J. Med.* **2012**, *367*, 1187-1197.

7.   Sternberg, C. N.; de Bono, J. S.; Chi, K. N.; Fizazi, K.; Mulders, P.; Cerbone, L.; Hirmand, M.; Forer, D.; Scher, H. I. Improved outcomes in elderly patients with metastatic castration-resistant prostate cancer treated with the androgen receptor inhibitor enzalutamide: results from the phase III AFFIRM trial. *Ann. Oncol.* **2014**, *25*, 429-434.

8.   Beer, T. M.; Armstrong, A. J.; Rathkopf, D. E.; Loriot, Y.; Sternberg, C. N.; Higano, C. S.; Iversen, P.; Bhattacharya, S.; Carles, J.; Chowdhury, S.; Davis, I. D.; de Bono, J. S.; Evans, C. P.; Fizazi, K.; Joshua, A. M.; Kim, C. S.; Kimura, G.; Mainwaring, P.; Mansbach, H.; Miller, K.; Noonberg, S. B.; Perabo, F.; Phung, D.; Saad, F.; Scher, H. I.; Taplin, M. E.; Venner, P. M.; Tombal, B. Enzalutamide in metastatic prostate cancer before chemotherapy. *N. Engl. J. Med.* **2014**, *371*, 424-433.

9.   Ryan, C. J.; Smith, M. R.; de Bono, J. S.; Molina, A.; Logothetis, C. J.; de Souza, P.; Fizazi, K.; Mainwaring, P.; Piulats, J. M.; Ng, S.; Carles, J.; Mulders, P. F.; Basch, E.; Small, E. J.; Saad, F.; Schrijvers, D.; Van Poppel, H.; Mukherjee, S. D.; Suttmann, H.; Gerritsen, W. R.; Flaig, T. W.; George, D. J.; Yu, E. Y.; Efstathiou, E.; Pantuck, A.; Winquist, E.; Higano, C. S.; Taplin, M. E.; Park, Y.; Kheoh, T.; Griffin, T.; Scher, H. I.; Rathkopf, D. E. Abiraterone in metastatic prostate cancer without previous chemotherapy. *N. Engl. J. Med.* **2013**, *368*, 138-148.

10.   Arora, V. K.; Schenkein, E.; Murali, R.; Subudhi, S. K.; Wongvipat, J.; Balbas, M. D.; Shah, N.; Cai, L.; Efstathiou, E.; Logothetis, C.; Zheng, D.; Sawyers, C. L. Glucocorticoid receptor confers resistance to antiandrogens by bypassing androgen receptor blockade. *Cell* **2013**, *155*, 1309-1322.

11.   Chang, K. H.; Li, R.; Kuri, B.; Lotan, Y.; Roehrborn, C. G.; Liu, J.; Vessella, R.; Nelson, P. S.; Kapur, P.; Guo, X.; Mirzaei, H.; Auchus, R. J.; Sharifi, N. A gain-of-function mutation in DHT synthesis in castration-resistant prostate cancer. *Cell* **2013**, *154*, 1074-1084.

12.   Li, Y.; Chan, S. C.; Brand, L. J.; Hwang, T. H.; Silverstein, K. A.; Dehm, S. M. Androgen receptor splice variants mediate enzalutamide resistance in castration-resistant prostate cancer cell lines. *Cancer Res.* **2013**, *73*, 483-489.

13.   Mostaghel, E. A.; Marck, B. T.; Plymate, S. R.; Vessella, R. L.; Balk, S.; Matsumoto, A. M.; Nelson, P. S.; Montgomery, R. B. Resistance to CYP17A1 inhibition with abiraterone in castration-resistant prostate cancer: induction of steroidogenesis and androgen receptor splice variants. *Clin. Cancer Res.* **2011**, *17*, 5913-5925.

14.   Nyquist, M. D.; Li, Y.; Hwang, T. H.; Manlove, L. S.; Vessella, R. L.; Silverstein, K. A.; Voytas, D. F.; Dehm, S. M. TALEN-engineered AR gene rearrangements reveal endocrine uncoupling of androgen receptor in prostate cancer. *Proc. Natl. Acad. Sci. U. S. A.* **2013**, *110*, 17492-17497.

15.   Mateo, J.; Smith, A.; Ong, M.; de Bono, J. S. Novel drugs targeting the androgen receptor pathway in prostate cancer. *Cancer Metastasis Rev.* **2014**, *33*, 567-579.

16.   Brand, L. J.; Dehm, S. M. Androgen receptor gene rearrangements: new perspectives on prostate cancer progression. *Curr. Drug Targets* **2013**, *14*, 441-449.

17.   Nyquist, M. D.; Dehm, S. M. Interplay between genomic alterations and androgen receptor signaling during prostate cancer development and progression. *Horm. Cancer* **2013**, *4*, 61-69.

18.   Andersen, R. J.; Mawji, N. R.; Wang, J.; Wang, G.; Haile, S.; Myung, J. K.; Watt, K.; Tam, T.; Yang, Y. C.; Banuelos, C. A.; Williams, D. E.; McEwan, I. J.; Wang, Y.; Sadar, M. D. Regression of castrate-recurrent prostate cancer by a small-molecule inhibitor of the amino-terminus domain of the androgen receptor. *Cancer cell* **2010**, *17*, 535-546.

19.   Myung, J. K.; Banuelos, C. A.; Fernandez, J. G.; Mawji, N. R.; Wang, J.; Tien, A. H.; Yang, Y. C.; Tavakoli, I.; Haile, S.; Watt, K.; McEwan, I. J.; Plymate, S.; Andersen, R. J.; Sadar, M. D. An androgen receptor N-terminal domain antagonist for treating prostate cancer. *J. Clin. Invest.* **2013**, *123*, 2948-2960.

20.   Dehm, S. M.; Tindall, D. J. Androgen receptor structural and functional elements: role and regulation in prostate cancer. *Mol. Endocrinol.* **2007**, *21*, 2855-2863.

21.   Claessens, F.; Denayer, S.; Van Tilborgh, N.; Kerkhofs, S.; Helsen, C.; Haelens, A. Diverse roles of androgen receptor (AR) domains in AR-mediated signaling. *Nucl. Recept. Signal.* **2008**, *6*, e008.

22.   Wright, H. M.; Clish, C. B.; Mikami, T.; Hauser, S.; Yanagi, K.; Hiramatsu, R.; Serhan, C. N.; Spiegelman, B. M. A synthetic antagonist for the peroxisome proliferator-activated receptor gamma inhibits adipocyte differentiation. *J. Biol. Chem.* **2000**, *275*, 1873-1877.

23.   Nakamuta, M.; Enjoji, M.; Uchimura, K.; Ohta, S.; Sugimoto, R.; Kotoh, K.; Kato, M.; Irie, T.; Muta, T.; Nawata, H. Bisphenol a diglycidyl ether (BADGE) suppresses tumor necrosis factor-alpha production as a PPARgamma

agonist in the murine macrophage-like cell line, RAW 264.7. *Cell Biol. Int.* **2002**, *26*, 235-241.

24.   Dworzanski, T.; Celinski, K.; Korolczuk, A.; Slomka, M.; Radej, S.; Czechowska, G.; Madro, A.; Cichoz-Lach, H. Influence of the peroxisome proliferator-activated receptor gamma (PPAR-gamma) agonist, rosiglitazone and antagonist, biphenol-A-diglicydyl ether (BADGE) on the course of inflammation in the experimental model of colitis in rats. *J. Physiol. Pharmacol.* **2010**, *61*, 683-693.

25.   Strand, D. W.; Jiang, M.; Murphy, T. A.; Yi, Y.; Konvinse, K. C.; Franco, O. E.; Wang, Y.; Young, J. D.; Hayward, S. W. PPARgamma isoforms differentially regulate metabolic networks to mediate mouse prostatic epithelial differentiation. *Cell Death Dis.* **2012**, *3*, e361.

26.   Kubota, T.; Koshizuka, K.; Williamson, E. A.; Asou, H.; Said, J. W.; Holden, S.; Miyoshi, I.; Koeffler, H. P. Ligand for peroxisome proliferator-activated receptor gamma (troglitazone) has potent antitumor effect against human prostate cancer both in vitro and in vivo. *Cancer Res.* **1998**, *58*, 3344-3352.

27.   Yang, C. C.; Wang, Y. C.; Wei, S.; Lin, L. F.; Chen, C. S.; Lee, C. C.; Lin, C. C. Peroxisome proliferator-activated receptor gamma-independent suppression of androgen receptor expression by troglitazone mechanism and pharmacologic exploitation. *Cancer Res.* **2007**, *67*, 3229-3238.

28.   Sikka, S.; Chen, L.; Sethi, G.; Kumar, A. P. Targeting PPARgamma Signaling Cascade for the Prevention and Treatment of Prostate Cancer. *PPAR Res.* **2012**, *2012*, 968040.

29.   Agatsuma, T.; Ogawa, H.; Akasaka, K.; Asai, A.; Yamashita, Y.; Mizukami, T.; Akinaga, S.; Saitoh, Y. Halohydrin and oxime derivatives of radicicol: synthesis and antitumor activities. *Bioorg. Med. Chem.* **2002**, *10*, 3445-3454.

30.   Hammarling, L.; Gustavsson, H.; Svensson, K.; Oskarsson, A. Migration of bisphenol-A diglycidyl ether (BADGE) and its reaction products in canned foods. *Food Addit. Contam.* **2000**, *17*, 937-943.

31.   Simal-Gandara, J.; Paz-Abuin, S.; Ahrne, L. A critical review of the quality and safety of BADGE-based epoxy coatings for cans: implications for legislation on epoxy coatings for food contact. *Crit. Rev. Food Sci. Nutr.* **1998**, *38*, 675-688.

32.   Delfosse, V.; Grimaldi, M.; le Maire, A.; Bourguet, W.; Balaguer, P. Nuclear receptor profiling of bisphenol-A and its halogenated analogues. *Vitam. Horm.* **2014**, *94*, 229-251.

33.   Olson, M. E.; Li, M.; Harris, R. S.; Harki, D. A. Small-molecule APOBEC3G DNA cytosine deaminase inhibitors based on a 4-amino-1,2,4-triazole-3-thiol scaffold. *ChemMedChem* **2013**, *8*, 112-117.